k - Version of Finite Element Method for Polymer Flows using Giesekus Constitutive Model

by

Kedar Mukund Deshpande

B.E., University of Pune, India, 2000

M.S.M.E., University of Kansas, 2004

Submitted to the Department of Mechanical Engineering and the Faculty of the Graduate School of the University of Kansas in partial fulfillment of the requirements for the Degree of Doctor of Philosophy

---

Dr Karan S. Surana (Advisor), Chair

Dr Peter W. Tenpas

Dr Ray Taghavi

Dr Robert M. Sorem

Dr Albert Romkes

Date defended

The Thesis committee for Kedar Mukund Deshpande certifies that this is the approved version of the following thesis:

k - Version of Finite Element Method for Polymer Flows using Giesekus Constitutive Model

Committee:

Dr Karan S. Surana (Advisor), Chair

Dr Peter W. Tenpas

Dr Ray Taghavi

Dr Robert M. Sorem

Dr Albert Romkes

Date approved

Acknowledgments

I would like to thank and express my sincere gratitude to my advisor and committee chair, Dr. Karan Surana(Deane E. Ackers Distinguished Professor of Mechanical Engineering) for providing able guidance and timely encouragement for successful completion of the work presented here. I would also like to thank Dr Peter W. Tenpas, Dr Ray Taghavi, Dr Robert M. Sorem and Dr Albert Romkes for serving as members of my thesis committee.

I would also like to extend my thanks to Dr. Karan Surana and the Department of Mechanical Engineering for providing me financial assistance during my graduate studies. The financial support provided by the DEPSCoR/AFOSR through grant number F49620-03-01-0298 to the University of Kansas, department of mechanical engineering and through grant number F49620-03-1-0201 to Texas A & M university are gratefully acknowledged. The seed grant provided by ARO through grant number FED46680 to the Univesity of Kansas, department of mechanical engineering is also achnowledged. The infrastructure provided by Computational Mechanics Laboratory (CML) is worth mentioning, as it helped immensly to complete this thesis work within time schedule.

Special thanks goes to my parents for encouraging and giving me good education, and for providing financial assistance during my graduate studies.

I appreciate and thank all of my friends and colleagues for providing good suggestions and fruitful discussions for completion of this work.

Abstract

One of the fundamental differences in the polymer flows compared to Newtonian or generalized Newtonian flow is the presence of elasticity due to polymer in addition to the viscosities of the solvent and the polymer. While for Newtonian and generalized Newtonian fluids viscous stresses are explicitly defined in terms of strain rates and transport properties, and thus can be completely eliminated from the governing differential equations (GDEs) by their substitution in the momentum and energy equations. This however is not possible in the case of polymer flows.

The mathematical models for polymer flows are derived using conservation laws in which many different choices of stresses as dependent variables are possible. In the published works it is generally accepted that GDEs in elastic stresses are meritorious in Galerkin method with weak form over other choices. However, regardless of the choices of stresses the GDEs always remain non-linear and hence, the Galerkin method with weak form yields variationally inconsistent integral forms for all possible choices of the stresses. Thus, one of the investigation in this study is to show the influence of the choices of stresses in the mathematical models on the computational processes when the integral forms are variationally consistent (VC).

Another significant issue in polymer flows is the issue of numerical solutions for higher Deborah numbers. For a given fluid and a given geometric configuration the choices of length (L_o) and relaxation time (λ) are generally fixed and hence high Deborah number flows are invariably associated with higher flow rates and thus higher velocities. In many standard model problems such as couette flow, lid driven cavity, expansion, contraction etc, severe deborah number (De) limitations are reported in the computational processes based on Galerkin method with weak form while there appears to be no such apparent limitation in the constitutive model such as Giesekus model. In this work we investigate if such Deborah number limitations exist in hpk framework or are such limitations a consequence of VIC integral form and C^0 local approximations. The work presented here considers boundary value problems (BVPs) as well as initial value problems (IVPs) using Giesekus constitutive model.

For BVPs, numerical studies are presented for (i) One dimensional fully developed

flow between parallel plates (ii)developing flow between parallel plates and (iii) lid driven square cavity. In case of one dimensional fully developed flow solutions are reported for Deborah numbers up to 6514.52 and there does not seem to be any limit of deborah number in 'hpk' framework. Solutions are reported for developing flow between parallel plates upto deborah number of 20.13. Excellent agreement is obtained between for one dimensional fully developed flow between parallel plates and developing flow between parallel plates. For lid driven square cavity, mathematical idealization of the physics at the corners where stationary walls intersect the lid is presented. It is shown that in the hpk framework when $h_d \rightarrow 0$ and $k \rightarrow \infty$, physics is approached where the lid meets the stationary vertical walls. Various numerical studies are presented upto deborah number of 2.4 for h_d = 0.1 and 0.05. The converged solutions independent of h, p and k are reported. The convergence of the Newton's method with line search slows down for high deborah numbers primarily due to the fact that the stokes flow is not in the close neighborhood of the solution sought. This problem is overcome by using the solution at lower deborah number as the initial solution for high deborah number i.e. continuation in Deborah number.

The numerical solutions of boundary value problem (BVP) and initial value problem (IVP) arising in Fiber spinning of polymers are presented using Least squares and space-time least squares finite element process in $H^{k,p}$ scalar product spaces. The parameter k, the order of the space defines the global differentiability of order (k-1) and is an independent parameter in all finite element computations in addition to characteristic length h and degree p of the approximations. This work discusses various mathematical models, assumptions employed in their derivations, integral forms and approximation spaces. The need and the importance of higher order spaces in space and time and the meritorious features of the variationally consistent (VC) integral forms are demonstrated. Numerical studies consist of four different benchmark problems used most frequently in the published work. Numerical studies are presented for different draw ratios and lengths of the physical domain. In all cases stationary states of the evolutions are compared with the solution of the corresponding BVP. Numerical studies show that for a given polymer there is a limiting value of draw ratio for a fixed length

beyond which computations will fail due to excessive stresses in the polymeric liquid indicating possibility of the onset and progression of damage. The higher order global differentiability of the approximations in space and time and VC (or STVC) integral forms are essential for incorporating the desired physics in the computational process and for unconditional stability of the computational processes.

Contents

List of Tables

List of Figures

Nomenclature

$\hat{\mathbf{U}}$	=	Velocity Vector
$\mathbf{U}$	=	Dimensionless Velocity Vector
$\hat{\rho}$	=	Density
ρ	=	Dimensionless Density
$\hat{\eta}$	=	Zero Shear Rate Shear Viscosity
η	=	Dimensionless Zero Shear Rate Shear Viscosity
$\hat{\boldsymbol{\tau}}$	=	Stress Tensor
$\boldsymbol{\tau}$	=	Dimensionless Stress Tensor
$\hat{\mathrm{p}}$	=	Pressure
p	=	Dimensionless Pressure
$\hat{u}$	=	Velocity in x direction
u	=	Dimensionless Velocity in x direction
$\hat{v}$	=	Velocity in x direction
v	=	Dimensionless Velocity in x direction
$\hat{\tau}_{xx}$	=	Normal Stress in x direction
τ_{xx}	=	Dimensionless Normal Stress in x direction
$\hat{\tau}_{yy}$	=	Normal Stress in y direction
τ_{yy}	=	Dimensionless Normal Stress in y direction
$\hat{\tau}_{xy}$	=	Shear Stress in xy plane
τ_{xy}	=	Dimensionless Shear Stress in xy plane
De	=	Deborah Number
Re	=	Reynolds Number
$\hat{x}$	=	x coordinate
x	=	Dimensionless x coordinate
$\hat{y}$	=	y coordinate

y	=	Dimensionless y coordinate
λ_1	=	Relaxation Time
τ_o	=	Reference Stress
ρ_o	=	Reference Density
u_o	=	Reference Velocity
L_o	=	Reference Length
η_o	=	Reference Viscosity
τ_o	=	Reference Stress
u_h	=	Interpolation of Velocity u over an element $'\mathrm{e}'$
v_h	=	Interpolation of Velocity$v$over an element $'\mathrm{e}'$
p_h	=	Interpolation of Pressure p over an element $'\mathrm{e}'$
τ_{xx}^h	=	Interpolation of normal stress τ_{xx} over an element $'\mathrm{e}'$
τ_{yy}^h	=	Interpolation of normal stress τ_{yy} over an element $'\mathrm{e}'$
τ_{xy}^h	=	Interpolation of shear stress τ_{xy} over an element $'\mathrm{e}'$
$\hat{\boldsymbol{\tau}}^p$	=	Polymer Stress Tensor
$\boldsymbol{\tau}^p$	=	Dimensionless Polymer Stress Tensor
$\hat{\boldsymbol{\tau}}^s$	=	Solvent Stress Tensor
$\boldsymbol{\tau}^s$	=	Dimensionless Solvent Stress Tensor
$\hat{\tau}_{xx}^p$	=	Polymer Normal Stress τ_{xx}
$\hat{\tau}_{yy}^p$	=	Polymer Normal Stress τ_{yy}
$\hat{\tau}_{xy}^p$	=	Polymer Shear Stress τ_{xy}
τ_{xx}^p	=	Dimensionless Polymer Normal Stress τ_{xx}
τ_{yy}^p	=	Dimensionless Polymer Normal Stress τ_{yy}
τ_{xy}^p	=	Dimensionless Polymer Shear Stress τ_{xy}
$\hat{\tau}_{xx}^s$	=	Solvent Normal Stress τ_{xx}
$\hat{\tau}_{yy}^s$	=	Solvent Normal Stress τ_{yy}
$\hat{\tau}_{xy}^s$	=	Solvent Shear Stress τ_{xy}

τ^s_{xx} = Dimensionless Solvent Normal Stress τ_{xx}

τ^s_{yy} = Dimensionless Solvent Normal Stress τ_{yy}

τ^s_{xy} = Dimensionless Solvent Shear Stress τ_{xy}

$\boldsymbol{\tau}^e$ = Dimensionless Elastic Stress Tensor

$\boldsymbol{\tau}^v$ = Dimensionless Viscous Stress Tensor

τ^e_{xx} = Dimensionless Elastic Normal Stress τ_{xx}

τ^e_{yy} = Dimensionless Elastic Normal Stress τ_{yy}

τ^e_{xy} = Dimensionless Elastic Shear Stress τ_{xy}

τ^v_{xx} = Dimensionless Viscous Normal Stress τ_{xx}

τ^v_{yy} = Dimensionless Viscous Normal Stress τ_{yy}

τ^v_{xy} = Dimensionless Viscous Shear Stress τ_{xy}

τ^{pv}_{xx} = Dimensionless Polymer Viscous Normal Stress τ_{xx}

τ^{pv}_{yy} = Dimensionless Polymer Viscous Normal Stress τ_{yy}

τ^p_{xy} = Dimensionless Polymer Viscous Shear Stress τ_{xy}

$\boldsymbol{\tau}_{(1)}$ = Convected Time Derivative of Dimensionless Stress Tensor

$\boldsymbol{\tau}^p_{(1)}$ = Convected Time Derivative of Dimensionless Polymer Stress Tensor

$\boldsymbol{\tau}^s_{(1)}$ = Convected Time Derivative of Dimensionless Solvent Stress Tensor

η_s = Dimensionless Shear Viscosity

η_p = Dimensionless Polymer Viscosity

I = Error Functional in Least Squares Finite Element Formulation

$\dot{\boldsymbol{\gamma}}$ = ShearRate

E^e_i = Element Error (or residual) equation for an element $'\mathrm{e}'$

$\nabla\mathbf{U}$ = Rate of Strain Tensor

dof = degrees of freedom

GDEs = Global Differential Equations

Chapter 1

Introduction, Literature review and Scope of work

1.1 Introduction

One of the fundamental differences in the polymer flows compared to Newtonian or generalized Newtonian flow is the presence of elasticity due to the polymer in addition to the viscosities of the solvent and the polymer. Even for dilute polymeric liquids the elasticity effects can be significant at higher flow rates, higher shear rates or higher elongational rates. When one examines the mathematical models for polymer flows and compares them with those for Newtonian, generalized Newtonian flows, one finds that the constitutive equation in case of polymers may be complicated partial differential equations in polymer stress, strain rates and transport properties. While for Newtonian and generalized Newtonian fluids viscous stresses are explicitly defined in terms of strain rates and transport properties, and can be substituted in the momentum and energy equations and thus can be completely eliminated from the mathematical models. This, however is not possible in case of polymer flows.

To illustrate this point further we consider two dimensional isothermal incompressible flow of a Newtonian and generalized Newtonian fluid. The GDEs for this case consist of continuity, momentum and constitutive equations. These can be derived in terms of u, v, p and $\boldsymbol{\tau}_{ij}$ (viscous stresses). These are a system of six first order partial

differential equations and hence will permit C^{00} local approximations when designing finite element processes for obtaining their numerical solution. If we substitute viscous stresses $\boldsymbol{\tau}_{ij}$ in the momentum equation then we only have a system of three partial differential equations in u, v, p, however, the momentum equations now contain upto second order derivatives of the velocities u and v. The finite element processes for these GDEs would require higher order continuity (higher than C^{00}) local approximations for u and v if we wish to maintain integrals in Riemann sense. In case of two dimensional polymer flows, the situation is much more complicated, as an example consider giesekus fluid. The continuity and momentum remain the same as in case of Newtonian and generalized Newtonian fluids, but the constitutive equations are in terms of polymer stress $\boldsymbol{\tau}^p_{ij}$. The momentum equation contain total stresses $\boldsymbol{\tau}_{ij} = \boldsymbol{\tau}^p_{ij} + \boldsymbol{\tau}^s_{ij} = \boldsymbol{\tau}^e_{ij} + \boldsymbol{\tau}^{pv}_{ij} + \boldsymbol{\tau}^s_{ij}$. $\boldsymbol{\tau}^{sv}_{ij}$ and $\boldsymbol{\tau}^{pv}_{ij}$ can be explicitly expressed in terms of strain rates and solvent and polymer viscosities. In this case there are many different alternatives to derive different forms of GDEs depending upon the choice of stress variables : (1) $u, v, p, \boldsymbol{\tau}^p_{ij}, \boldsymbol{\tau}^{sv}_{ij}$: a first order system of partial differential equations. (2) $u, v, p, \boldsymbol{\tau}^p_{ij}$: in this case $\boldsymbol{\tau}^{sv}_{ij}$ have been substituted in the momentum equation in terms of strain rates and solvent viscosity and hence, the momentum equations contain upto second order derivatives of the velocities. (3) $u, v, p, \boldsymbol{\tau}^e_{ij}$: in this case $\boldsymbol{\tau}^{pv}_{ij}$ and $\boldsymbol{\tau}^{sv}_{ij}$ have been substituted in terms of strain rates and polymer and solvent viscosities. Here, we find that momentum as well as constitutive equations contain upto second order derivatives of the velocities. (4) Other choices such as $u, v, p, \boldsymbol{\tau}^e_{ij}, \boldsymbol{\tau}^{pv}_{ij}, \boldsymbol{\tau}^{sv}_{ij}$; $u, v, p, \boldsymbol{\tau}^e_{ij}, \boldsymbol{\tau}^{pv}_{ij}$; $u, v, p, \boldsymbol{\tau}^e_{ij}, \boldsymbol{\tau}^{sv}_{ij}$ etc. are possible as well. The first order system of GDEs permit use of C^{00} local approximations but at the expense of increased number of dependent variable and hence loss of computational efficiency. The GDEs containing upto second order derivatives result in reduced number of dependent variable but require higher order global differentiability local approximations. However, regardless of the choices of the stress variables, the resulting mathematical models remain a system of non-linear partial differential equations.

In the published work [1, 2] it is reported that some form of the GDEs are meritorious over the others. In particular the GDEs in $u, v, p, \boldsymbol{\tau}^e_{ij}$ are considered meritorious

in Galerkin method with weak form in which integration by parts is generally used to lower the differentiation in the velocity terms. Our view point is that since the GDEs are always non-linear, Galerkin method with weak form is always variationally inconsistent [3] regardless of the choices of dependent variables and hence undoubtedly require use of upwinding methods for some choices of h, p and k ranges of dimensional parameters and boundary conditions. Thus, the influence of the choices of stress variables on the performance of the computational processes in hpk framework with VC (or STVC) integral form is an area of investigation.

Another significant issue in polymer flows is the issue of numerical simulations for higher Deborah numbers ($De = \lambda.u_o/L_o$). For a given fluid and a given geometric configuration the choices of λ and L_o (reference value) are generally fixed and hence high Deborah number flows are invariably associated with higher flow rates and higher velocities. In many standard model problems such as Couette flow, lid driven cavity, expansion, contraction etc, Deborah number limitations are reported in the computational process based on Galerkin method with weak form while there appears to be no apparent limitation in the constitutive model such as Giesekus model. In this work we investigate if such Deborah number limitations exist in hpk framework or are such limitations a consequence of VIC integral form and C^0 local approximations.

1.2 Literature review

There is vast amount of literature published on numerical methods for polymer flows using finite difference, finite volume and finite element methodologies. The reasons for the failure or less than satisfying performance of computational processes at higher De are not clear but in general it is concluded that better computational methods are needed. That is, whether it is due to :(1) the choice of variables in the mathematical models, (2) the choice of the method of approximation or (3) the choice of local approximations.

Rajagopalan et al. [1] reported formulation based on finite element elastic-viscous splitting in the momentum equations (EVSS/FEM) and concluded this formulation

to be the most robust at high Deborah number flows. The same formulation is used by Rajagopalan et al. [4] to study steady two dimensional rimming flow of Newtonian and viscoelastic liquid films. A new decoupled finite element method for integral models (INT/FEM) was also reported by Rajagopalan et al. [5] for two dimensional viscoelastic flows. The performance of INT/FEM method is reported to be comparable with EVSS/FEM method at high Deborah number flows for shear thinning fluids.

Guenette and Fortin [6] developed a mixed finite element method by introduction of the rate of deformation tensor as an additional unknown. The constitutive equation was used in its original form without explicit change of stress variable as done in EVSS method. The numerical strategy used is a decoupled iterative scheme as a preconditioner for the Generalized Minimal Residual (GMRES) algorithm. Arigo et al. [7] presented a comparison of experimental and numerical results for sphere sedimenting axially under the gravity through a cylindrical tube containing viscoelastic fluid, the numerical computations are performed using EVSS formulation and computations are done upto Deborah number of 2.2 with mesh refinements. In [8, 9], a modified EVSS method with rate of deformation as an additional variable is used to simulate the 4:1 contraction flow and stokes flow problem. Matallah et al. [10] presented numerical studies for various recovery and stress-splitting schemes for an Oldroyd-B model within the framework of Taylor Galerkin/pressure correction method. The authors claim the recovery scheme to be more accurate and stable than the conventional EVSS method at high Deborah number flows.

An adaptive viscosity vorticity (DAVSS-ω) formulation is developed by Dou and Thien [11] for the polymer flow past a circular cylinder. The stability of the viscoelastic flows at high Deborah numbers is achieved by combining discrete adaptive elastic viscous split stress (DAVSS) formulation with the independent interpolation of the vorticity to arrive at the DAVSS-ω method. A new stabilized formulation MIX1 (Galerkin/Least Squares formulation) based on the incompressibility residual of the finite element discretizations is introduced by Fan et al [12]. The success of MIX1 method over EVSS and DEVSS was claimed for solving the benchmark problems. Baijens [13] reported a comprehensive review of the application of mixed finite element method to

solve viscoelastic flow problems. It was concluded that the DEVSS based methods in combination with SUPG formulation, DG formulation or other upwind schemes provide the most robust formulation to study viscoelastic flows for high Deborah number. In recent development, Thais et al. [14] formed simplified algebraic explicit stress models (AES-1 and AES-2) and compared the numerical results from AES models with the Oldroyd-B model for flows of viscoelastic fluid in a 180^o bent planar channel and in a 4:1 contraction flow. The main goal for developing AES models was to save computational cost as compared with the differential constitutive models.

Lim and schowalter[15] studied the stability of pressure driven flow between parallel plates using pseudo-spectral methods, authors also presented analytical solution for α = 0.5 (mobility factor). Brezzi et al. [16] introduced mixed finite element method based on simplices and cubes for second order elliptic problems. A Spectral method and pseudo spectral method is used in [17, 18], to analyze the performance of giesekus constitutive equation for the undulating channel steady state flow as well as the axisymmetric flow of Oldroyd fluid. In reference [19, 20, 21], finite element method is used for numerical simulation of polymer melts using various differential constitutive models, numerical results are compared with the experimental results. It is concluded that the Phan Thein Tanner (PTT) model gives the best quantitative fit to the experimental data in these investigations. A higher order galerkin method (hp type) is used by Talwar and Khomami [22, 23] for steady creeping flow and inertial flow of shear thinning viscoelastic fluids past periodic square array for a variety of constitutive models.

Szady et al. [24] presented a new mixed finite element method (EVSS-G/FEM) that is reported to satisfy the compatibility condition between velocity gradients and elastic stress by the use of same degree polynomial approximation for elastic stress and velocity gradients. Yurun [25] compared the performance of discontinuous galerkin (DG) method and the continuous streamline upwinding petrov galerkin method (SUPG) using EVSS formulation and pure mixed formulation (MIX). The abrupt contraction, stick slip problem and smooth flow of UCM fluid around a sphere were used as model problems. Authors concluded that the DG/EVSS method is more stable than SUPG/EVSS

method for 4:1 contraction problem. A second order accurate finite volume/finite element hybrid scheme is developed by Wapperom et al.[26] using oldroyd-B model. Liu et al.[27] investigated the flow of polymer solutions around a periodic, linear array of cylinders using Giesekus constitutive equation, the finite extensible, nonlinear elastic dumbbell model with Peterlin's approximation (FENE-P) and the FENE dumbbell model of Chilcott-Rallison (CR) using finite element method and EVSS-G and DEVSS-G formulations. The lid driven cavity flow has been studied by Grillet et al. [28, 29] experimentally using video image analysis and as well as numerically using a convergent and highly accurate mixed finite element technique to investigate the onset of elastic instability. Mckinley et al. [30, 31, 32] established a dimensionless stability criterion to provide a consistent framework for analyzing pure elastic instabilities in a wide range of simple and complex flow geometries. Oliveria [33] investigated the numerical aspects of the implementation of Giesekus constitutive model in a finite volume method specifically for decomposition of stress equations to maximize diagonal dominance, and imposition of boundary conditions for the normal stresses and pressure.

Chauverie and Owens [34] investigated flow past a cylinder for Oldoroyd-B and PTT constitutive models using a stabilized spectral element method for accurate integration of the mixed elliptic-hyperbolic system. Bonvin and picasso [35] proposed finite element/Monte-Carlo method for solving the flow of a dilute polymeric liquid in 4:1 abrupt contraction. The performance of the stabilized Galerkin/Least Squares finite element formulation using a new definition of the stabilization parameter for the constitutive equation is presented by Behr et al. [36]. A defect correction method is proposed by Ervin and Lee [37] for viscoelastic fluid flows for high Deborah numbers. The main difficulty of lack of convergence for non linear iteration process is alleviated to some extent by using defect step in which the constitutive equation is solved with an artificially reduced Deborah numbers for stability and the resulting error is corrected in the correction step. Coronado et al [38] introduced four field galerkin-least squares formulation that uses a separate variable for velocity gradient. The numerical studies using GLS indicate that GLS method is comparable to DEVSS-G/SUPG method and yields results at lower computational cost compared to DEVSS type methods.

Remarks

Based on the literature review presented in this section, we make several remarks

1. Regardless of the specific forms of the GDEs in the mathematical models depending upon the choices of stress variables, the resulting governing differential equations always remain non-linear.

2. Use of finite difference, finite volume and Galerkin method with weak form for obtaining the numerical solutions of the BVPs and IVPs resulting from these mathematical models requires upwinding methods in some form or the other to stabilize computations. Thus the success of these methods for high Deborah number flows may largely depend upon whether the upwinding method retain adequate physics to the computational processes.

3. The upwinding methods neither have mathematical basis nor physical, so failure of computations for higher De based on these methods may not be surprising at all.

4. In finite element processes we construct integral form based on fundamental lemma [3, 39, 40] which is then used for discretization containing elements (or space-time elements). Whether the integrals over the discretized domain are Riemann or Lebesgue influences the physics that is incorporated in the computational process. Almost all currently used finite element processes are of class C^0 in space and time. This obviously makes all integrals in the Lebesgue sense and hence, limited physics.

5. Even when so called 'benchmark quality' solutions are reported the concept of convergence is rarely demonstrated. For example in the currently used finite element technology solutions that are independent of h, the characteristic length and p, the degree of local approximation are generally not available. Thus, how close C^0 solutions come to the real physics (continuity and differentiability of certain order of the dependent variables) is rarely demonstrated.

6. In summary, when the numerical computations fail beyond a certain Deborah

number, in our view, the reasons for the failure are difficult to establish due to too many questionable strategies in the design of the computations.

Recently Surana et al. [3, 39, 40] presented k-version of finite element method and h, p, k mathematical and computational framework for BVPs. The author shows that the k, the order of the approximation space is an independent parameter in all finite element computations in addition to h and p used currently. k, provides global differentiability of (k - 1) of approximations in space. h, p and hp-adaptive processes cannot alter k. For example local approximation of class C^0 (i.e. k = 1) remain of class C^0 regardless of mesh refinement and p-level increase. Authors in references [3, 39, 40] introduced the concepts of variational consistency and variational inconsistency of the integral forms by establishing a link between the integral forms resulting from the methods of approximations and the elements of calculus of variations. Surana et al. showed that the VC integral forms satisfy all three elements (existence of functional I, $\delta I = 0$ necessary condition yielding the integral form and $\delta^2 I$ yielding a unique extremum principle) of the calculus of variation. The coefficient matrices in the algebraic systems resulting from VC integral forms are symmetric, positive definite with real basis and eigen values greater than zero and thus, the computations are unconditionally stable. VIC integral forms on the other hand do not always ensure unconditionally stable computational processes. These may even totally degenerate in which case the computations cease. By classifying the differential operators into three groups: self-adjoint, non-self adjoint and non-linear, surana et al. [3, 39, 40] showed that the methods of approximations based on Galerkin method, weighted residual method, petrov-galerkin method are always VIC for all three classes of differential operators. Galerkin method with weak form is only VC for self adjoint operators when the bilinear functional B(.,.) is symmetric. The least squares method is always VC regardless of the differential operator. Based on [3, 39, 40], only LSP is a viable finite element computational methodology for non-linear boundary value problems and hence is used in the work presented here.

Surana et al. [41] extended the work presented in references [3, 39, 40] for BVPs to IVPs. The authors showed that the space-time differential operators can be math-

ematically classified into two groups: non-self adjoint and non-linear either by using the entire space-time domain or by using a space-time strip (or slab). A link between various space-time methods of approximations and calculus of variations for the two classes of operators shows that all methods of approximation are space-time variationally inconsistent except space-time least squares process. Authors in reference [41] also demonstrated STLSP utilizing space-time strip or slab with time marching are highly meritorious in terms of accuracy (or error control) and computational efficiency. In the work presented here we utilize this approach for IVPs.

1.3 Scope of present study

The mathematical and computational framework utilized in the work presented here for BVPs and IVPs in polymer flows has two important features that distinguishes it from all other methodologies used currently.

1. The mathematical and computational framework is based on h, the characteristic length, p, the degree of local approximation and k, the order of the approximation space as three independent computational parameters [3, 39, 40, 41] as opposed to h, p used currently. k, the order of the approximation space permits global differentiability of order (k - 1) in space and time. This is necessiated by the physics and the higher order global differentiability characteristics of the theoretical solutions. In terms of mathematics it translates into being able to maintain integrals in Riemann sense as opposed to Lebesgue sense. The higher order global differentiability approximation yield lower residuals, better convergence, better accuracy for reduced degrees of freedom.

2. The second important aspect of the work is that the integral forms are ensured to be variationally consistent (BVPs) and space-time variationally consistent (IVPs). VC and STVC integral forms ensure unconditionally stable computational process for all choices of h, p and k. The coefficient matrices in the algebraic system are always symmetric with real basis and eigen values greater than zero. Since, the differential operators in the mathematical models for the BVPs as well

as IVPs are non-linear only least-squares process and space-time least squares are VC and STVC and hence, used in the work presented here.

Details of the mathematical models including Giesekus constitutive equations are given in chapter 2. Various choices of stress variables are considered in the mathematical models. The least squares finite element formulation for BVPs and space-time least squares finite element formulation for IVPs are presented in chapter 3. Minimally conforming spaces and their influence on the computational processes is also discussed in chapter 3. One dimensional fully developed flow between parallel plates and lid driven square cavity are used as model problems for BVPs. The numerical studies are presented in chapter 4.

The mathematical models for BVPs and IVPs in fiber spinning are derived and the inconsistencies in the currently used models are pointed out. A variety of numerical studies are presented for both BVPs and IVPs. Limiting values of draw ratios are demonstrated for a given polymer and a given length. Chapter 5 contains brief literature review on fiber spinning and development of mathematical models is presented in chapter 6. The numerical studies for BVPs and IVPs in fiber spinning are presented in chapter 7. Summary and conclusions drawn from this work are given in chapter 8.

Chapter 2

Mathematical models for Steady Polymer Flows using Giesekus Constitutive equations.

2.1 GDEs for steady polymer flows using Giesekus constitutive model

For isothermal flow of an incompressible fluid the conservation of mass and newton's second law for a control volume yield well known continuity equation and momentum equations (using Bird's notation for stress [42])

$$\hat{\boldsymbol{\nabla}} \cdot \hat{\mathbf{U}} = 0 \tag{2.1}$$

$$\hat{\rho}\big(\hat{\mathbf{U}} \cdot \hat{\boldsymbol{\nabla}}\big)\hat{\mathbf{U}} - \hat{\boldsymbol{\nabla}} \cdot \hat{\boldsymbol{\sigma}} = 0 \tag{2.2}$$

$$\forall(\hat{x}, \hat{y}) \in \Omega_{\hat{x},\hat{y}}$$

In which $\hat{\rho}$ is density and $\hat{\boldsymbol{\sigma}}$ are the total stresses. Using stokes hypothesis we can write (using Bird's notation [42])

$$\hat{\boldsymbol{\sigma}} = -\hat{p}\boldsymbol{I} - \hat{\boldsymbol{\tau}} \tag{2.3}$$

In (2.3), $\hat{\boldsymbol{\tau}}$ are stress deviations, we assume that the following holds.

$$\hat{\boldsymbol{\tau}} = \hat{\boldsymbol{\tau}}^p + \hat{\boldsymbol{\tau}}^s \tag{2.4}$$

$$\hat{\boldsymbol{\tau}} = \hat{\boldsymbol{\tau}}^e + \hat{\boldsymbol{\tau}}^{pv} + \hat{\boldsymbol{\tau}}^s \tag{2.5}$$

The superscripts s, p refer to solvent and polymer and e, pv mean elastic and polymer viscous. Thus, $\hat{\boldsymbol{\tau}}^s$ is the solvent stress (i.e. purely viscous), $\hat{\boldsymbol{\tau}}^{pv}$ is the viscous stress due to polymer and $\hat{\boldsymbol{\tau}}^e$ is the elastic stress. Furthermore, using Newton's law of viscosity, we have,

$$\hat{\boldsymbol{\tau}}^s = -\hat{\eta}_s \hat{\dot{\boldsymbol{\gamma}}} \tag{2.6}$$

$$\hat{\boldsymbol{\tau}}^{pv} = -\hat{\eta}_p \hat{\dot{\boldsymbol{\gamma}}} \tag{2.7}$$

where, $\hat{\eta}_s$ and $\hat{\eta}_p$ are solvent and polymer viscosities.

The Giesekus constitutive equation describing the behavior of the polymer melts or dense polymeric liquid [43] can be written as,

$$\hat{\boldsymbol{\tau}}^p + \lambda_1 \hat{\boldsymbol{\tau}}^p_{(1)} - \left(\frac{\lambda_1 \alpha}{\hat{\eta}_p}\right)(\hat{\boldsymbol{\tau}}^p \cdot \hat{\boldsymbol{\tau}}^p) + \hat{\eta}_p \hat{\dot{\boldsymbol{\gamma}}} = 0 \tag{2.8}$$

In (2.8), λ_1 is relaxation time and α is called the mobility factor.

We non dimensionalize all of the above equations using following dimensionless variables and reference quantities.

$$x = \hat{x}/L_0, \quad y = \hat{y}/L_0, \quad \mathbf{U} = \hat{\mathbf{U}}/u_0, \quad \boldsymbol{\tau} = \hat{\boldsymbol{\tau}}/\tau_0, \quad \boldsymbol{\tau}^p = \hat{\boldsymbol{\tau}}^p/\tau_0, \quad \boldsymbol{\tau}^s = \hat{\boldsymbol{\tau}}^s/\tau_0$$

$$\boldsymbol{\tau}^e = \hat{\boldsymbol{\tau}}^e/\tau_0, \quad \boldsymbol{\tau}^{pv} = \hat{\boldsymbol{\tau}}^{pv}/\tau_0, \quad \mathrm{p} = \hat{\mathrm{p}}/\tau_0, \quad \rho = \hat{\rho}/\rho_0, \quad \eta = \hat{\eta}/\eta_0, \quad \eta_p = \hat{\eta}_p/\eta_0$$

$$\eta_s = \hat{\eta}_s/\eta_0, \quad \eta_0 = \hat{\eta}_p + \hat{\eta}_s \tag{2.9}$$

Where L_0, u_0, ρ_0, η_0 and τ_0 are reference length, velocity, density, viscosity and stress.

we obtain the following for the (2.1) - (2.8).

$$\boldsymbol{\nabla} \cdot \mathbf{U} = 0 \tag{2.10}$$

$$f_1 \rho(\mathbf{U} \cdot \boldsymbol{\nabla})\mathbf{U} + \boldsymbol{\nabla} \mathrm{p} + \boldsymbol{\nabla} \cdot \boldsymbol{\tau} = 0 \tag{2.11}$$

$$\boldsymbol{\tau}^p + De.\boldsymbol{\tau}^p_{(1)} - \frac{De.\alpha}{\eta_p.f_2}(\boldsymbol{\tau}^p \cdot \boldsymbol{\tau}^p) + \eta_p.f_2\dot{\boldsymbol{\gamma}} = 0 \tag{2.12}$$

$$\boldsymbol{\tau}^s + \eta_s.f_2\dot{\boldsymbol{\gamma}} = 0 \tag{2.13}$$

$$\boldsymbol{\tau} = \boldsymbol{\tau}^p + \boldsymbol{\tau}^s \tag{2.14}$$

$\forall (x, y) \in \Omega_{x,y}$

$$where \;\; f_1 = \begin{cases} 1 & if\ \tau_0 = \rho_0 u_0^2 = (\tau_0)_{cke} \\ Re & if\ \tau_0 = \eta_0 u_0 / L_0 = (\tau_0)_{cvs} \end{cases} \tag{2.15}$$

$$f_2 = \begin{cases} 1/Re & if\ \tau_0 = \rho_0 u_0^2 = (\tau_0)_{cke} \\ 1 & if\ \tau_0 = \eta_0 u_0 / L_0 = (\tau_0)_{cvs} \end{cases} \tag{2.16}$$

$Where, (\tau_0)_{cke}$: reference stress based on characteristic kinetic energy.

$(\tau_0)_{cvs}$: reference stress based on characteristic viscous stress.

$De = (\lambda_1.u_0/L_0)$

The choice of τ_0 is not arbitrary and has serious consequences on the convergence of iterative solution procedure for non-linear algebraic equations. It was shown in [44, 45] that $\tau_0 = max((\tau_0)_{cvs}, (\tau_0)_{cke})$ is the best choice for non denationalizing stresses and pressure in the GDEs and hence we adopt this for all further studies. GDEs (2.10)-(2.16) contain $\mathbf{U}$, p, $\boldsymbol{\tau}$, $\boldsymbol{\tau}^p$ and $\boldsymbol{\tau}^s$ as dependent variables. At this stage several choices of dependent variables are possible.

(i) $\mathbf{U},\ \mathrm{p},\ \boldsymbol{\tau},\ \boldsymbol{\tau}^s$

(ii) $\mathbf{U},\ \mathrm{p},\ \boldsymbol{\tau}^p,\ \boldsymbol{\tau}^s$

(iii) $\mathbf{U},\ \mathrm{p},\ \boldsymbol{\tau}^e,\ \boldsymbol{\tau}^s,$ assuming $\boldsymbol{\tau}^p = \boldsymbol{\tau}^e + \boldsymbol{\tau}^{pv}$ in which $\boldsymbol{\tau}^{pv} = -\eta_p.f_2\dot{\boldsymbol{\gamma}}$ and $\boldsymbol{\tau}^e$ is the

elastic stress tensor.

(iv) $\mathbf{U},\ \mathrm{p},\ \boldsymbol{\tau}^e,\ \boldsymbol{\tau}^v$, where $\boldsymbol{\tau}^v = \boldsymbol{\tau}^{pv} + \boldsymbol{\tau}^s$.

(v) $\mathbf{U},\ \mathrm{p},\ \boldsymbol{\tau}^p$

(vi) $\mathbf{U},\ \mathrm{p},\ \boldsymbol{\tau}^e$

(vii) $\mathbf{U},\ \mathrm{p},\ \boldsymbol{\tau}$

A few basic guidelines may be observed for the choice of dependent variables to ensure that the GDEs

(a) Do not have redundancies.

(b) Contain fundamental variables. That is, the variables chosen cannot be expressed explicitly in terms of others. This is helpful in avoiding inconsistencies that may be created in the computational process due to the choice of local approximations.

(c) Contain as few dependent variables as possible in order to maintain efficiency of computations.

(d) Are in as simple a form as possible, even though the computational framework is not sensitive to this. This argument is essentially due to computational efficiency reasons.

Based on the above guidelines, first we note that solvent stresses $\boldsymbol{\tau}^s$ and polymer viscous stresses $\boldsymbol{\tau}^{pv}$ due to their explicit dependence on strain rate tensor can be eliminated from the GDEs. Since Giesekus constitutive equations are derived in terms of $\boldsymbol{\tau}^p$, it is perhaps natural to treat $\boldsymbol{\tau}^p$ as variable to maintain simplicity in the constitutive equations. Thus $\mathbf{U}$, p, $\boldsymbol{\tau}^p$ choice of dependent variable is perhaps worthy of consideration. Secondly , if $\boldsymbol{\tau}^p = \boldsymbol{\tau}^e + \boldsymbol{\tau}^{pv}$, then $\mathbf{U}$, p, $\boldsymbol{\tau}^e$ choice appears equally worthy of consideration except the fact that in this case the constitutive equations are more complicated. However we do not consider$\boldsymbol{\tau}^{pv}$ as dependent variables in the computations for the same reasons that precludes $\boldsymbol{\tau}^s$ as a dependent variables. Also $\mathbf{U}$, p, $\boldsymbol{\tau}$ can be considered as dependent variables, this choice

also leads to slightly more complicated form of GDEs. The GDEs in variable $\mathbf{U}$, p, $\boldsymbol{\tau}^p$ will be referred to as 'strong form' of the GDEs. These equations have sound choice of variables, contain no redundancies and create no inconsistencies due to local approximations in the finite element process.

2.2 GDEs in variables U, p, τ^p (Strong form of GDEs):

Using the substitutions suggested above, we obtain the following GDEs from (2.10) - (2.14).

$$\boldsymbol{\nabla} \cdot \mathbf{U} = 0 \tag{2.17}$$

$$f_1(\mathbf{U} \cdot \boldsymbol{\nabla})\mathbf{U} + \boldsymbol{\nabla}\mathrm{p} + \boldsymbol{\nabla} \cdot \boldsymbol{\tau}^p - \eta_s.f_2.\boldsymbol{\nabla} \cdot \big(\boldsymbol{\nabla}\mathbf{U} + (\boldsymbol{\nabla}\mathbf{U})^T\big) = 0 \tag{2.18}$$

$$\boldsymbol{\tau}^p + De.\boldsymbol{\tau}^p_{(1)} - \frac{De.\alpha}{\eta_p.f_2}(\boldsymbol{\tau}^p \cdot \boldsymbol{\tau}^p) + \eta_p.f_2.\big(\boldsymbol{\nabla}\mathbf{U} + (\boldsymbol{\nabla}\mathbf{U})^T\big) = 0 \tag{2.19}$$

For steady flows,

$$\boldsymbol{\tau}^p_{(1)} = (\mathbf{U} \cdot \boldsymbol{\nabla})\boldsymbol{\tau}^p - (\boldsymbol{\nabla}\mathbf{U})^T \cdot \boldsymbol{\tau}^p - (\boldsymbol{\tau}^p \cdot \boldsymbol{\nabla}\mathbf{U}) \tag{2.20}$$

Substituting for $\boldsymbol{\tau}^p_{(1)}$ in (2.19) we obtain the following,

$$\boldsymbol{\nabla} \cdot \mathbf{U} = 0 \tag{2.21}$$

$$f_1(\mathbf{U} \cdot \boldsymbol{\nabla})\mathbf{U} + \boldsymbol{\nabla}\mathrm{p} + \boldsymbol{\nabla} \cdot \boldsymbol{\tau}^p - \eta_s.f_2.\boldsymbol{\nabla} \cdot \big(\boldsymbol{\nabla}\mathbf{U} + (\boldsymbol{\nabla}\mathbf{U})^T\big) = 0 \tag{2.22}$$

$$\begin{aligned}\boldsymbol{\tau}^p + De.\big((\mathbf{U} \cdot \boldsymbol{\nabla})\boldsymbol{\tau}^p - (\boldsymbol{\nabla}\mathbf{U}\big)^T \cdot \boldsymbol{\tau}^p - (\boldsymbol{\tau}^p \cdot \boldsymbol{\nabla}\mathbf{U})) - \frac{De.\alpha}{\eta_p.f_2}(\boldsymbol{\tau}^p \cdot \boldsymbol{\tau}^p) \\ +\eta_p.f_2.\big(\boldsymbol{\nabla}\mathbf{U} + (\boldsymbol{\nabla}\mathbf{U})^T\big) = 0\end{aligned} \tag{2.23}$$

$\forall (x, y) \in \Omega_{x,y}$

2.3 GDEs for 2D flow in variables U, p, τ^p (Strong form of GDEs):

Using (2.17) - (2.23), expanded form of the GDEs for two dimensional steady state flow can be written as,

$$\frac{\partial u}{\partial x} + \frac{\partial v}{\partial y} = 0 \tag{2.24}$$

$$f_1\left(u\frac{\partial u}{\partial x} + v\frac{\partial u}{\partial y}\right) + \frac{\partial \mathrm{p}}{\partial x} + \frac{\partial \tau^p_{xx}}{\partial x} + \frac{\partial \tau^p_{xy}}{\partial y} - \eta_s.f_2.\left(2\frac{\partial^2 u}{\partial x^2} + \frac{\partial^2 u}{\partial y^2} + \frac{\partial^2 v}{\partial x \partial y}\right) = 0 \tag{2.25}$$

$$f_1\left(u\frac{\partial v}{\partial x} + v\frac{\partial v}{\partial y}\right) + \frac{\partial \mathrm{p}}{\partial y} + \frac{\partial \tau^p_{xy}}{\partial x} + \frac{\partial \tau^p_{yy}}{\partial y} - \eta_s.f_2.\left(2\frac{\partial^2 v}{\partial y^2} + \frac{\partial^2 u}{\partial x \partial y} + \frac{\partial^2 v}{\partial x^2}\right) = 0 \tag{2.26}$$

$$\begin{aligned}&\tau^p_{xx} + De.\left(u\frac{\partial \tau^p_{xx}}{\partial x} + v\frac{\partial \tau^p_{xx}}{\partial y} - 2\tau^p_{xx}\frac{\partial u}{\partial x} - 2\tau^p_{xy}\frac{\partial u}{\partial y}\right)\\ &\quad -\frac{De.\alpha}{\eta_p.f_2}\left((\tau^p_{xx})^2 + (\tau^p_{xy})^2\right) + 2\eta_p.f_2.\frac{\partial u}{\partial x} = 0\end{aligned} \tag{2.27}$$

$$\begin{aligned}&\tau^p_{xy} + De.\left(u\frac{\partial \tau^p_{xy}}{\partial x} + v\frac{\partial \tau^p_{xy}}{\partial y} - \tau^p_{xx}\frac{\partial v}{\partial x} - \tau^p_{yy}\frac{\partial u}{\partial y} - \tau^p_{xy}\left(\frac{\partial u}{\partial x} + \frac{\partial v}{\partial y}\right)\right)\\ &\quad -\frac{De.\alpha}{\eta_p.f_2}(\tau^p_{xy}(\tau^p_{xx} + \tau^p_{yy})) + \eta_p.f_2.(\frac{\partial u}{\partial y} + \frac{\partial v}{\partial x}) = 0\end{aligned} \tag{2.28}$$

$$\begin{aligned}&\tau^p_{yy} + De.\left(u\frac{\partial \tau^p_{\mathrm{yy}}}{\partial x} + v\frac{\partial \tau^p_{yy}}{\partial y} - 2\tau^p_{yy}\frac{\partial v}{\partial y} - 2\tau^p_{xy}\frac{\partial v}{\partial x}\right)\\ &\quad -\frac{De.\alpha}{\eta_p.f_2}\left((\tau^p_{yy})^2 + (\tau^p_{xy})^2\right) + 2\eta_p.f_2.\frac{\partial v}{\partial y} = 0\end{aligned} \tag{2.29}$$

$\forall (x, y) \in \Omega_{x,y}$

These equations contain upto second order derivatives of the velocities but only first order derivatives of the stresses. Furthermore, no further substitutions of any kind are possible in (2.24) - (2.29). These system of equations will be referred to as strong form of GDEs for 2D steady flow.

2.4 GDEs in variables U, p, $\boldsymbol{\tau}^p$ and $\boldsymbol{\tau}^s$ (Weak form of GDEs):

By examining (2.24) - (2.29), we observe that these contain second derivatives of the velocity $\mathbf{U}$, hence will preclude the use of C^0 local approximations in approximation methods such as Least Squares process. If we maintain $\mathbf{U}$, p and $\boldsymbol{\tau}^p$ as variables of choice then the only other choice left is to use $\boldsymbol{\tau}^s$ as additional variables so that (2.24)-(2.29) can be recast as a system of first order differential equations in $\mathbf{U}$, p, $\boldsymbol{\tau}^p$ and $\boldsymbol{\tau}^s$ and thereby permitting use of C^0 local approximations. We remark that $\boldsymbol{\tau}^s$ equations do represent inconsistencies due to choice of local approximations in finite element process but such inconsistencies cannot be avoided, if we wish the GDEs to be a system of first order partial differential equations.

$$\boldsymbol{\nabla} \cdot \mathbf{U} = 0 \tag{2.30}$$

$$f_1.(\mathbf{U} \cdot \boldsymbol{\nabla})\mathbf{U} + \boldsymbol{\nabla}\mathrm{p} + \boldsymbol{\nabla} \cdot \boldsymbol{\tau}^p + \boldsymbol{\nabla} \cdot \boldsymbol{\tau}^s = 0 \tag{2.31}$$

$$\boldsymbol{\tau}^p + De.\big((\mathbf{U} \cdot \boldsymbol{\nabla})\boldsymbol{\tau}^p - (\boldsymbol{\nabla}\mathbf{U})^T \cdot \boldsymbol{\tau}^p - \boldsymbol{\tau}^p \cdot \boldsymbol{\nabla}\mathbf{U}\big) - \frac{De.\alpha}{\eta_p.f_2}(\boldsymbol{\tau}^p \cdot \boldsymbol{\tau}^p)$$

$$+\eta_p.f_2.\big(\boldsymbol{\nabla}\mathbf{U} + (\boldsymbol{\nabla}\mathbf{U})^T\big) = 0 \tag{2.32}$$

$$\boldsymbol{\tau}^s + \eta_s.f_2.(\boldsymbol{\nabla}\mathbf{U} + (\boldsymbol{\nabla}\mathbf{U})^T) = 0 \tag{2.33}$$

$$\forall (x, y) \in \Omega_{x,y}$$

Expanded form of (2.30) - (2.33) for two dimensional steady flow are given in the following,

$$\frac{\partial u}{\partial x} + \frac{\partial v}{\partial y} = 0 \tag{2.34}$$

$$f_1.\left(u\frac{\partial u}{\partial x} + v\frac{\partial u}{\partial y}\right) + \frac{\partial \mathrm{p}}{\partial x} + \frac{\partial \tau^p_{xx}}{\partial x} + \frac{\partial \tau^p_{xy}}{\partial y} + \frac{\partial \tau^s_{xx}}{\partial x} + \frac{\partial \tau^s_{xy}}{\partial y} = 0 \tag{2.35}$$

$$f_1.\left(u\frac{\partial v}{\partial x} + v\frac{\partial v}{\partial y}\right) + \frac{\partial \mathrm{p}}{\partial y} + \frac{\partial \tau^p_{xy}}{\partial x} + \frac{\partial \tau^p_{yy}}{\partial y} + \frac{\partial \tau^s_{xy}}{\partial x} + \frac{\partial \tau^s_{yy}}{\partial y} = 0 \tag{2.36}$$

$$\tau^p_{xx} + De.\left(u\frac{\partial \tau^p_{xx}}{\partial x} + v\frac{\partial \tau^p_{xx}}{\partial y} - 2\tau^p_{xx}\frac{\partial u}{\partial x} - 2\tau^p_{xy}\frac{\partial u}{\partial y}\right)$$

$$-\frac{De.\alpha}{\eta_p.f_2}.\left((\tau_{xx}^p)^2+(\tau_{xy}^p)^2\right)+2\eta_p.f_2.\frac{\partial u}{\partial x}=0 \tag{2.37}$$

$$\tau_{xy}^p+De.\left(u\frac{\partial\tau_{xy}^p}{\partial x}+v\frac{\partial\tau_{xy}^p}{\partial y}-\tau_{xx}^p\frac{\partial v}{\partial x}-\tau_{yy}^p\frac{\partial u}{\partial y}-\tau_{xy}^p\left(\frac{\partial u}{\partial x}+\frac{\partial v}{\partial y}\right)\right)$$

$$-\frac{De.\alpha}{\eta_p.f_2}.(\tau_{xy}^p(\tau_{xx}^p+\tau_{yy}^p))+\eta_p.f_2.\left(\frac{\partial u}{\partial y}+\frac{\partial v}{\partial x}\right)=0 \tag{2.38}$$

$$\tau_{yy}^p+De.\left(u\frac{\partial\tau_{yy}^p}{\partial x}+v\frac{\partial\tau_{yy}^p}{\partial y}-2\tau_{yy}^p\frac{\partial v}{\partial y}-2\tau_{xy}^p\frac{\partial v}{\partial x}\right)$$

$$-\frac{De.\alpha}{\eta_p.f_2}((\tau_{yy}^p)^2+(\tau_{xy}^p)^2)+2\eta_p.\ f_2.\frac{\partial v}{\partial y}=0 \tag{2.39}$$

$$\tau_{xx}^s+2\eta_s.f_2.\left(\frac{\partial u}{\partial x}\right)=0 \tag{2.40}$$

$$\tau_{xy}^s+f_2.\eta_s.\left(\frac{\partial u}{\partial y}+\frac{\partial v}{\partial x}\right)=0 \tag{2.41}$$

$$\tau_{yy}^s+2\eta_s.f_2.\left(\frac{\partial v}{\partial y}\right)=0 \tag{2.42}$$

$\forall(x,y)\in\Omega_{x,y}$

2.5 GDEs for 1D fully developed flow between parallel plates

One of the main thrust of this work is to investigate the importance of the choice of different dependent variables in the GDEs. The one dimensional fully developed flow between parallel plates is used for this purpose using **U**, p, $\boldsymbol{\tau}^p$; **U**, p, $\boldsymbol{\tau}^e$ and **U**, p, $\boldsymbol{\tau}$ as dependent variables.

(a) using **U**, p, $\boldsymbol{\tau}^p$ as variables :

The expanded form of the GDEs for one dimensional fully developed flow between parallel plates (figure 4.1(a)) in variables **U**, p and $\boldsymbol{\tau}^p$ are given by :

$$\frac{\partial \mathrm{p}}{\partial x}+\frac{\partial\tau_{xy}^p}{\partial y}-\eta_s.f_2.\frac{\partial^2 u}{\partial y^2}=0 \tag{2.43}$$

$$\frac{\partial \mathrm{p}}{\partial y} + \frac{\partial \tau_{yy}^{p}}{\partial y} = 0 \tag{2.44}$$

$$\tau_{xx}^{p} - 2.De.\tau_{xy}^{p}\frac{\partial u}{\partial y} - \frac{De.\alpha}{\eta_p.f_2}\big((\tau_{xx}^{p})^2 + (\tau_{xy}^{p})^2\big) = 0 \tag{2.45}$$

$$\tau_{xy}^{p} - De.\tau_{yy}^{p}\frac{\partial u}{\partial y} - \frac{De.\alpha}{\eta_p.f_2}(\tau_{xy}^{p}(\tau_{xx}^{p} + \tau_{yy}^{p})) + \eta_p.f_2.(\frac{\partial u}{\partial y}) = 0 \tag{2.46}$$

$$\tau_{yy}^{p} - \frac{De.\alpha}{\eta_p.f_2}\big((\tau_{yy}^{p})^2 + (\tau_{xy}^{p})^2\big) = 0 \tag{2.47}$$

(b) using **U**, p and $\boldsymbol{\tau}^{e}$ as variables :

Substituting $\boldsymbol{\tau}^{p} = \boldsymbol{\tau}^{e} + \boldsymbol{\tau}^{pv}$ in which $\boldsymbol{\tau}^{pv} = -\eta_p.f_2\dot{\boldsymbol{\gamma}}$ the expanded form of the GDEs for one dimensional fully developed flow between parallel plates with elastic stress as dependent variable can be written as follows,

$$\frac{\partial \mathrm{p}}{\partial x} + \frac{\partial \tau_{xy}^{e}}{\partial y} - f_2.\frac{\partial^2 u}{\partial y^2} = 0 \tag{2.48}$$

$$\frac{\partial \mathrm{p}}{\partial y} + \frac{\partial \tau_{yy}^{e}}{\partial y} = 0 \tag{2.49}$$

$$\tau_{xx}^{e} - 2.De.\tau_{xy}^{e}\frac{\partial u}{\partial y} + 2.De.\eta_p.f_2(\frac{\partial u}{\partial y})^2 - \frac{De.\alpha}{\eta_p.f_2}\big((\tau_{xx}^{e})^2 + (\tau_{xy}^{e})^2$$

$$-2.\eta_p f_2.\tau_{xy}^{e} + (\eta_p.f_2\frac{\partial u}{\partial y})^2\big) = 0 \tag{2.50}$$

$$\tau_{xy}^{e} - \eta_p f_2\frac{\partial u}{\partial y} - De.\tau_{yy}^{e}\frac{\partial u}{\partial y} - \frac{De.\alpha}{\eta_p.f_2}\big(\tau_{xy}^{e}\tau_{xx}^{e} + \tau_{xy}^{e}\tau_{yy}^{e}$$

$$-\eta_p.f_2.\frac{\partial u}{\partial y}\tau_{xx}^{e} - \eta_p.f_2.\frac{\partial u}{\partial y}\tau_{yy}^{e}\big) + \eta_p f_2\frac{\partial u}{\partial y} = 0 \tag{2.51}$$

$$\tau_{yy}^{e} - \frac{De.\alpha}{\eta_p.f_2}\big((\tau_{yy}^{e})^2 + (\tau_{xy}^{e})^2 - 2\eta_p.f_2.\frac{\partial u}{\partial y}\tau_{xy}^{e} + (\eta_p.f_2\frac{\partial u}{\partial y})^2\big) = 0 \tag{2.52}$$

(c) Using **U**, p and $\boldsymbol{\tau}$ as variables :

Similarly substituting $\boldsymbol{\tau}^{p} = \boldsymbol{\tau} - \boldsymbol{\tau}^{s}$ in which $\boldsymbol{\tau}^{s} = -\eta_s.f_2\dot{\boldsymbol{\gamma}}$. The expanded form of GDES for one dimensional fully developed flow between parallel plates with total stress as dependent variable can be obtained.

$$\frac{\partial \mathrm{p}}{\partial x} + \frac{\partial \tau_{xy}}{\partial y} = 0 \tag{2.53}$$

$$\frac{\partial \mathrm{p}}{\partial y} + \frac{\partial \tau_{yy}}{\partial y} = 0 \tag{2.54}$$

$$\begin{aligned}\tau_{xx} - 2.De.\big(\tau_{xy}\frac{\partial u}{\partial y} + \eta_s.f_2(\frac{\partial u}{\partial y})^2\big) \\ -\frac{De.\alpha}{\eta_p.f_2}\big(\tau_{xx}^2 + \tau_{xy}^2 + 2.\eta_s.f_2\frac{\partial u}{\partial y}\tau_{xy} + (\eta_s.f_2\frac{\partial u}{\partial y})^2\big) = 0\end{aligned} \tag{2.55}$$

$$\begin{aligned}\tau_{xy} + \eta_s.f_2\frac{\partial u}{\partial y} - De.\tau_{yy}\frac{\partial u}{\partial y} \\ -\frac{De.\alpha}{\eta_p.f_2}\big(\tau_{xx}\tau_{xy} + \tau_{xy}\tau_{yy} + \eta_s.f_2\frac{\partial u}{\partial y}\tau_{xx} + \eta_s.f_2\frac{\partial u}{\partial y}\tau_{yy}\big) + \eta_p.f_2\frac{\partial u}{\partial y} = 0\end{aligned} \tag{2.56}$$

$$\tau_{yy} - \frac{De.\alpha}{\eta_p.f_2}\big((\tau_{yy})^2 + (\tau_{xy})^2 + 2\eta_s.f_2.\frac{\partial u}{\partial y}\tau_{xy} + (\eta_s.f_2\frac{\partial u}{\partial y})^2\big) = 0 \tag{2.57}$$

Remarks :

1. First, we note that GDEs in section 2.3 and 2.5 are in variables $\mathbf{U}$, p and $\boldsymbol{\tau}^p$; $\mathbf{U}$, p and $\boldsymbol{\tau}^e$; $\mathbf{U}$, p and $\boldsymbol{\tau}$. These contain first order derivatives of p, $\boldsymbol{\tau}^p$, $\boldsymbol{\tau}^e$ and $\boldsymbol{\tau}$ but upto second order derivatives of velocity $\mathbf{U}$. whereas GDEs in section 2.4 are first order in $\mathbf{U}$, p, $\boldsymbol{\tau}^p$, $\boldsymbol{\tau}^s$.

2. A theoretical solution of these equations is not possible even for highly simplified case such as fully developed flow between parallel plates.

3. If we assume that the theoretical solutions of the GDEs (though may not be obtainable) are analytic i.e. $\mathbf{U}$, p, $\boldsymbol{\tau}^p$ or $\boldsymbol{\tau}^p$ and $\boldsymbol{\tau}^s$ are analytic, then $\mathbf{U}$, p, $\boldsymbol{\tau}^p$ or $\boldsymbol{\tau}^p$ and $\boldsymbol{\tau}^s$ are algebraic polynomials of infinite degree in x and y. Such solutions are obviously of class $C^\infty(\Omega_{xy})$ in which derivatives of all orders of the dependent variables exist, are continuous and differentiable and are square integrable as well. This feature of the theoretical solution is significant and permits us to design a precise mathematical and computational framework to address their numerical simulation.

2.6 Summary

In this chapter, mathematical models for polymer flows using Giesekus constitutive equations are presented for various choices of stresses as dependent variables. These mathematical models are specialized for 1-D and 2-D steady polymer flows. Regardless of the choices of stresses as dependent variables the governing differential equations remain a system of non-linear partial differential equations in the dependent variables. Since the derivation of the constitutive model for Giesekus fluid utilizes $\boldsymbol{\tau}^p$ as dependent variables it is perhaps fitting to maintain $\boldsymbol{\tau}^p$ as variables in the development of the momentum equations. This avoids unnecessary complexities in the constitutive equations. The total stress $\boldsymbol{\tau}$ in the momentum equations is decoupled into $\boldsymbol{\tau}^p$ and $\boldsymbol{\tau}^{sv}$ or $\boldsymbol{\tau}^s$. This results in a system of first order partial differential equations in $\mathbf{U}$, p, $\boldsymbol{\tau}^p$ and $\boldsymbol{\tau}^s$ referred to as weak form of GDEs. Substitution of $\boldsymbol{\tau}^s$ in terms of strain rates in the momentum equations eliminates $\boldsymbol{\tau}^s$ as variables but results in upto second order derivatives of the velocities in the momentum equations. The resulting mathematical model is referred to as strong form of GDEs. Based on Surana et al. [46] the strong form of GDEs are free of inconsistencies during finite element process when choosing local approximations. Additionally, elimination of $\boldsymbol{\tau}^s$ as variables results in reduction of the dependent variables and hence improved computational efficiency in the finite element processes.

Chapter 3

Least Squares Formulation for steady polymer flows

In this chapter we present details of the least squares processes for steady polymer flows (BVPs). From the mathematical models presented in chapter 2, we note that regardless of the choices of variables and the type of flow (1-D or 2-D) the GDEs are always a system of non-linear PDEs in the dependent variables. Thus, based on [3, 39, 40] only integral form based on least squares process is variationally consistent and hence considered here.

3.1 Least Squares Process in Ω (no discretization)

In this section we present details of the LSP in general for Ω which is then specialized for discretization of Ω for 1-D, 2-D polymer flows. Let n_e be the number of equations in the GDEs defined over the domain Ω. Let φ be the vector of 'n_e' variables. Let φ_h be the approximation of φ over Ω, then upon substituting φ_h in the 'n_e' equations we obtain 'n_e' residuals, E_i, i = 1,2,...,n_e

For subsequent details, consider GDEs in **U**, p and $\boldsymbol{\tau}^p$. The treatment for the other set of GDEs is similar.Upon substituting these approximations in the GDEs, we obtain

residual equations for Ω given by,

$$E_i(\varphi_h); i = 1, 2, ..., n_e \tag{3.1}$$

In LSP, we begin with construction of a functional I using residual equations (3.1)

(i) Existence of functional I :

$$I_{(\varphi_h)} = \sum_{i=1}^{n_e}(E_i, E_i) = \sum_{i=1}^{n_e}\int_{\Omega}(E_i)^2\, d\Omega \tag{3.2}$$

Clearly I describes a convex manifold and furthermore the convexity of the manifold is independent of the differential operator.

(ii) Necessary conditions :

Necessary conditions are obtained by setting $\delta I(\varphi_h)$ = 0 (provided $I(\varphi_h)$ is differentiable in φ_h),

$$\delta I = \sum_{i=1}^{n_e}(E_i, \delta E_i) = \{\mathrm{g}(\varphi_h)\} = 0 \tag{3.3}$$

(iii) Sufficient Condition (extremum principle) :

Second variation of $I(\varphi_h)$ i.e. $\delta^2 I(\varphi_h)$ (provided $I(\varphi_h)$ is differentiable twice in φ_h) provides sufficient condition or extremum principle. Based on [25-27], we can write ,

$$\delta^2 I(\varphi_h) \approx \sum_{i=1}^{n_e}(\delta E_i, \delta E_i) > 0 \tag{3.4}$$

(i) - (iii) clearly establish that the Least Squares process is variationally consistent.

(iv) We must now find solution φ_h that satisfies (3.4). However, since $\{\mathrm{g}(\varphi_\mathrm{h})\}$ is a nonlinear function of φ_h due to the fact that the GDEs are non-linear, we must find φ_h iteratively. Following Surana et al. [27], if φ_h^o is a starting or assumed solution, then $\{\mathrm{g}(\varphi_\mathrm{h})\}$ can be expanded in Taylor series about φ_h^o, and limiting to

first order approximation (Newton's linear method) we obtain the following,

$$\varphi_h = \varphi_h^o + \alpha \Delta\varphi_h$$

$$\Delta\varphi_h = -\left[\delta^2 I(\varphi_h)\right]^{-1}_{\varphi_h^o} \{\mathrm{g}(\varphi_h)\}_{\varphi_h^o} \tag{3.5}$$

in which α is constant, generally between 0 and 2 determined such that $I(\varphi_h) \leq I(\varphi_h^o)$. This procedure is termed as Newton's method with line search.

we already have expressions for $E_i, i = 1...n_e$ in (3.1) and approximation φ_h involving unknown constant and basis functions. All that we need now are expressions for $\delta E_i,\ i = 1, ...n_e$, which can be easily obtained using $E_i,\ i = 1, ...n_e$ and differentiating them with respect to the constants used in the approximation φ_h.

Remarks

(1) First, we note that the coefficient matrix in $\Delta\varphi_h$ calculation is given by $\delta^2 I(\varphi_h)|_{\varphi_h^o}$(in 3.5). Since $\delta^2 I(\varphi_h)|_{\varphi_h^o} > 0$, for any choices of computational and physical parameters, the coefficient matrix is always positive definite.

(2) (3.4) assures that a solution φ_h minimizes $I(\varphi_h)$ in (3.2).

(3) Global minima of $I(\varphi_h)$ is zero, which is only possible when $E_i \equiv 0 \text{ in } \Omega_{\text{xy}}$ (i.e in the pointwise sense) i.e minima of $I(\varphi_h)$ in (i) - (iv) also satisfies GDEs and hence is solution of the BVP.

(4) Since approximation φ_h is global over Ω_x (without discretization), there are no issues of global differentiability of φ_h.

3.2 Least Squares Finite Element Process

Let $\bar{\Omega}^T = \bigcup_e^M \bar{\Omega}^e$ be discretization of $\bar{\Omega}$ containing 'M' subdomains in which $\bar{\Omega}^e$ is a subdomain (element) 'e'. Let φ_h^e be local approximations of φ over $\bar{\Omega}^e$, then φ_h, the

global approximation of φ over $\bar{\Omega}^T$ is given by,

$$\varphi_h = \bigcup_{e}^{M} \varphi_h^e \tag{3.6}$$

The details presented in section (3.1) for LSP over Ω can be recast for the discretization $\bar{\Omega}^T$,

(i) Existence of functional $I(\varphi)_h \; for \; \bar{\Omega}^T$:

$$I(\varphi_h) = \sum_{e=1}^{M} \sum_{i=1}^{n_e} (E_i^e, E_i^e) = \sum_{e=1}^{M} \sum_{i=1}^{n_e} \int_{\Omega^e} (E_i)^2 \, d\Omega \tag{3.7}$$

in which the E_i^e are the element residuals equations obtained from GDEs in section 2.1 by substituting φ_h^e.

(ii) Necessary conditions :

These are obtained by setting $\delta I(\varphi_h) = 0$, provided $I(\varphi_h)$ is differentiable in φ_h,

$$\delta I(\varphi_h) = \sum_{e=1}^{M} \sum_{i=1}^{n_e} (E_i^e, \delta E_i^e) = \sum_{e=1}^{M} \{\mathrm{g}^e(\varphi_h^e)\} = \{\mathrm{g}(\varphi_h)\} = \mathbf{0} \tag{3.8}$$

(iii) Sufficient Condition (extremum principle) :

If $I(\varphi_h)$ is differentiable twice in φ_h, then $\delta^2 I(\varphi_h)$ provides the extremum principle, and based on [27] we have,

$$\delta^2 I(\varphi_h) \approx \sum_{e=1}^{M} \sum_{i=1}^{n_e} (\delta E_i^e, \delta E_i^e) = \sum_{e=1}^{M} \delta^2 I^e(\varphi_h^e) \tag{3.9}$$

(iv) Newton's method with line search becomes,

$$\varphi_h = \varphi_h^o + \alpha \Delta \varphi_h$$

$$\Delta \varphi_h = - \left[\sum_{e=1}^{M} \delta^2 I(\varphi_h) \right]_{\varphi_h^o}^{-1} \{\mathrm{g}(\varphi_\mathrm{h})\}_{\varphi_h^o} \tag{3.10}$$

Remarks

(1) Variational consistency of this Least Square finite element process stems from the Variational consistency of LSP over Ω presented in section 3.1. Hence the remarks presented in section 3.1 , hold here as well.

(2) The nature of local approximation φ_h^e is crucial so that we can establish the scalar product spaces containing basis functions for local approximations φ_h^e .

3.3 1-D fully developed flow between parallel plates : LSFEP

In this case $\bar{\Omega} = \bar{\Omega}_y$, $\bar{\Omega}^T = \bigcup \bar{\Omega}_y^e$, n_e = 5 and $\varphi_h^e = [u^e, \mathrm{p}^e, (\tau^p{}_{xx})^e, (\tau^p{}_{xy})^e, (\tau^p{}_{yy})^e]^t$; if we use u, p and $\boldsymbol{\tau}^p$ as variables, $E_i^e; i = 1, ..., 5$ becomes,

$$
\begin{aligned}
E_1^e &= \frac{\partial \mathrm{p}_\mathrm{h}^\mathrm{e}}{\partial x} + \frac{\partial (\tau_{xy}^p)_h^e}{\partial y} - \eta_s.f_2.\frac{\partial^2 u_h^e}{\partial y^2} \\
E_2^e &= \frac{\partial \mathrm{p}_\mathrm{h}^\mathrm{e}}{\partial y} + \frac{\partial (\tau_{yy}^p)_h^e}{\partial y} = 0 \\
E_3^e &= (\tau_{xx}^p)_h^e - 2.De.(\tau_{xy}^p)_h^e \frac{\partial u_h^e}{\partial y} - \frac{De.\alpha}{\eta_p.f_2}\big(((\tau_{xx}^p)_h^e)^2 + ((\tau_{xy}^p)_h^e)^2\big) = 0 \\
E_4^e &= (\tau_{xy}^p)_h^e - De.(\tau_{yy}^p)_h^e \frac{\partial u_h^e}{\partial y} - \frac{De.\alpha}{\eta_p.f_2}\big((\tau_{xy}^p)_h^e.(\tau_{xx}^p)_h^e + (\tau_{xy}^p)_h^e.(\tau_{yy}^p)_h^e\big) \\
&\quad + \eta_p.f_2.(\frac{\partial u_h^e}{\partial y}) = 0 \\
E_5^e &= (\tau_{yy}^p)_h^e - \frac{De.\alpha}{\eta_p.f_2}\big(((\tau_{yy}^p)_h^e)^2 + ((\tau_{xy}^p)_h^e)^2\big) = 0
\end{aligned}
\tag{3.11}
$$

3.4 2-D steady flow of Giesekus fluid

In this case $\bar{\Omega} = \bar{\Omega}_x y$, $\bar{\Omega}^T = \bigcup \bar{\Omega}_x y^e$, n_e = 6 and $\varphi_h^e = [u^e, v^e, \mathrm{p}^e, (\tau^p{}_{xx})^e, (\tau^p{}_{xy})^e, (\tau^p{}_{yy})^e]^t$; if we use u, p and $\boldsymbol{\tau}^p$ as variables, $E_i^e; i = 1, ..., 6$ becomes,

$$E_1^e = \frac{\partial u_h^e}{\partial x} + \frac{\partial v_h^e}{\partial x}$$

$$E_2^e = f_1 \left(u_h^e \frac{\partial u_h^e}{\partial x} + v_h^e \frac{\partial u_h^e}{\partial y} \right) + \frac{\partial \mathrm{p}_h^e}{\partial x} + \frac{\partial (\tau_{xx}^p)_h^e}{\partial x} + \frac{\partial (\tau_{xy}^p)_h^e}{\partial y}$$
$$-\eta_s . f_2 . \left(2\frac{\partial^2 u_h^e}{\partial y^2} + \frac{\partial^2 v_h^e}{\partial x \partial y} + \frac{\partial^2 u_h^e}{\partial x^2} \right)$$

$$E_3^e = f_1 \left(u_h \frac{\partial v_h}{\partial x} + v_h \frac{\partial v_h}{\partial y} \right) + \frac{\partial \mathrm{p}_h}{\partial y} + \frac{\partial (\tau_{xy}^p)_h}{\partial x} + \frac{\partial (\tau_{yy}^p)_h}{\partial y}$$
$$-\eta_s . f_2 . \left(2\frac{\partial^2 v_h^e}{\partial y^2} + \frac{\partial^2 u_h^e}{\partial x \partial y} + \frac{\partial^2 v_h^e}{\partial x^2} \right)$$

$$E_4^e = (\tau_{xx}^p)_h^e + De. \left(u_h^e \frac{\partial (\tau_{xx}^p)_h^e}{\partial x} + v_h^e \frac{\partial (\tau_{xx}^p)_h^e}{\partial y} - 2(\tau_{xx}^p)_h^e \frac{\partial u_h^e}{\partial x} - 2(\tau_{xy}^p)_h^e \frac{\partial u_h^e}{\partial y} \right) \quad (3.12)$$
$$-\frac{De.\alpha}{\eta_p . f_2} \left(((\tau_{xx}^p)_h^e)^2 + \left((\tau_{xy}^p)_h^e)^2 \right) \right) + 2\eta_p . f_2 . \frac{\partial u_h^e}{\partial x}$$

$$E_5^e = (\tau_{xy}^p)_h^e + De. \left(u_h^e \frac{\partial (\tau_{xy}^p)_h^e}{\partial x} + v_h^e \frac{\partial (\tau_{xy}^p)_h^e}{\partial y} - (\tau_{xx}^p)_h^e \frac{\partial v_h^e}{\partial x} - (\tau_{yy}^p)_h^e \frac{\partial u_h^e}{\partial y} \right.$$
$$\left. -(\tau_{xy}^p)_h^e \left(\frac{\partial u_h^e}{\partial x} + \frac{\partial v_h^e}{\partial y} \right) \right) - \frac{De.\alpha}{\eta_p . f_2} . \left((\tau_{xy}^p)_h^e ((\tau_{xx}^p)_h^e + (\tau_{yy}^p)_h^e) \right)$$
$$+\eta_p . f_2 . \left(\frac{\partial u_h^e}{\partial y} + \frac{\partial\, v_h^e}{\partial x} \right)$$

$$E_6^e = (\tau_{yy}^p)_h^e + De. \left(u_h^e \frac{\partial (\tau_{yy}^p)_h^e}{\partial x} + v_h^e \frac{\partial (\tau_{yy}^p)_h^e}{\partial y} - 2(\tau_{yy}^p)_h^e \frac{\partial v_h^e}{\partial y} - 2(\tau_{xy}^p)_h^e \frac{\partial v_h^e}{\partial x} \right)$$
$$-\frac{De.\alpha}{\eta_p . f_2} . \left(((\tau_{yy}^p)_h^e)^2 + ((\tau_{xy}^p)_h^e)^2 \right) + 2\eta_p . f_2 . \frac{\partial v_h^e}{\partial y}$$

3.5 Local approximation spaces for LSFEP for GDEs in U, p, $\boldsymbol{\tau}^p$

The GDEs in $\mathbf{U}$, p and $\boldsymbol{\tau}^p$contains only first order derivatives of p and $\boldsymbol{\tau}^p$ but upto second order derivatives of velocity $\mathbf{U}$. Hence, the highest order derivatives of p, $\boldsymbol{\tau}^p$ appearing in the integrands of the LSP are one whereas those of $\mathbf{U}$ are two. That is $H^{2,p}(\bar{\Omega}_{xy}^e)$ is the minimally conforming space for p_h^e and $(\boldsymbol{\tau}^p)_h^e$ and $H^{3,p}(\bar{\Omega}_{xy})^e$ is the minimally conforming space for $\mathbf{U}_h^e$. We note that p_h^e and $(\boldsymbol{\tau}^p)_h^e$ of class $C^2(\bar{\Omega}_{xy}^e)$ are

also admissible in the integrands. Thus, it is perhaps convenient and computationally more advantageous to consider $H^{3,p}(\bar{\Omega}^e_{xy})$ as minimally conforming space for φ^e_h. Hence we have the following,

$$\varphi_h \in H^k(\bar{\Omega}^T_{xy});\ k \geq 3$$

$$\varphi^e_h \in H^{k,p}(\bar{\Omega}^e_{xy});\ k \geq 3 \tag{3.13}$$

Scalar product spaces of order higher than 3 (minimally conforming space) are needed if the computed solutions are to possess the same global differentiability (upto same order) as the theoretical solutions.

3.6 Local approximations spaces for LSFEP for GDEs in U, p, $\boldsymbol{\tau}^p$, $\boldsymbol{\tau}^s$:

Since the GDEs in **U**, p, $\boldsymbol{\tau}^p$, $\boldsymbol{\tau}^s$ are a set of first order differential equations, following the same reasoning as in section 3.5, we have the following,

$$\varphi_h \in H^k(\bar{\Omega}^T_{xy});\ k \geq 2$$

$$\varphi^e_h \in H^{k,p}(\bar{\Omega}^e_{xy});\ k \geq 2 \tag{3.14}$$

In (3.14), k=2 corresponds to the minimally conforming space. Here also, the need for higher order spaces is obvious for same reason as given in section (3.5)

3.7 Summary

The mathematical models presented in chapter 2 show that regardless of the choice of stresses, the governing differential equations resulting from the mathematical models remain non-linear partial differential equations. While there may be some advantages in using some variables in constructing finite element processes when using Galerkin method with weak form [1, 2], however, based on Surana et al. [3], the

integral forms based on all methods of approximations remain variationally inconsistent except least squares method when the system of non-linear algebraic equations are solved using Newton's linear method with approximation of the second variation of the least squares functional [3]. Thus, the choice of integral forms is not dictated by the integral forms but rather other considerations, simplicity of the GDEs being one of them. The least squares finite element processes dont depend upon the specific types of non-linearities in the GDEs. The fact that all form of GDEs regardless of the choices of stresses are non-linear partial differential equations is sufficient to consider a general Least squares finite element formulation applicable to all non-linear PDEs process. Such formulation has been presented for weak form as well as strong form of GDEs for 1-D and 2-D flows. The choices of approximation spaces including minimally conforming spaces have been discussed. The weak form of GDEs permit C^0 local approximations but the integrals are lebesgue. When the local approximations are of class C^j ; $j >= 1$, the integrals in the LSPs are Riemann. The strong form of the GDEs contain upto second order derivatives of the velocity thereby necessitating the use of local approximations of class $C^j, j >= 2$ for the velocities if the integrals are to be Riemann. If we consider equal order, equal degree local approximations for all variable, then $H^{k,p}\ (\bar{\Omega}^e); k >= 3$ are minimally conforming spaces for the strong form of GDEs in **U**, p, $\boldsymbol{\tau}^p$.

Chapter 4

Numerical Studies : 1-D and 2-D BVPs

The two major issues in the numerical simulations of polymer flows are : (i) choice of dependent variables (specially stresses) in the mathematical models and the performance of these models for BVPs and IVPs (ii) and the computations of numerical solutions for high Deborah numbers that are associated with higher flow rates for a given configuration and a given polymeric liquid. Both of these aspects are investigated by using standard model problems. The numerical studies are designed to demonstrate the following

(1) For a given order of the approximation space i.e (k) and a fixed discretization (h) it is possible to obtain a converging sequence of solutions with progressively increasing p-level.

(2) The process in (1) is carried out for progressively increasing values of k that is shown to converge. Hence, here we obtain a converged solution that is independent of p and k.

(3) The process in (1) and (2) is repeated for as many progressively refined uniform (or quasi-uniform) discretizations as needed until the converged solutions from (2) for two successive discretizations are in close agreement and thus yielding solution that is independent of h, p, and k.

One dimensional fully developed flow between parallel plates, developing flow between parallel plates and lid driven square cavity are used as model problems. One dimensional fully developed flow studies are presented for Deborah number as high as $De = 6514.52$. For developing flow between parallel plates, studies are presented upto $De = 20.13$. For lid driven cavity numerical studies are given upto $De = 2.4$.

4.1 One dimensional fully developed flow between parallel plates

The purpose of this study is to determine the influence of choice of the dependent variables on the performance of computational process for high Deborah number flows. Figure 4.1(a) shows a schematic of computational domain and the dimensions for the one dimensional fully developed flow. Figure 4.1(b) shows a uniform 10 element discretization used for pressure gradient starting from dp/dx = -0.10 till dp/dx = -2.70. The numerical strategy to compute solution at higher deborah numbers incorporates the use of solutions at lower deborah numbers as the starting solutions when computing solutions fro higher Deborah numbers i.e. continuation in Deborah number. The one dimensional fully developed flow studies are performed using three different choices of dependent variables, $\mathbf{U}, p, \boldsymbol{\tau}^p$; $\mathbf{U}, p, \boldsymbol{\tau}^e$ and $\mathbf{U}, p, \boldsymbol{\tau}$. $(\tau_0)_{cke}$ is used for non-dimensionalizing the stresses and pressure. We choose PIB/C14 [20] fluid with following properties:

$\hat{\rho}$ = 800 Kg/m^3, $\hat{\eta}_s$ = 0.002 Pa.s, $\hat{\eta}_p$ = 1.424 Pa.s, λ_1 = 0.06 s, $\hat{\eta} = \hat{\eta}_s + \hat{\eta}_p$ = 1.426 Pa.s, α = 0.15. If we choose reference viscosity $\eta_0 = \hat{\eta}$, then $\hat{\eta}$ = 1 and $\eta_s = \hat{\eta}_s/\eta_0$ = 0.0015, $\eta_p = \hat{\eta}_p/\eta_0$ = 0.9985 and the dimensionless parameters, Reynolds number (Re) and Deborah number (De), are given by $Re = (\rho_0 L_0/\eta_0)u_0$ = 1.7812062.u_0, $De = (\lambda_1/L_0)u_0$ = $18.8976378.u_0$.

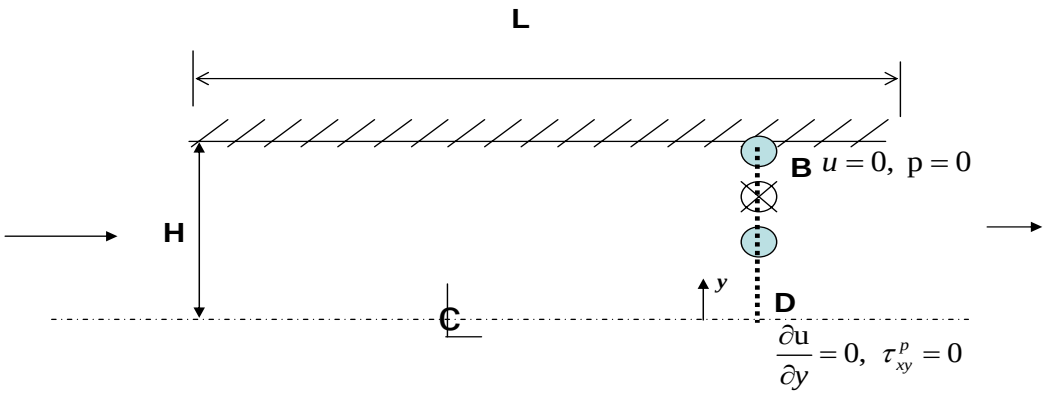

(a) Schematic of 1-D developed flow between parallel plates

Edge	Element Length				
$\overrightarrow{BD}$	0.1	0.1	0.1	0.1	0.1
	0.1	0.1	0.1	0.1	0.1

(b) 10 element uniform mesh discretization

Figure 4.1: Schematic and Mesh Discretization for 1-D fully developed flow between parallel plates

We present studies for all the three choices of dependent variables for 10 and 20 element uniform discretizations. Since, the analytical solution is smooth (though not known) based on the physics of the flow, we can entertain solutions of class C^1 i.e local approximations in $H^{2,p}(\bar{\Omega}^e_{xy})$ space and expect these to converge to class C^2 in the weak sense. For this reason we consider local approximations in spaces $H^{k,p}(\bar{\Omega}^e_{xy})$; $k = 2$ first, and if there is need we may increase k. For both discretizations at various flow rates, Newton's method with line search is used to obtain converged solution of the non-linear algebraic equation. When $|\mathrm{g_i}|_{max} \leq 10^{-6}$, the iterative process for nonlinear algebraic equations is considered converged. The order of approximation spaces k, p-level, residual function I, $|\mathrm{g_i}|_{\mathrm{max}}$, total degrees of freedom (dofs) and the number of iterations for various studies are presented in tables (4.1-4.4).

The p-convergence of least squares functional (LSF) I in $H^{2,p}(\bar{\Omega}^e_{xy})$ space for 10 element discretization at De = 0.48, De = 21.05, De = 317.28 and De = 6514.52 is shown in the figure 4.2. For De = 0.48 the I values O(10^{-15}) are obtained for all the p levels indicating that the solution is converged at lowest p level of 5 and further p refinement is not necessary as there is no significant decrease in the I values for higher p levels. For all other studies, the value of I increases with increasing De numbers for fixed dofs as expected. For the De = 21.05 value of I O(10^{-18}), for De = 317.28 value of I O(10^{-15}) and for De = 6514.52 value of I O(10^{-8}) are achieved upon convergence indicating that the computed solutions satisfy GDEs quite well. Figure 4.3 shows comparison of plots for velocity u for different flow rates (i.e. Deborah number) using the polymer stress formulation. Solutions are reported until deborah number of $De = 6514.52$. Similarly, figures 4.4-4.6 shows the comparison for τ^p_{xx}, τ^p_{xy}, τ^p_{yy} at various deborah numbers for solutions of class C^1. Mesh convergence for the $De = 134.38$ and $De = 6514.52$ is reported in figures 4.7 and 4.8 respectively using uniform 10 element and 20 element discretization. Excellent agreement of the solutions from both the meshes indicate that the solutions are indeed converged and independent of h. Solutions are also calculated using elastic stress and total stress formulations, figure 4.9 shows comparison between the polymer stress formulation, elastic stress formulation and total stress formulation for 10 element discretization. A good agreement is seen between all three formulations

until $De = 21.05$ after which the elastic stress formulation begins to experience convergence problems and hence further computations using elastic stress formulation were not possible. The total stress formulation and polymer stress formulation shows good agreement of the solution for higher flow rates. Figure 4.10 shows comparison for polymer stress formulation and total stress formulation at very high deborah number of 6514.52. Based on these studies, we make following remarks

(1) Computations of numerical solutions for very high deborah numbers for fully developed flow between parallel plates are possible using polymer stress formulation and total stress formulation. The solutions are reported upto $De = 6514.52$ and there does not seem to be a limit of deborah number in numerical simulations using h, p, k framework with VC integral form.

(2) The elastic stress formulation reported in the literature [1, 2] to be meritorious (for Galerkin method with weak form) begins to experience convergence problem after $De = 21.05$. The h, p, k refinement does not help alleviate the convergence problem either.

(3) For all Deborah numbers, the least squares functional (LSF) I is O (10^{-8}) − O (10^{-18}) indicating that the GDEs are satisfied quite well by the computed solutions.

(4) With increasing De, in general, the Newton's method with line search require many more iterations for convergence, this finding has also been reported in the literature by others [37, 47, 48]. This problem has been resolved to some extent by using the converged solutions at lower deborah number as the initial solution for solving higher deborah number flows.

Table 4.1: 10 Element uniform mesh (De = 0.48)

Formulation	Order of Space k	p-level	LSF (I)	$\|g_i\|$max	dof	Iterations
$\mathbf{U}, p, \boldsymbol{\tau}^p$	1	11	0.2195554773E-15	0.370673E-07	506	4
$\mathbf{U}, p, \boldsymbol{\tau}^e$	1	11	0.2195554780E-15	0.696531E-07	506	4
$\mathbf{U}, p, \boldsymbol{\tau}$	1	11	0.2195554776E-15	0.370216E-07	506	4

Table 4.2: 10 Element uniform mesh (De = 21.05)

Formulation	Order of Space k	p-level	LSF (I)	$\|g_i\|$max	dof	Iterations
$\mathbf{U}, p, \boldsymbol{\tau}^p$	1	11	0.1339022475E-18	0.282744E-08	506	6
$\mathbf{U}, p, \boldsymbol{\tau}^e$	1	11	0.9093348101E-14	0.962507E-06	506	22
$\mathbf{U}, p, \boldsymbol{\tau}$	1	11	0.1329200854E-18	0.282692E-08	506	6

Table 4.3: 10 Element uniform mesh (De = 317.28)

Formulation	Order of Space k	p-level	LSF (I)	$\|g_i\|$max	dof	Iterations
$\mathbf{U}, p, \boldsymbol{\tau}^p$	1	11	0.3153466778E-15	0.576797E-09	506	5
$\mathbf{U}, p, \boldsymbol{\tau}^e$	1	11	0.8980004290E-05	0.113551E+01	506	50
$\mathbf{U}, p, \boldsymbol{\tau}$	1	11	0.3087741652E-15	0.545815E-09	506	5

Table 4.4: 10 Element uniform mesh (De = 6514.52)

Formulation	Order of Space k	p-level	LSF (I)	$\|g_i\|$max	dof	Iterations
$\mathbf{U}, p, \boldsymbol{\tau}^p$	1	11	0.2726340796E-08	0.290854E-06	506	8
$\mathbf{U}, p, \boldsymbol{\tau}$	1	11	0.2620915595E-08	00.376258E-06	506	7

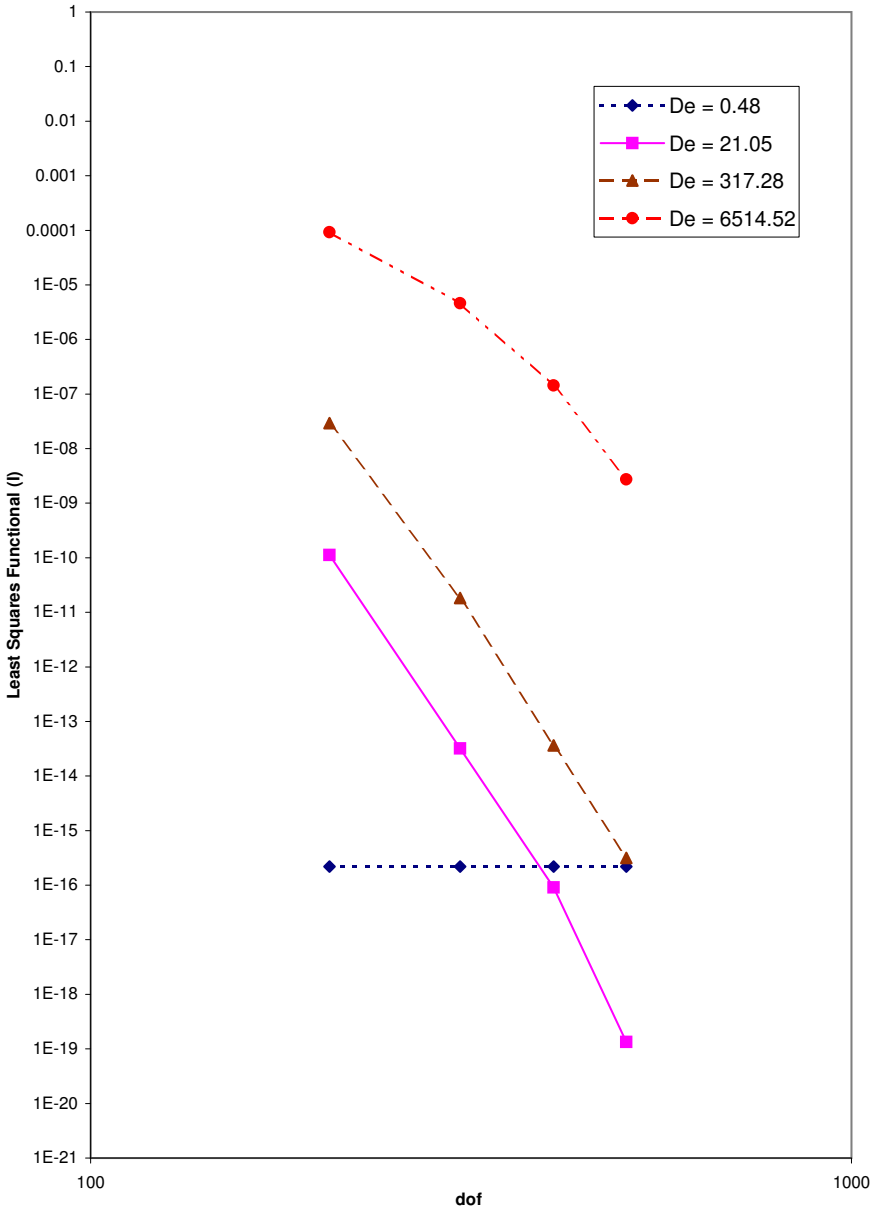

Figure 4.2: p - convergence of LSF (I), Solutions of class C^1 for 10 element uniform mesh , Fully Developed Flow between parallel plates

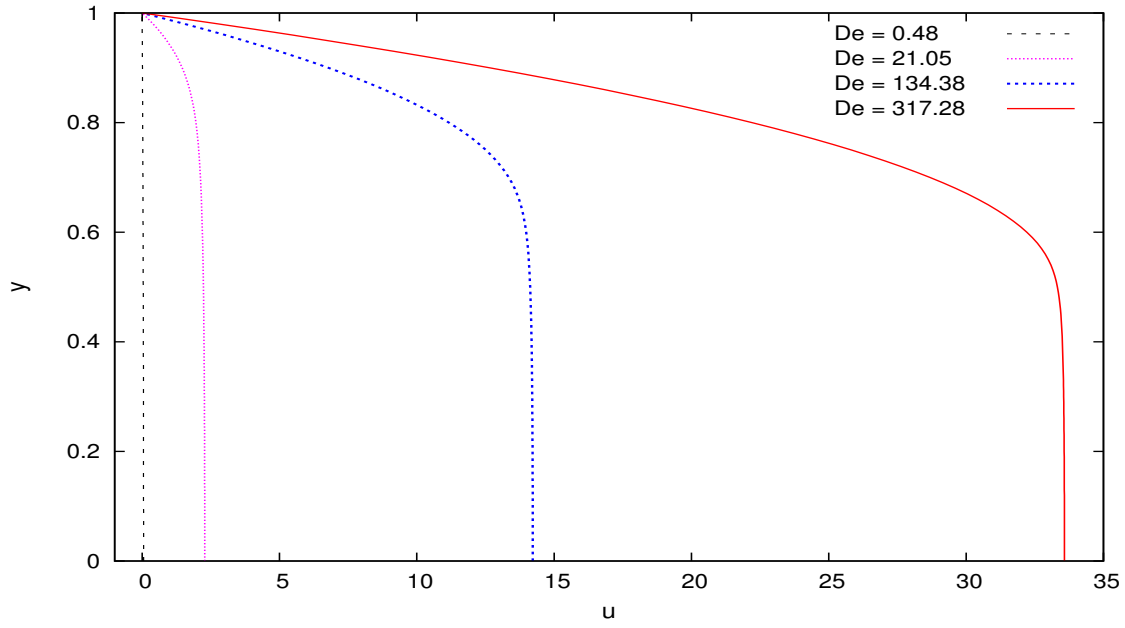

(a) velocity u versus y

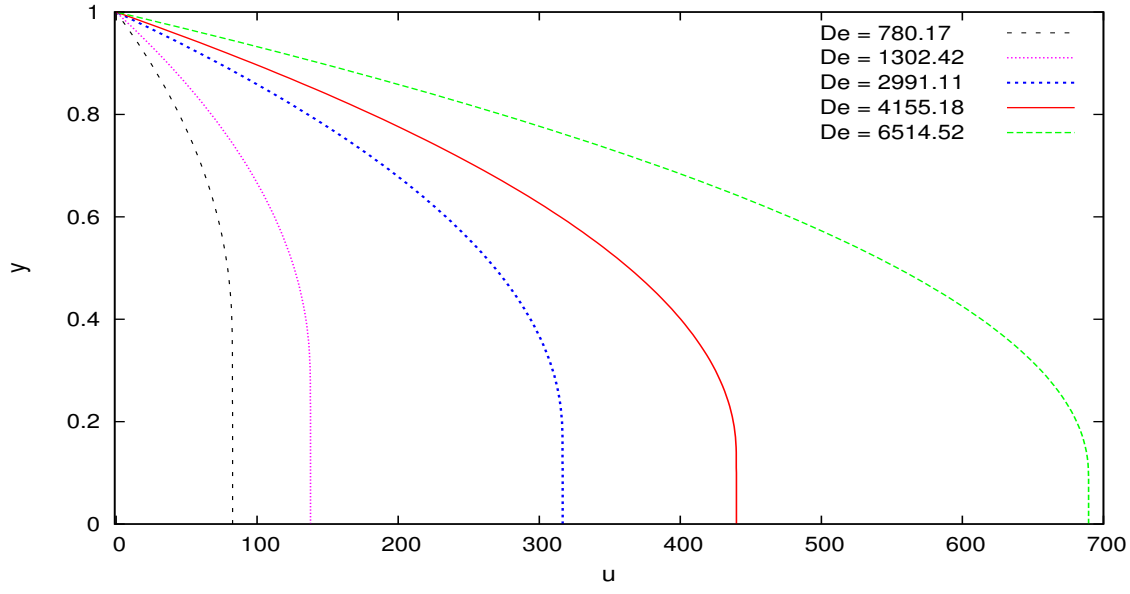

(b) velocity u versus y

Figure 4.3: Fully developed flow between parallel plates : solutions of class C^1 for 10 element uniform mesh at p=11 using polymer stress formulation

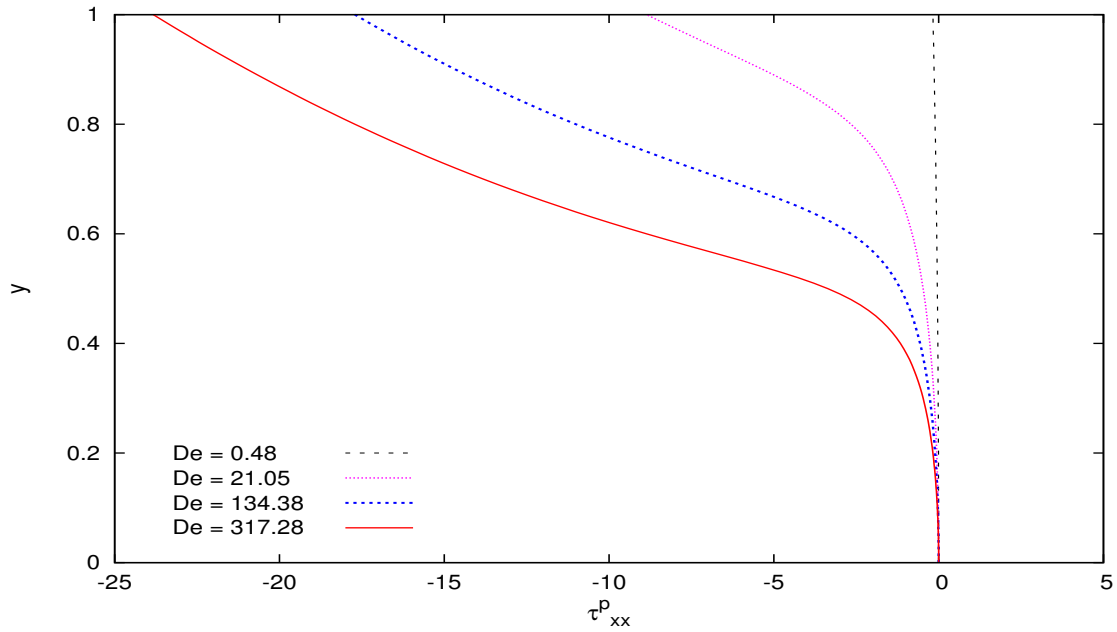

(a) Normal stress τ_{xx}^{p} versus y

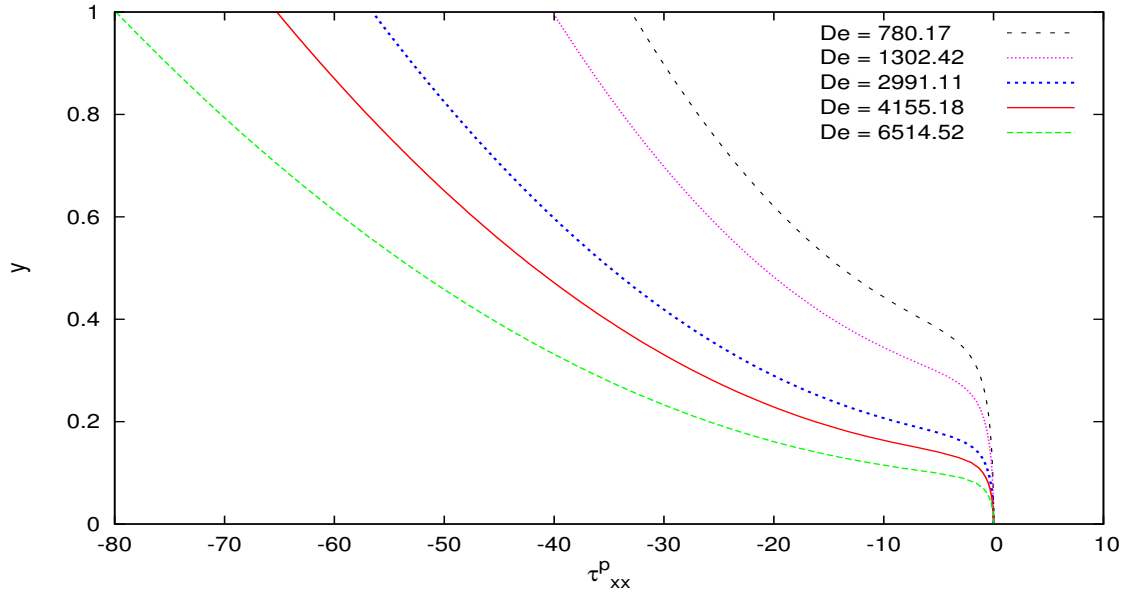

(b) Normal stress τ_{xx}^{p} versus y

Figure 4.4: Fully developed flow between parallel plates : solutions of class C^1 for 10 element uniform mesh at p=11 using polymer stress formulation

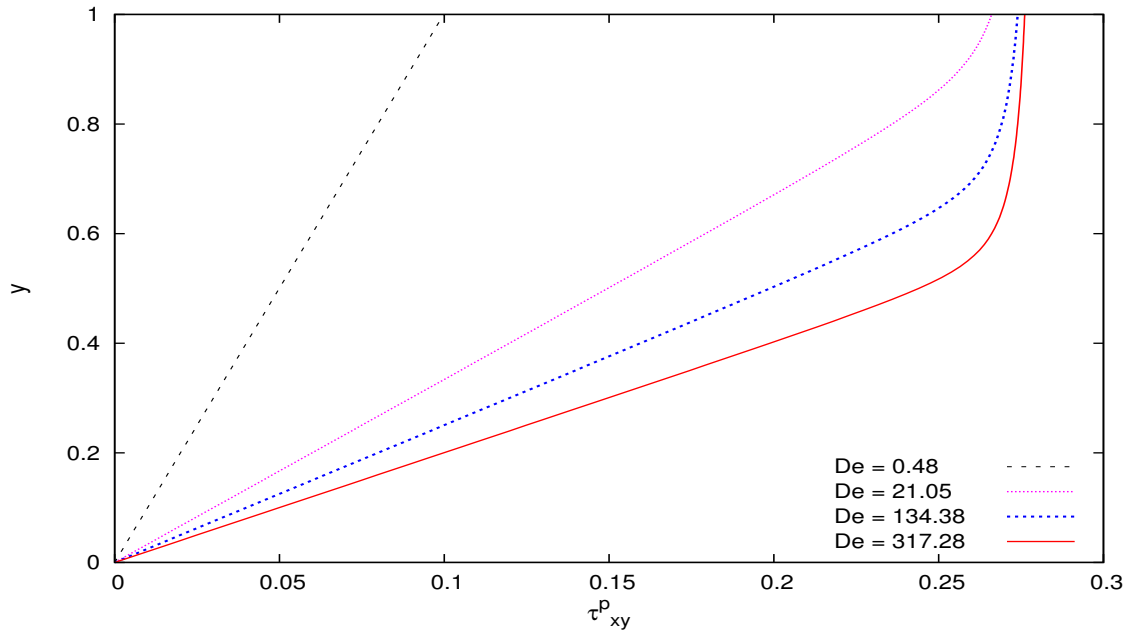

(a) Shear stress τ^p_{xy} versus y

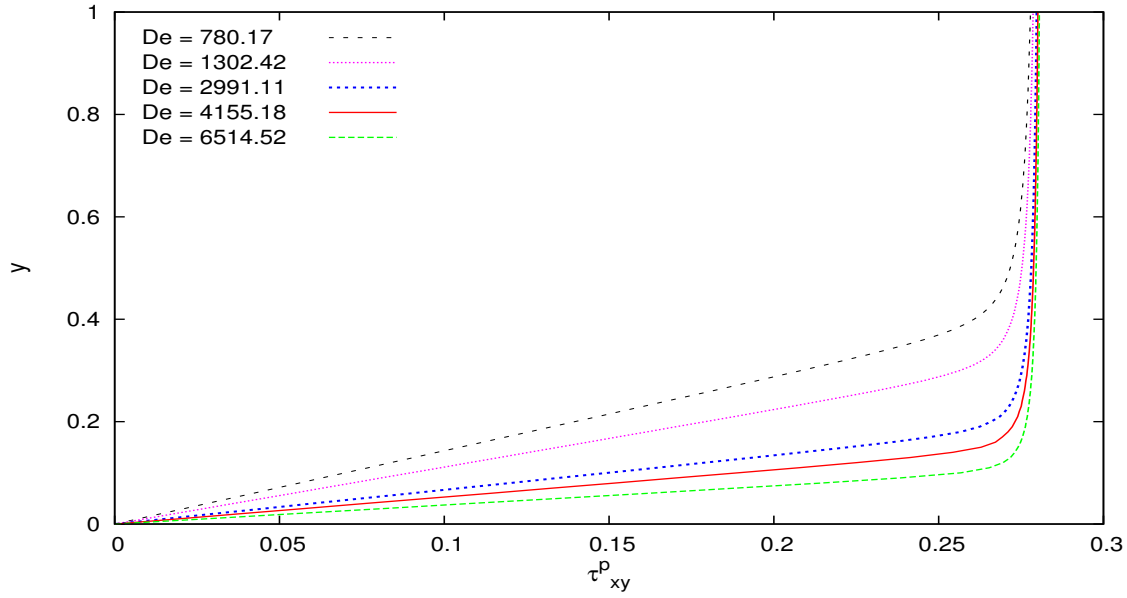

(b) Shear stress τ^p_{xy} versus y

Figure 4.5: Fully developed flow between parallel plates : solutions of class C^1 for 10 element uniform mesh at p=11 using polymer stress formulation

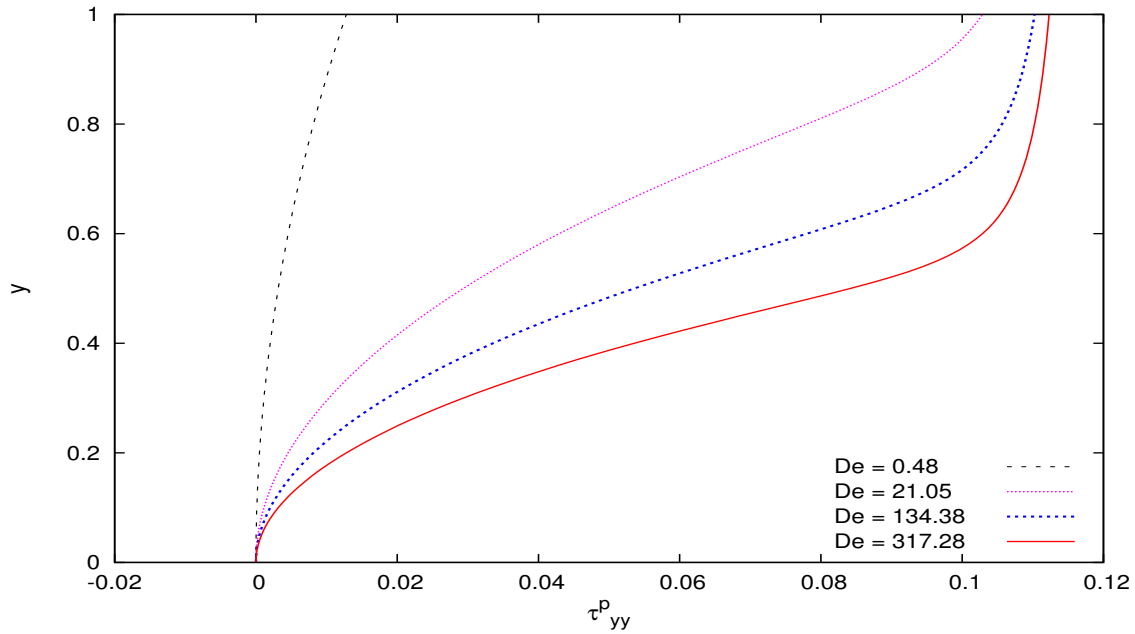

(a) Normal stress τ^p_{yy} versus y

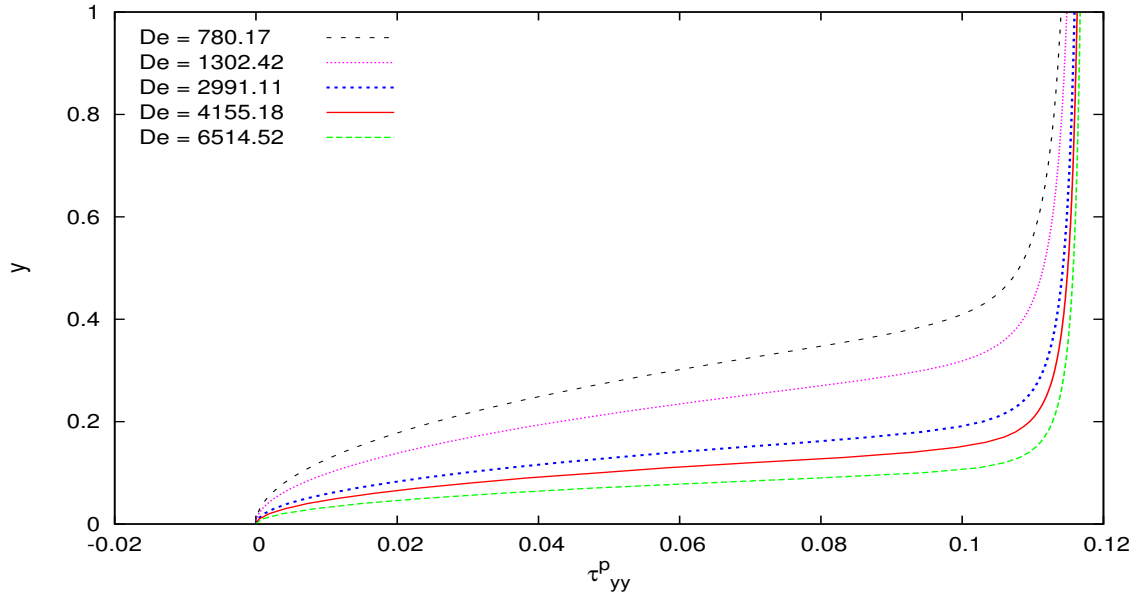

(b) Normal stress τ^p_{yy} versus y

Figure 4.6: Fully developed flow between parallel plates : solutions of class C^1 for 10 element uniform mesh at p=11 using polymer stress formulation

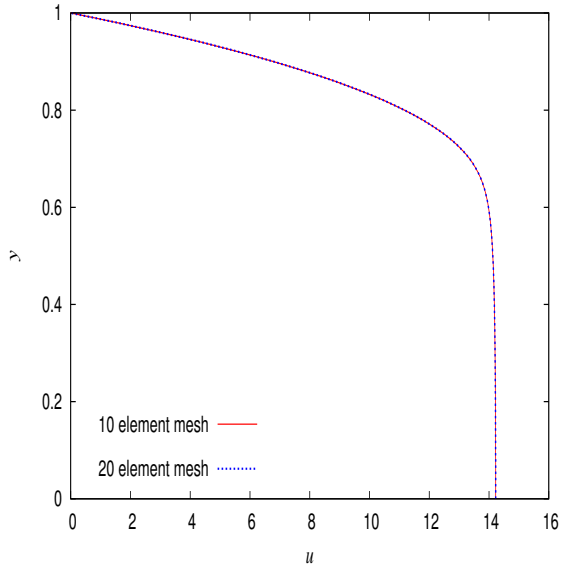

(a) Velocity u versus y

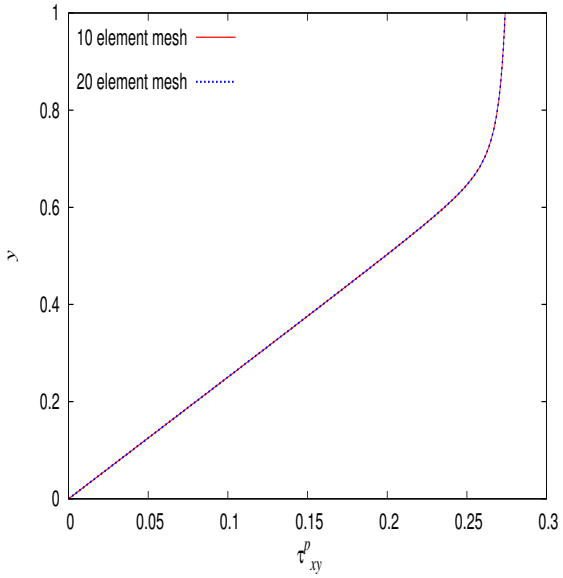

(b) Shear stress τ^p_{xy} versus y

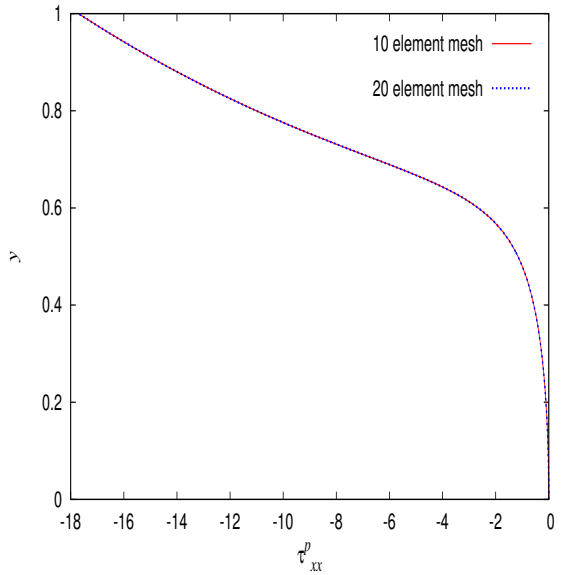

(c) Normal stress τ^p_{xx} versus y

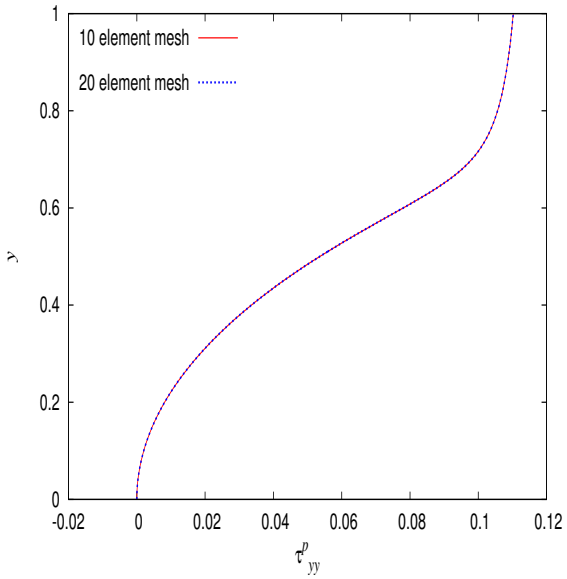

(d) Normal stress τ^p_{yy} versus y

Figure 4.7: Solutions of class C^1 for fully developed flow between parallel plates; 10 and 20 element uniform mesh p=11 for polymer stress formulation; De = 134.38

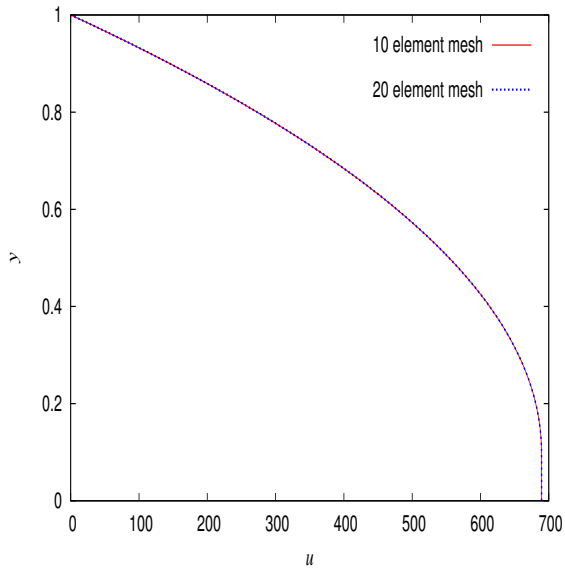

(a) Velocity u versus y

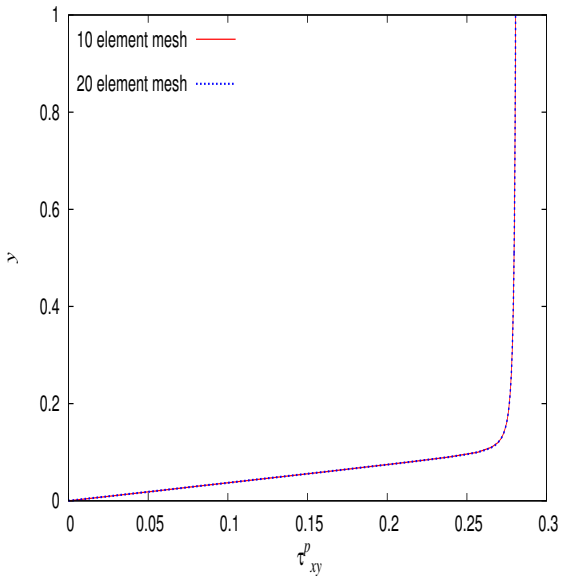

(b) Shear stress τ^p_{xy} versus y

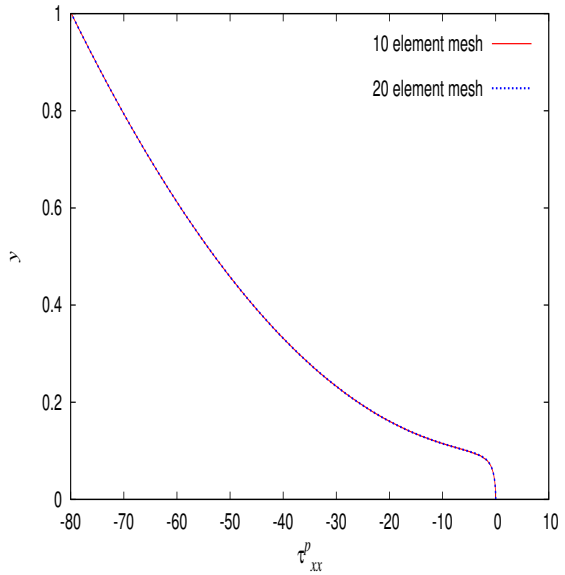

(c) Normal stress τ^p_{xx} versus y

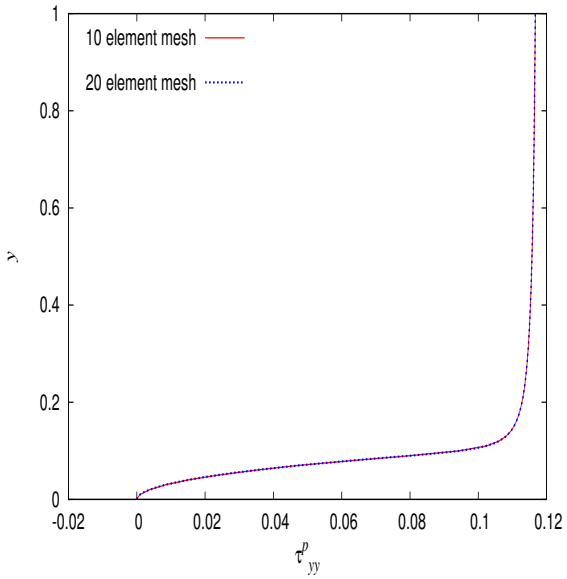

(d) Normal stress τ^p_{yy} versus y

Figure 4.8: Solutions of class C^1 for fully developed flow between parallel plates; 10 and 20 element uniform mesh at p=11 for polymer stress formulation; De = 6514.52

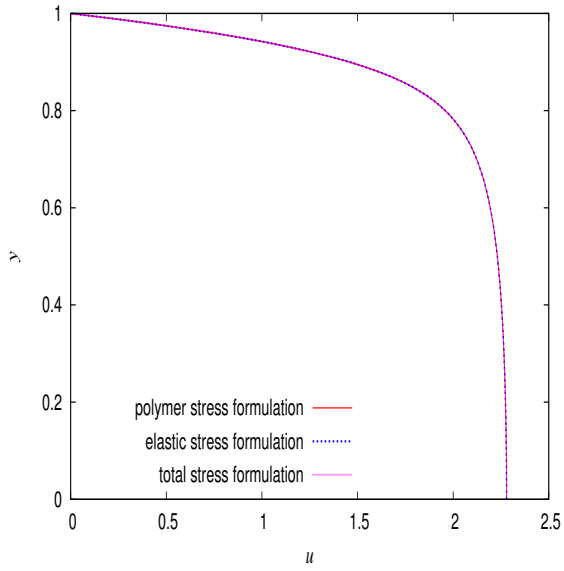

(a) Velocity u versus y

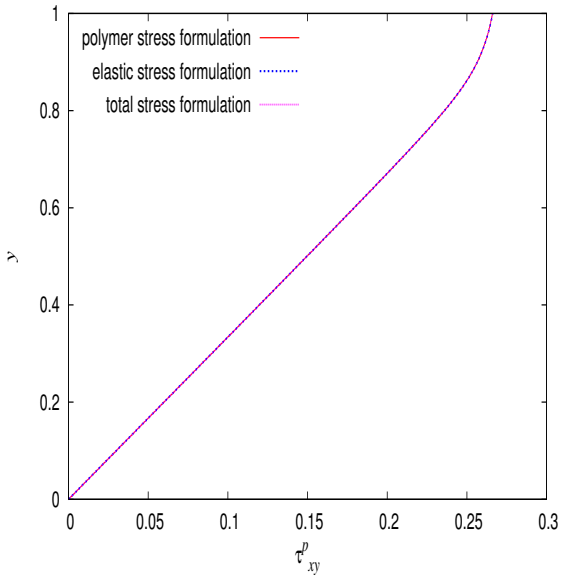

(b) Shear stress τ^p_{xy} versus y

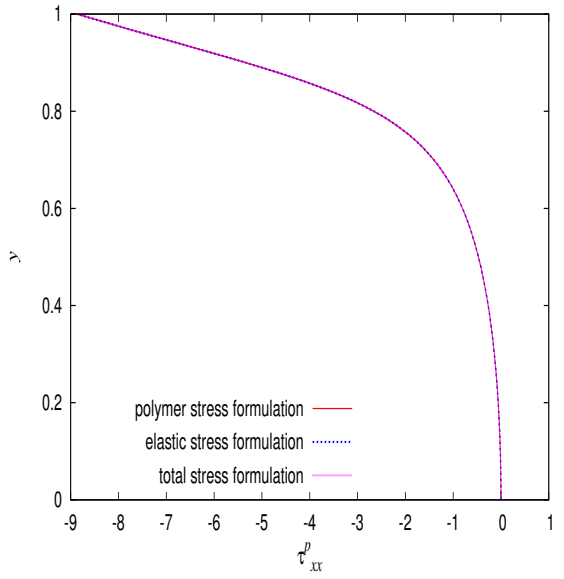

(c) Normal stress τ^p_{xx} versus y

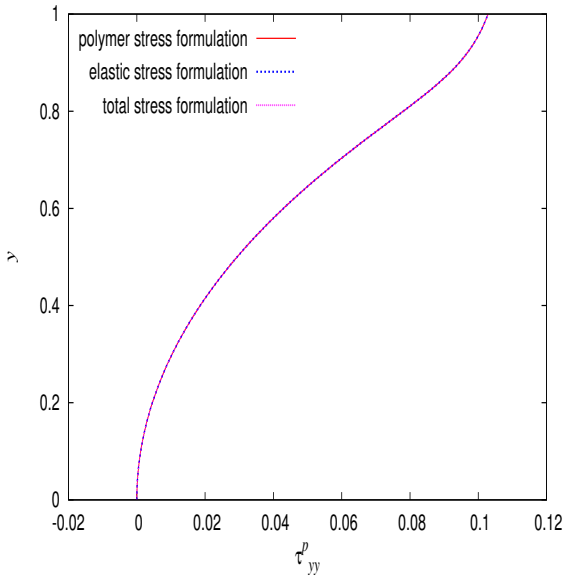

(d) Normal stress τ^p_{yy} versus y

Figure 4.9: Solutions of class C^1 for fully developed flow between parallel plates; 10 element uniform mesh at p=11; De = 21.05

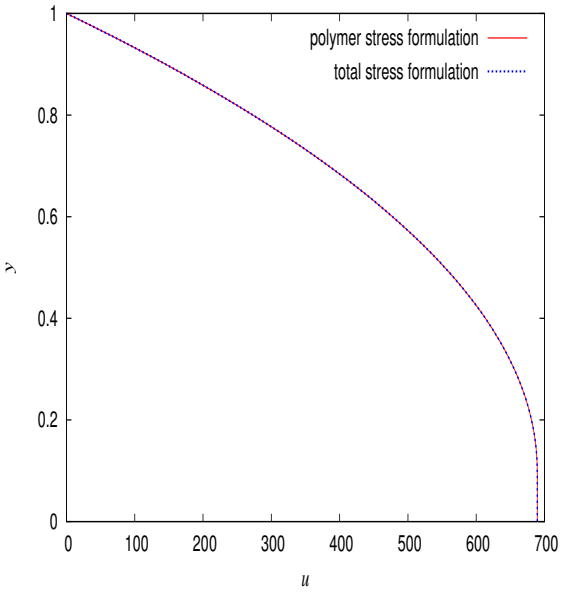

(a) Velocity u versus y

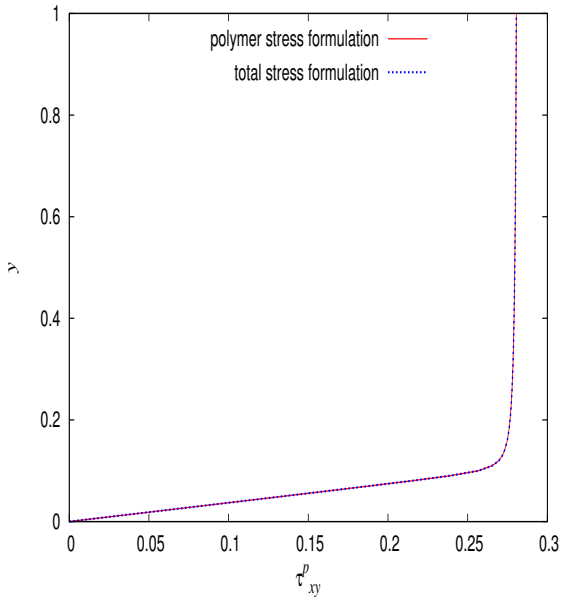

(b) Shear stress τ^p_{xy} versus y

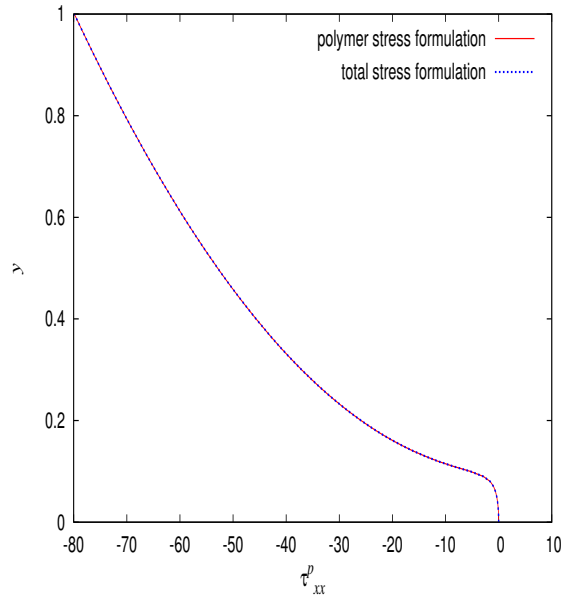

(c) Normal stress τ^p_{xx} versus y

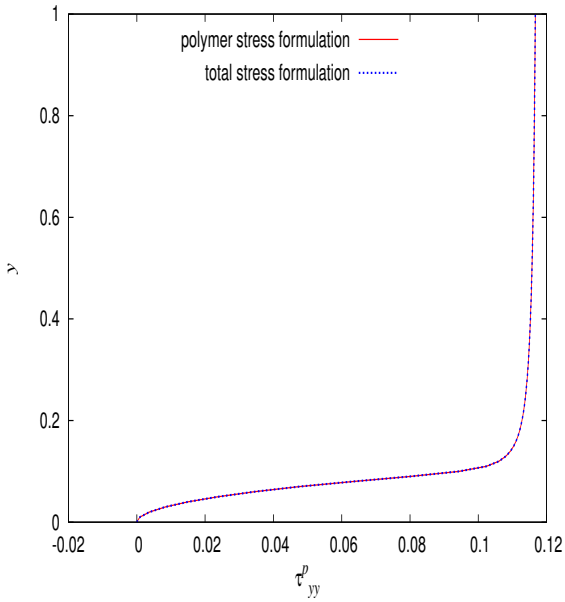

(d) Normal stress τ^p_{yy} versus y

Figure 4.10: Solutions of class C^1 for fully developed flow between parallel plates; uniform 10 element mesh p=11; De = 6514.52

4.2 Developing flow between parallel plates:

Figure 4.11(a) shows a schematic and computational domain for developing flow between parallel plates. At inlet (boundary CA) uniform velocity is applied which changes from constant value to zero over an element located at A along AC with continuous and differentiable higher order distribution. Boundary conditions on various boundaries are also shown in figure 4.11(a). The length L is chosen sufficiently large to ensure that fully developed flow conditions do exist at the outflow boundary DB. Figure 4.11(b) shows a uniform 200 finite element discretization used for u_0 = 0.00214, u_0 = 0.1, u_0 = 0.5, u_0 = 1.0 corresponding to Deborah number, $De = 0.053$, $De = 2.3$, $De = 10.28$, $De = 20.13$. $(\tau_0)_{cke}$ is used for non-dimensionalizing the stresses and pressure due to the fact that it is larger than $(\tau_0)_{cvs}$ for all velocities considered here. Since, the analytical solution is smooth (though not known) based on the physics of the flow, we can entertain solutions of class C^{11} i.e local approximations in $H^{2,p}(\bar{\Omega}^e_{xy})$ space and expect these to converge to class C^{22} in the weak sense. For this reason we consider local approximations in spaces $H^{k,p}(\bar{\Omega}^e_{xy})$; $k = 2, 3$ first, and if there is need we may increase k.

For the 200 element mesh at various flow rates, the p-levels are increased uniformly in x and y directions(or ξ, η)and Newton's method with line search is used to obtain converged solution of the non-linear algebraic equations. When $|\mathrm{g_i}|_{\max} \leq 10^{-6}$, the iterative process for nonlinear algebraic equations is considered converged. The order of approximation spaces k, p-level, residual function I, $|\mathrm{g_i}|_{\max}$, total degrees of freedom (dofs) and the number of iterations for various studies are presented in Tables (4.5-4.8). With increasing p-levels values of I O(10^{-5}) are achieved indicating that the computed solutions satisfy GDEs quite well.

Figure 4.12 shows the comparison for velocity u at $De = 0.053$, $De = 2.3$, $De = 10.3$ and $De = 20.13$ for the local approximations of class C^{22}, as the Deborah number increases the fluid elasticity increases and flow develops a constant core. Also boundary layer gets more thinner as seen in the figures 4.12. Figure 4.13 shows the comparison for velocity v at $De = 0.053$, $De = 2.3$, $De = 10.3$ and $De = 20.13$. The velocity v is zero over the most of domain except near the inlet boundary as expected. Figures 4.14-4.16

shows the comparison for normal stress τ^p_{xx}, τ^p_{yy} and shear stress τ^p_{xy} respectively at $De = 0.053$, $De = 2.3$, $De = 10.3$ and $De = 20.13$. With increasing flow rate the value of normal stresses (τ^p_{xx}, τ^p_{yy}) and shear stress (τ^p_{xy}) increases near the wall. Solutions of class $C^1 1$ show identical behaviors (not shown for sake of brevity). Figure 4.17 shows plots of u, τ^p_{xy}, τ^p_{xx},τ^p_{yy} versus y at the outflow boundary for the solutions of classes C^1 at p = 5 for all ranges of De considered. Figure 4.18 shows the comparison of solution of class C^1 and C^2 for $De = 20.13$. Figure 4.19 shows the comparison of one dimensional fully developed flow solutions and the two dimensional developing flow solution for $De = 20.13$. We make the following remarks.

(1) With increasing flow rates and hence increasing De, the fully developed flow begins to develop a constant velocity core that grows in the y direction and thus developing progressively thinner boundary layer near the plate.

(2) With increasing De, in general, the Newton's method with line search require many more iterations for convergence, This finding has also been reported in the literature by others [37, 47, 48]. This problem has been resolved to some extent by using the solution at lower deborah number as the initial solution for solving higher deborah number flows.

(3) For all Deborah numbers, the least squares functional (LSF) I is O (10^{-3}) – O (10^{-5}) indicating that the GDEs are satisfied quite well by the computed solutions.

(4) This problem has no theoretical solution. However, a comparison of one dimensional fully developed flow results with those of developing flow at the outflow boundary show excellent agreement.

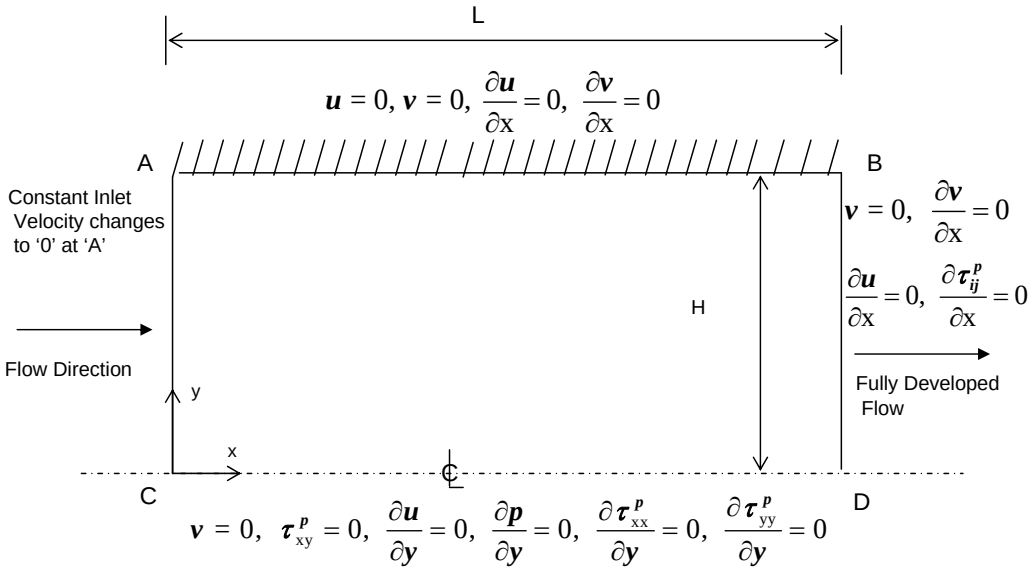

If $L_0 = \hat{H} = 0.003175$ then $H = 1$

(a) Schematic of Developing Flow Between Parallel Plates

Edge	Element Length									
$\rightarrow$ AB	10	10	10	10	10	10	10	10	10	10
	10	10	10	10	10	10	10	10	10	10
$\rightarrow$ CA	0.1	0.1	0.1	0.1	0.1	0.1	0.1	0.1	0.1	0.1

$\hat{L} = 0.635\text{m}, \text{ hence } L = 200$

(b) A 200 element discretization for developing flow between parallel plates

Figure 4.11: Schematic and Mesh Discretization for 2-D developing flow between parallel plates

Table 4.5: 200 Element mesh (De = 0.053)

Order of Space k	p-level	LSF (I)	$\|g_i\|$max	dof	Iterations
1	5	0.3544583809E-05	0.513797E-06	19692	3
2	5	0.4624431915E-05	0.764750E-06	11600	4

Table 4.6: 200 Element mesh (De = 2.3000)

Order of Space k	p-level	LSF (I)	$\|g_i\|$max	dof	Iterations
1	5	0.7710480610E-04	0.696761E-06	19692	26
2	5	0.9212874819E-04	0.978168E-06	11600	43

Table 4.7: 200 Element mesh (De = 10.28)

Order of Space k	p-level	LSF(I)	$\|g_i\|$max	dof	Iterations
1	5	0.3073972046E-03	0.446729E-06	19692	172
2	5	0.3723806687E-03	0.732956E-06	11600	37

Table 4.8: 200 Element mesh (De = 20.13)

Order of Space k	p-level	LSF(I)	$\|g_i\|$max	dof	Iterations
1	5	0.7178945536E-03	0.466364E-06	19692	191
2	5	0.7644771797E-03	0.932955E-06	11600	166

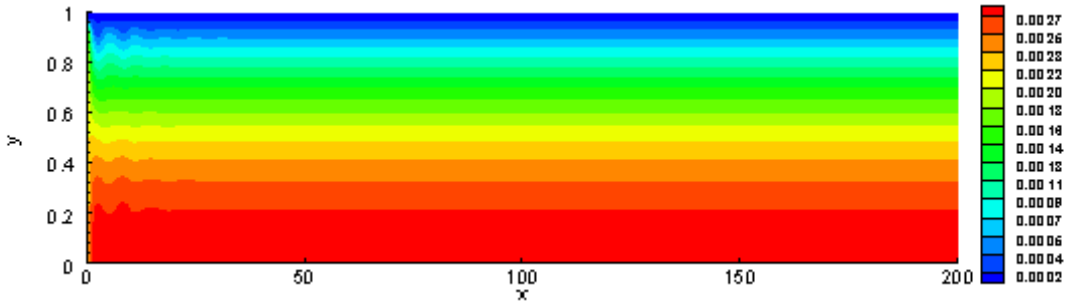

(a) Velocity u , $De = 0.0533$

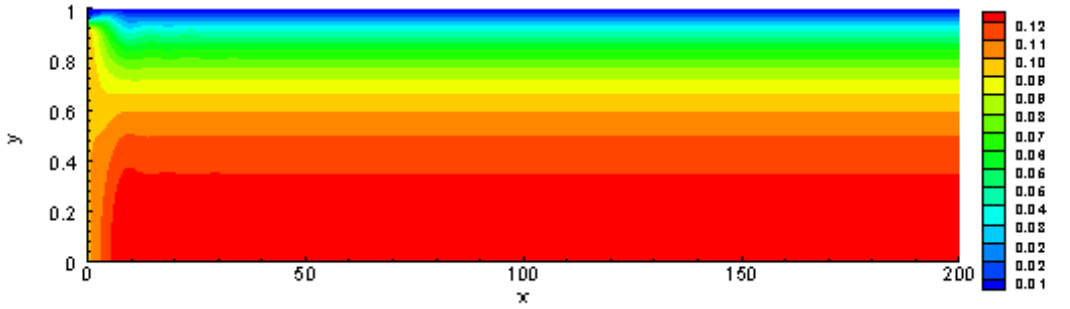

(b) Velocity u , $De = 2.3$

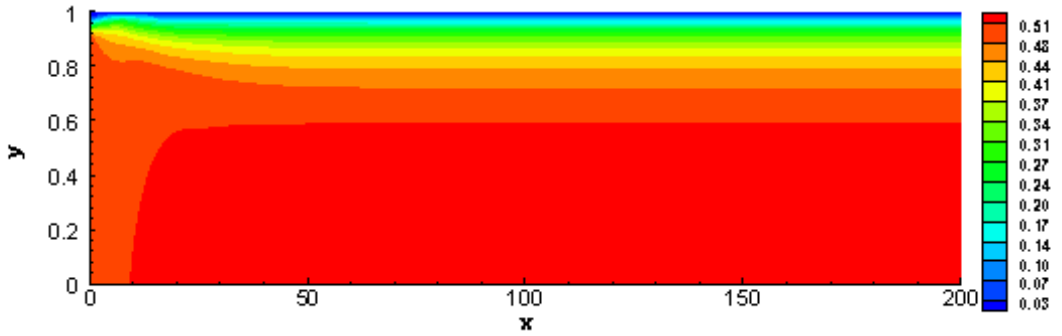

(c) Velocity u , $De = 10.3$

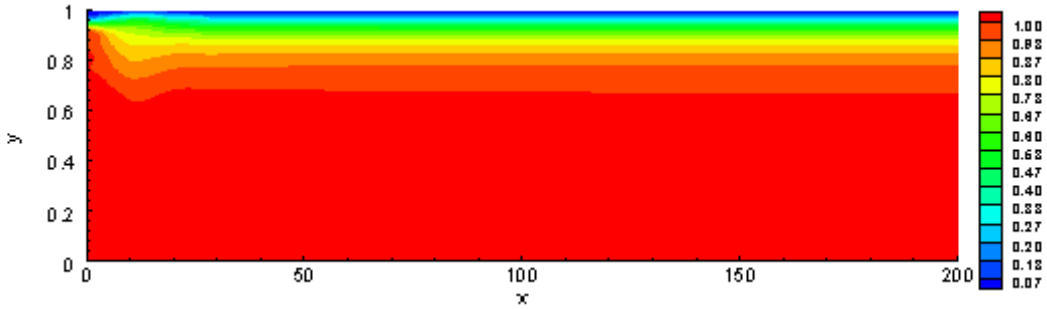

(d) Velocity u , $De = 20.13$

Figure 4.12: Solutions of class C^{22} , p = 5 for 200 element mesh

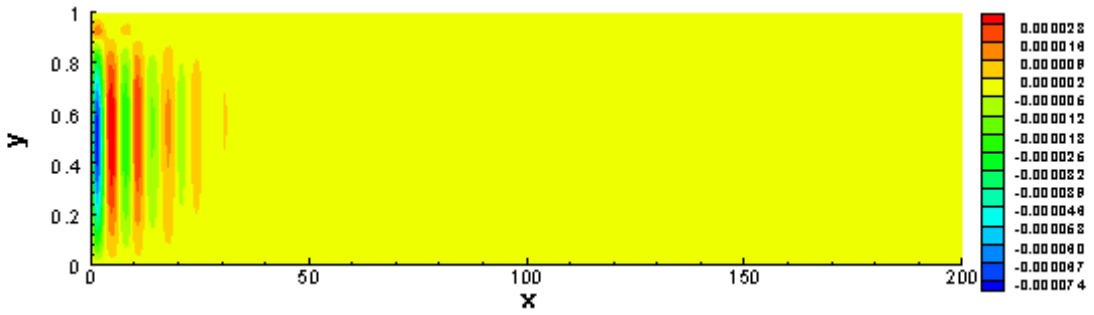

(a) Velocity v , $De = 0.0533$

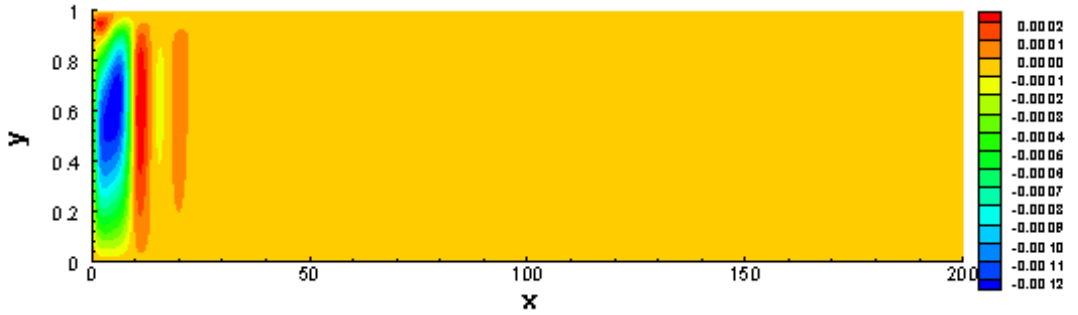

(b) Velocity v , $De = 2.3$

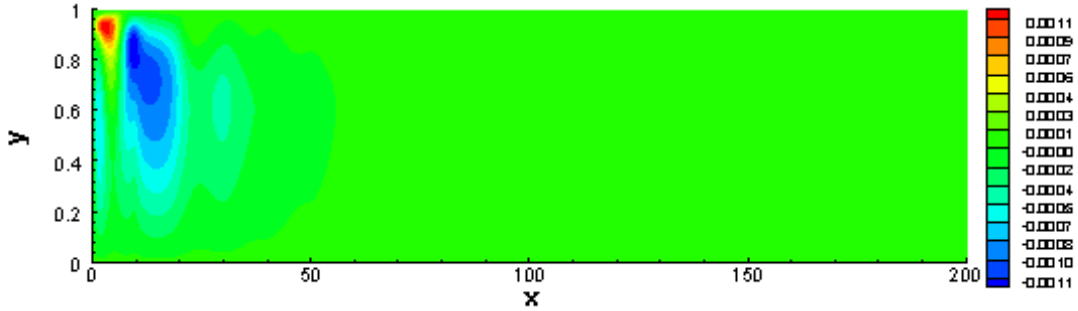

(c) Velocity v , $De = 10.3$

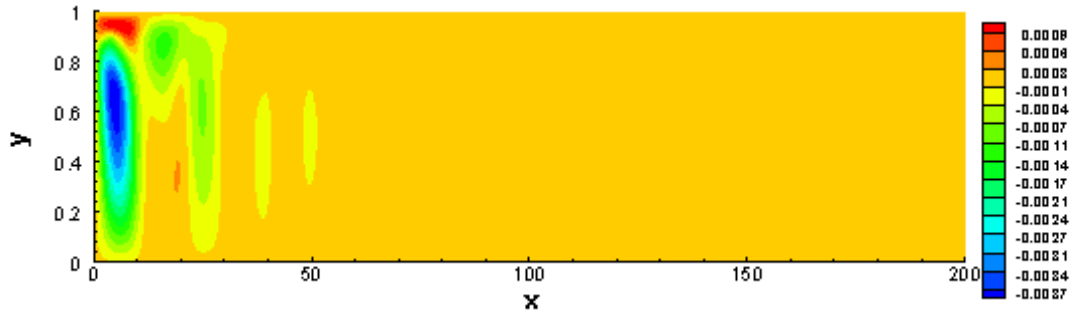

(d) Velocity v , $De = 20.13$

Figure 4.13: Solutions of class C^{22} , p = 5 for 200 element mesh

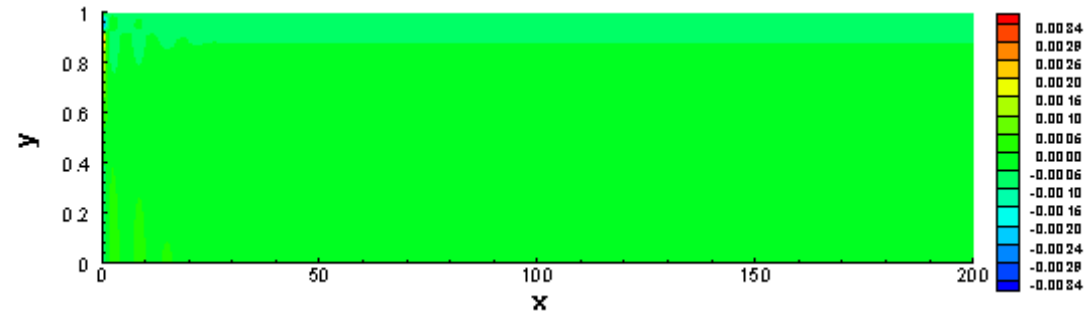

(a) Normal stress τ_{xx}^{p} , $De = 0.0533$

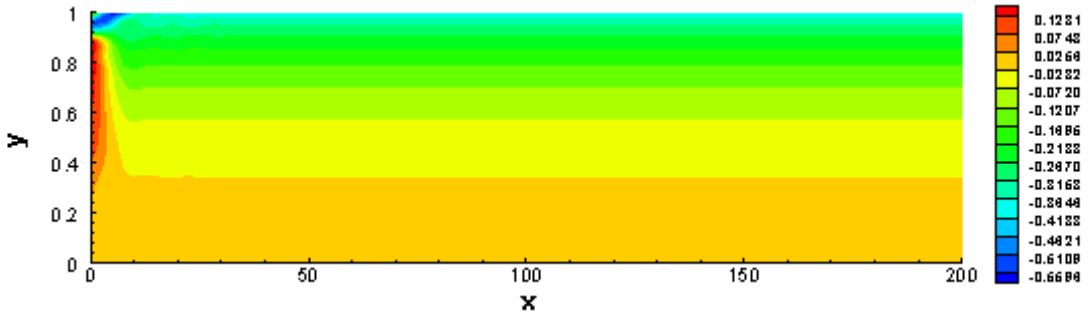

(b) Normal stress τ_{xx}^{p} , $De = 2.3$

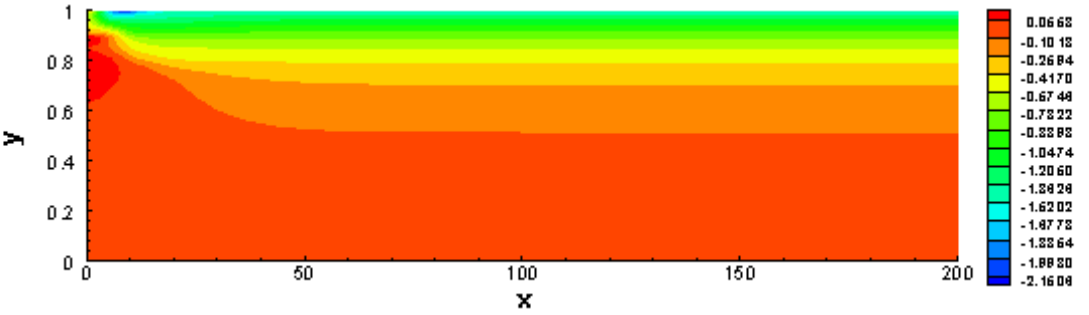

(c) Normal stress τ_{xx}^{p} , $De = 10.3$

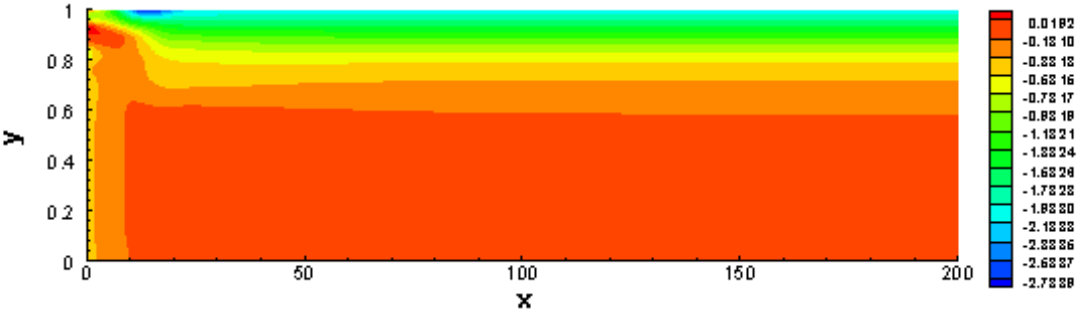

(d) Normal stress τ_{xx}^{p} , $De = 20.13$

Figure 4.14: Solutions of class C^{22} , p = 5 for 200 element mesh

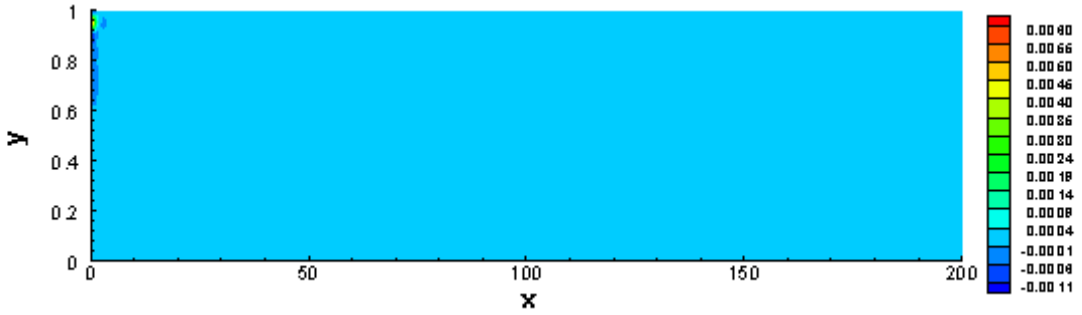

(a) Normal stress τ_{yy}^{p} , $De = 0.0533$

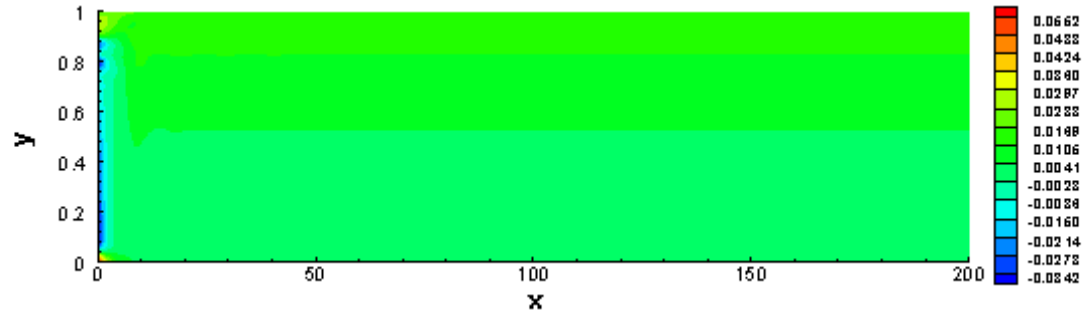

(b) Normal stress τ_{yy}^{p} , $De = 2.3$

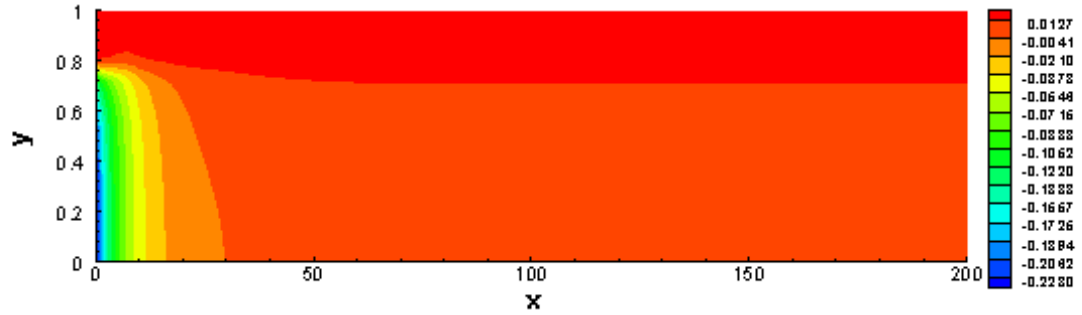

(c) Normal stress τ_{yy}^{p} , $De = 10.3$

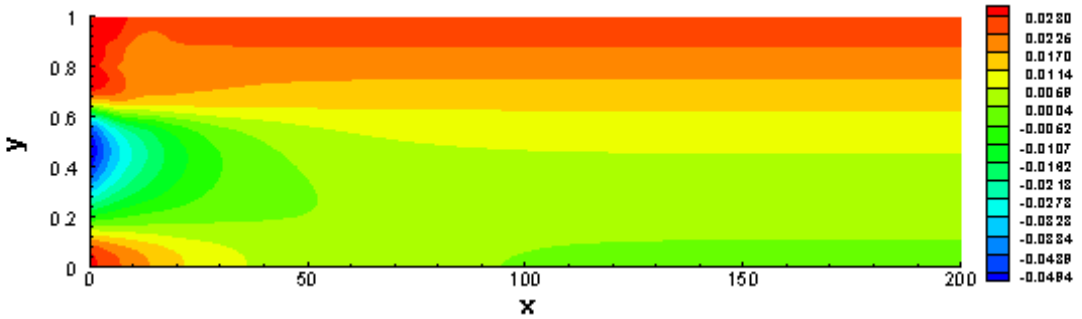

(d) Normal stress τ_{yy}^{p} , $De = 20.13$

Figure 4.15: Solutions of class C^{22} , p = 5 for 200 element mesh

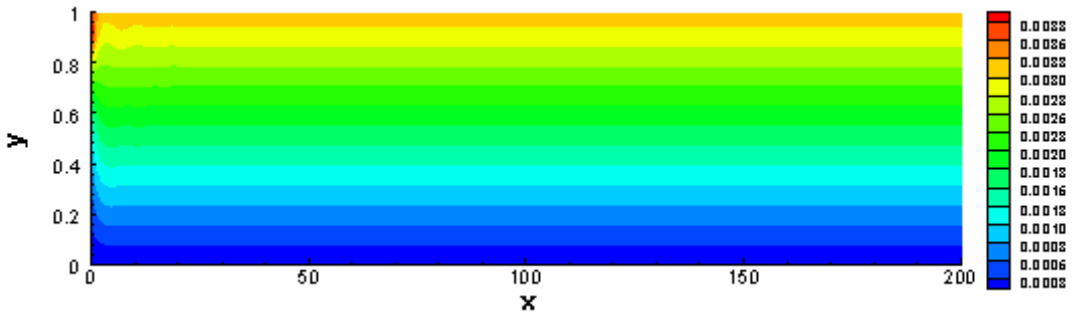

(a) Shear stress τ_{xy}^{p} , $De = 0.0533$

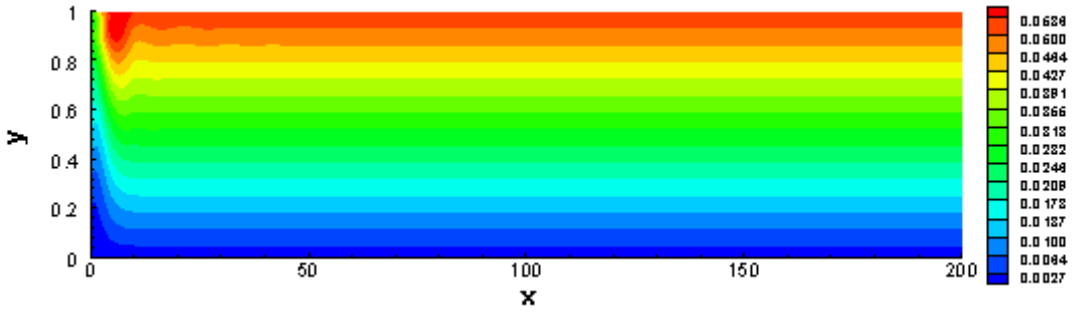

(b) Shear stress τ_{xy}^{p} , $De = 2.3$

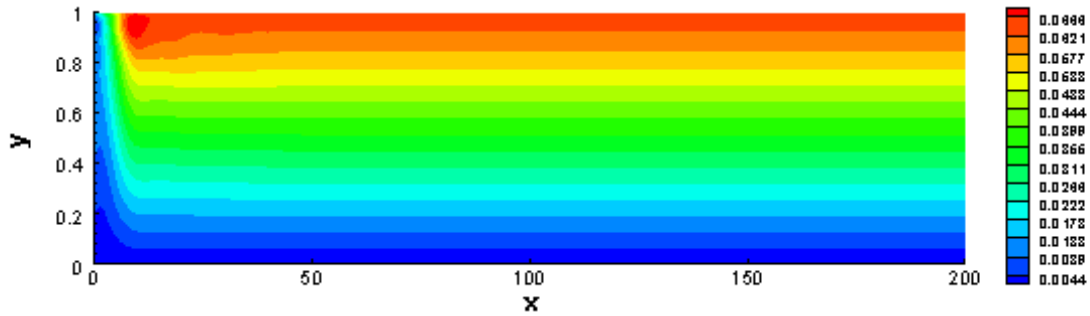

(c) Shear stress τ_{xy}^{p} , $De = 10.3$

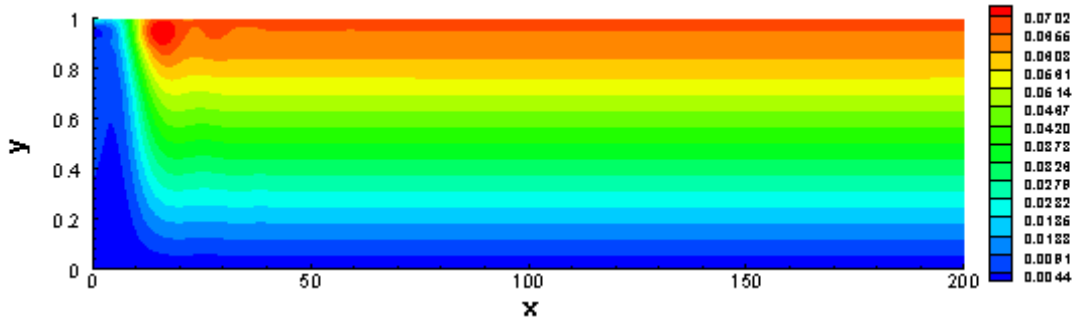

(d) Shear stress τ_{xy}^{p} , $De = 20.13$

Figure 4.16: Solutions of class C^{22} , p = 5 for 200 element mesh

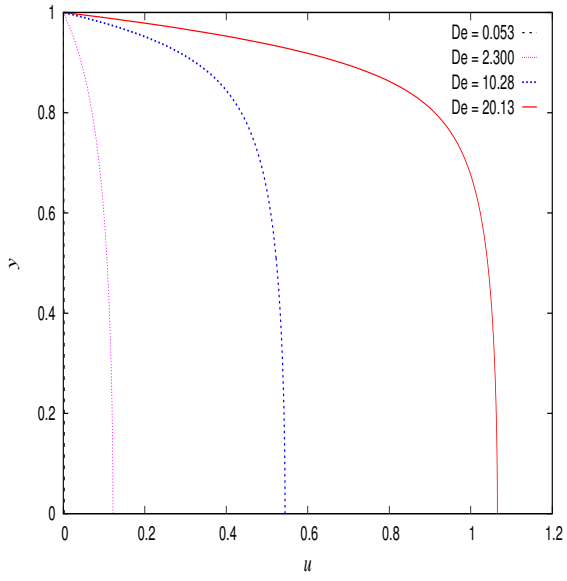

(a) Velocity u versus y

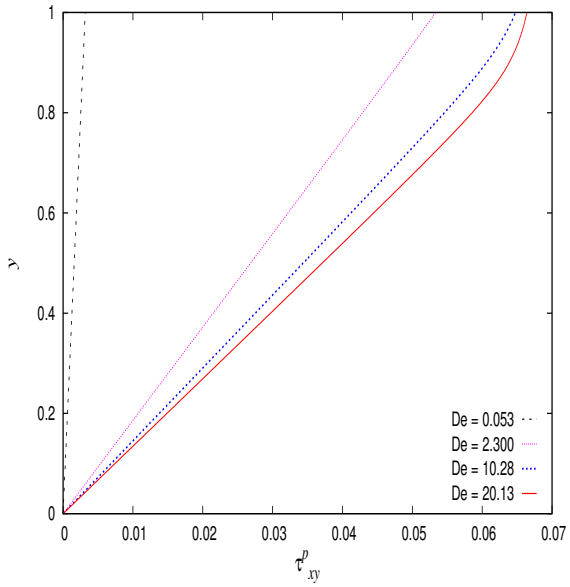

(b) Shear stress τ^p_{xy} versus y

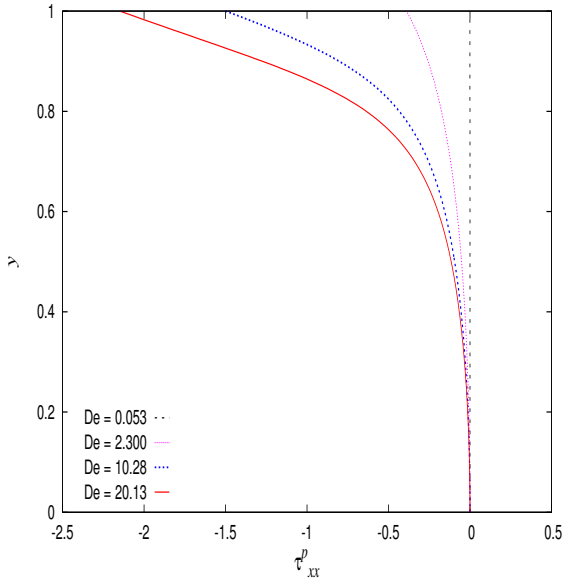

(c) Normal stress τ^p_{xx} versus y

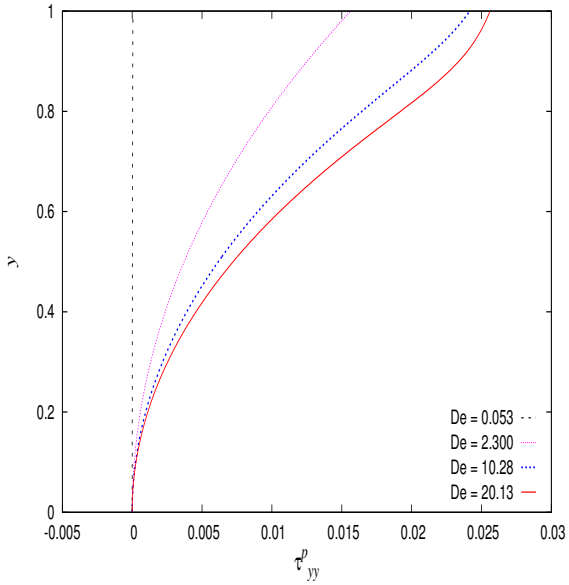

(d) Normal stress τ^p_{yy} versus y

Figure 4.17: Developing flow solutions of class C^1 at the outflow for 200 element mesh; p=5

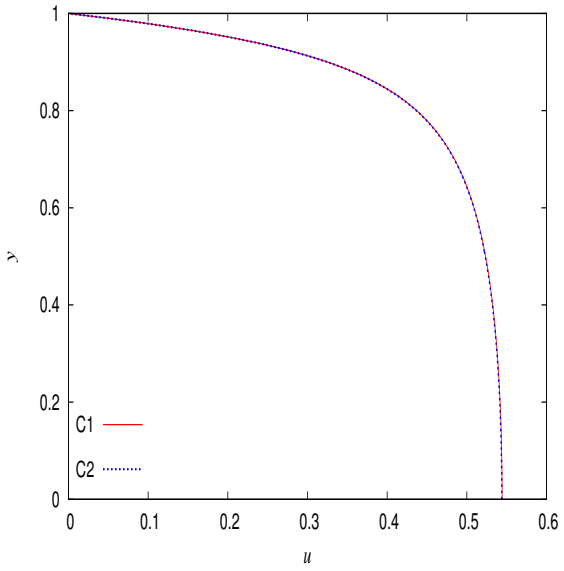

(a) Velocity u versus y

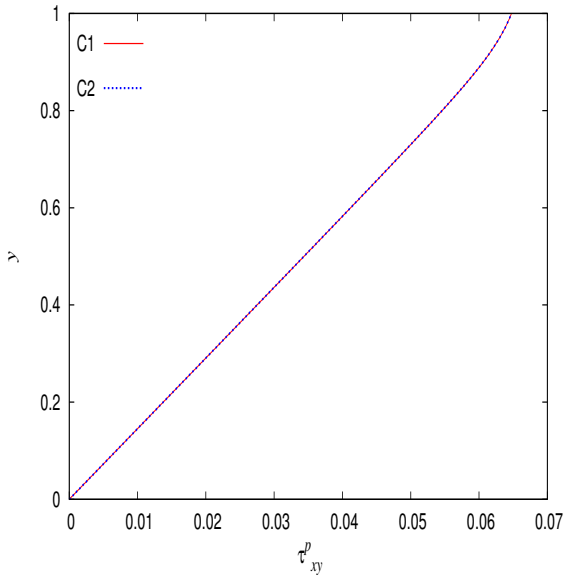

(b) Shear stress τ^p_{xy} versus y

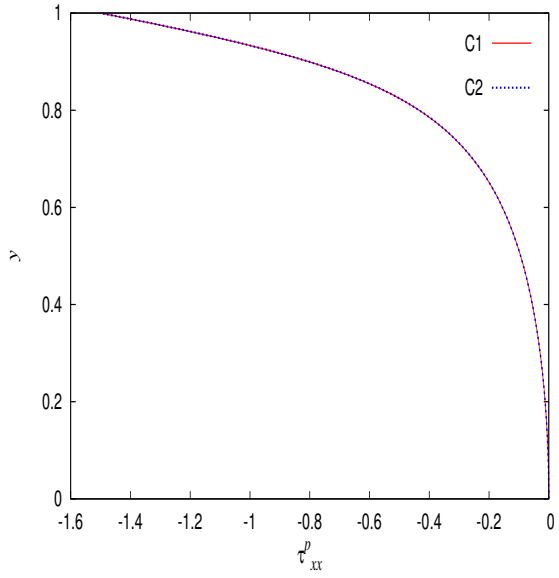

(c) Normal stress τ^p_{xx} versus y

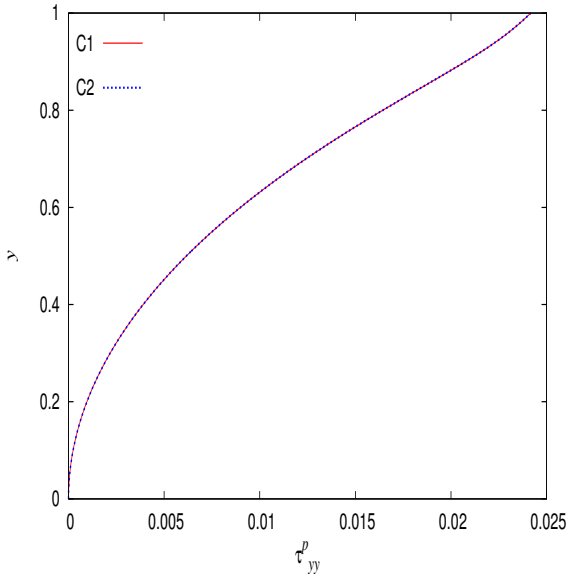

(d) Normal stress τ^p_{yy} versus y

Figure 4.18: Developing flow solutions of class C^1 and C^2 at the outflow for 200 element mesh for $De = 20.13$; p=5

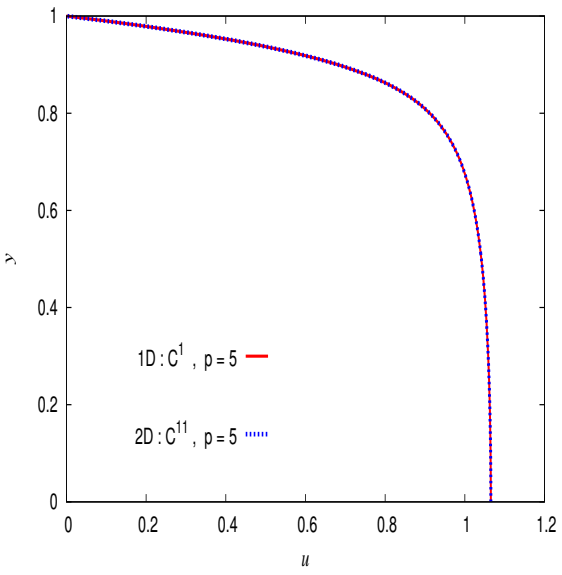

(a) Velocity u versus y

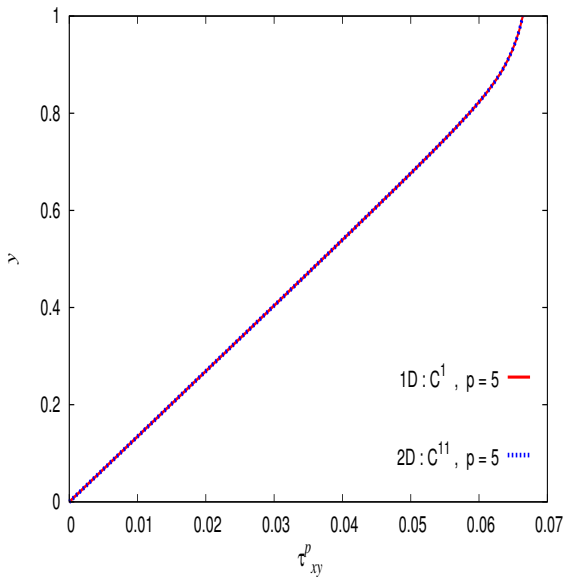

(b) Shear stress τ^p_{xy} versus y

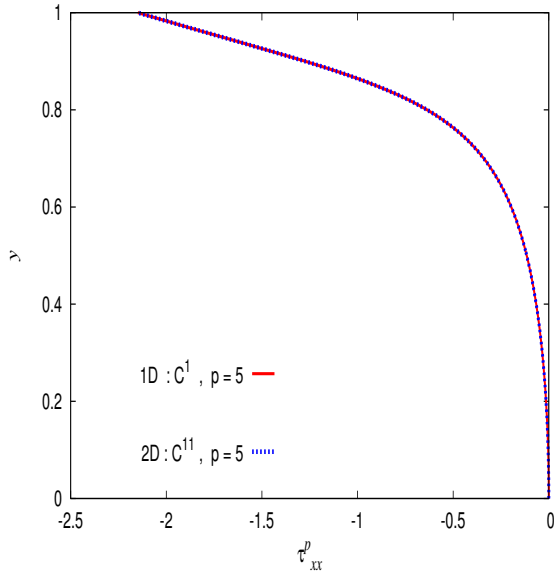

(c) Normal stress τ^p_{xx} versus y

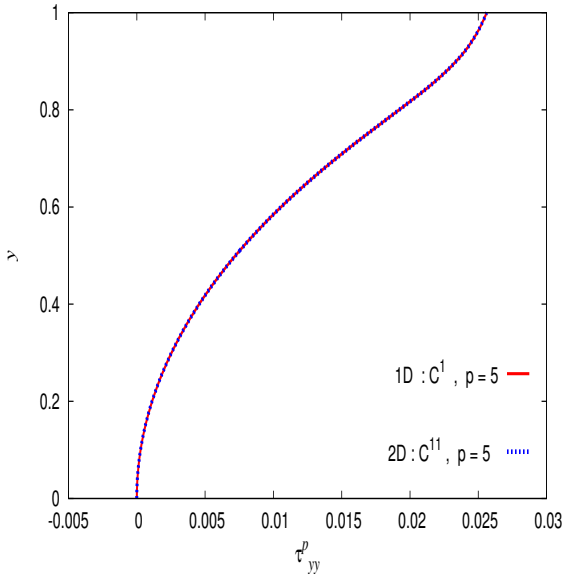

(d) Normal stress τ^p_{yy} versus y

Figure 4.19: Comparison of 1D and 2D fully developed flow solutions of class C^1, De = 20.13

4.3 Lid Driven Cavity

In this study we consider a lid driven cavity (figures 4.20(a) and 4.20(b)). We use the same fluid properties as considered for flow between parallel plates (section 4.1). Figure 4.20(b) shows an idealization of the cavity physics. The points A and B where the moving lid meets the stationary vertical walls of the cavity represent locations where velocity u is non-unique. Figure 4.20(b) shows a velocity distribution from u = 0 at points A and B to u = 1 at a distance h_d away from the corners. As one increases the order of the space k such that $k \rightarrow \infty$ and reduces h_d such that $h_d \rightarrow 0$, the physics of the cavity in figure 4.20(a) at corners A and B is recovered, hence the rationale for idealization shown in figure 4.20(b) for computations. A fixed value of h_d represents specific idealization of the physics for which limit points independent of h, p and k are essential to demonstrate. A reduced value of h_d is closer to the real physics but represents a different idealization of the physics. In the present study we demonstrate converged solutions independent of h, p and k for each of the progressively reduced values of h_d.

Figure 4.20(c)-4.20(f) show details of four different discretizations. Figure 4.20(c) has details of a quasi-uniform discretization in which h_d = 0.1. The discretization in figure 4.20(d) is a 10×10 uniform mesh in which each element is 0.1×0.1. These two meshes are used to demonstrate h, p, k independence of the solution h_d = 0.1. Figure 4.20(e) show a 49 element quasi-uniform discretization in which h_d = 0.05 (half of that used in 36 and 100 element meshes). Discretization shown in figure 4.20(f) is 400 element uniform discretization in which h_d = 0.05 also. Meshes in figures 4.20(e) and figure 4.20(f) are used to demonstrate h, p and k independent solutions for h_d = 0.05. The h-convergence studies are performed by uniform mesh refinement in the x and y direction. For h_d value of 0.1, a 100 element uniform mesh is used to start the h-convergence studies followed by uniform 400, 1600 and 6400 element meshes. For h_d value of 0.05, a 400 element uniform mesh is used to start the h-convergence studies followed by uniform 1600 and 6400 element meshes. The order of approximation spaces k, p-level, residual function I, $|\mathrm{g_i}|_{\max}$, total degrees of freedom (dofs) and the number of iterations for various studies are presented in Tables (4.9-4.24). In specific

for $De = 0.24$ the least squares functional (I) values are reported for 36 element mesh, 100 element mesh, 49 element mesh and 400 element mesh in tables 4.13, 4.14, 4.15 and 4.16 respectively. In tables 4.17, 4.18, 4.19 and 4.20 the I values are reported for $De = 1.2$ and for $De = 2.4$ the I values are reported in tables 4.21, 4.22, 4.23 and 4.24 respectively.

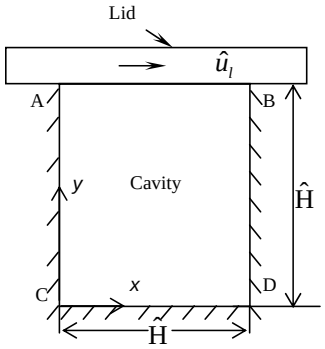

$\hat{H} = 0.05m, L_0 = 0.05m, H = 1$

(a) Schematic of Lid Driven Cavity

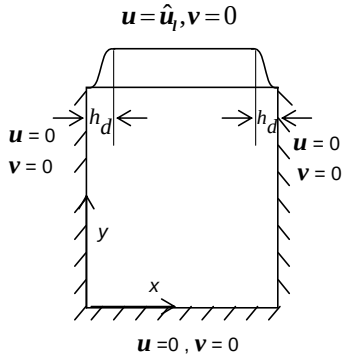

(b) Idealization of Lid Driven Cavity in (a) : computational domain and boundary conditions.

Edge	Element Lengths					
$\vec{AB}$	0.1	0.1	0.3	0.3	0.1	0.1
$\vec{CA}$	0.2	0.2	0.2	0.2	0.1	0.1

(c) A 36 element discretization : mesh M1; $h_d = 0.1$

Edge	Element Lengths									
$\vec{AB}$	0.1	0.1	0.1	0.1	0.1	0.1	0.1	0.1	0.1	0.1
$\vec{CA}$	0.1	0.1	0.1	0.1	0.1	0.1	0.1	0.1	0.1	0.1

(d) A 100 element discretization : mesh M2 ; $h_d = 0.1$

Edge	Element Lengths						
$\vec{AB}$	0.05	0.05	0.25	0.3	0.25	0.05	0.05
$\vec{CA}$	0.25	0.25	0.25	0.075	0.075	0.05	0.05

(e) A 49 element discretization : mesh M3 ; $h_d = 0.05$

Edge	Element Length									
$\vec{AB}$	0.05	0.05	0.05	0.05	0.05	0.05	0.05	0.05	0.05	0.05
	0.05	0.05	0.05	0.05	0.05	0.05	0.05	0.05	0.05	0.05
$\vec{CA}$	0.05	0.05	0.05	0.05	0.05	0.05	0.05	0.05	0.05	0.05
	0.05	0.05	0.05	0.05	0.05	0.05	0.05	0.05	0.05	0.05

(f) A 400 element discretization : mesh M4 ; $h_d = 0.05$

Figure 4.20: Schematic and Mesh Discretizations for lid driven cavity flow

Table 4.9: p-convergence : 36 Element Mesh, h_d = 0.1; De = 0.24

Order of space k	p-level	LSF (I)	$\|g_i\|$max	dof	Iterations
1	3	2.18E-04	7.23E-07	1071	7
1	5	1.48E-05	7.09E-07	3855	13
1	7	5.62E-06	2.93E-07	8367	18
1	9	2.97E-06	7.68E-07	14607	25

Table 4.10: h-convergence : h_d = 0.1; De = 0.24

Order of space k	No. of elements	LSF (I)	$\|g_i\|$max	dof	Iterations
1	100	2.02E-04	4.71E-07	2735	8
1	400	2.80E-05	6.61E-07	10255	11
1	1600	9.49E-06	9.34E-07	39695	9
1	6400	7.66E-06	6.88E-07	156175	34

Table 4.11: p-convergence : 49 Element Mesh, h_d = 0.05; De = 0.24

Order of space k	p-level	LSF (I)	$\|g_i\|$max	dof	Iterations
1	3	2.24E-04	7.43E-07	1415	11
1	5	1.37E-05	8.82E-07	5167	23
1	7	5.25E-06	5.49E-07	11271	22
1	9	2.87E-06	7.42E-07	19727	45

Table 4.12: h-convergence : h_d = 0.05; De = 0.24

Order of space k	No. of elements	LSF (I)	$\|g_i\|$max	dof	Iterations
1	400	1.99E-04	7.67E-07	10255	12
1	1600	2.65E-05	8.56E-07	39695	55
1	6400	8.23E-06	8.34E-07	156175	22

Table 4.13: Mesh M1 : 36 Element h_d = 0.1; De = 0.24.

Order of space k	p-level	LSF (I)	$\|g_i\|$max	dof	Iterations
1	9	0.2965416205E-05	0.768159E-06	14607	25
2	9	0.3892978839E-05	0.718093E-06	11797	18
3	9	0.4463720416E-05	0.678038E-06	9287	19

Table 4.14: Mesh M2 : 100 Element h_d = 0.1; De = 0.24.

Order of space k	p-level	LSF (I)	$\|g_i\|$max	dof	Iterations
1	7	0.5615314525E-05	0.814295E-06	22575	16
2	7	0.6470077099E-05	0.920932E-06	16437	13
3	7	0.8378516819E-05	0.853004E-06	11271	10

Table 4.15: Mesh M3 : 49 Element h_d = 0.05; De = 0.24.

Order of space k	p-level	LSF (I)	$\|g_i\|$max	dof	Iterations
1	9	0.2870859006E-05	0.741661E-06	19727	45
2	9	0.3178692652E-05	0.956144E-06	15815	33
3	9	0.3518269206E-05	0.926907E-06	12335	41

Table 4.16: Mesh M4 : 400 Element h_d = 0.05; De = 0.24.

Order of space k	p-level	LSF (I)	$\|g_i\|$max	dof	Iterations
2	7	0.5354709266E-05	0.826557E-06	62837	31
3	7	0.7232218426E-05	0.650345E-06	41671	25

Table 4.17: Mesh M1 : 36 Element h_d = 0.1; De = 1.2.

Order of space k	p-level	LSF (I)	$\|g_i\|$max	dof	Iterations
1	9	0.2124422969E-04	0.768159E-06	14607	34
2	9	0.2341483466E-04	0.875510E-06	11797	56
3	9	0.2914594562E-04	0.898962E-06	9287	62

Table 4.18: Mesh M2 : 100 Element h_d = 0.1; De = 1.2.

Order of space k	p-level	LSF (I)	$\|g_i\|$max	dof	Iterations
1	7	0.5047652416E-04	0.973286E-06	22575	24
2	7	0.6280254481E-04	0.616040E-06	16437	33
3	7	0.1545348839E-03	0.981246E-06	11271	57

Table 4.19: Mesh M3 : 49 Element h_d = 0.05; De = 1.2.

Order of space k	p-level	LSF (I)	$\|g_i\|$max	dof	Iterations
1	9	0.1715939870E-04	0.968332E-06	19727	76
2	9	0.1723529107E-04	0.769330E-06	15815	80
3	9	0.2326119629E-04	0.825836E-06	12335	87

Table 4.20: Mesh M4 : 400 Element h_d = 0.05; De = 1.2.

Order of space k	p-level	LSF (I)	$\|g_i\|$max	dof	Iterations
2	7	0.4370511624E-04	0.799688E-06	62837	96
3	7	0.1281517820E-03	0.812982E-06	41671	43

Table 4.21: Mesh M1 : 36 Element h_d = 0.1; De = 2.4.

Order of space k	p-level	LSF (I)	$\|g_i\|$max	dof	Iterations
1	9	0.1604293787E-03	0.875467E-06	14607	54
2	9	0.2005714926E-03	0.993710E-06	11797	85
3	9	0.3411018537E-03	0.899275E-06	9287	32

Table 4.22: Mesh M2 : 100 Element h_d = 0.1; De = 2.4.

Order of space k	p-level	LSF (I)	$\|g_i\|$max	dof	Iterations
2	7	0.1160697938E-02	0.964009E-06	16437	42
3	7	0.2882296939E-02	0.979572E-06	11271	49

Table 4.23: Mesh M3 : 49 Element h_d = 0.05; De = 2.4.

Order of space k	p-level	LSF (I)	$\|g_i\|$max	dof	Iterations
1	9	0.1059424859E-03	0.915642E-06	19727	97
2	9	0.1474726727E-03	0.972523E-06	15815	47
3	9	0.2561442103E-03	0.755750E-06	12335	40

Table 4.24: Mesh M4 : 400 Element h_d = 0.05; De = 2.4.

Order of space k	p-level	LSF (I)	$\|g_i\|$max	dof	Iterations
3	7	0.2597939275E-02	0.986013E-06	41671	74

Firstly, we present a comparison between p-convergence and h-convergence studies of the least squares functional (LSF) I in H^2 space in figure 4.21. The h-convergence studies are performed for h_d value of 0.1 using a uniform 100, 400, 1600 and 6400 element meshes. The order of approximation spaces k, p-level, residual function I, $|\mathrm{g_i}|_{\max}$, total degrees of freedom (dofs) and the number of iterations for various studies are presented in tables (4.9 - 4.12). A comparison between p-convergence studies obtained by using a graded 36 element mesh for h_d = 0.1 and h-convergence studies is presented in figure 4.21 which clearly demonstrates adequacy of the use of graded 36 element mesh for further studies presented in this work. The least squares functional value (I) for 36 element mesh is much lower than the 6400 element mesh which has the ten times degrees of freedom (dofs) as compared to the 36 element mesh. Thus the 36 element graded mesh is computationally more efficient both in regards of CPU time and numerical accuracy and is the preferred choice for computations. A comparison of velocity u for different meshes for h_d = 0.1 is shown in figure 4.22. Clearly the 36 element mesh at p level 9 produces the same results as 1600 element mesh which has more than twice the dofs as 36 element mesh and hence obviates the need of further h-convergence studies. Similar comparison is presented in figure 4.23 for velocity v which shows that results are identical for 36 element mesh and 1600 element mesh. For h_d value of 0.05, a 400 element uniform mesh is used to start the h-convergence studies followed by 1600 and 6400 uniform element meshes. From figure 4.21 we can observe that the least squares functional (I) for 49 element mesh is much lower than the 6400 element mesh which has almost the ten times degrees of freedom (dofs) compared to the 49 element mesh. Thus the 49 element graded mesh is computationally more efficient both in regards of CPU time and numerical accuracy and is the preferred choice for computations. A comparison of velocity u for different meshes for h_d = 0.05 is shown in figure 4.24. Clearly the 49 element mesh at p level 9 produces same results as 6400 element mesh. Similar comparison is presented in figure 4.25 for velocity v which shows that results are identical for 49 element mesh and 6400 element mesh.

A representative p-convergence study of the least squares functional I in spaces $H^{k,p}(\bar{\Omega}^e_{xy})$, $2 \leq k \leq 4$ is presented in figure 4.26 for 36 element discretization. Conver-

gence rates in all three spaces are roughly the same but in general slightly lower values of I are obtained with higher k. p levels are uniformly increased in x or y (or ξ and η) for each element of the discretization. A similar representative p-convergence study of the least squares functional I in spaces $H^{k,p}(\bar{\Omega}^e_{xy})$, $2 \leq k \leq 4$ is presented in figure 4.27 for 49 element discretization at De = 0.24.

In the next study, we consider 36 element discretization with h_d = 0.1. The distribution of velocity u is shown at De = 0.24 and De = 2.4 in figures 4.28(a) and 4.28(b) respectively. For De = 0.24, there is recirculation of the flow at the center of the cavity, the maximum velocity is at the top of the cavity where the lid is in motion. For De = 2.4, the boundary layer is more isolated near the top of the cavity as compared to De = 0.24. Figures 4.28(c) and 4.28(d) show a comparison for velocity v for De = 0.24 and De = 2.4, for De = 2.4 the recirculation at the top downstream corner is stronger than the De = 0.24. The pressure plots for De = 0.24 and De = 2.4 in figures 4.28(e) and 4.28(f) show higher pressure values of De = 2.4. The distribution of the stress τ^p_{xx} is presented in figure 4.29(a) for De = 0.24 and in figure 4.29(b) for De = 2.4. The magnitude of the stress τ^p_{xx} is positive near the upper left corner as the polymer is being pulled by the lid and hence is in tension, as we move away from the upper left corner towards the downstream side the polymer is being pushed and hence is in compression resulting in negative values of the τ^p_{xx}. A similar distribution of the stress τ^p_{xx} is presented for De = 2.4 except that in this case the magnitude of the axial stress is much higher compared to De = 0.24. The distribution of the stress τ^p_{yy} is presented in figure 4.29(c) and 4.29(d) respectively, the magnitude of the axial stress is positive at the top of the cavity for both the deborah numbers but with higher magnitude for De = 2.4 compared to De = 0.24. Figures 4.29(e) and 4.29(f) shows the comparison of shear stress τ^p_{xy} for De = 0.24 and De = 2.4 respectively. In case of De = 2.4 the magnitude of the shear stresses is higher than those for De = 0.24.

We consider a 36 element discretization with h_d = 0.1, and compute converged solutions in spaces $H^{k,p}(\bar{\Omega}^e_{xy})$; $2 \leq k \leq 4$ i.e solutions of class C^1, C^2 and C^3. Figures 4.30-4.34 show comparison of the solution of class C^2 at p = 9 for deborah number of 0.24, 0.72, 1.20, 2.40 for $u,\ v,\ \tau^p_{xx},\ \tau^p_{xy},\ \tau^p_{yy}$ respectively. The Solutions are shown at

the center of the cavity i.e at x = 0.5 and y = 0.5, and also near the top of the cavity at y = 0.99. The Deborah number of 0.24 is a moderate value for which solutions are reported in the literature, but Deborah number of 2.4 is considered to be high for which published solutions are not available in the literature. Figures 4.35-4.39 show the comparison of the solutions of class C^1, C^2 and C^3 for $De = 0.24$ at p = 9. A good agreement is observed between the solutions of class C^2 and C^3 at the center of the cavity as well as near the lid (y = 0.99). Similarly figures 4.40-4.44 show comparisons of the solution of class C^1, C^2 and C^3 for $De = 1.20$ and figures 4.45-4.49 show the same comparisons for Deborah number of 2.4. Influence of the order of the space is clearly observed in some graphs specially in areas of peak values. For all practical purposes, solution of class C^3 can be considered as p, k independent solution for the 36 element mesh with h_d = 0.1.

To show the mesh independence of the solutions for h_d = 0.1, we consider 100 element mesh with h_d = 0.1 (same as for 36 element mesh) and obtain converged solutions for approximations of classes $C^1, C^2 \text{ and } C^3$ by progressively increasing p-level. Comparisons of the converged solutions of classes $C^1, C^2 \text{ and } C^3$ show similar behavior as for 36 element mesh (omitted for the sake of brevity). Figures 4.50-4.54 show a comparison of the solution of class C^2 for the 36 and 100 element discretizations for h_d = 0.1 at $De = 0.24$. Similarly figures 4.55-4.59 shows mesh independent solutions of class C^2 at $De = 1.2$ using 36 and 100 element meshes.

In the next study we consider 49 and 400 element discretizations with the h_d = 0.05. This study is parallel to the one presented for h_d = 0.1 using 36 and 100 element discretizations. Figures 4.60-4.64 show comparisons of the solution of class C^3 at p = 9 using 49 element mesh for De of 0.24, 0.72, 1.20, 2.40 for $u,\ v,\ \tau^p_{xx},\ \tau^p_{xy},\ \tau^p_{yy}$ respectively. A comparison of the solutions in $H^{k,p}(\bar{\Omega}^e)$; k = 2, 3, 4 spaces is shown in figures 4.65-4.69. We observe that while in some isolated areas (specially near peaks) the solution are not converged even for k = 4, but the overall behavior shows solutions of classes C^3 to be quite close to the converged solution. Similarly, figures 4.70-4.74 show comparison of the solution of class C^1, C^2 and C^3 at $De = 1.20$ and figures 4.75-4.79 show the same comparisons for Deborah number of 2.4.

Similar studies were also conducted for 400 element mesh with findings parallel to those reported here for 49 element mesh. Figures 4.80-4.84 show comparisons of the limit points for 49 and 400 element discretizations for $De = 0.24$. Results from the two discretizations are in excellent agreement indicating the h-independence of the solutions. Figures 4.85-4.89 shows mesh independent solutions at $De = 1.2$.

The results shown in figures 4.90-4.94 are the comparisons of the solutions for 36 and 49 element discretization in which h_d = 0.1 and 0.05 respectively at $De = 0.24$. Overall, the two compare very well, except in the vicinity of the corners where the stationary wall meets the lid. The 49 element discretization in which h_d = 0.05 naturally produces higher local gradients compared to 36 element mesh with h_d = 0.1 in the vicinity of points A and B but do not influence the far field solution significantly. These local gradients will continue to increase with progressively reduced h_d but will also become more localized. Reduction of h_d beyond a certain value (say O(10^{-3})) is obviously of very little practical consequence. However, the mechanism discussed here will allow one to approach the true physical situation when $h_d \to 0$ and $k \to \infty$. Similarly figures 4.95-4.99 show the comparison of solutions for 36 and 49 element mesh at $De = 1.20$ and figures 4.100-4.104 show similar comparisons at $De = 2.4$. The thrust of the studies presented here is to demonstrate that h, p and k independent solutions are possible and that with additional parameters k, it is possible to approach the true physics at points A and B in the computational process.

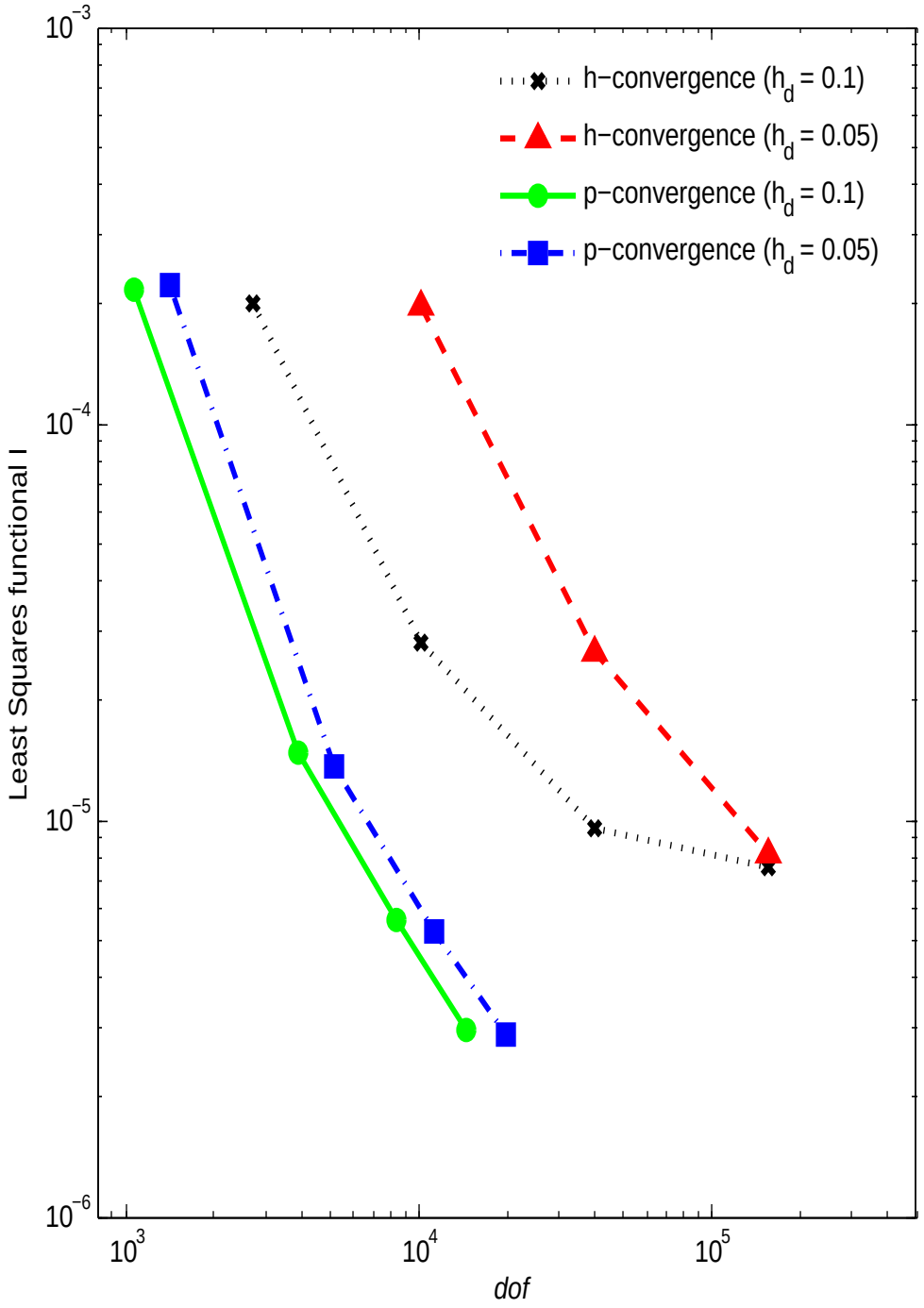

Figure 4.21: Least Squares functional I for solutions of class C^{11}, h-convergence using $p = 3$, $De = 0.24$

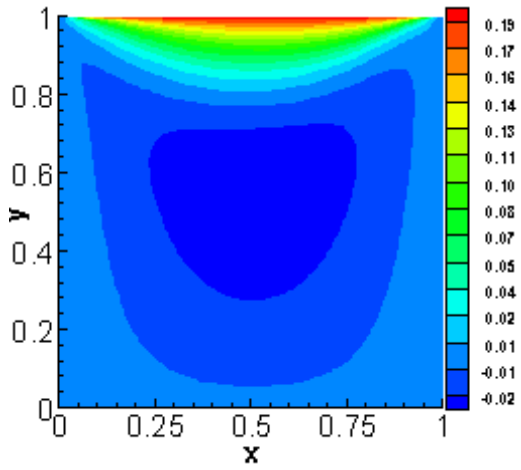

(a) 36 element mesh, C^{11}, $p = 9$

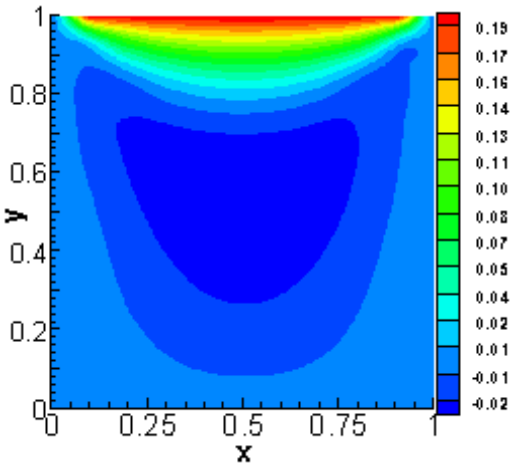

(b) 100 element mesh, C^{11}, $p = 3$

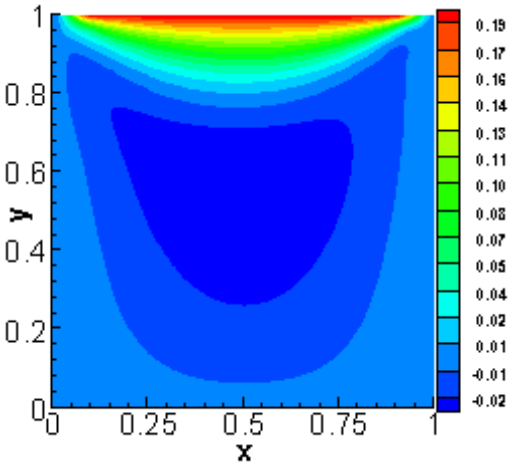

(c) 400 element mesh, C^{11}, $p = 3$

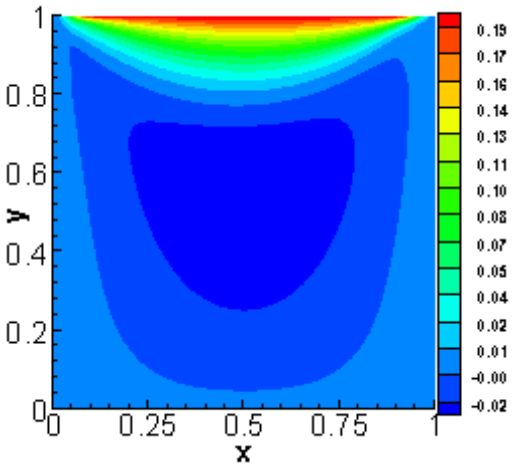

(d) 1600 element mesh, C^{11}, $p = 3$

Figure 4.22: Comparison of Velocity u, p-convergence studies using 36 element graded discretization (h_d = 0.1) and h-convergence studies using 100, 400 and 1600 element uniform discretization (h_d = 0.1); De = 0.24

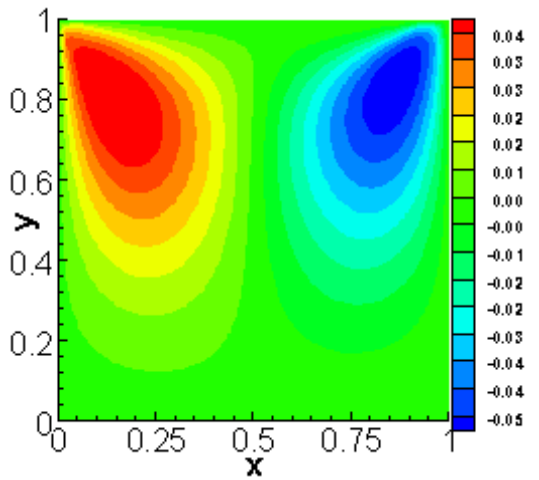

(a) 36 element mesh, C^{11}, $p = 9$

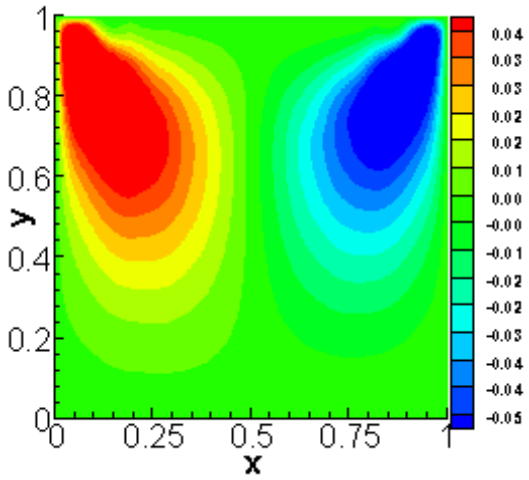

(b) 100 element mesh, C^{11}, $p = 3$

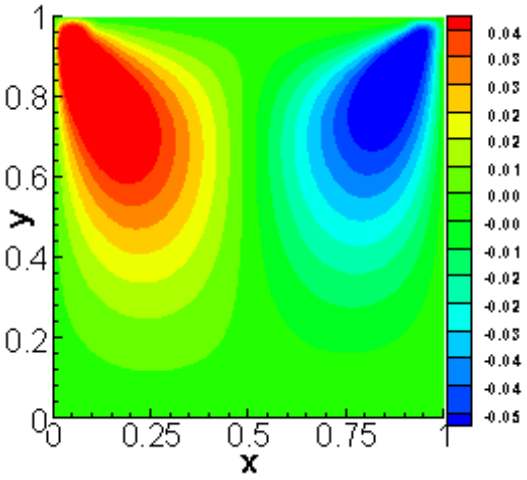

(c) 400 element mesh, C^{11}, $p = 3$

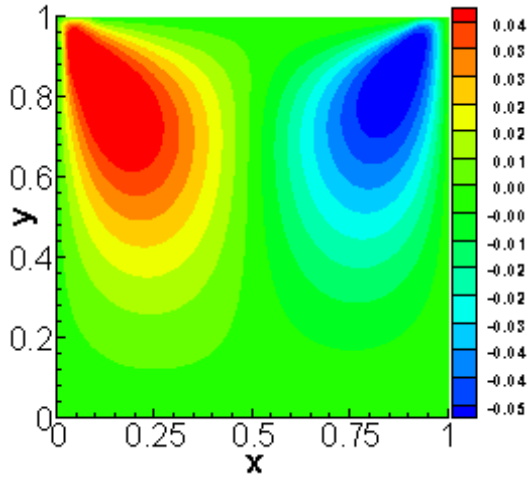

(d) 1600 element mesh, C^{11}, $p = 3$

Figure 4.23: Comparison of Velocity v, p-convergence studies using 36 element graded discretization (h_d = 0.1) and h-convergence studies using 100, 400 and 1600 element uniform discretization (h_d = 0.1); De = 0.24

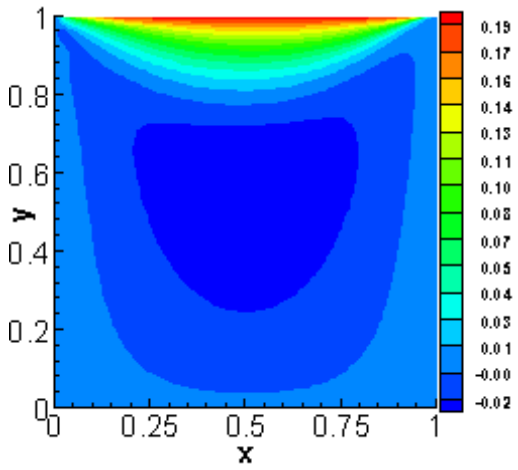

(a) 49 element mesh, C^{11}, $p = 9$

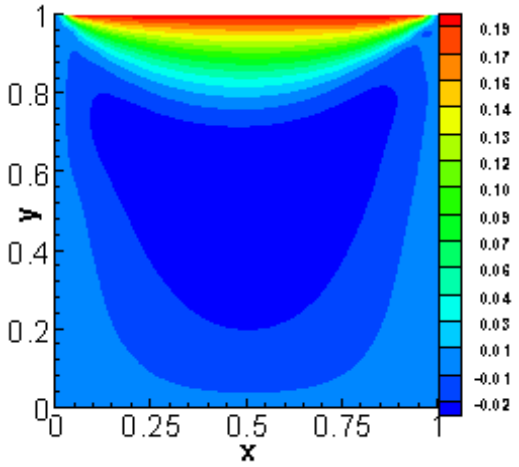

(b) 400 element mesh, C^{11}, $p = 3$

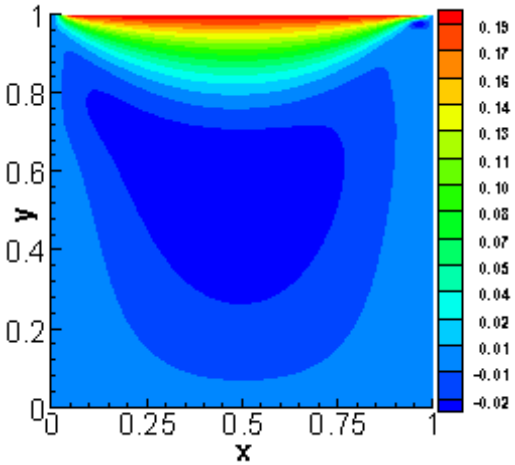

(c) 1600 element mesh, C^{11}, $p = 3$

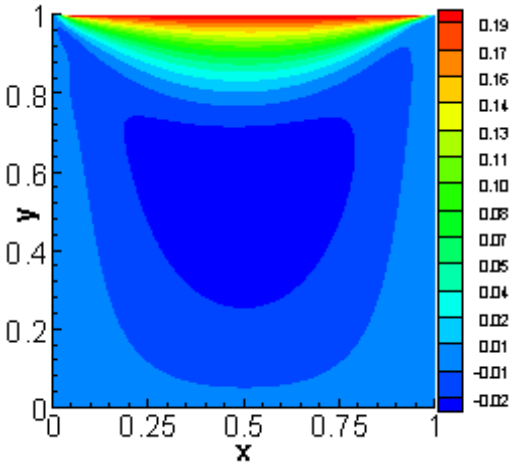

(d) 6400 element mesh, C^{11}, $p = 3$

Figure 4.24: Comparison of Velocity u, p-convergence studies using 49 element graded discretization (h_d = 0.05) and h-convergence studies using 400, 1600 and 6400 element uniform discretization (h_d = 0.05); De = 0.24

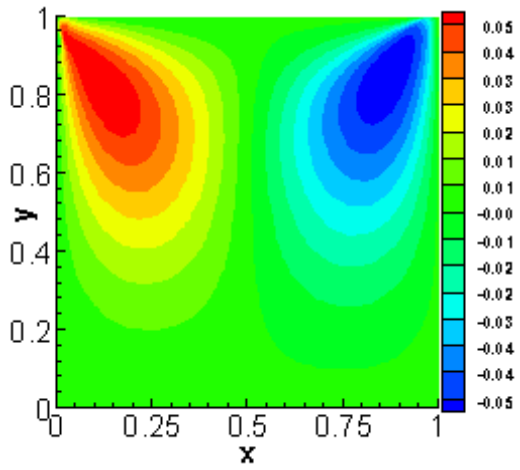

(a) 49 element mesh, C^{11}, $p = 9$

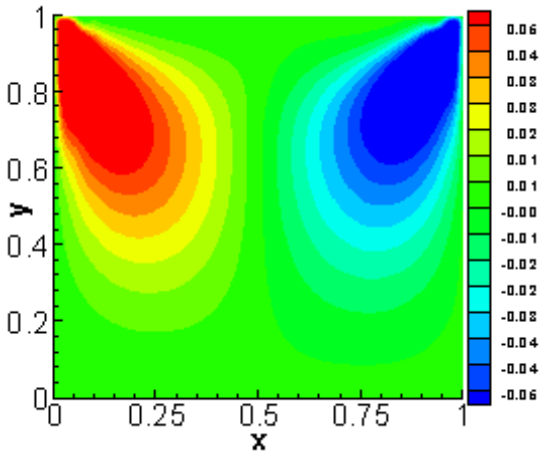

(b) 400 element mesh, C^{11}, $p = 3$

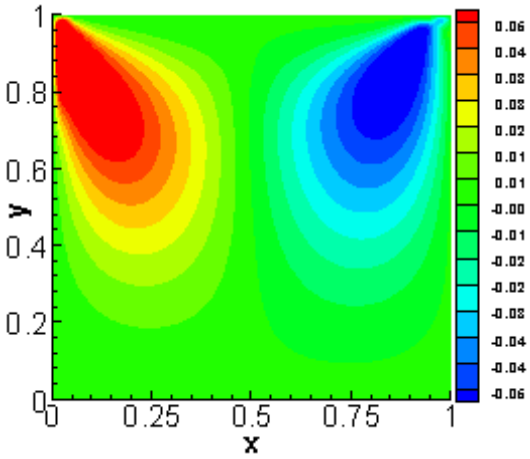

(c) 1600 element mesh, C^{11}, $p = 3$

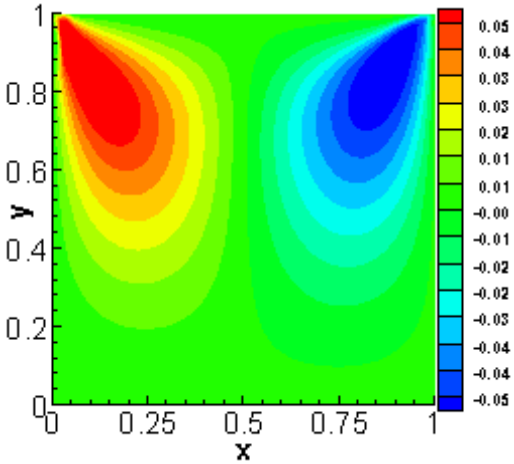

(d) 6400 element mesh, C^{11}, $p = 3$

Figure 4.25: Comparison of Velocity v, p-convergence studies using 49 element graded discretization (h_d = 0.05) and h-convergence studies using 400, 1600 and 6400 element uniform discretization (h_d = 0.05); De = 0.24

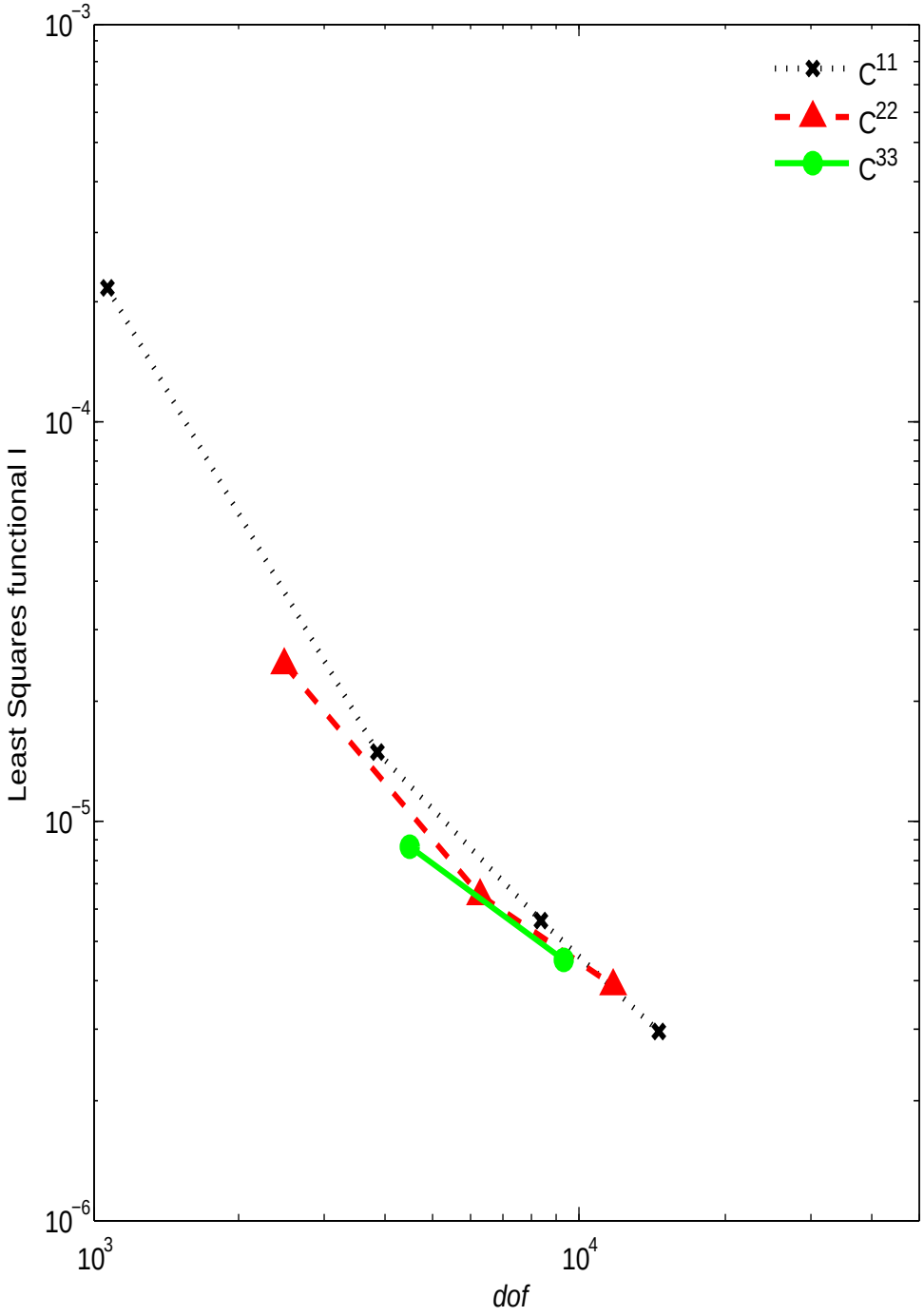

Figure 4.26: Least Squares functional I for 36 element mesh $h_d = 0.1$, $De = 0.24$

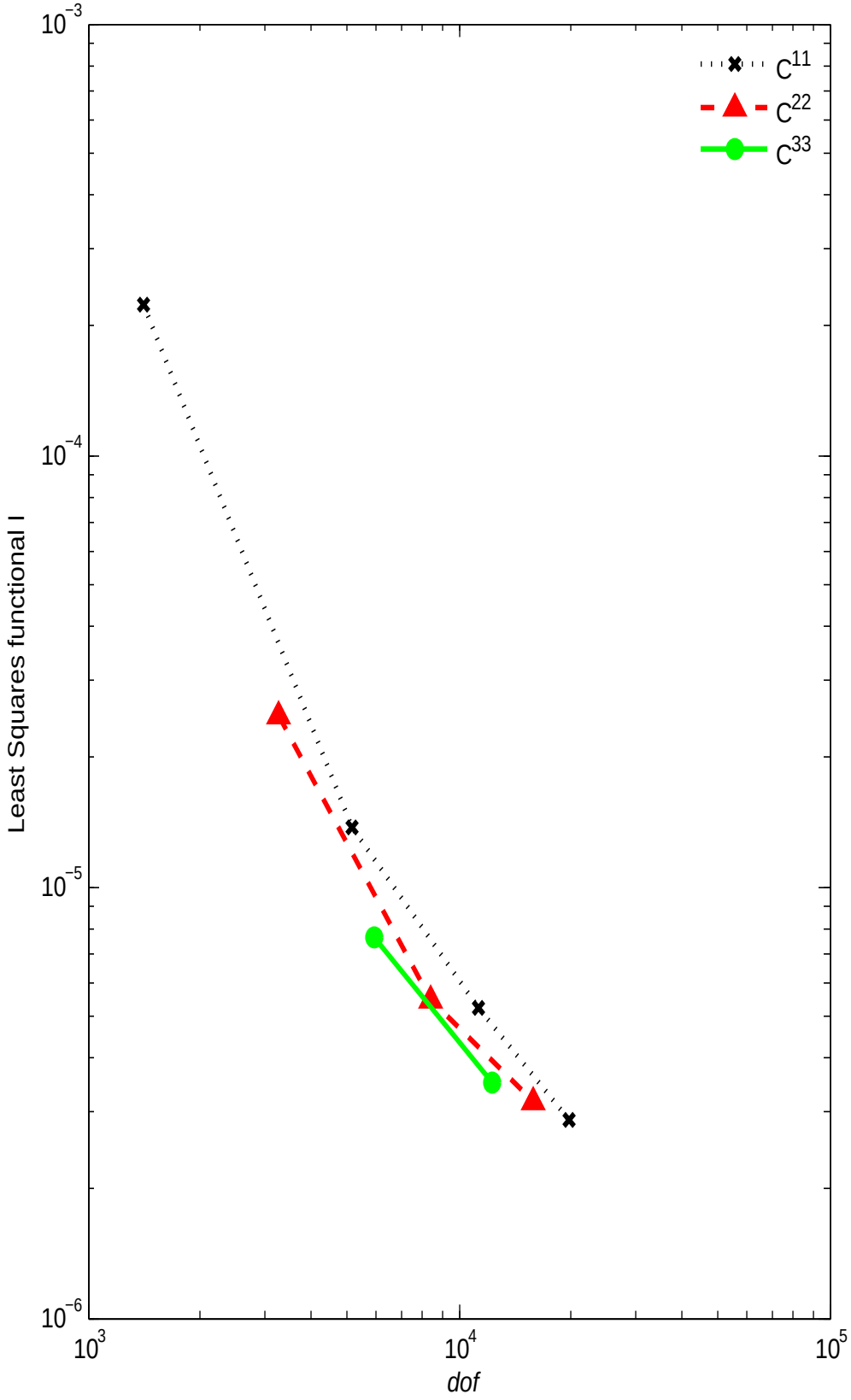

Figure 4.27: Least Squares functional I for 49 element mesh $h_d = 0.05$, $De = 0.24$

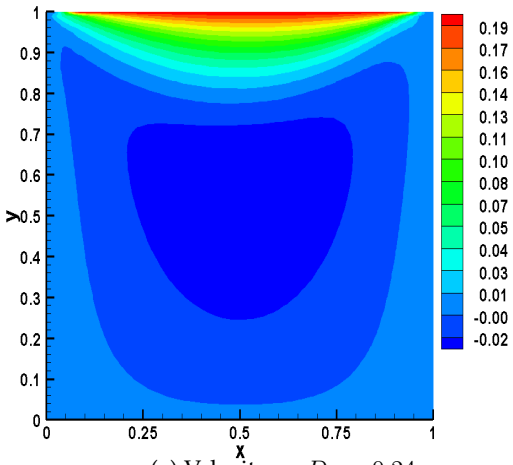

(a) Velocity u , $De = 0.24$

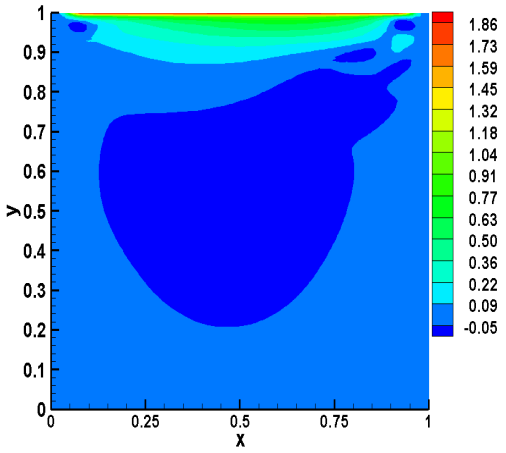

(b) Velocity u , $De = 2.4$

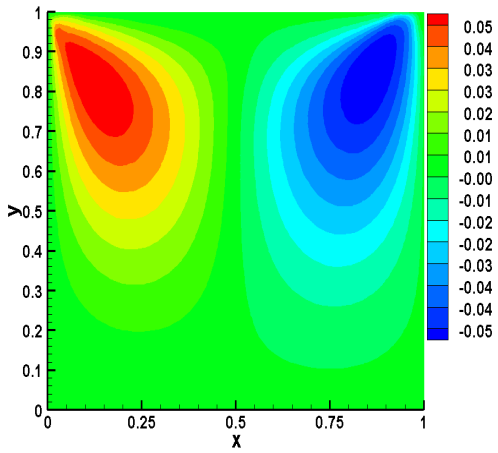

(c) Velocity v , $De = 0.24$

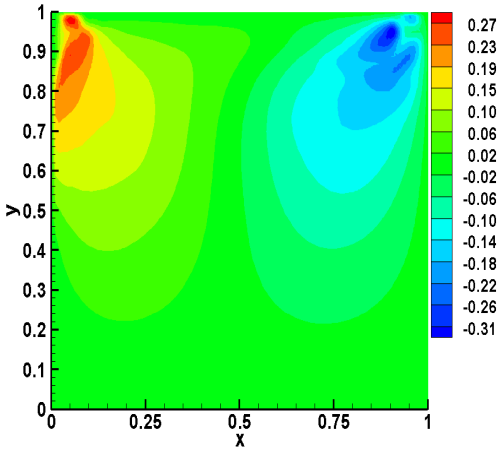

(d) Velocity v , $De = 2.4$

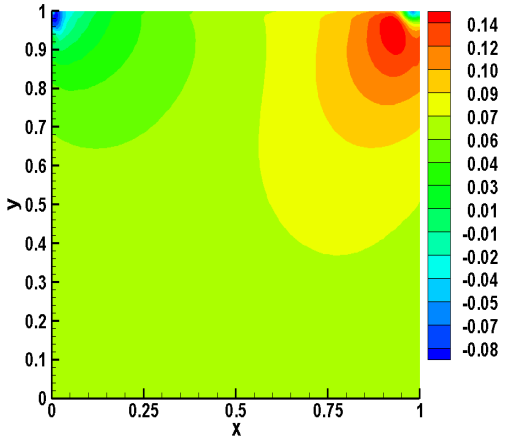

(e) Pressure p , $De = 0.24$

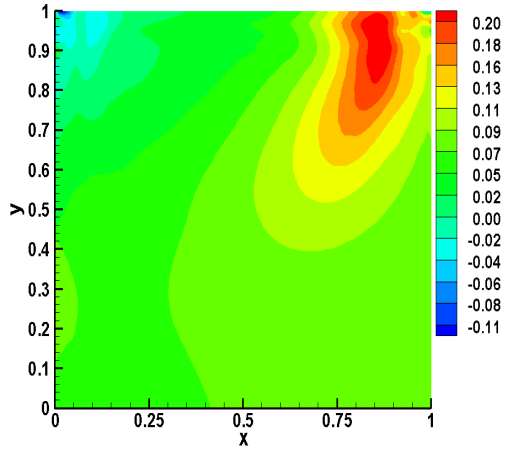

(f) Pressure p , $De = 2.4$

Figure 4.28: Solutions of class C^{33} , $p = 9$ for 36 element mesh , $h_d = 0.1$

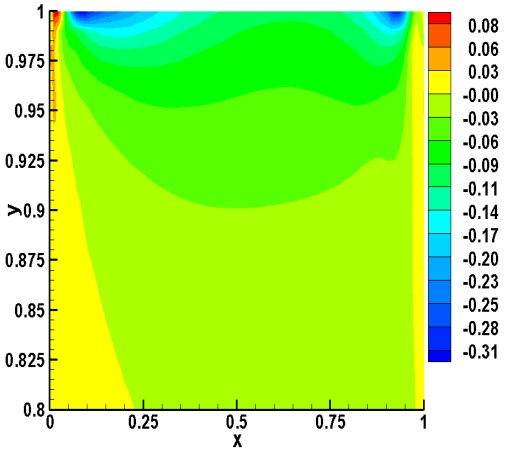

(a) Normal Stress τ_{xx}^p , $De = 0.24$ (exploded view near the lid)

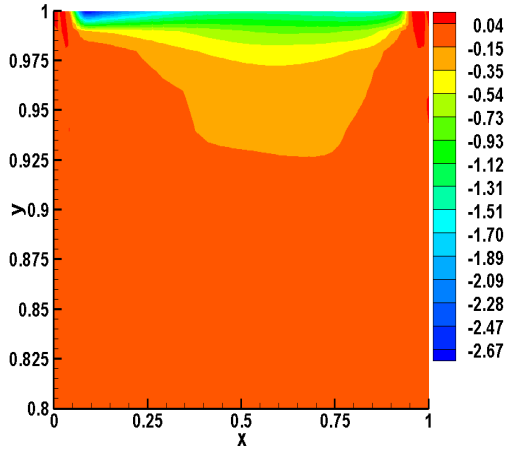

(b) Normal Stress τ_{xx}^p, $De = 2.4$ (exploded view near the lid)

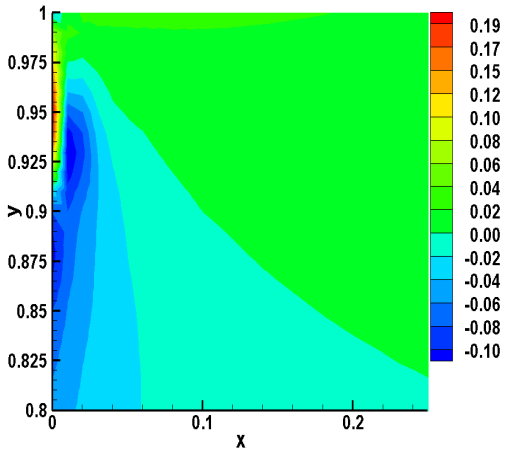

(c) Normal Stress τ_{yy}^p , $De = 0.24$ (exploded view near the lid)

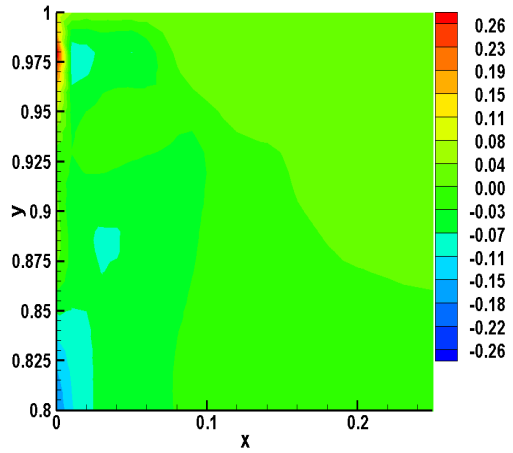

(d) Normal Stress τ_{yy}^p , $De = 2.4$ (exploded view near the lid)

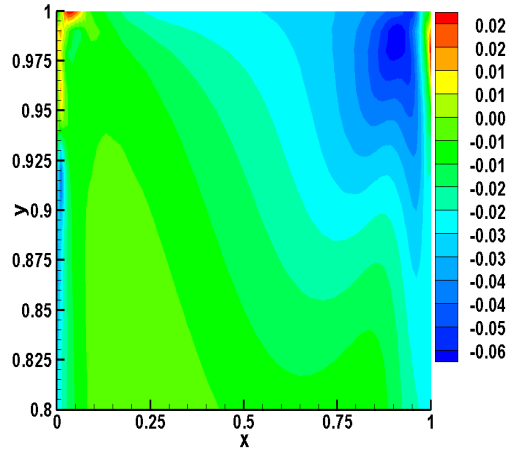

(e) Shear Stress τ_{xy}^p , $De = 0.24$ (exploded view near the lid)

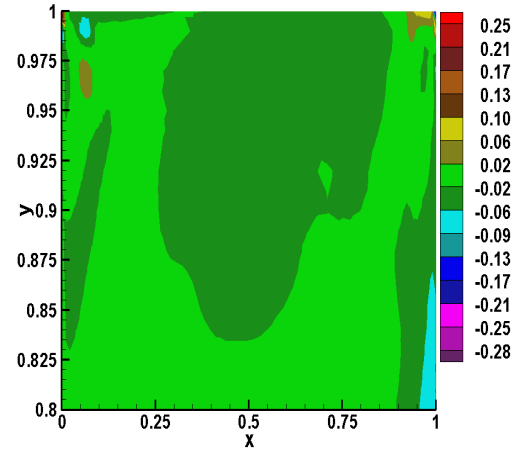

(f) Shear Stress τ_{xy}^p , $De = 2.4$ (exploded view near the lid)

Figure 4.29: Solutions of class C^{33} , p = 9 for 36 element mesh , h_d = 0.1

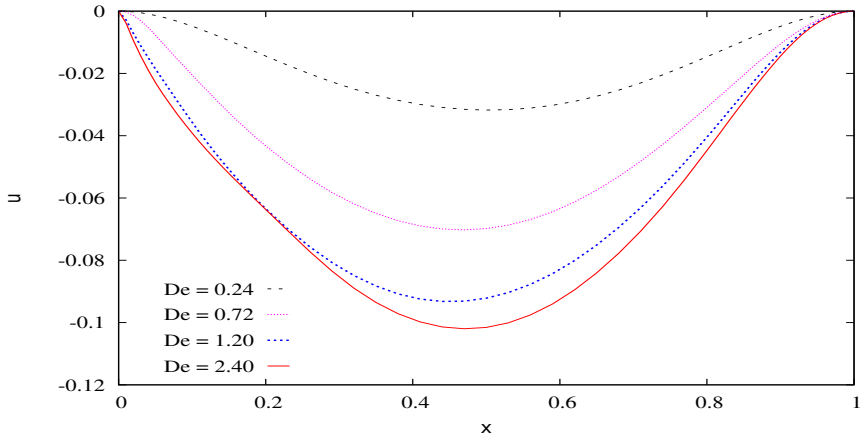

(a) Velocity u versus x at y=0.5

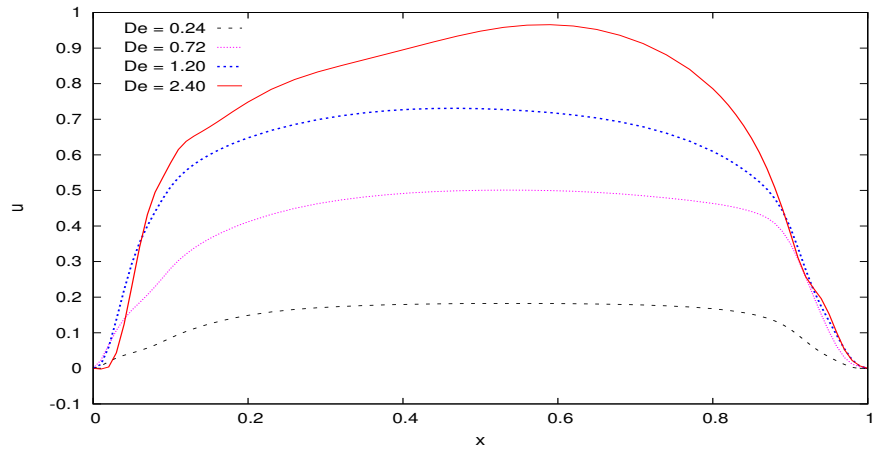

(b) Velocity u versus x at y=0.99

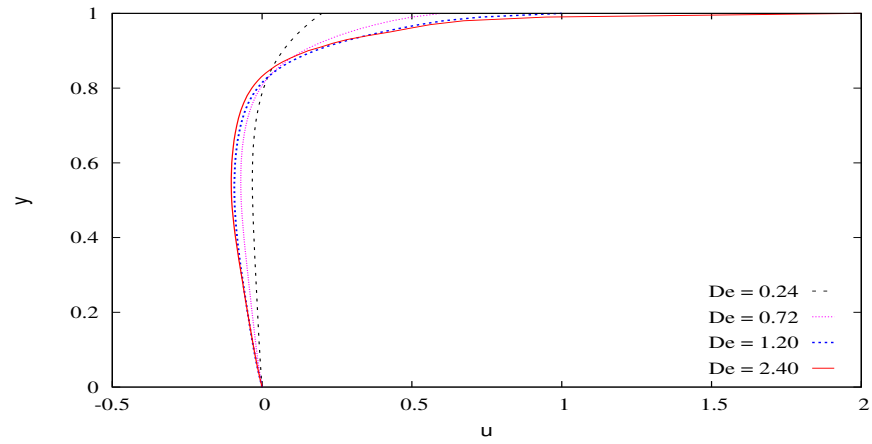

(c) Velocity u versus y at x=0.5

Figure 4.30: Solutions of class C^2 for lid driven cavity for Mesh M1 (36 elm , $h_d = 0.1$); $p = 9$

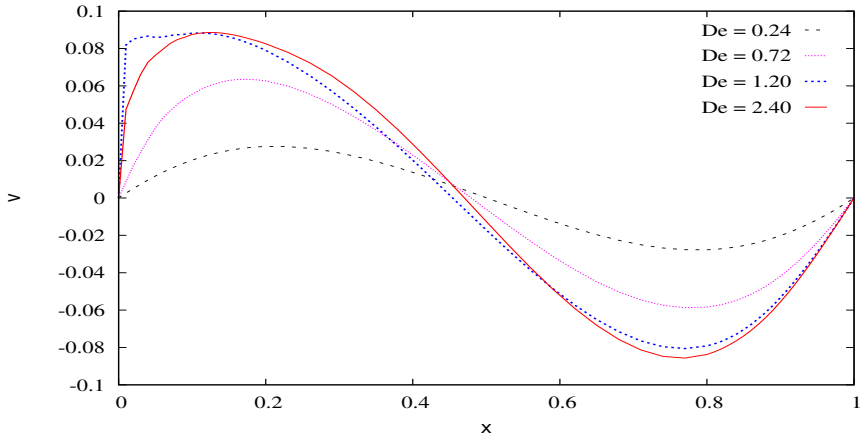

(a) Velocity v versus x at y=0.5

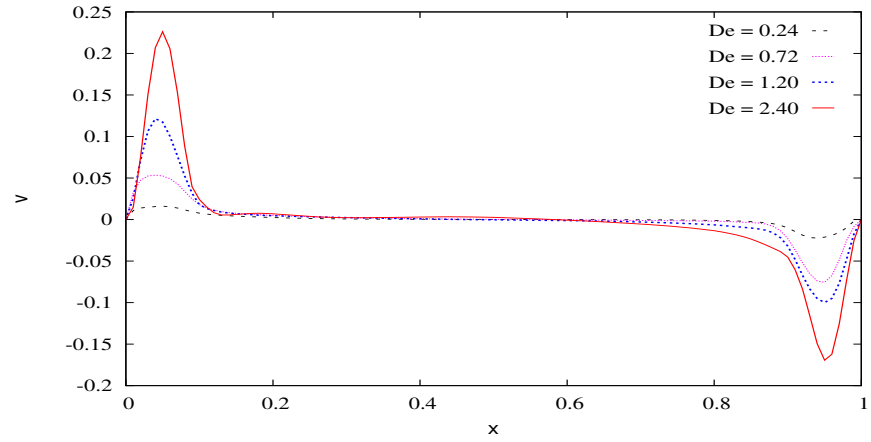

(b) Velocity v versus x at y=0.99

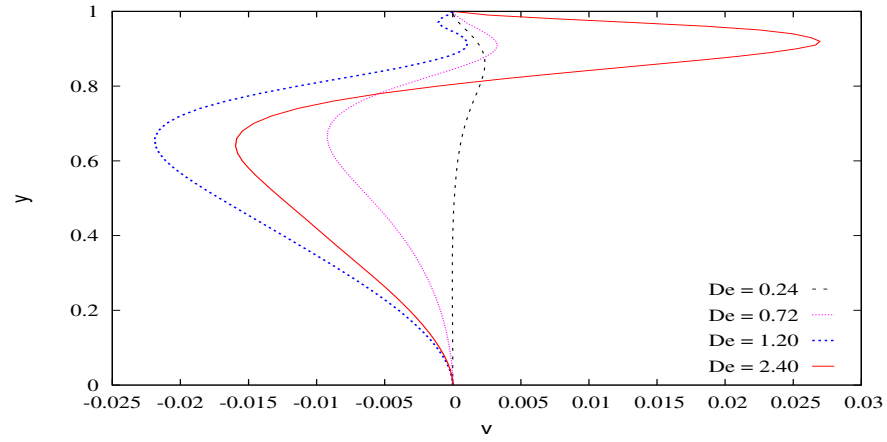

(c) Velocity v versus y at x=0.5

Figure 4.31: Solutions of class C^2 for lid driven cavity for Mesh M1 (36 elm , $h_d = 0.1$); $p = 9$

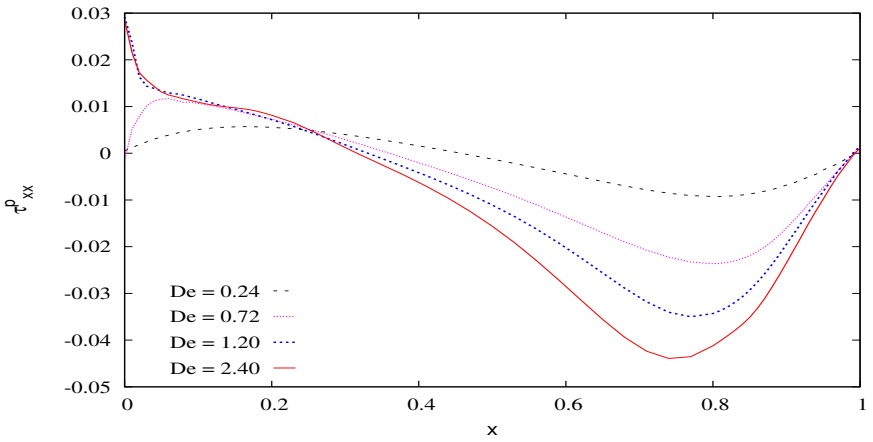

(a) Normal Stress τ^p_{xx} versus x at y=0.5

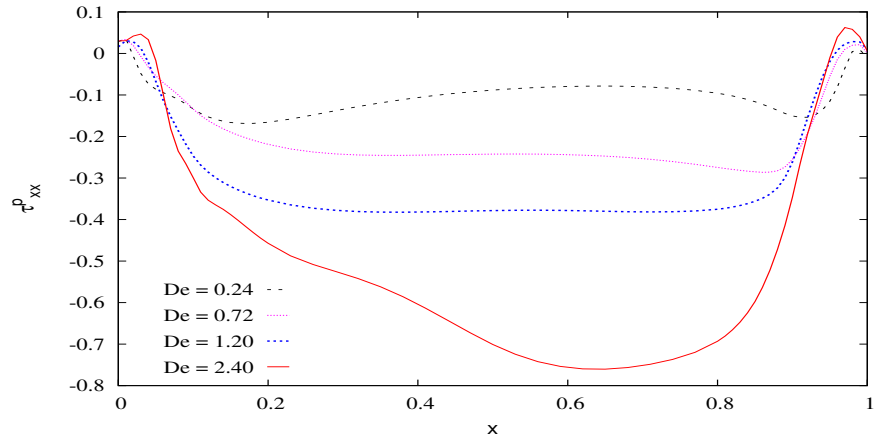

(b) Normal Stress τ^p_{xx} versus x at y=0.99

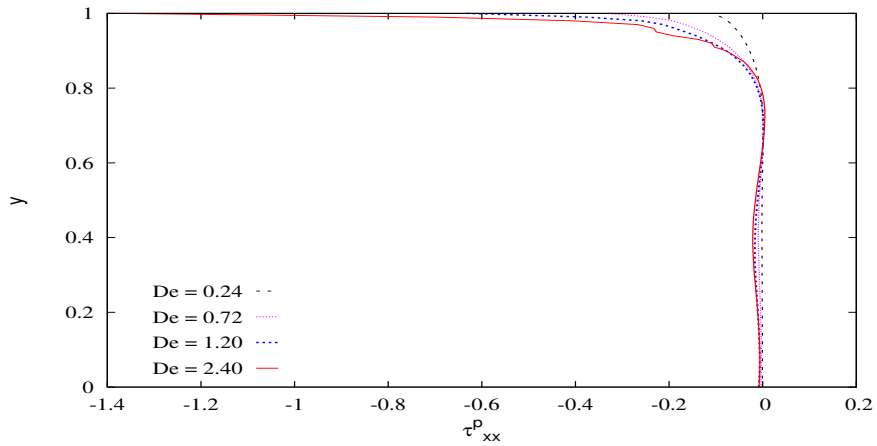

(c) Normal Stress τ^p_{xx} versus y at x=0.5

Figure 4.32: Solutions of class C^2 for lid driven cavity for Mesh M1 (36 elm , $h_d = 0.1$); $p = 9$

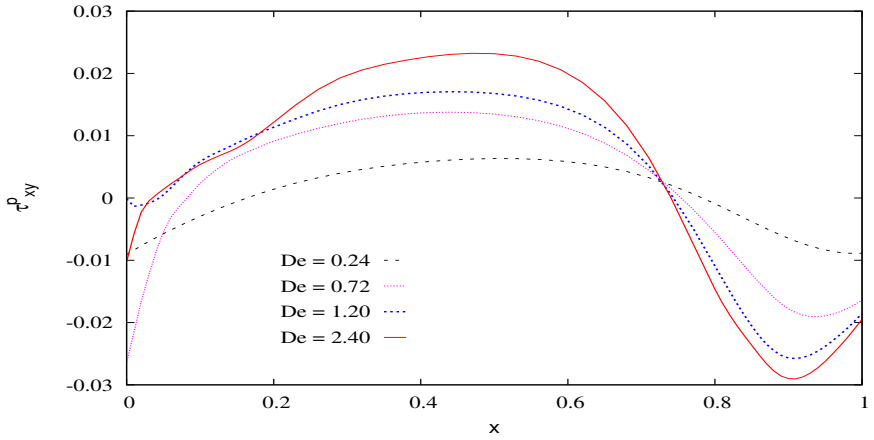

(a) Shear Stress τ^p_{xy} versus x at y=0.5

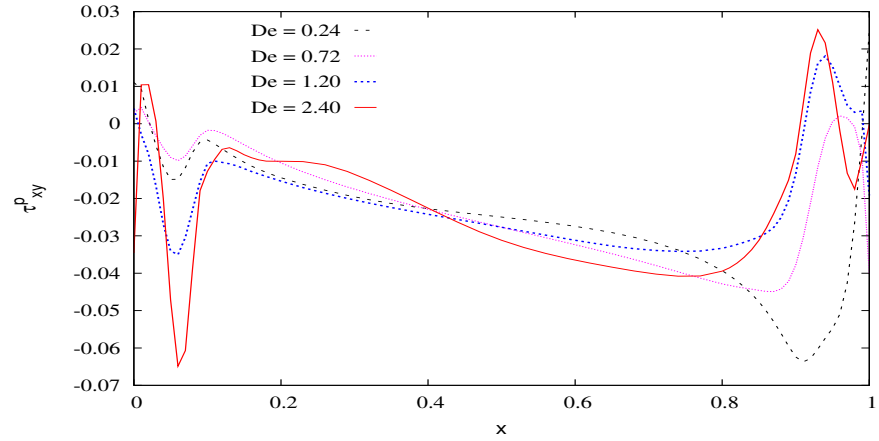

(b) Shear Stress τ^p_{xy} versus x at y=0.99

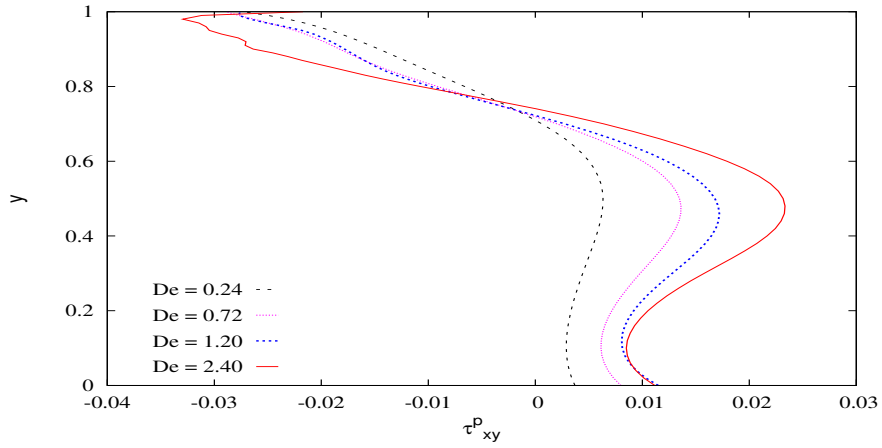

(c) Shear Stress τ^p_{xy} versus y at x=0.5

Figure 4.33: Solutions of class C^2 for lid driven cavity for Mesh M1 (36 elm , $h_d = 0.1$); $p = 9$

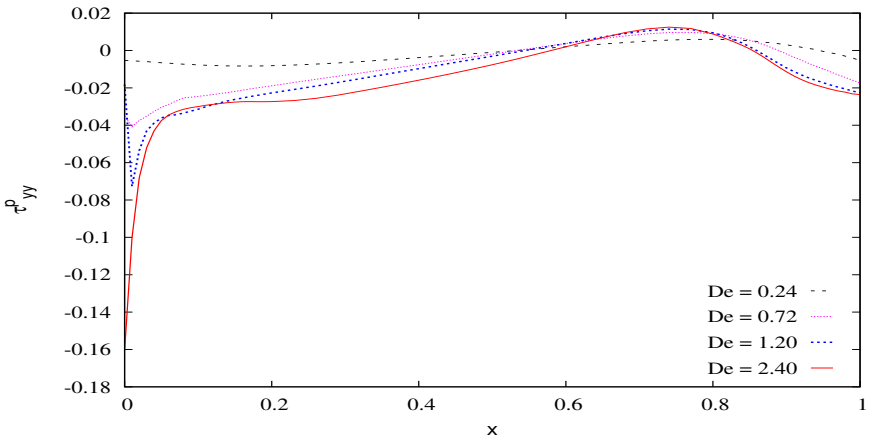

(a) Normal Stress τ^p_{yy} versus x at y=0.5

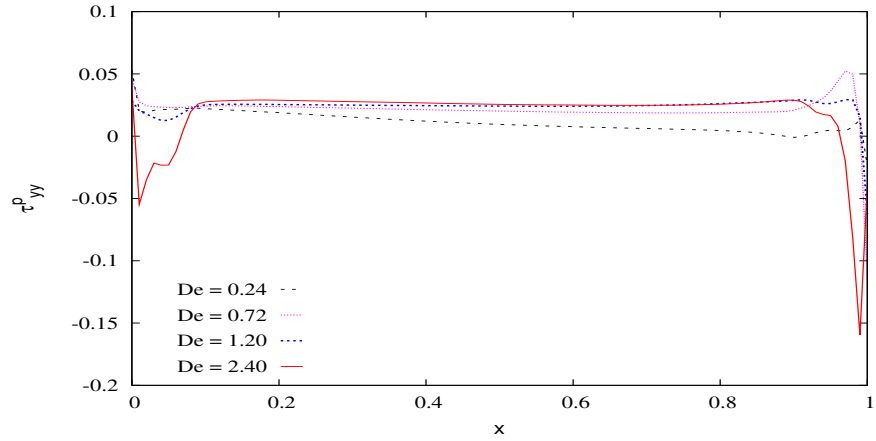

(b) Normal Stress τ^p_{yy} versus x at y=0.99

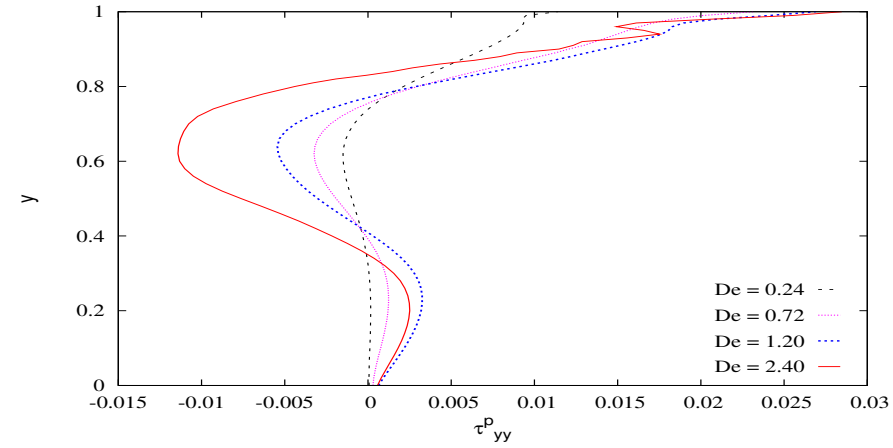

(c) Normal Stress τ^p_{yy} versus y at x=0.5

Figure 4.34: Solutions of class C^2 for lid driven cavity for Mesh M1 (36 elm , $h_d = 0.1$); $p = 9$

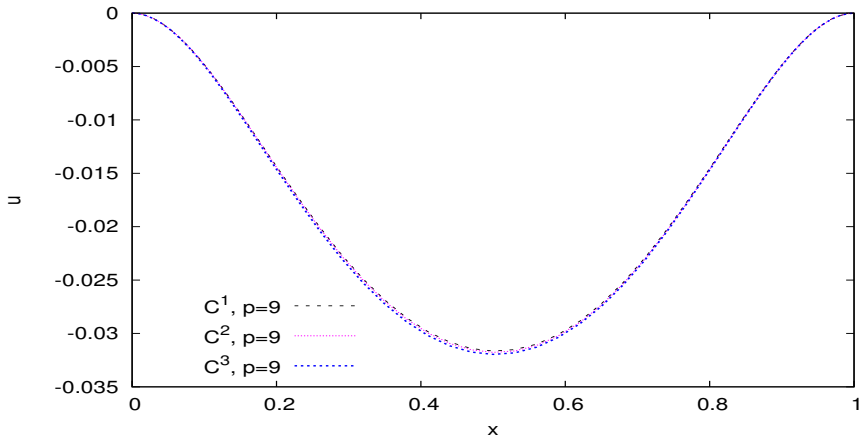

(a) Velocity u versus x at y=0.5

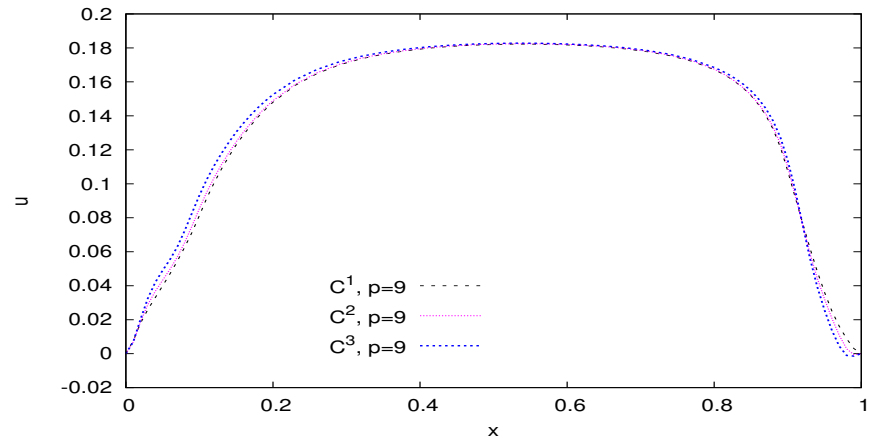

(b) Velocity u versus x at y=0.99

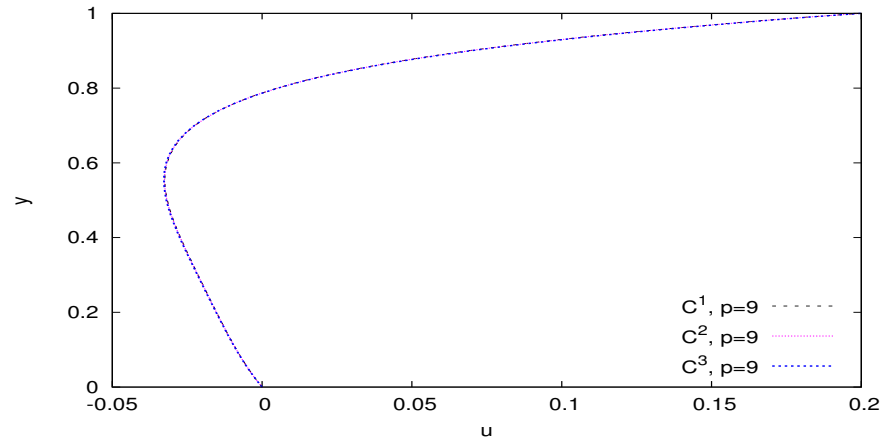

(c) Velocity u versus y at x=0.5

Figure 4.35: Comparison of solutions for mesh M1 (36 elm, h_d = 0.1); $De = 0.24$

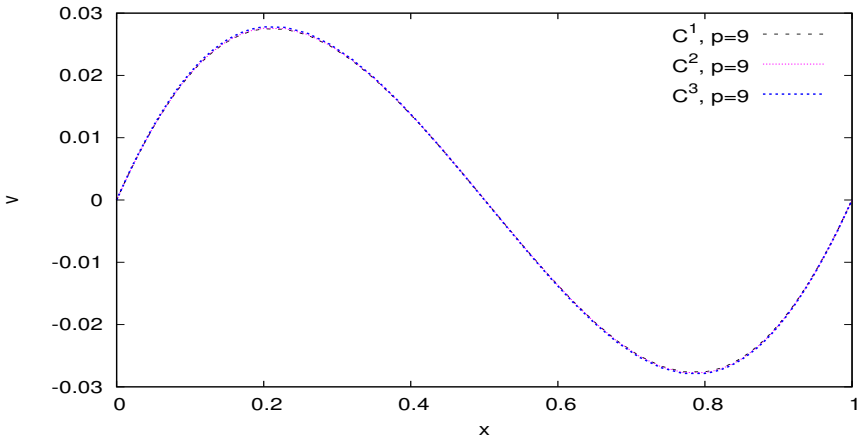

(a) Velocity v versus x at y=0.5

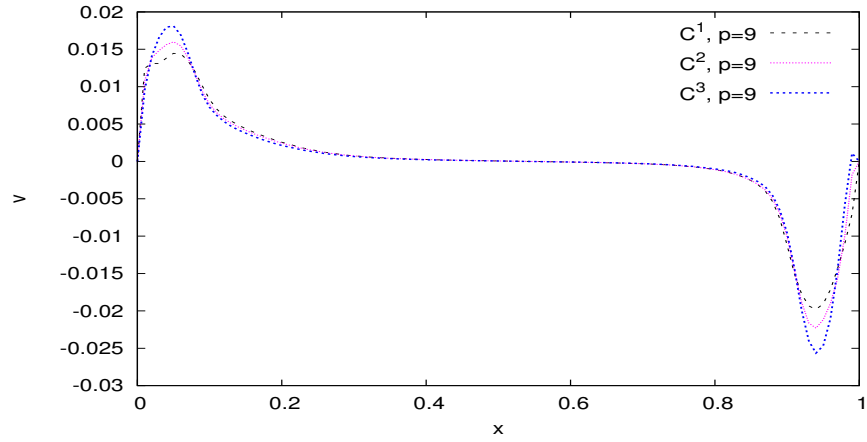

(b) Velocity v versus x at y=0.99

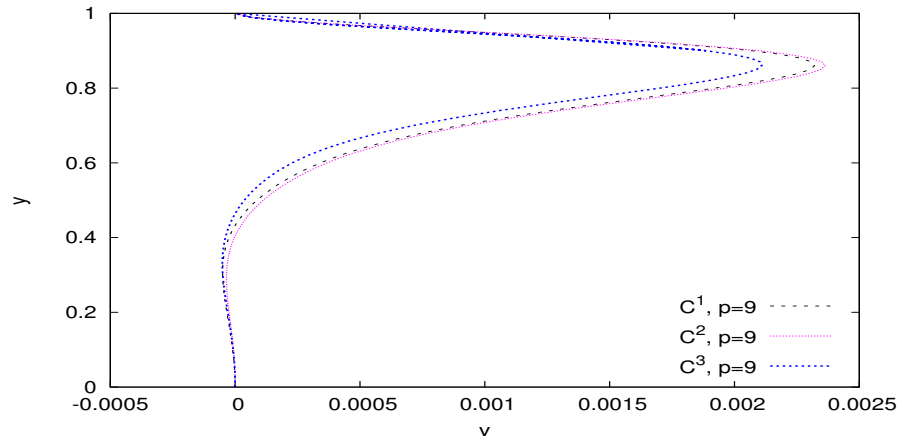

(c) Velocity v versus y at x=0.5

Figure 4.36: Comparison of solutions for mesh M1 (36 elm, h_d = 0.1); $De = 0.24$

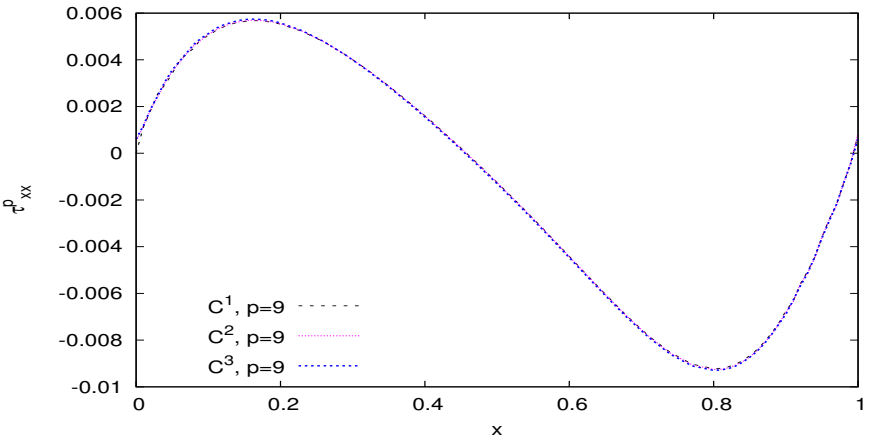

(a) Normal Stress τ^p_{xx} versus x at y=0.5

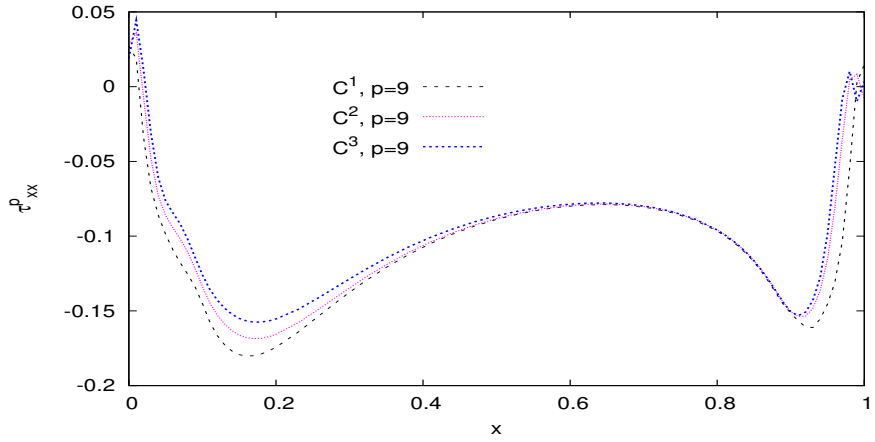

(b) Normal Stress τ^p_{xx} versus x at y=0.99

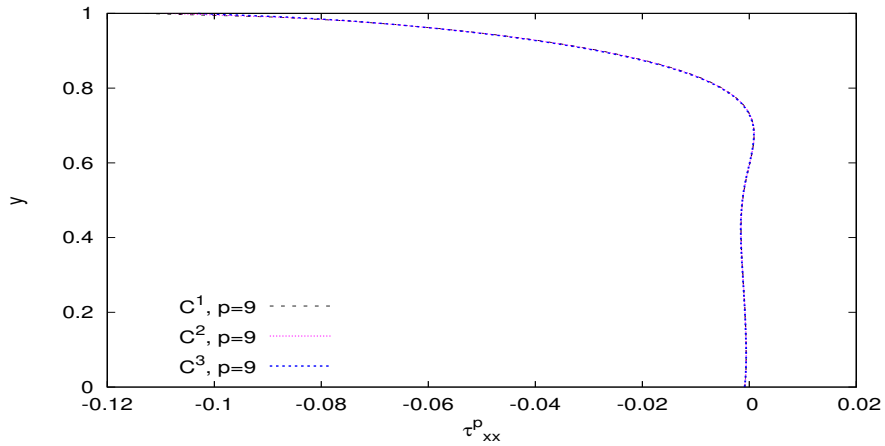

(c) Normal Stress τ^p_{xx} versus y at x=0.5

Figure 4.37: Comparison of solutions for mesh M1 (36 elm, h_d = 0.1); $De = 0.24$

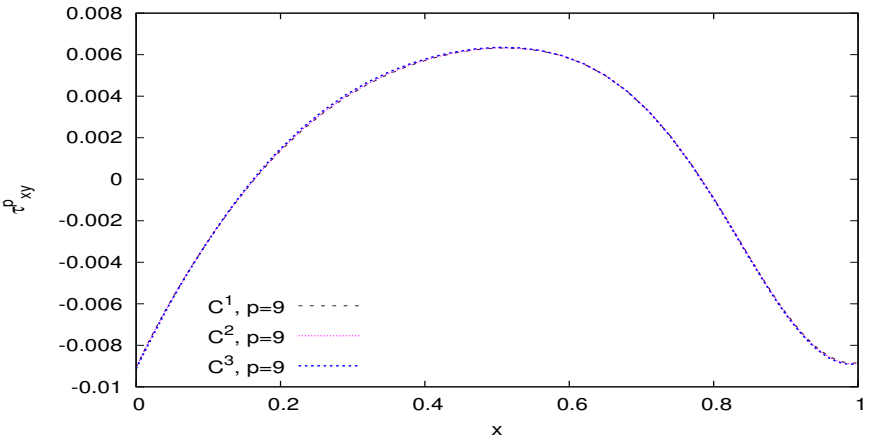

(a) Shear Stress τ^p_{xy} versus x at y=0.5

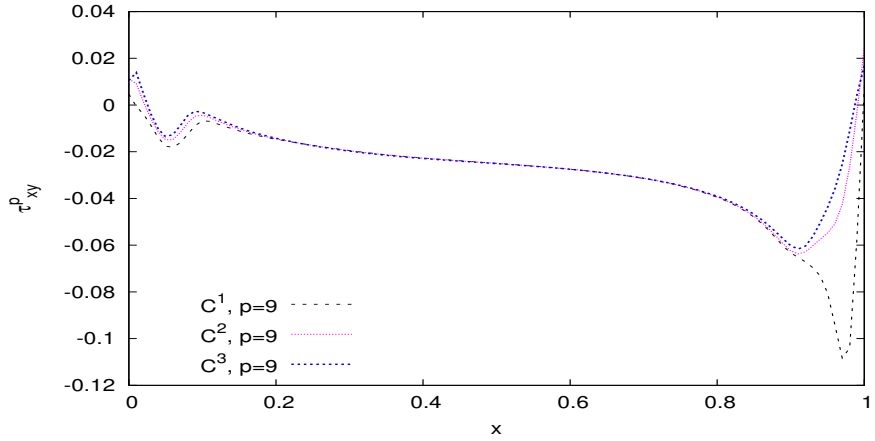

(b) Shear Stress τ^p_{xy} versus x at y=0.99

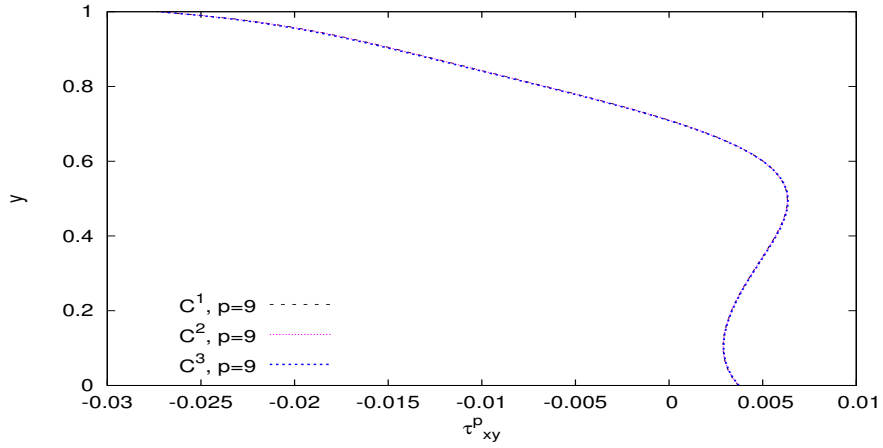

(c) Shear Stress τ^p_{xy} versus y at x=0.5

Figure 4.38: Comparison of solutions for mesh M1 (36 elm, h_d = 0.1); $De = 0.24$

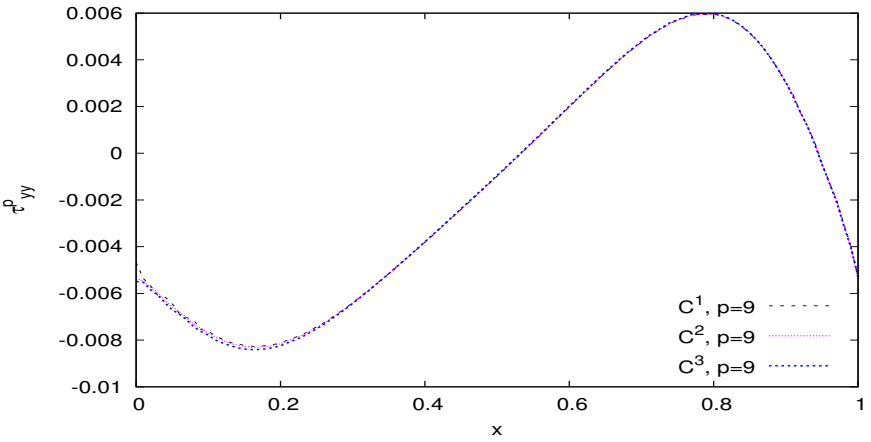

(a) Normal Stress τ^p_{yy} versus x at y=0.5

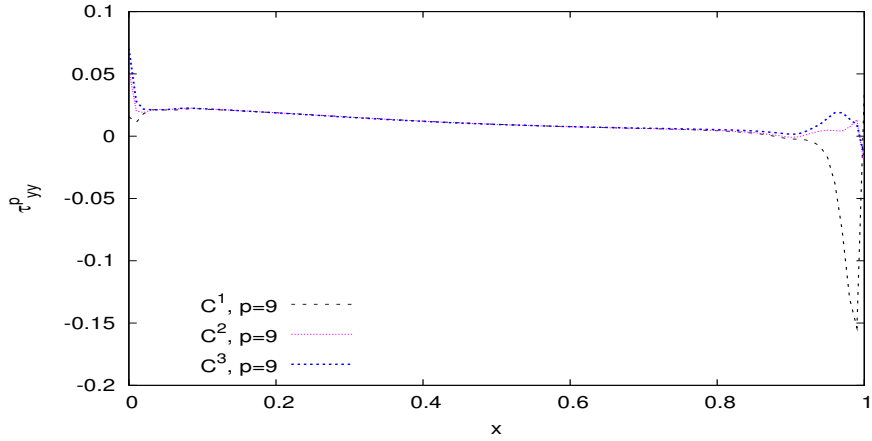

(b) Normal Stress τ^p_{yy} versus x at y=0.99

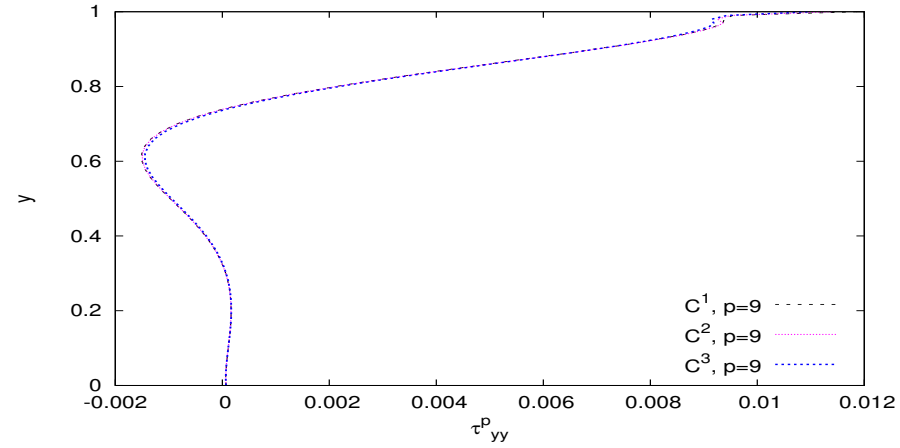

(c) Normal Stress τ^p_{yy} versus y at x=0.5

Figure 4.39: Comparison of solutions for mesh M1 (36 elm, h_d = 0.1); $De = 0.24$

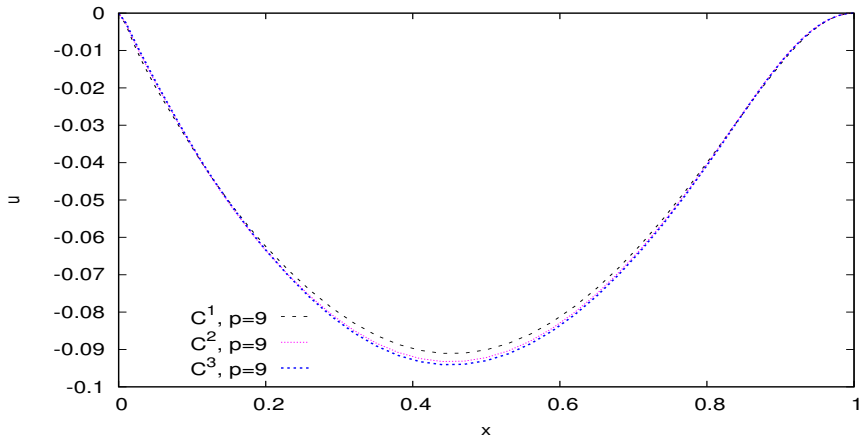

(a) Velocity u versus x at y=0.5

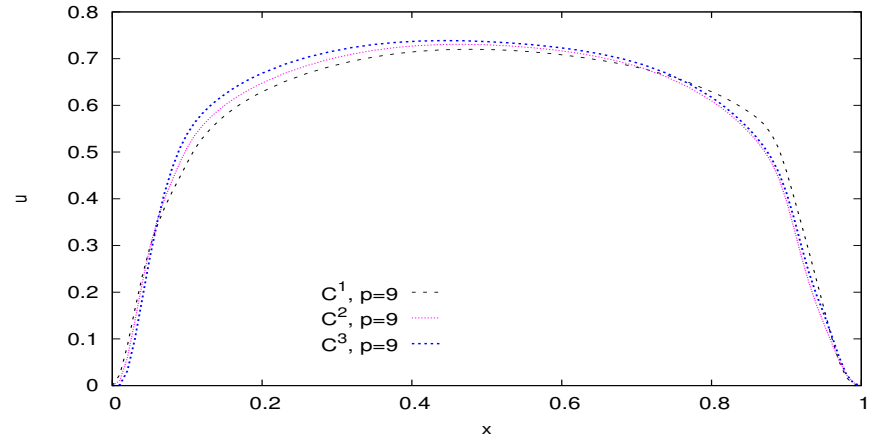

(b) Velocity u versus x at y=0.99

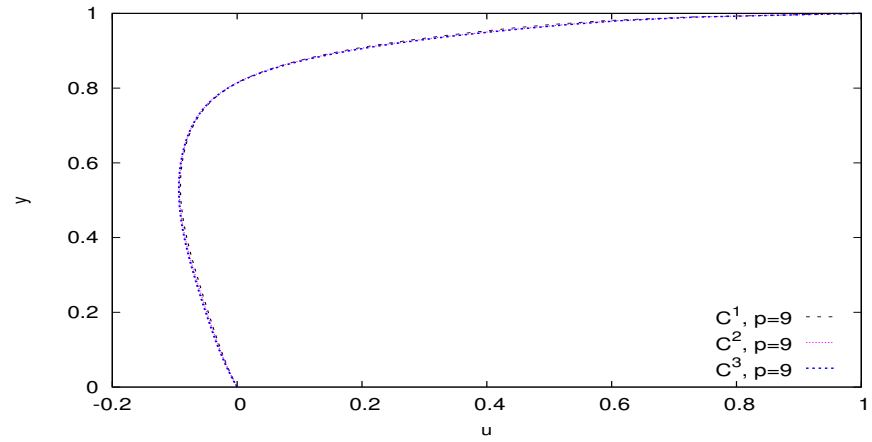

(c) Velocity u versus y at x=0.5

Figure 4.40: Comparison of solutions for mesh M1 (36 elm, h_d = 0.1); $De = 1.2$

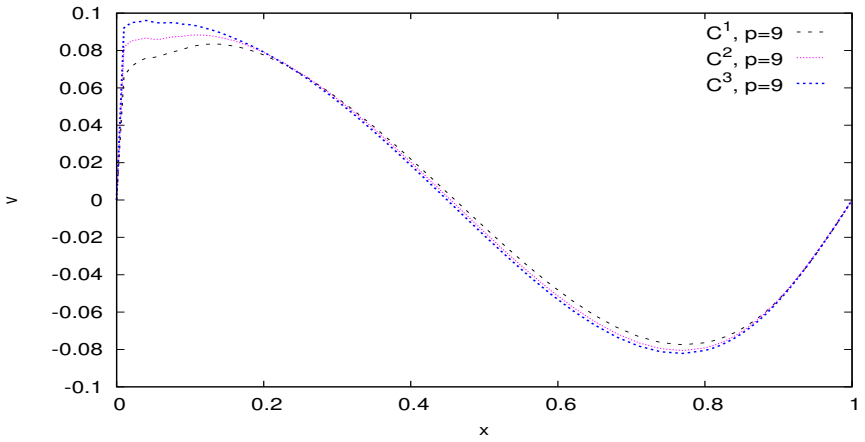

(a) Velocity v versus x at y=0.5

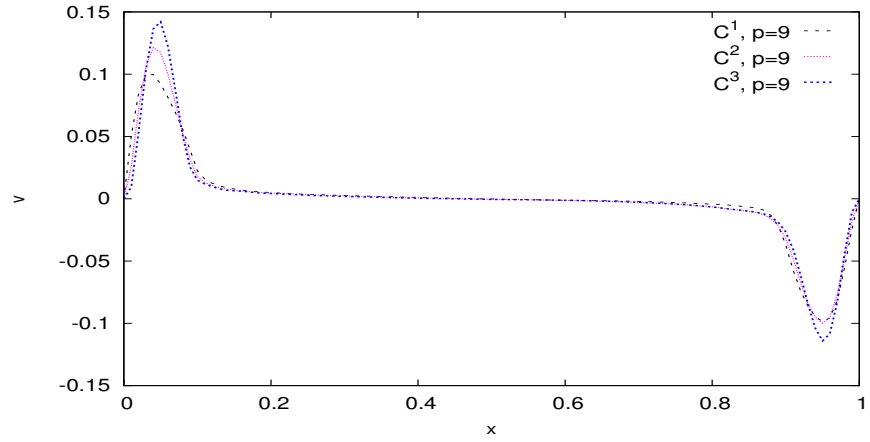

(b) Velocity v versus x at y=0.99

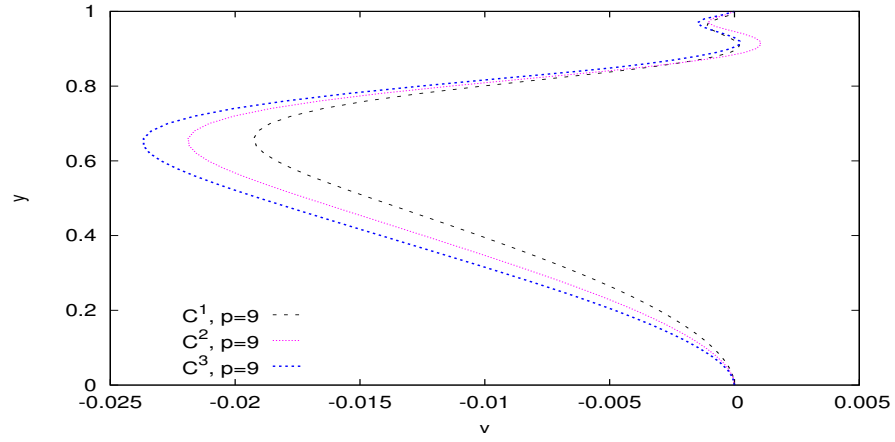

(c) Velocity v versus y at x=0.5

Figure 4.41: Comparison of solutions for mesh M1 (36 elm, h_d = 0.1); $De = 1.2$

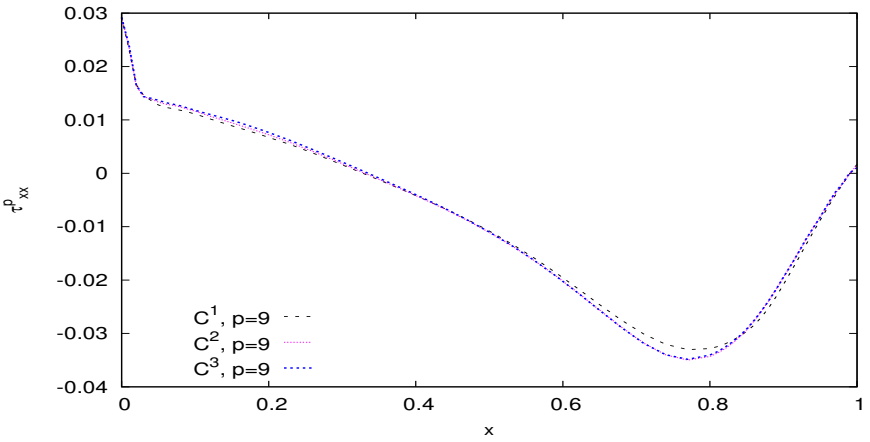

(a) Normal Stress τ^p_{xx} versus x at y=0.5

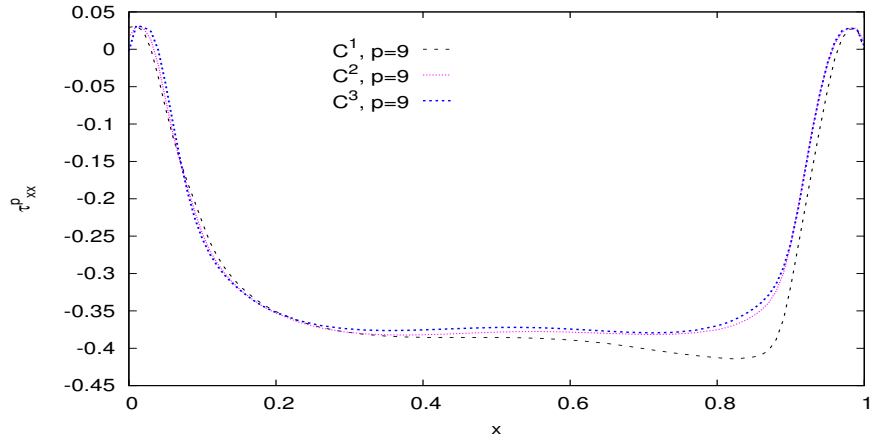

(b) Normal Stress τ^p_{xx} versus x at y=0.99

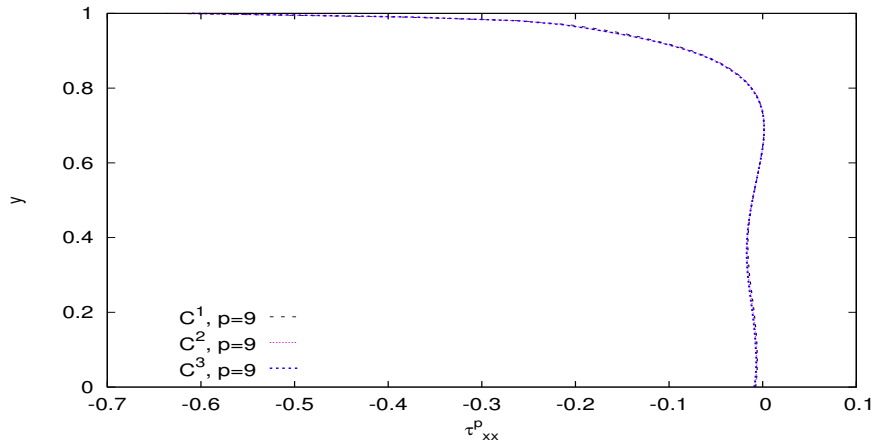

(c) Normal Stress τ^p_{xx} versus y at x=0.5

Figure 4.42: Comparison of solutions for mesh M1 (36 elm, h_d = 0.1); $De = 1.2$

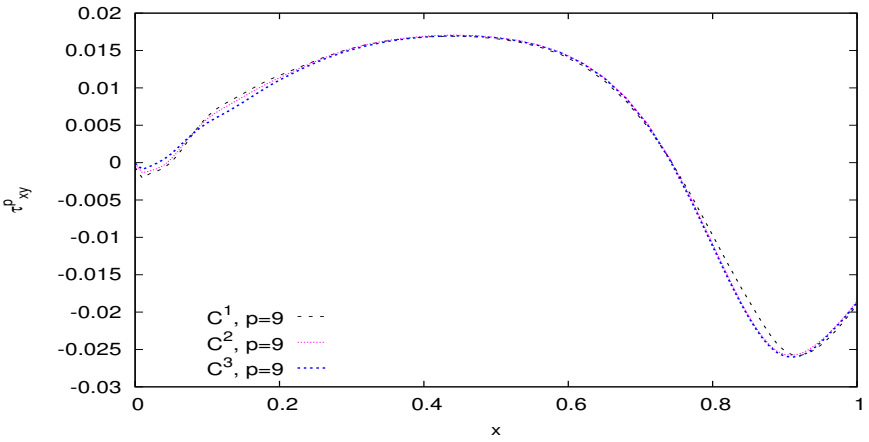

(a) Shear Stress τ^p_{xy} versus x at y=0.5

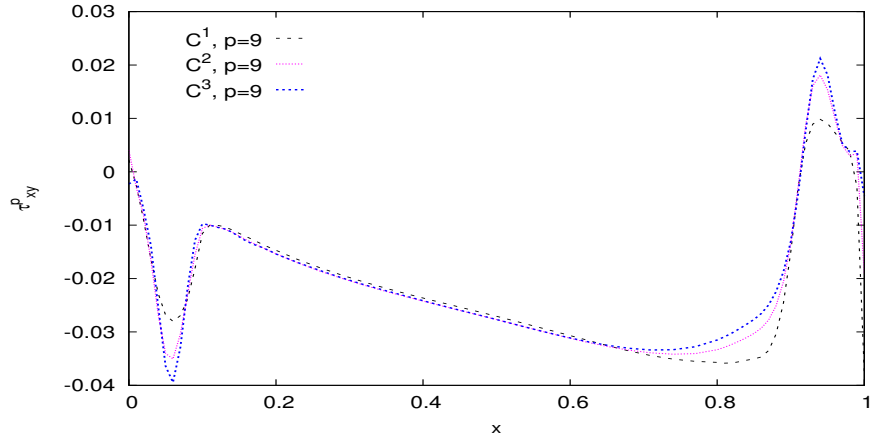

(b) Shear Stress τ^p_{xy} versus x at y=0.99

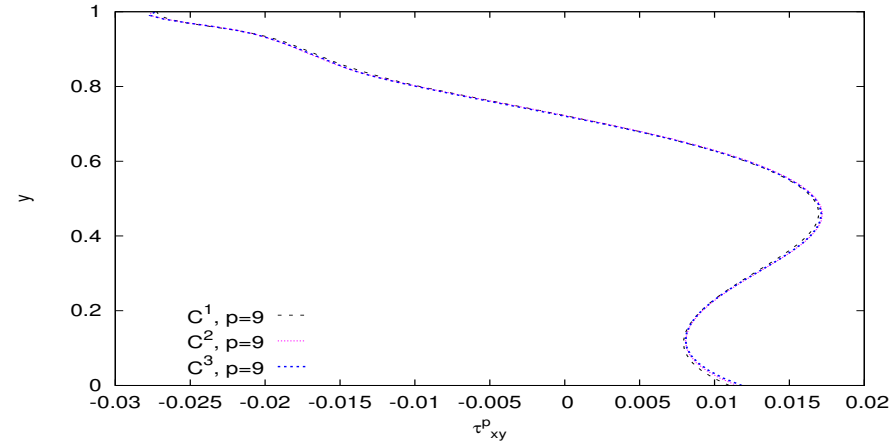

(c) Shear Stress τ^p_{xy} versus y at x=0.5

Figure 4.43: Comparison of solutions for mesh M1 (36 elm, h_d = 0.1); $De = 1.2$

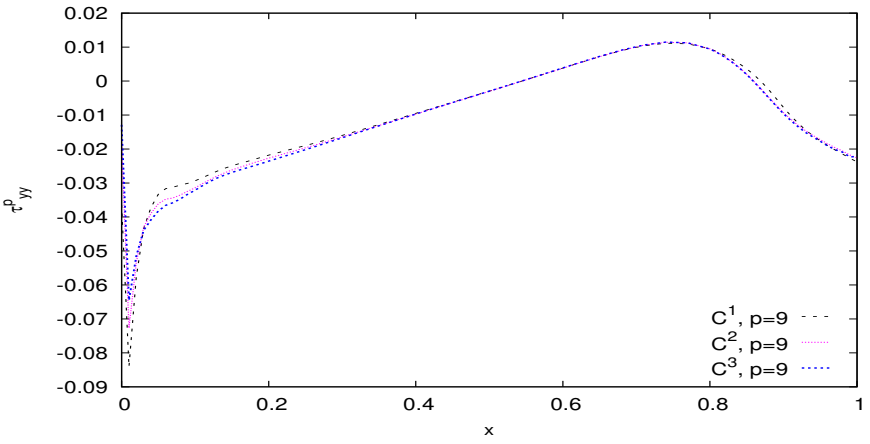

(a) Normal Stress τ^p_{yy} versus x at y=0.5

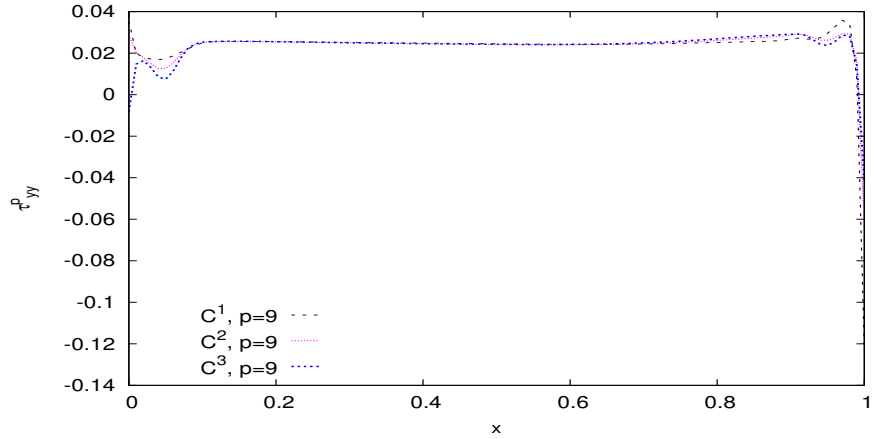

(b) Normal Stress τ^p_{yy} versus x at y=0.99

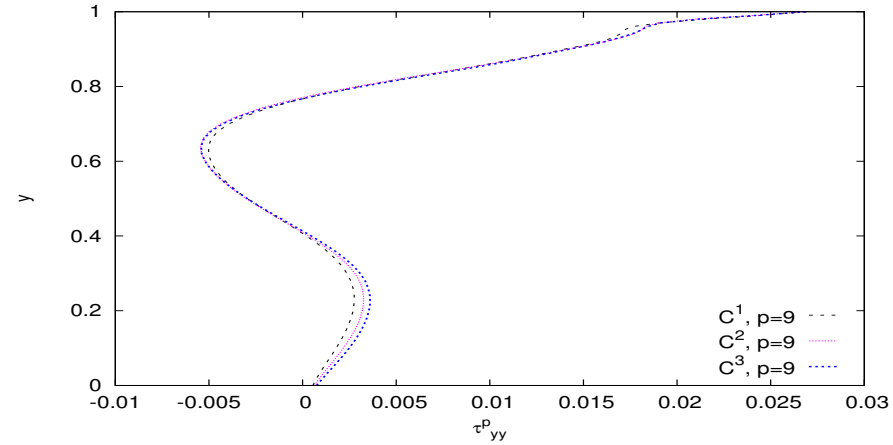

(c) Normal Stress τ^p_{yy} versus y at x=0.5

Figure 4.44: Comparison of solutions for mesh M1 (36 elm, h_d = 0.1); $De = 1.2$

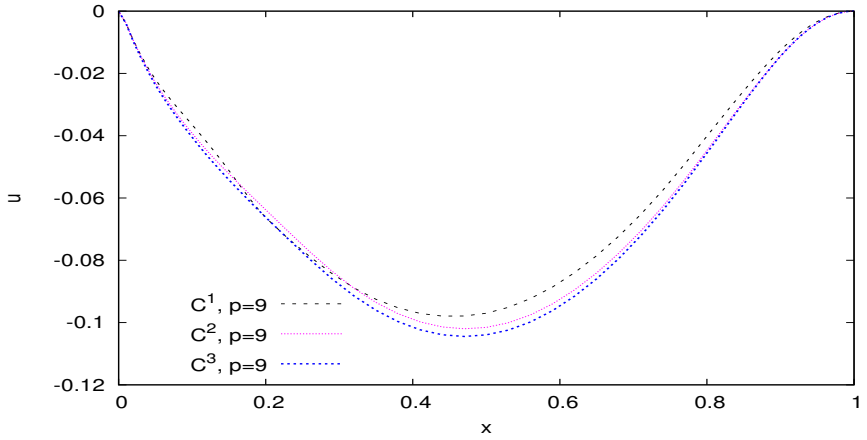

(a) Velocity u versus x at y=0.5

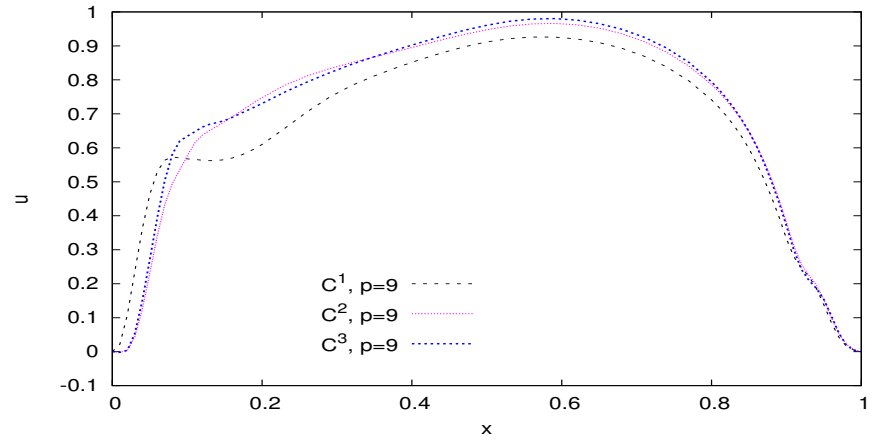

(b) Velocity u versus x at y=0.99

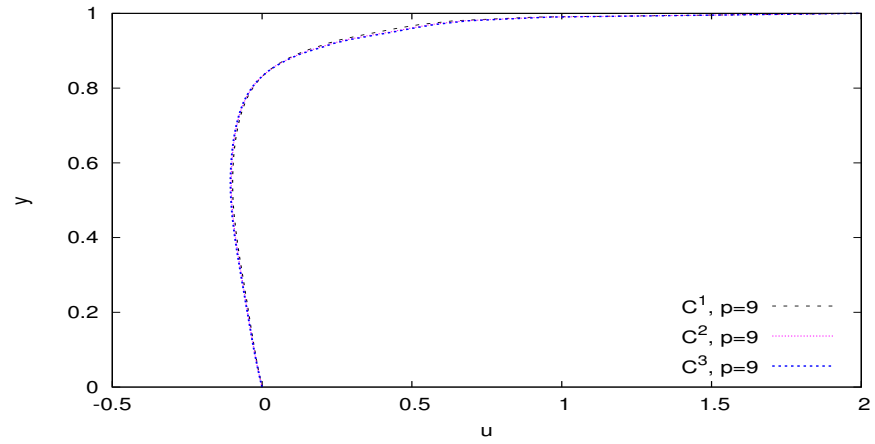

(c) Velocity u versus y at x=0.5

Figure 4.45: Comparison of solutions for mesh M1 (36 elm, h_d = 0.1); $De = 2.4$

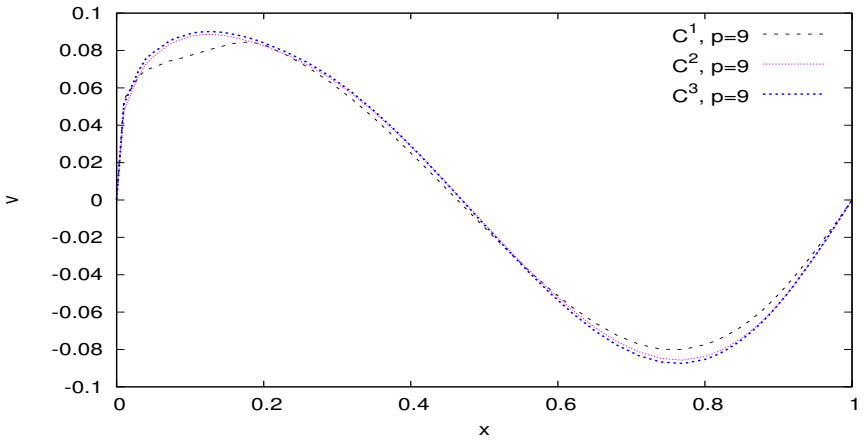

(a) Velocity v versus x at y=0.5

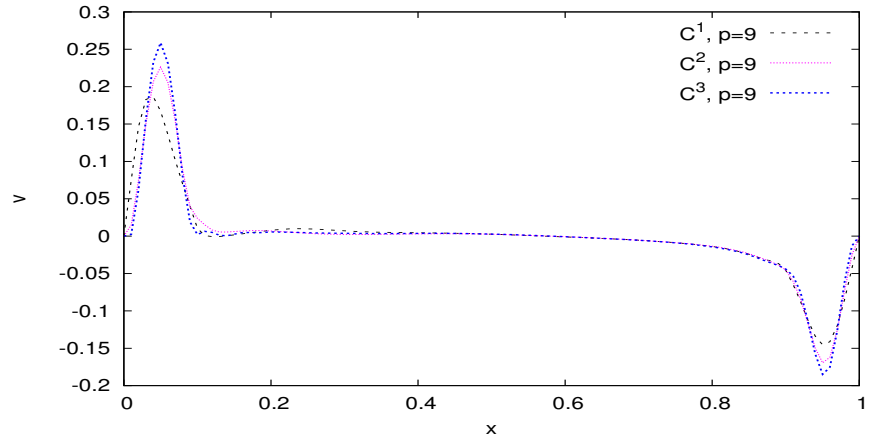

(b) Velocity v versus x at y=0.99

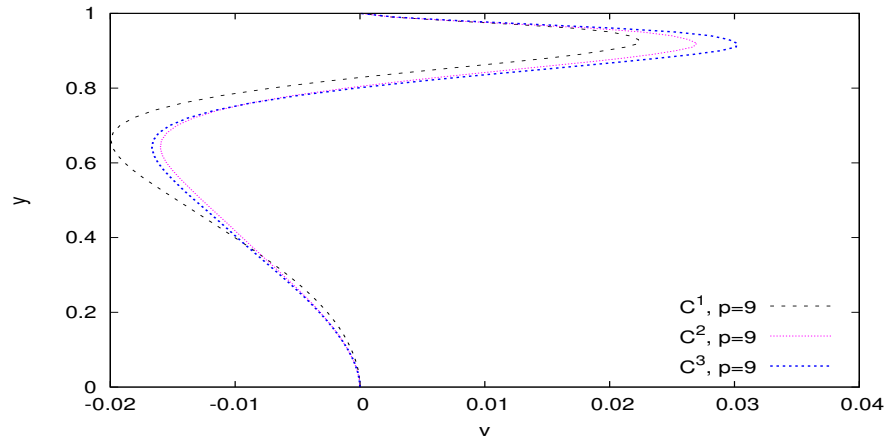

(c) Velocity v versus y at x=0.5

Figure 4.46: Comparison of solutions for mesh M1 (36 elm, h_d = 0.1); $De = 2.4$

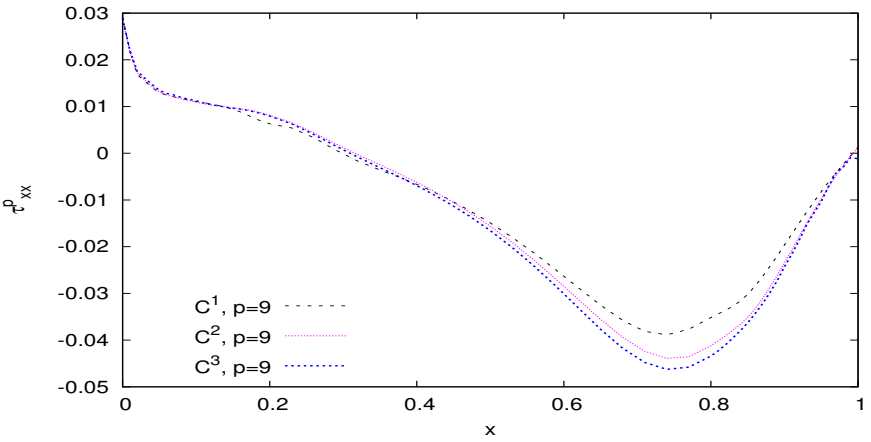

(a) Normal Stress τ^p_{xx} versus x at y=0.5

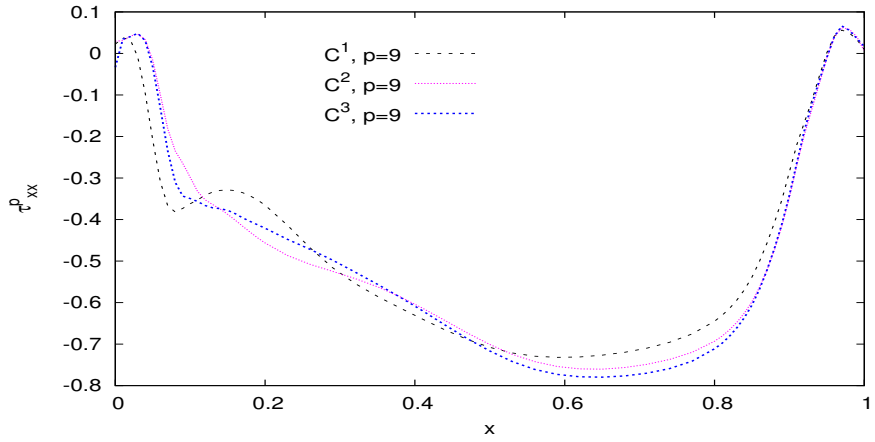

(b) Normal Stress τ^p_{xx} versus x at y=0.99

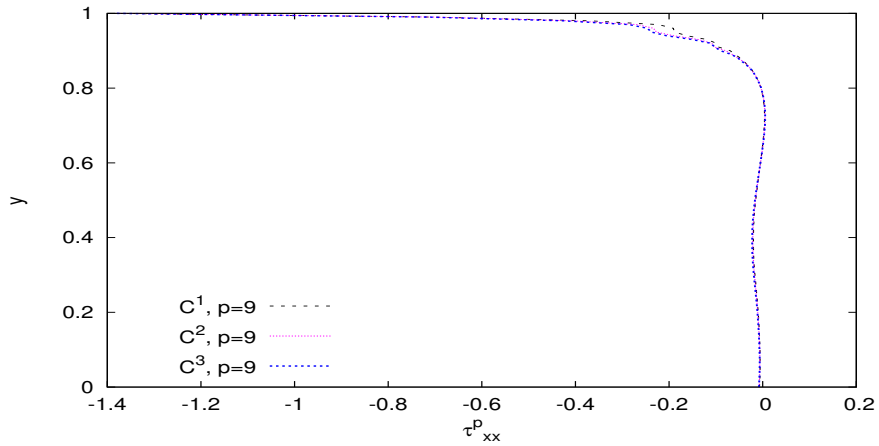

(c) Normal Stress τ^p_{xx} versus y at x=0.5

Figure 4.47: Comparison of solutions for mesh M1 (36 elm, h_d = 0.1); $De = 2.4$

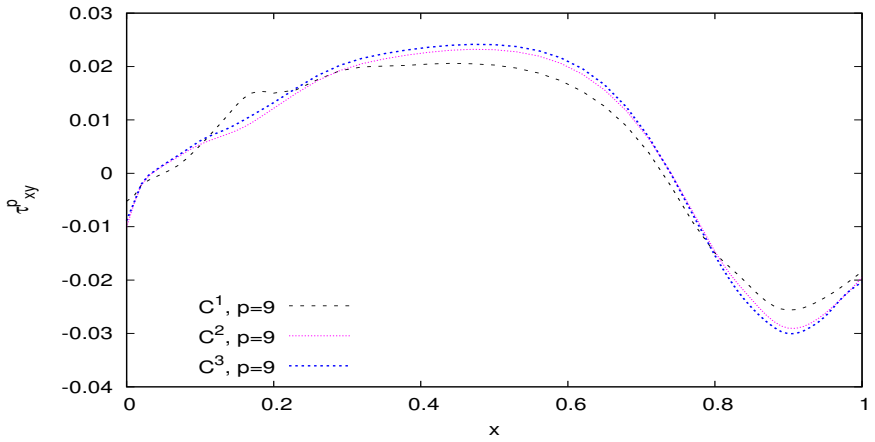

(a) Shear Stress τ^p_{xy} versus x at y=0.5

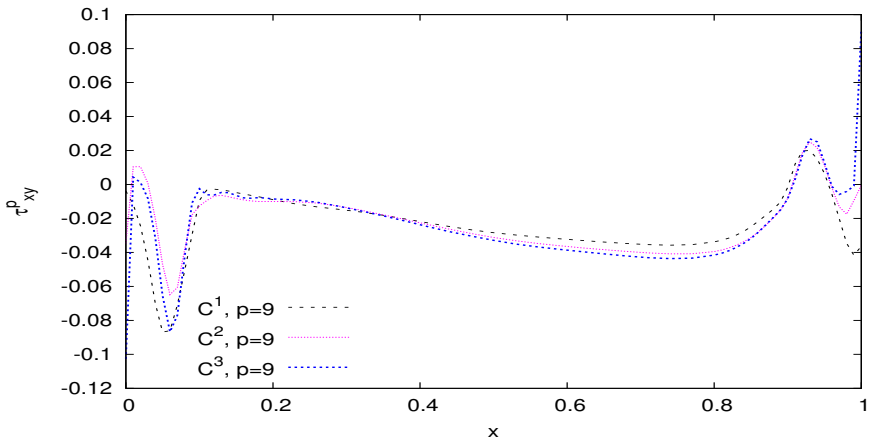

(b) Shear Stress τ^p_{xy} versus x at y=0.99

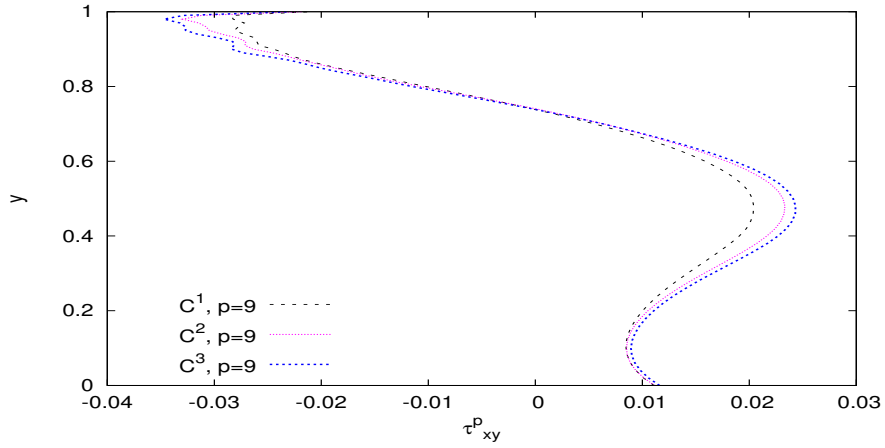

(c) Shear Stress τ^p_{xy} versus y at x=0.5

Figure 4.48: Comparison of solutions for mesh M1 (36 elm, h_d = 0.1); $De = 2.4$

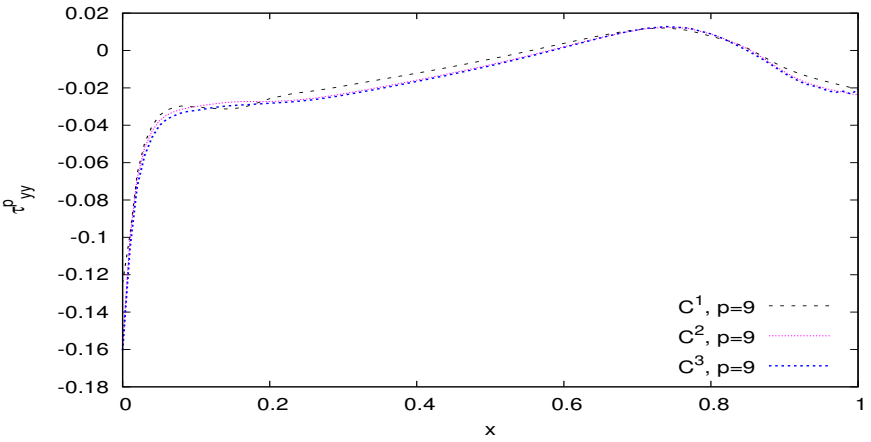

(a) Normal Stress τ^p_{yy} versus x at y=0.5

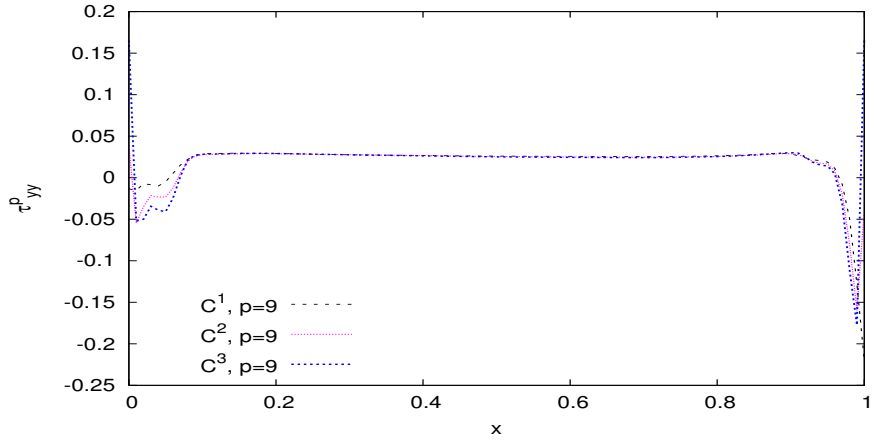

(b) Normal Stress τ^p_{yy} versus x at y=0.99

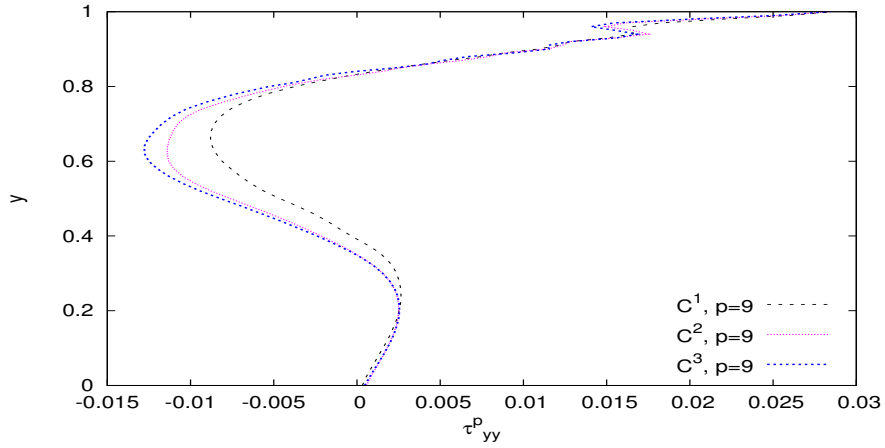

(c) Normal Stress τ^p_{yy} versus y at x=0.5

Figure 4.49: Comparison of solutions for mesh M1 (36 elm, h_d = 0.1); $De = 2.4$

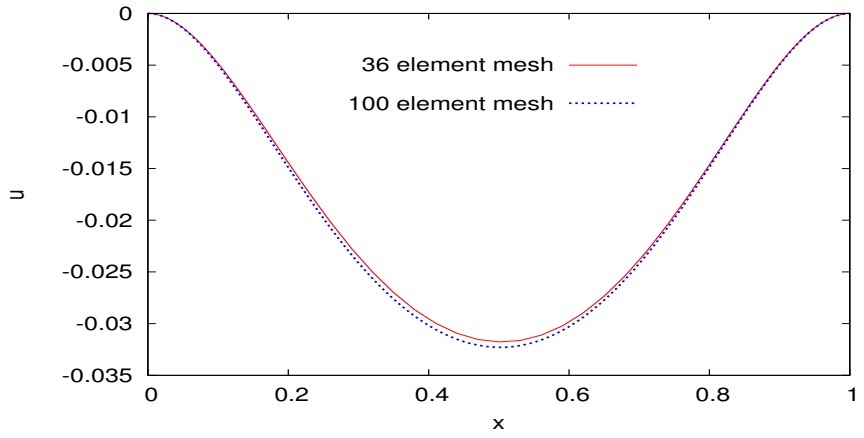

(a) Velocity u versus x at y=0.5

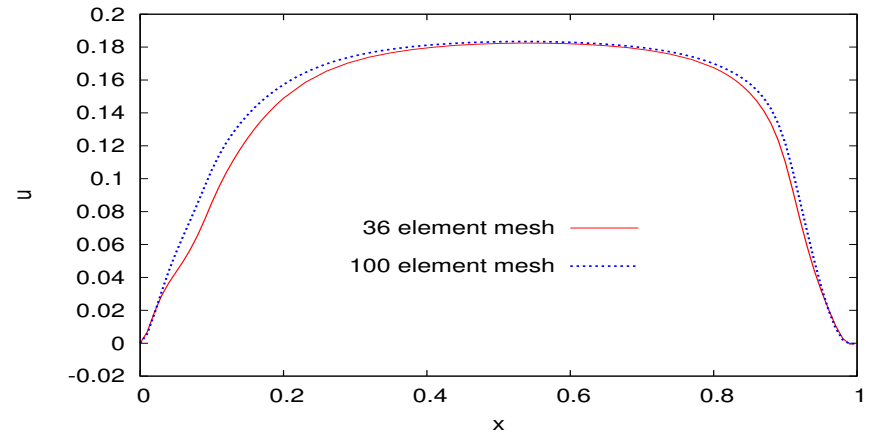

(b) Velocity u versus x at y=0.99

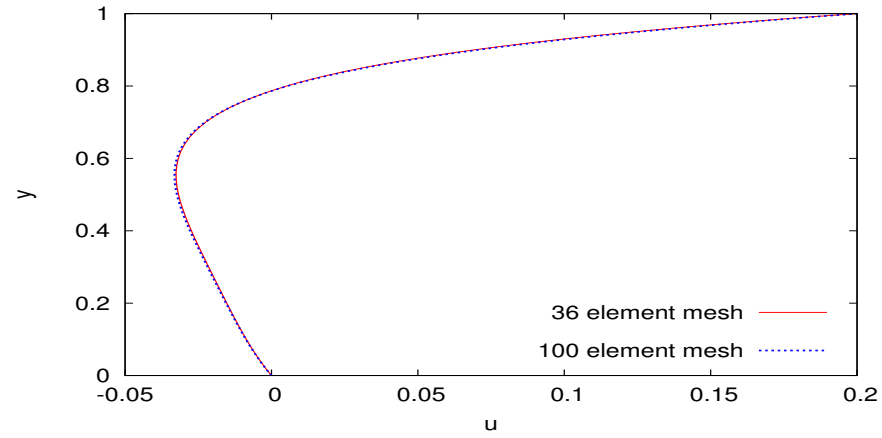

(c) Velocity u versus y at x=0.5

Figure 4.50: Solutions of class C^2 for mesh M1 (h_d = 0.1) ; p=9 and mesh M2 (h_d = 0.1) ; p=7, $De = 0.24$

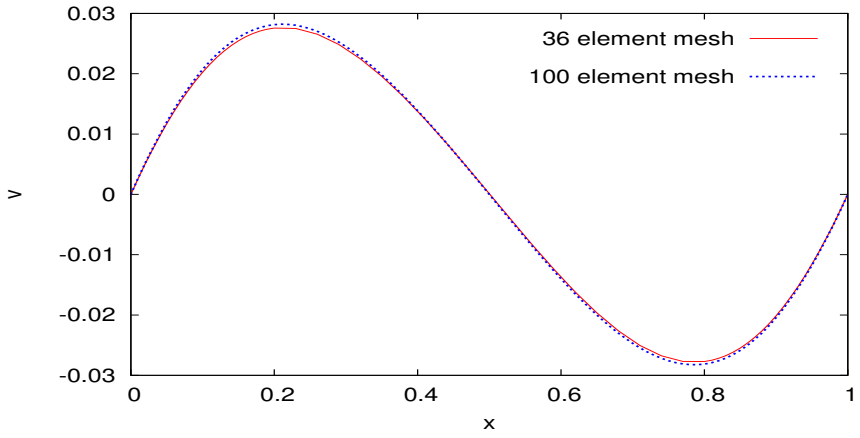

(a) Velocity v versus x at y=0.5

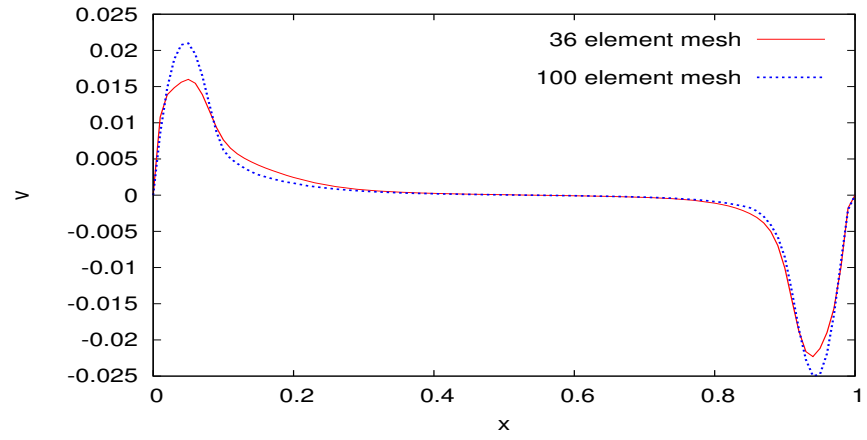

(b) Velocity v versus x at y=0.99

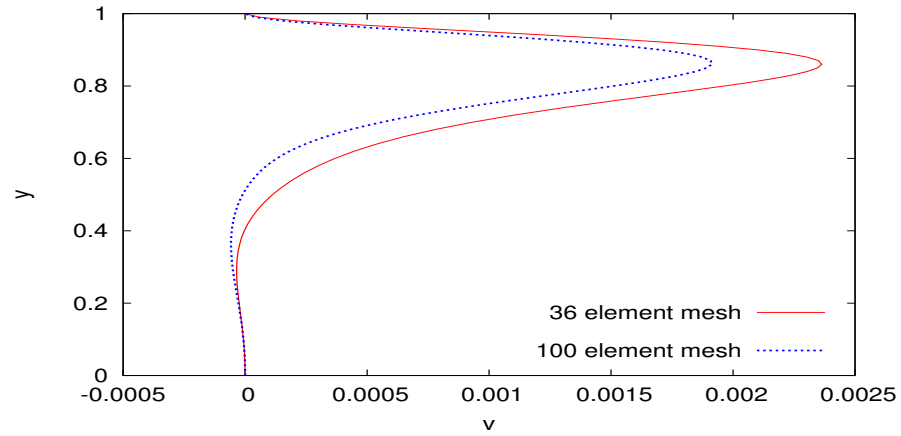

(c) Velocity v versus y at x=0.5

Figure 4.51: Solutions of class C^2 for mesh M1 (h_d = 0.1) ; p=9 and mesh M2 (h_d = 0.1) ; p=7, $De = 0.24$

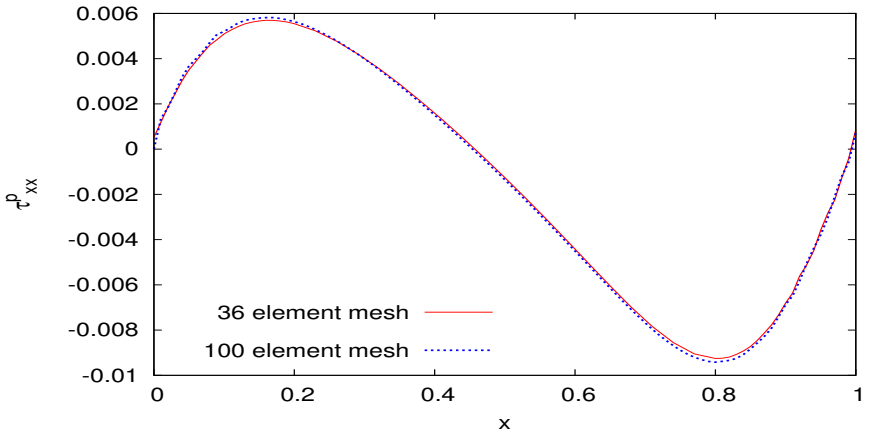

(a) Normal Stress τ^p_{xx} versus x at y=0.5

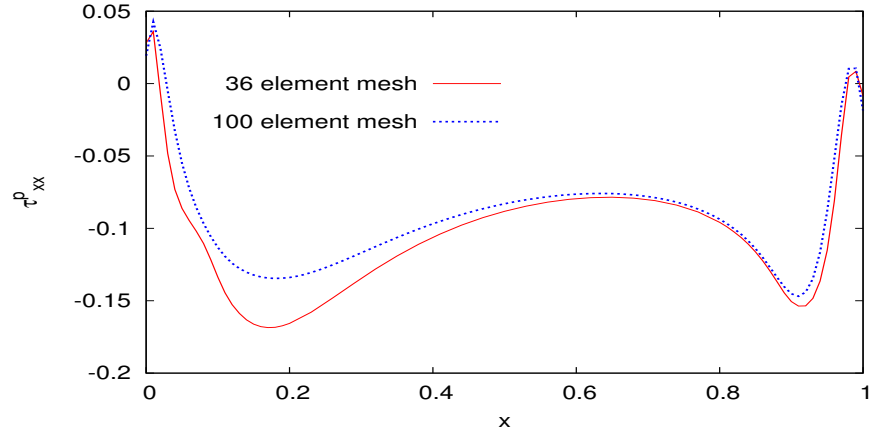

(b) Normal Stress τ^p_{xx} versus x at y=0.99

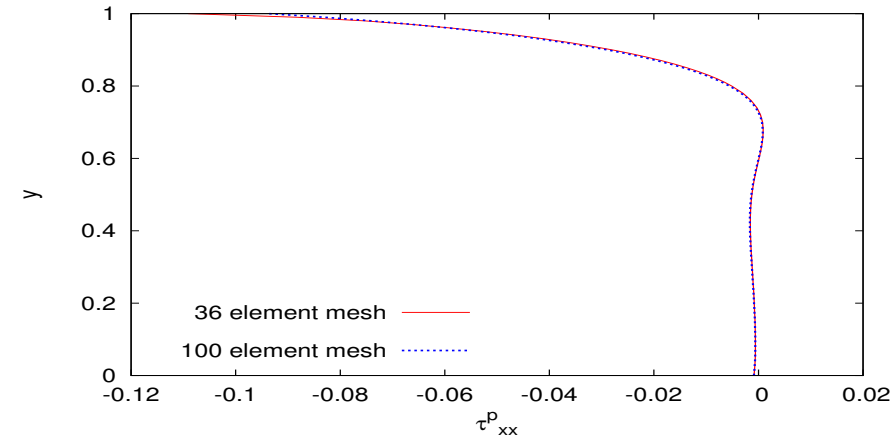

(c) Normal Stress τ^p_{xx} versus y at x=0.5

Figure 4.52: Solutions of class C^2 for mesh M1 (h_d = 0.1) ; p=9 and mesh M2 (h_d = 0.1) ; p=7, $De = 0.24$

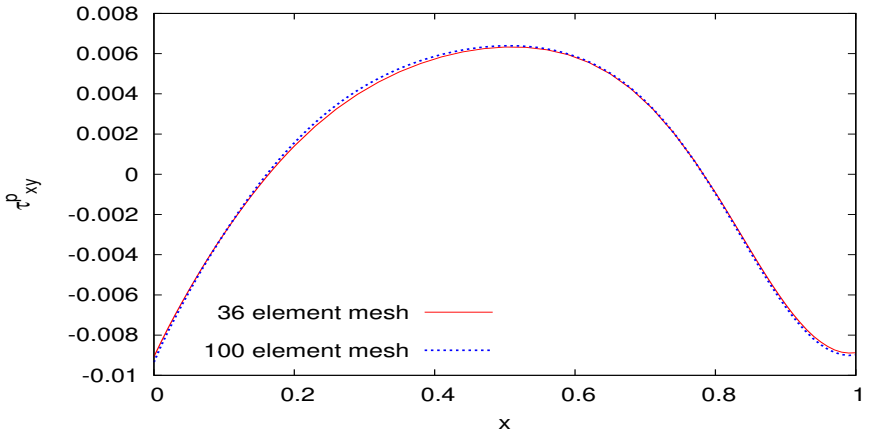

(a) Shear Stress τ^p_{xy} versus x at y=0.5

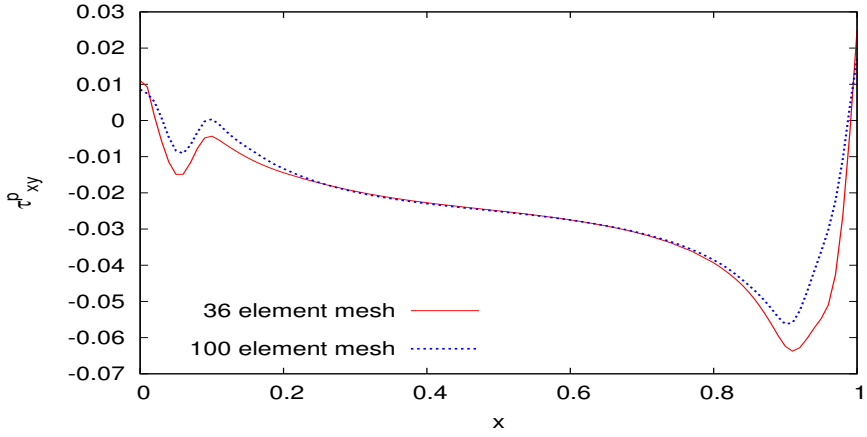

(b) Shear Stress τ^p_{xy} versus x at y=0.99

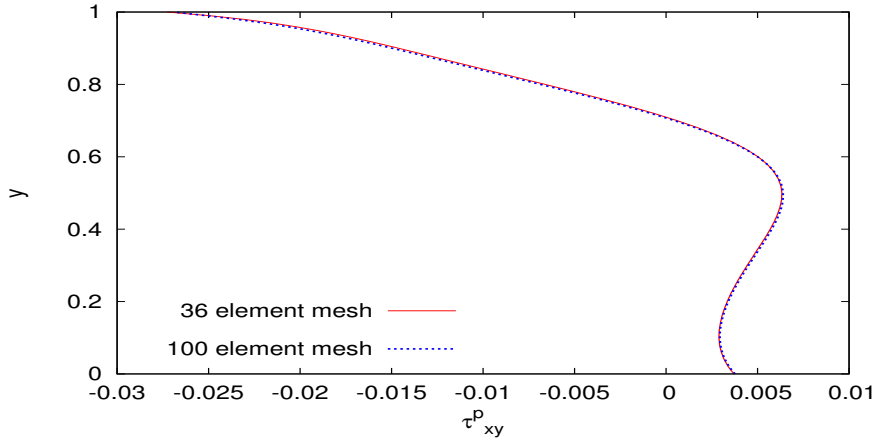

(c) Shear Stress τ^p_{xy} versus y at x=0.5

Figure 4.53: Solutions of class C^2 for mesh M1 (h_d = 0.1) ; p=9 and mesh M2 (h_d = 0.1) ; p=7, $De = 0.24$

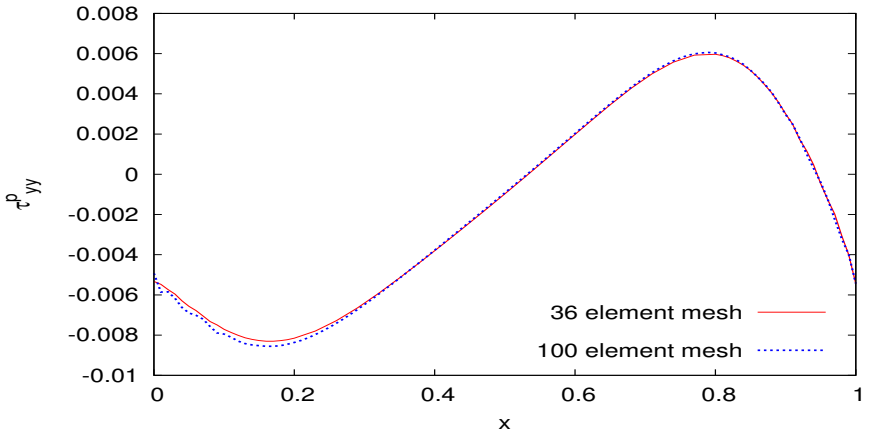

(a) Normal Stress τ^p_{yy} versus x at y=0.5

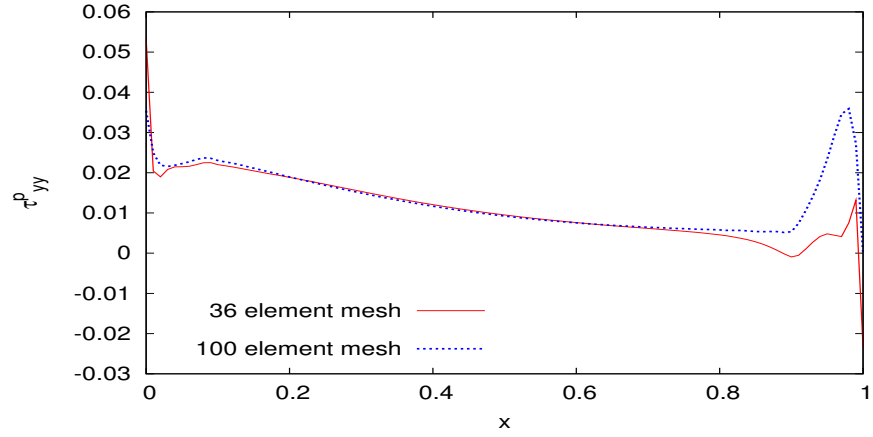

(b) Normal Stress τ^p_{yy} versus x at y=0.99

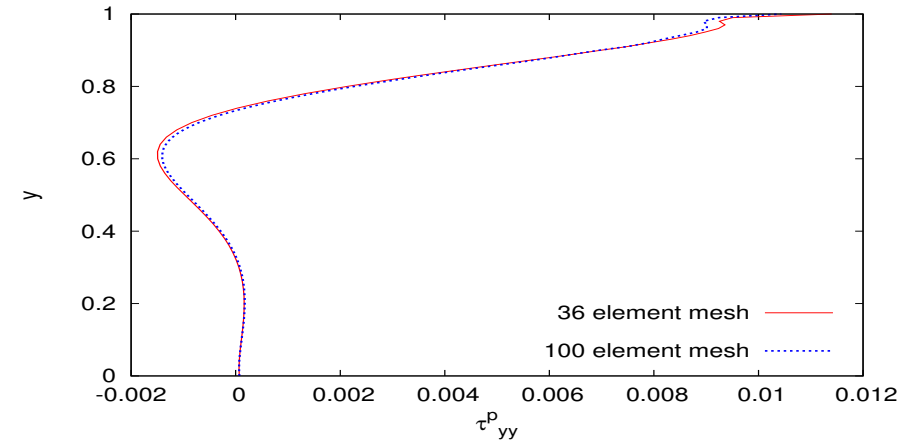

(c) Normal Stress τ^p_{yy} versus y at x=0.5

Figure 4.54: Solutions of class C^2 for mesh M1 (h_d = 0.1) ; p=9 and mesh M2 (h_d = 0.1) ; p=7, $De = 0.24$

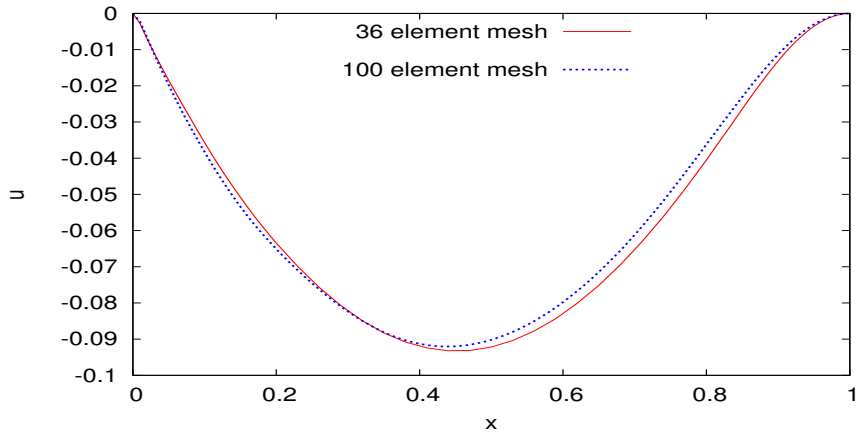

(a) Velocity u versus x at y=0.5

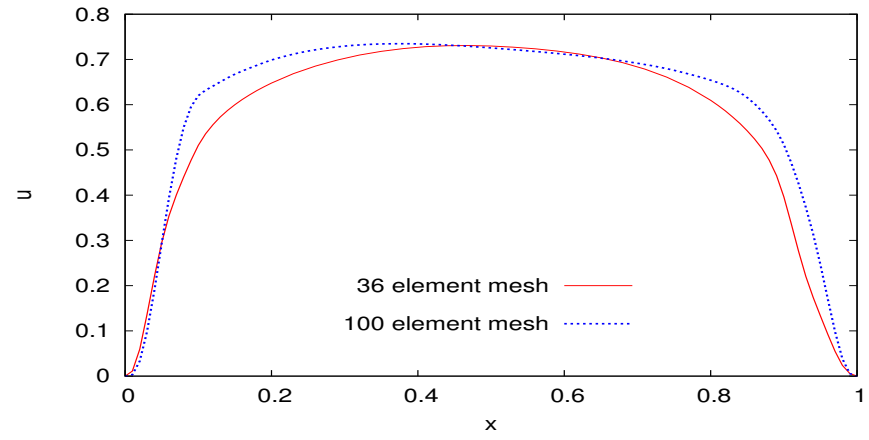

(b) Velocity u versus x at y=0.99

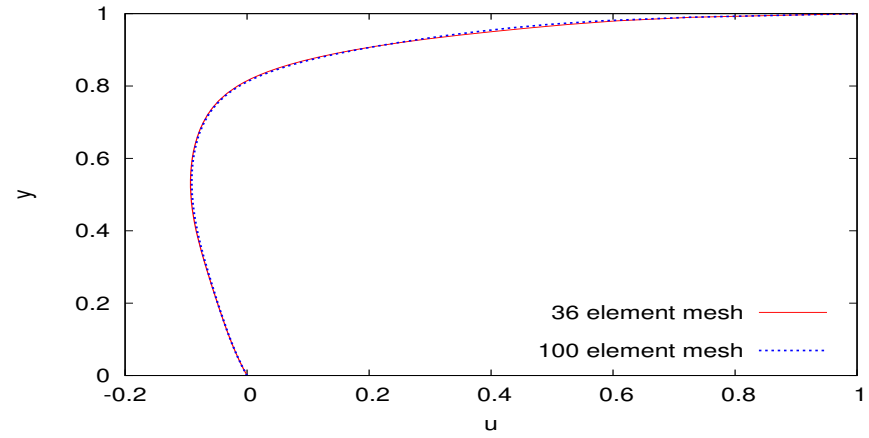

(c) Velocity u versus y at x=0.5

Figure 4.55: Solutions of class C^2 for mesh M1 (h_d = 0.1) ; p=9 and mesh M2 (h_d = 0.1) ; p=7, $De = 1.2$

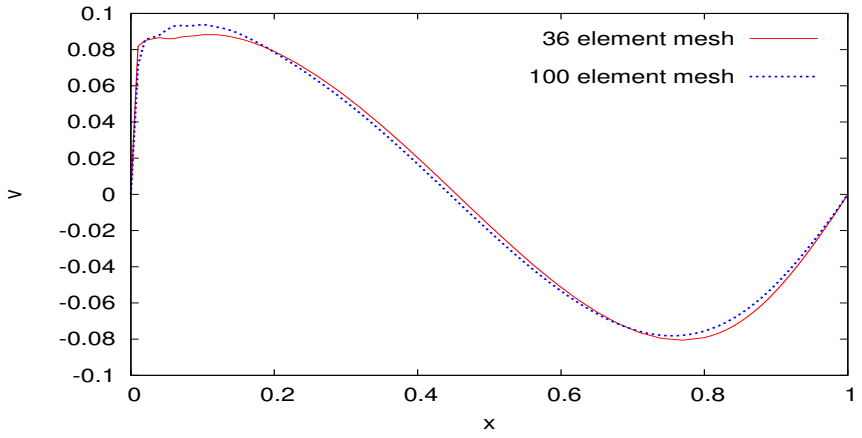

(a) Velocity v versus x at y=0.5

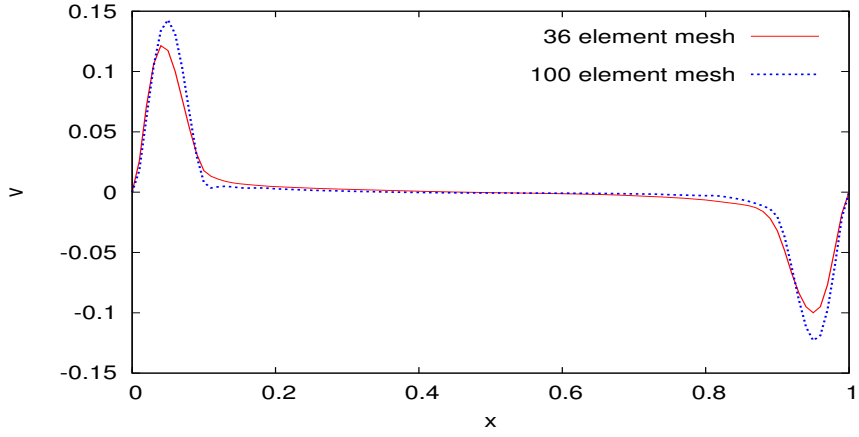

(b) Velocity v versus x at y=0.99

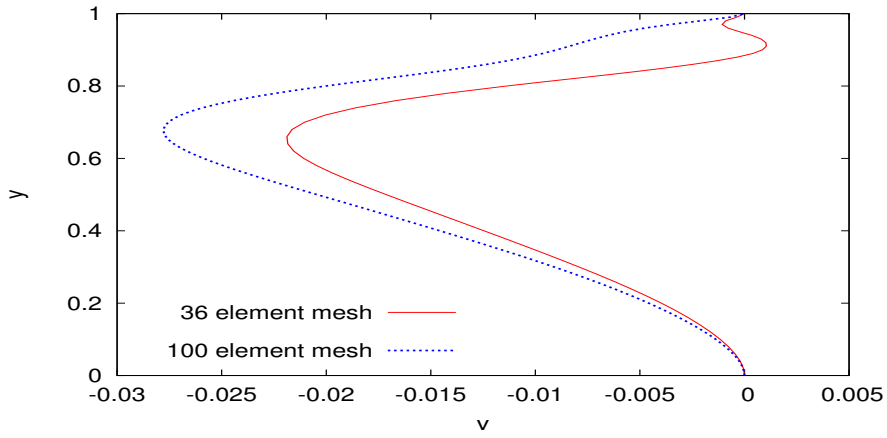

(c) Velocity v versus y at x=0.5

Figure 4.56: Solutions of class C^2 for mesh M1 (h_d = 0.1) ; p=9 and mesh M2 (h_d = 0.1) ; p=7, $De = 1.2$

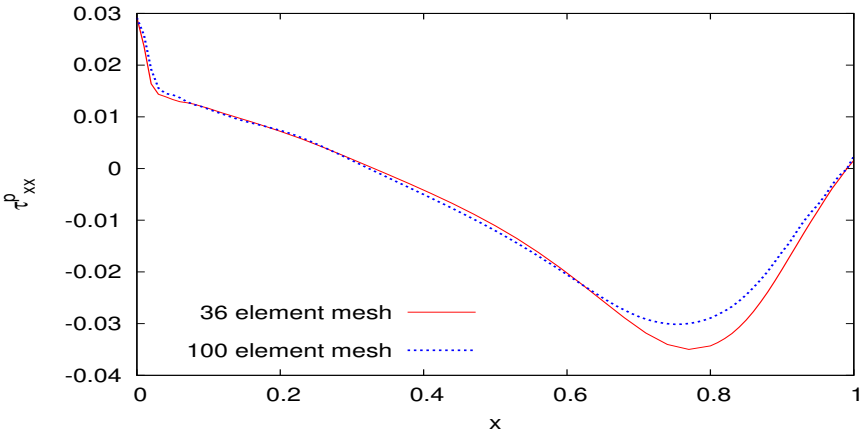

(a) Normal Stress τ^p_{xx} versus x at y=0.5

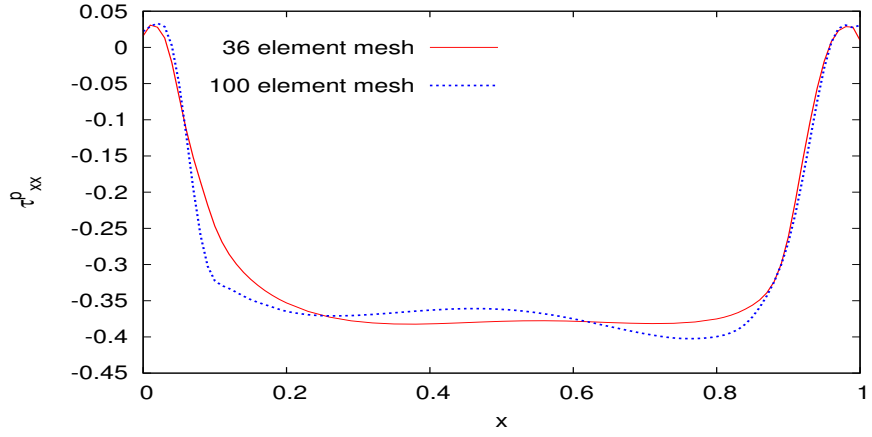

(b) Normal Stress τ^p_{xx} versus x at y=0.99

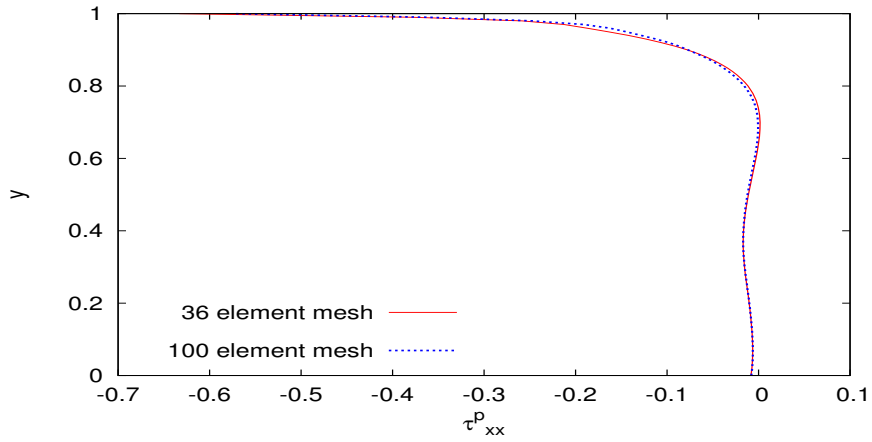

(c) Normal Stress τ^p_{xx} versus y at x=0.5

Figure 4.57: Solutions of class C^2 for mesh M1 (h_d = 0.1) ; p=9 and mesh M2 (h_d = 0.1) ; p=7, $De = 1.2$

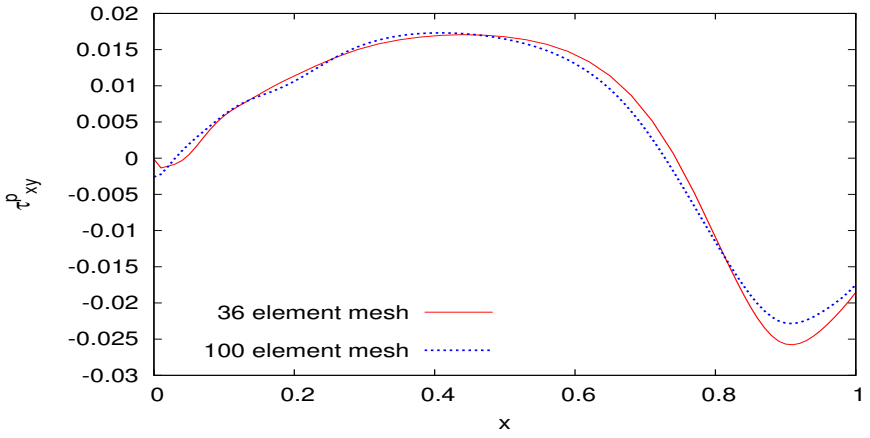

(a) Shear Stress τ^p_{xy} versus x at y=0.5

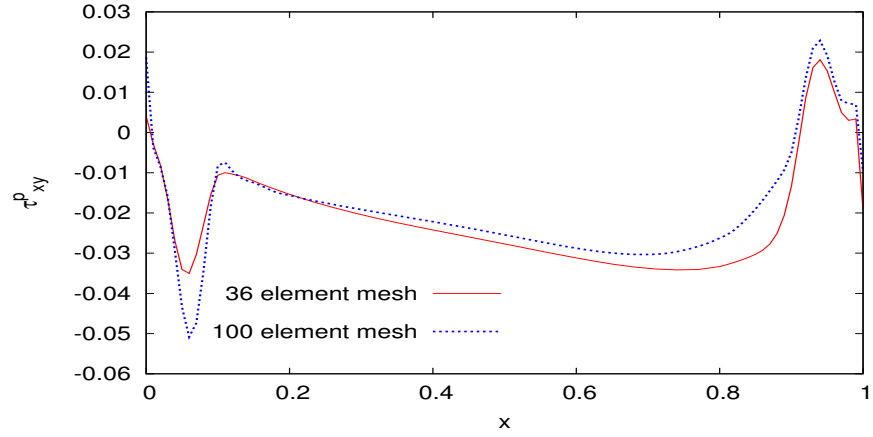

(b) Shear Stress τ^p_{xy} versus x at y=0.99

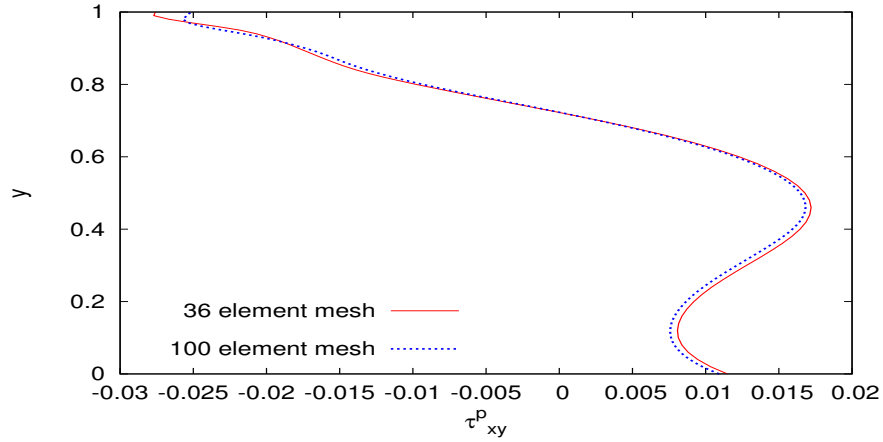

(c) Shear Stress τ^p_{xy} versus y at x=0.5

Figure 4.58: Solutions of class C^2 for mesh M1 (h_d = 0.1) ; p=9 and mesh M2 (h_d = 0.1) ; p=7, $De = 1.2$

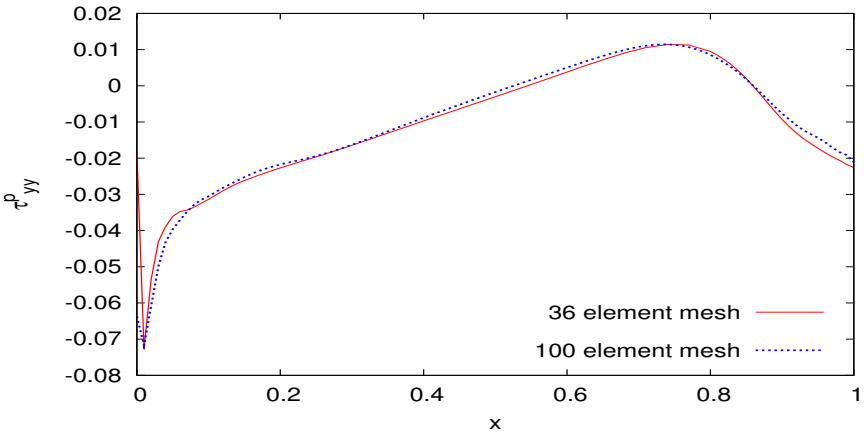

(a) Normal Stress τ^p_{yy} versus x at y=0.5

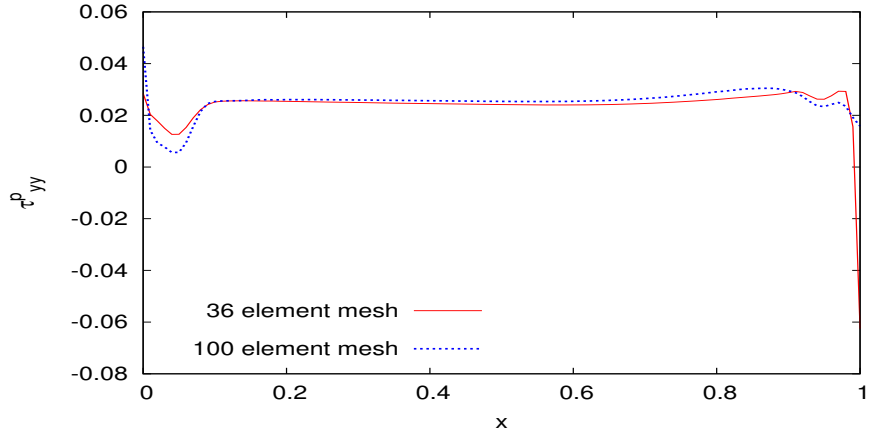

(b) Normal Stress τ^p_{yy} versus x at y=0.99

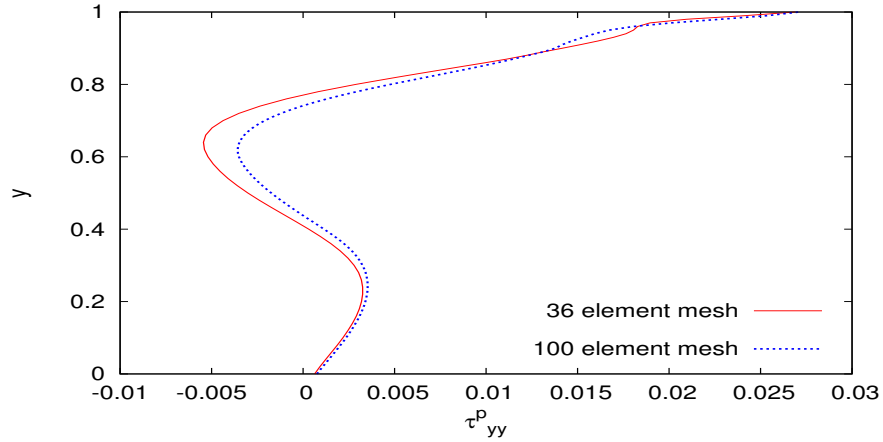

(c) Normal Stress τ^p_{yy} versus y at x=0.5

Figure 4.59: Solutions of class C^2 for mesh M1 (h_d = 0.1) ; p=9 and mesh M2 (h_d = 0.1) ; p=7, $De = 1.2$

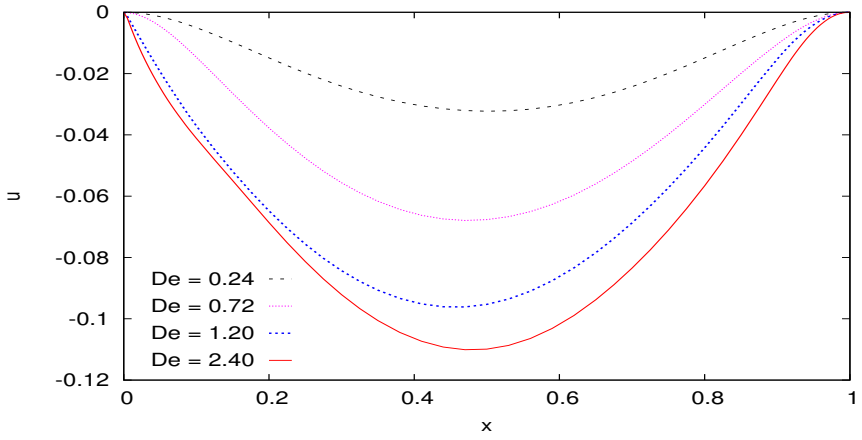

(a) Velocity u versus x at y=0.5

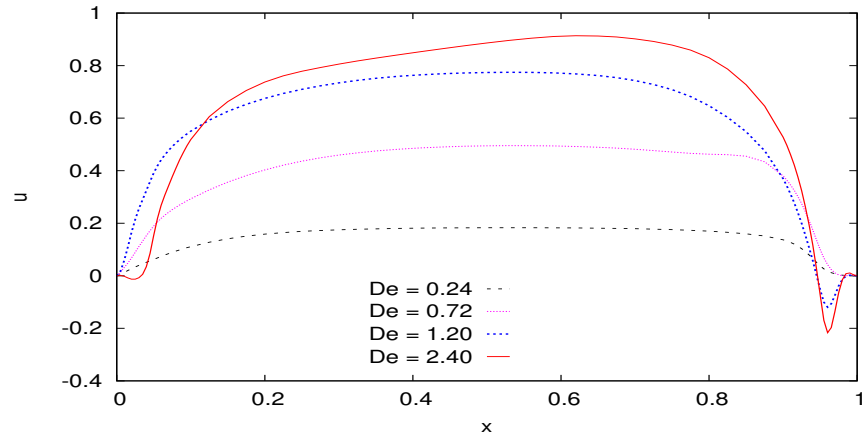

(b) Velocity u versus x at y=0.99

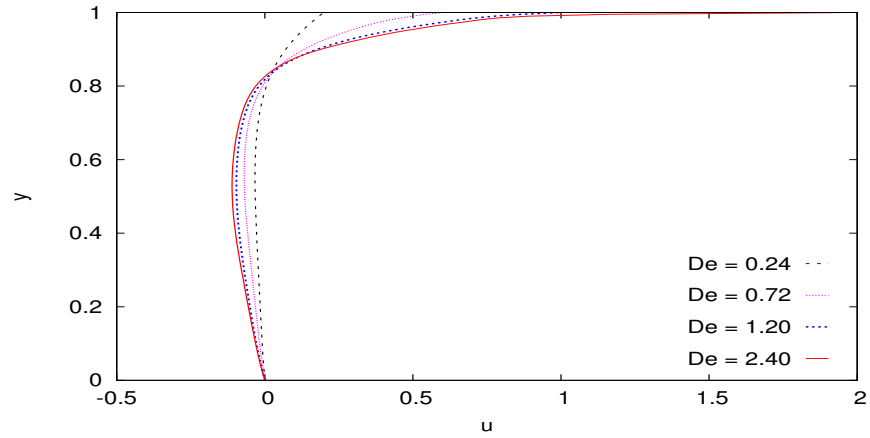

(c) Velocity u versus y at x=0.5

Figure 4.60: Solutions of class C^2 for lid driven cavity for Mesh M3 (49 elm , $h_d = 0.05$); $p = 9$

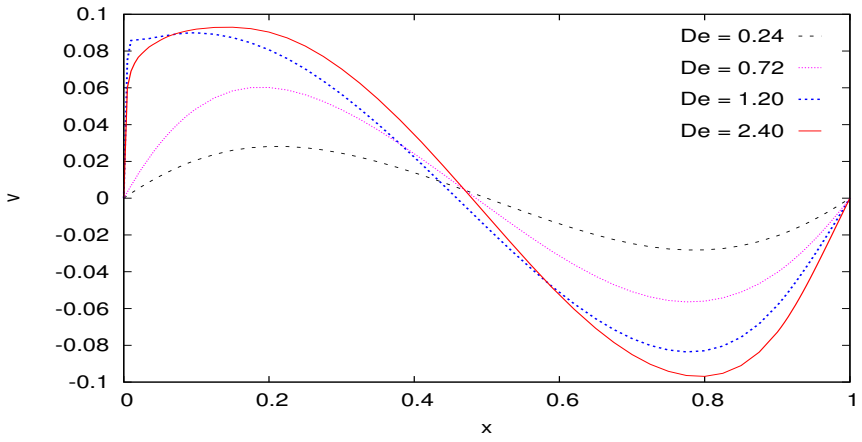

(a) Velocity v versus x at y=0.5

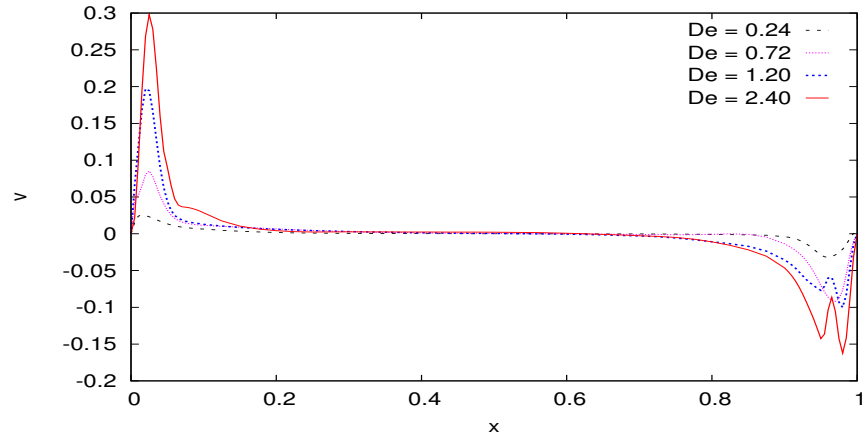

(b) Velocity v versus x at y=0.99

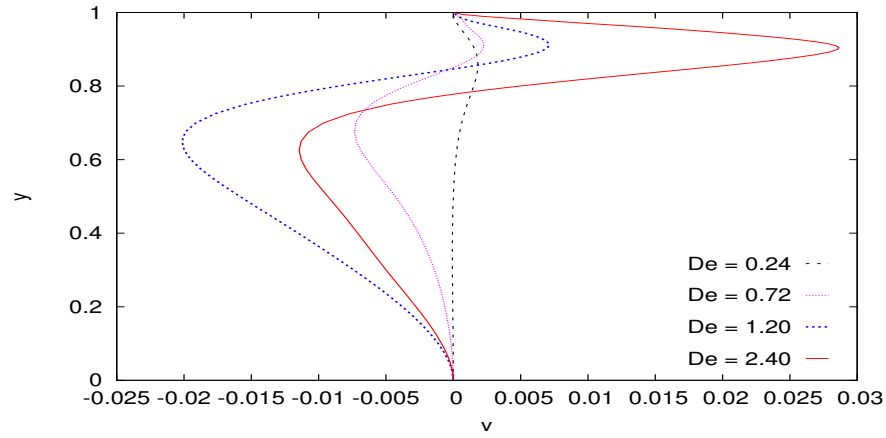

(c) Velocity v versus y at x=0.5

Figure 4.61: Solutions of class C^2 for lid driven cavity for Mesh M3 (49 elm , $h_d = 0.05$); $p = 9$

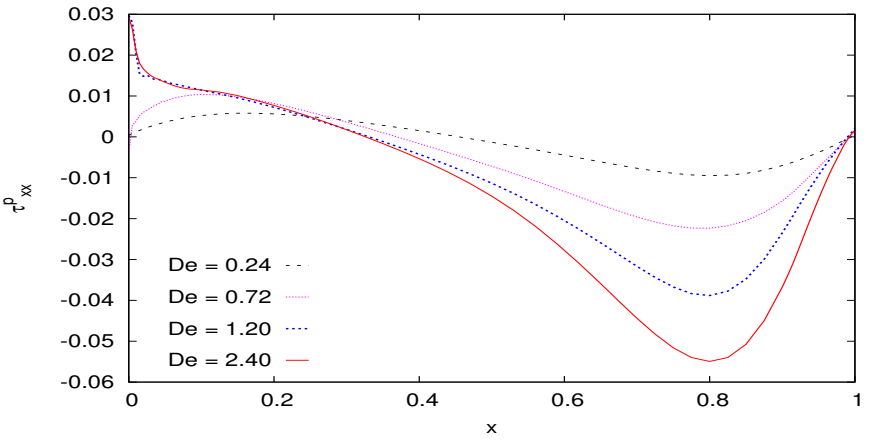

(a) Normal Stress τ^p_{xx} versus x at y=0.5

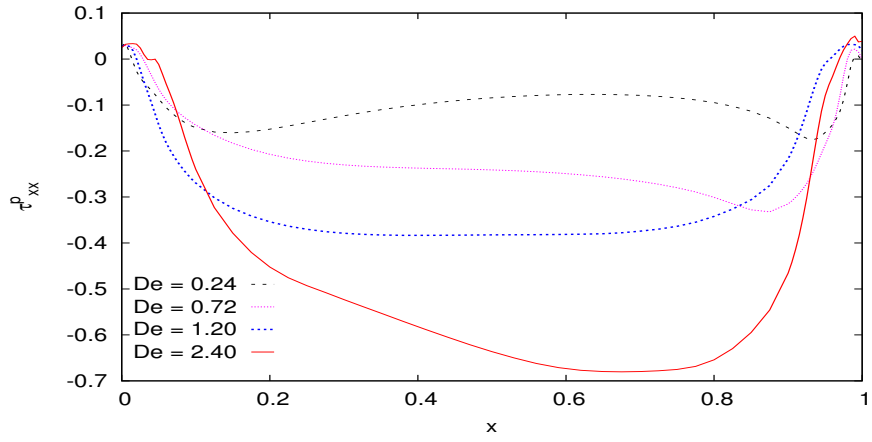

(b) Normal Stress τ^p_{xx} versus x at y=0.99

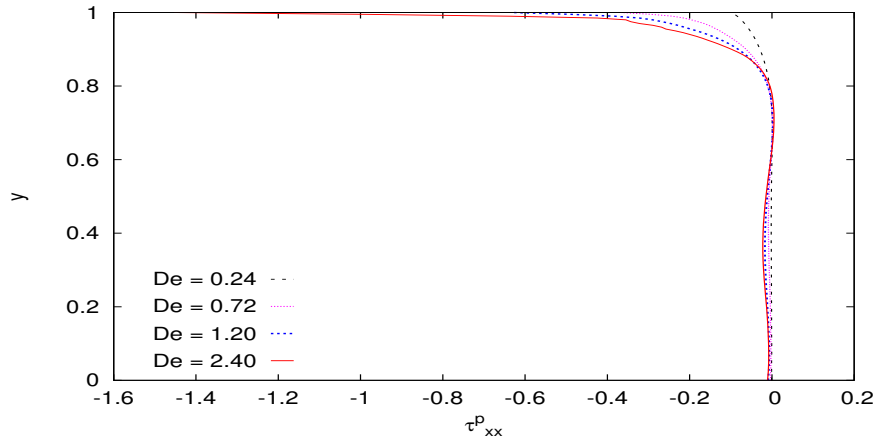

(c) Normal Stress τ^p_{xx} versus y at x=0.5

Figure 4.62: Solutions of class C^2 for lid driven cavity for Mesh M3 (49 elm , $h_d = 0.05$); $p = 9$

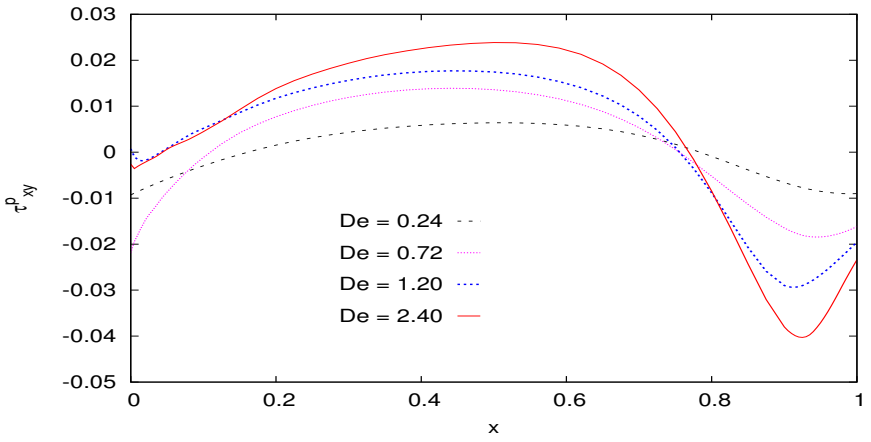

(a) Shear Stress τ^p_{xy} versus x at y=0.5

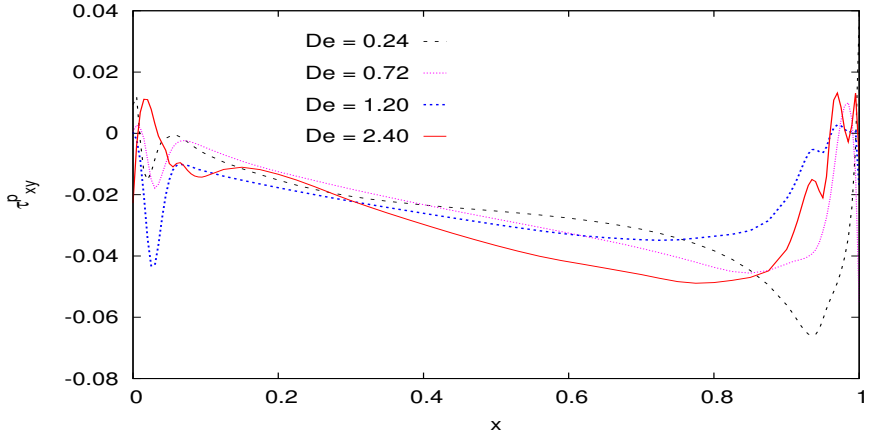

(b) Shear Stress τ^p_{xy} versus x at y=0.99

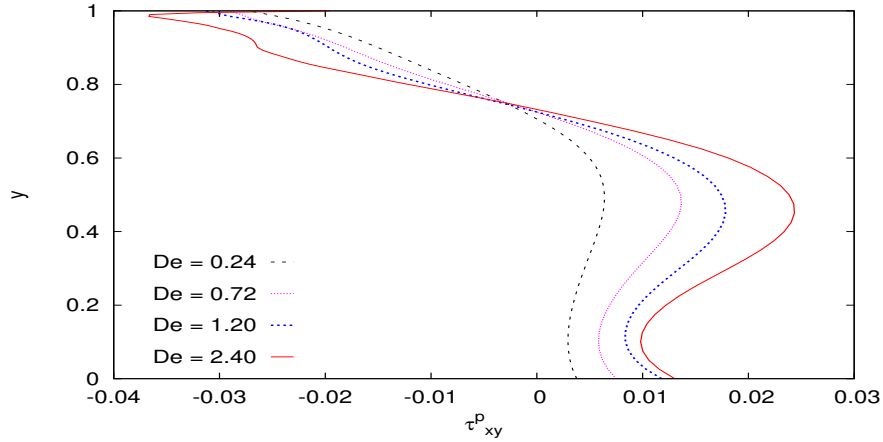

(c) Shear Stress τ^p_{xy} versus y at x=0.5

Figure 4.63: Solutions of class C^2 for lid driven cavity for Mesh M3 (49 elm , $h_d = 0.05$); $p = 9$

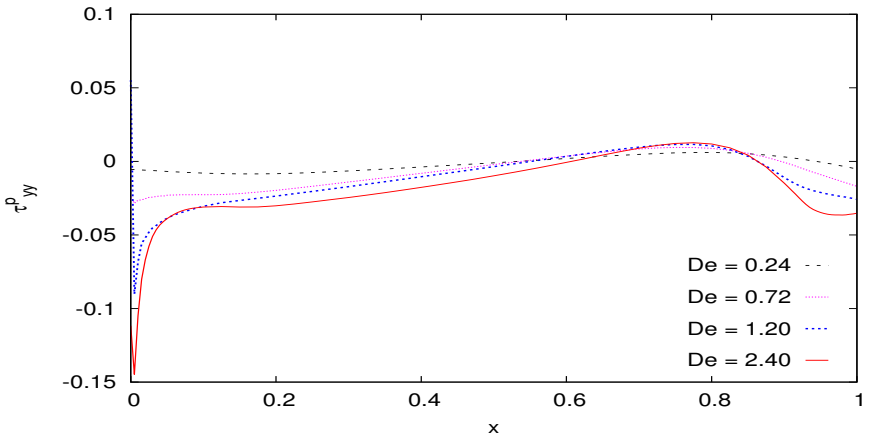

(a) Normal Stress τ^p_{yy} versus x at y=0.5

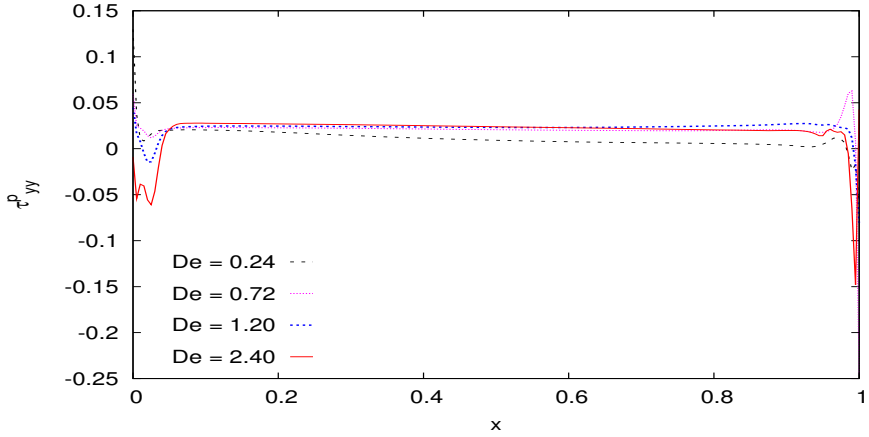

(b) Normal Stress τ^p_{yy} versus x at y=0.99

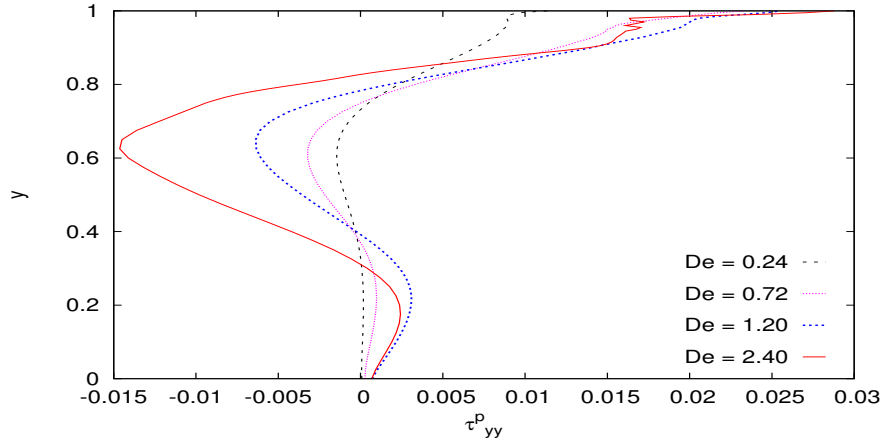

(c) Normal Stress τ^p_{yy} versus y at x=0.5

Figure 4.64: Solutions of class C^2 for lid driven cavity for Mesh M3 (49 elm , $h_d = 0.05$); $p = 9$

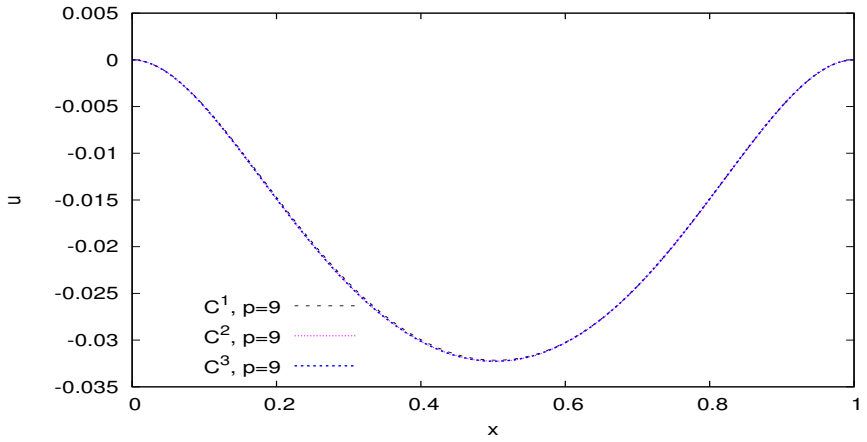

(a) Velocity u versus x at y=0.5

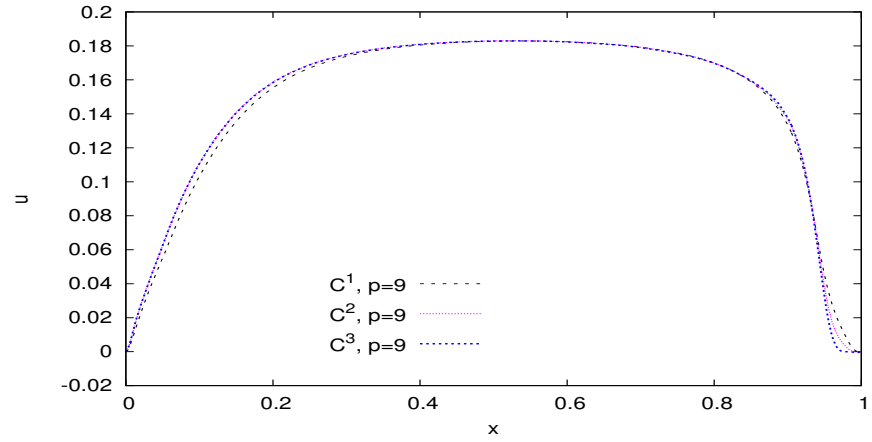

(b) Velocity u versus x at y=0.99

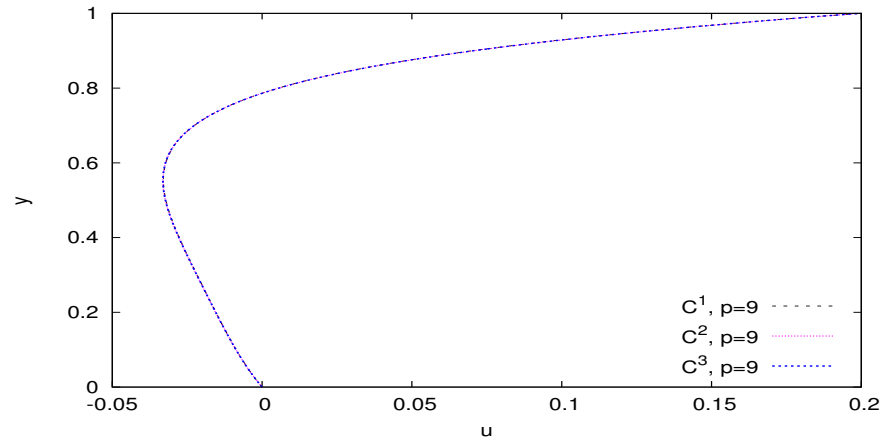

(c) Velocity u versus y at x=0.5

Figure 4.65: Comparison of solutions for mesh M3 (49 elm, h_d = 0.05); $De = 0.24$

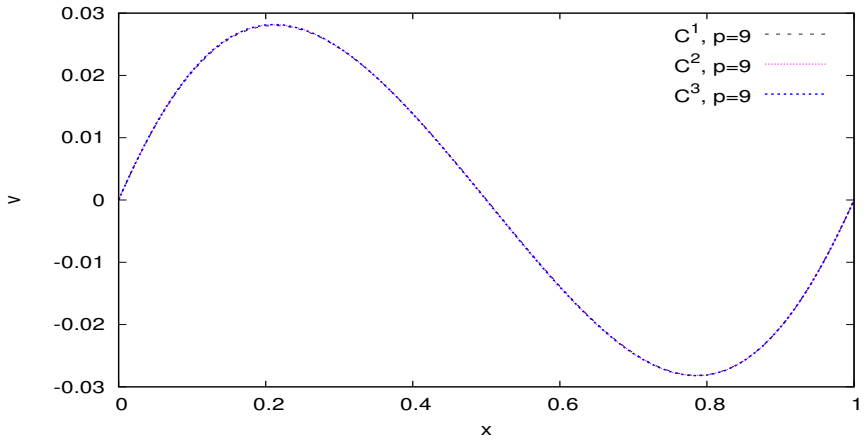

(a) Velocity v versus x at y=0.5

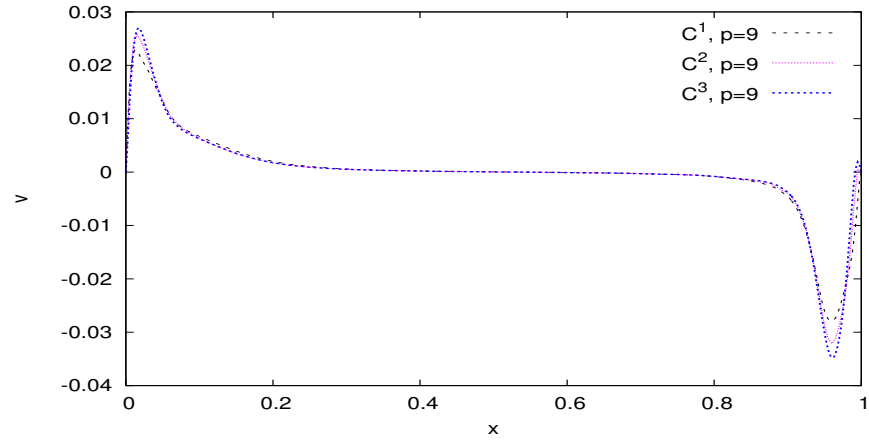

(b) Velocity v versus x at y=0.99

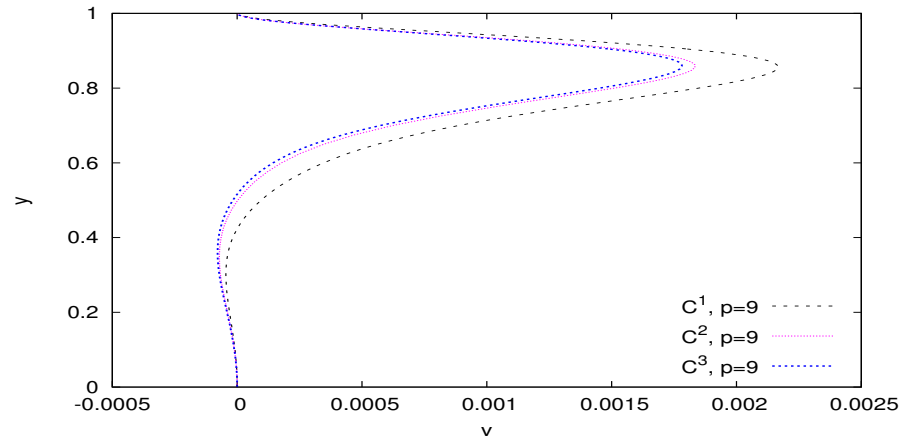

(c) Velocity v versus y at x=0.5

Figure 4.66: Comparison of solutions for mesh M3 (49 elm, h_d = 0.05); $De = 0.24$

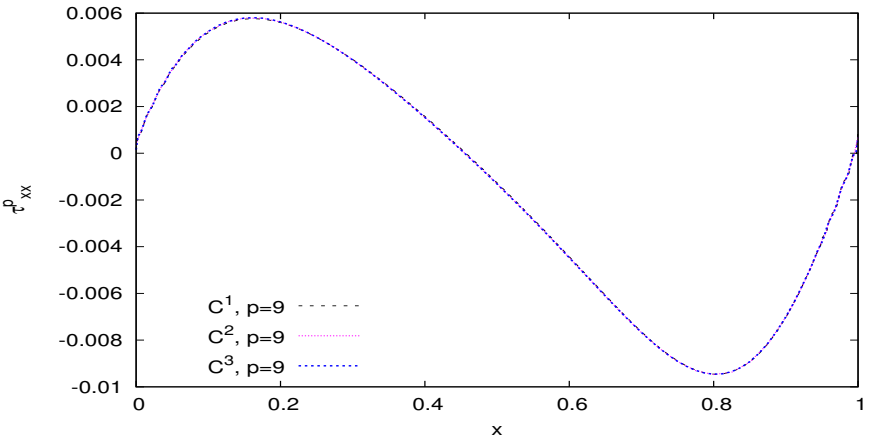

(a) Normal Stress τ^p_{xx} versus x at y=0.5

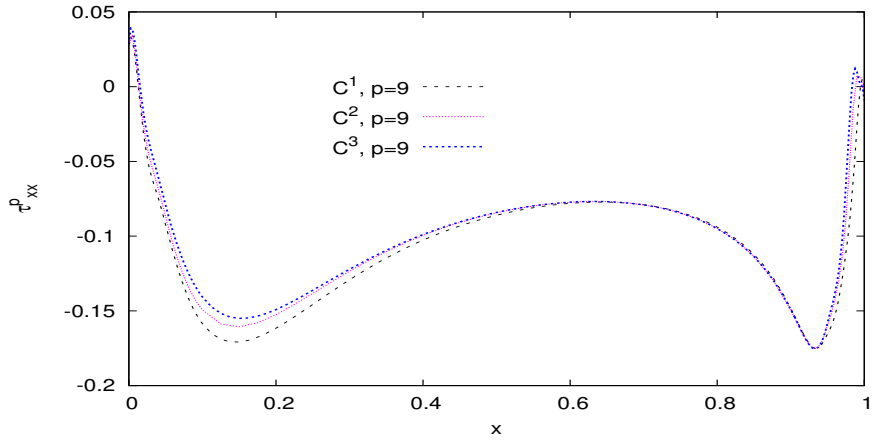

(b) Normal Stress τ^p_{xx} versus x at y=0.99

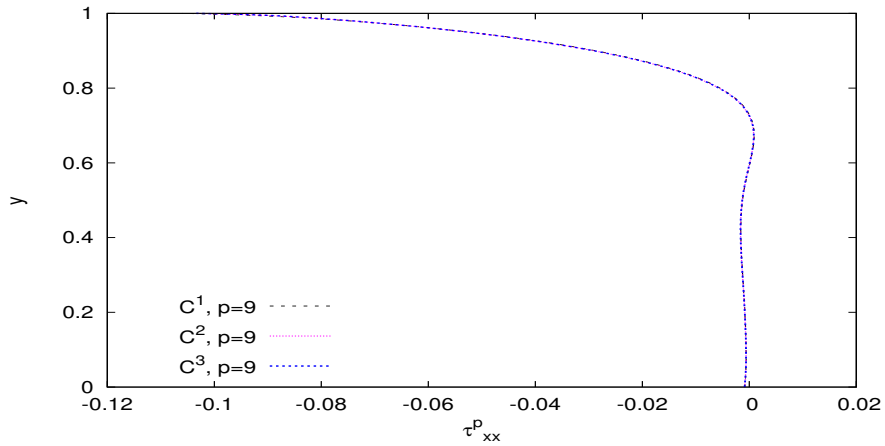

(c) Normal Stress τ^p_{xx} versus y at x=0.5

Figure 4.67: Comparison of solutions for mesh M3 (49 elm, h_d = 0.05); $De = 0.24$

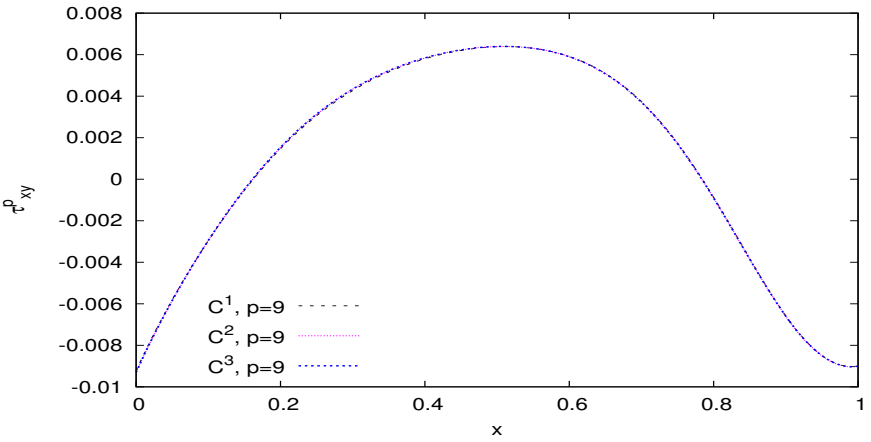

(a) Shear Stress τ^p_{xy} versus x at y=0.5

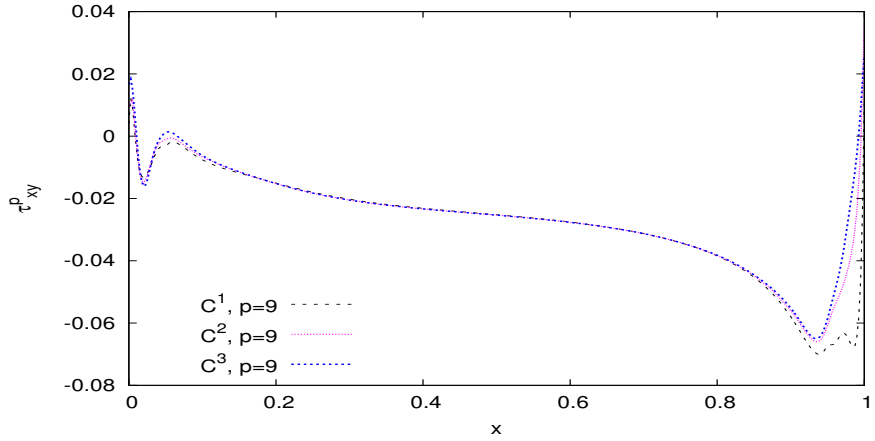

(b) Shear Stress τ^p_{xy} versus x at y=0.99

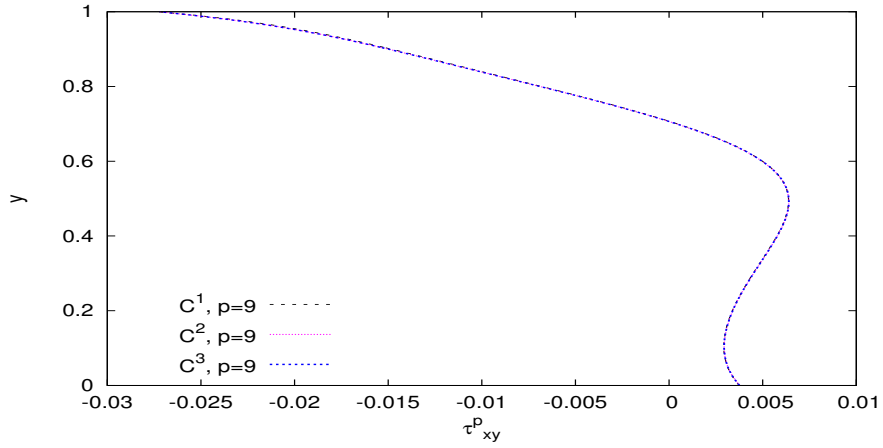

(c) Shear Stress τ^p_{xy} versus y at x=0.5

Figure 4.68: Comparison of solutions for mesh M3 (49 elm, h_d = 0.05); $De = 0.24$

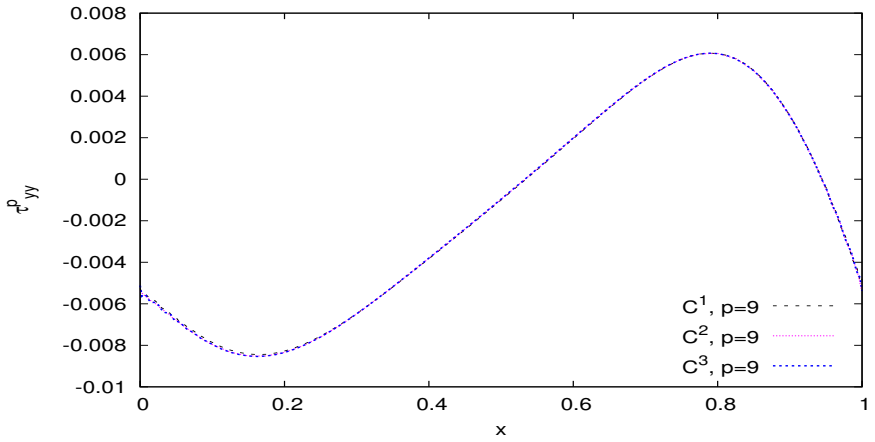

(a) Normal Stress τ^p_{yy} versus x at y=0.5

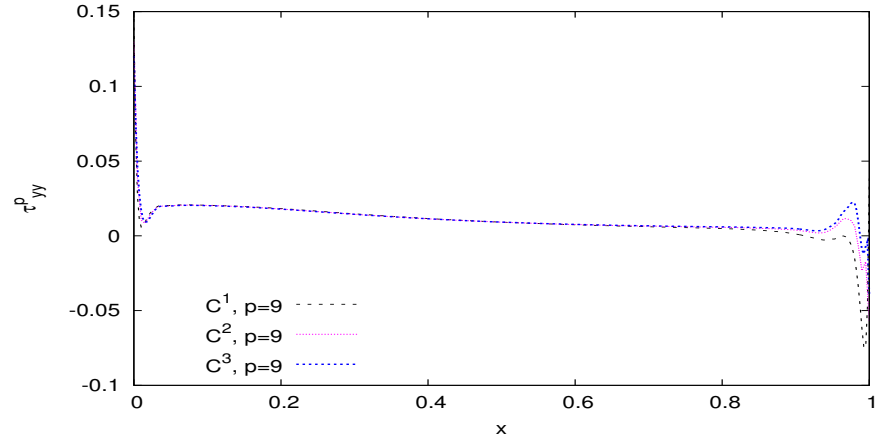

(b) Normal Stress τ^p_{yy} versus x at y=0.99

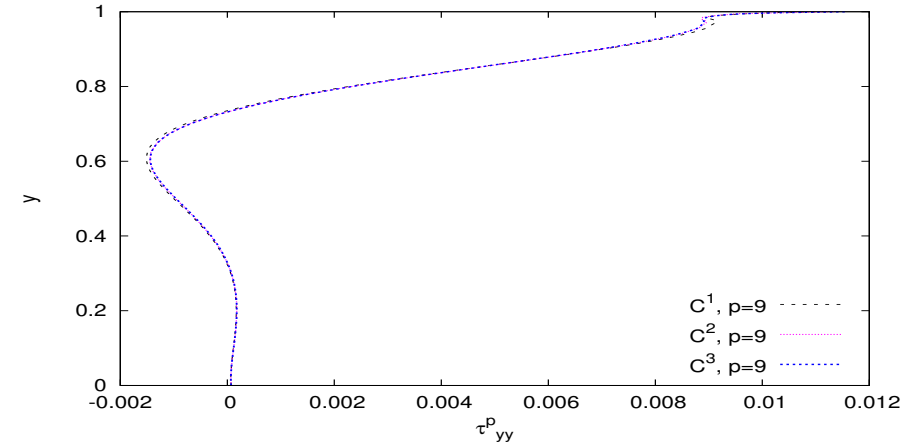

(c) Normal Stress τ^p_{yy} versus y at x=0.5

Figure 4.69: Comparison of solutions for mesh M3 (49 elm, h_d = 0.05); $De = 0.24$

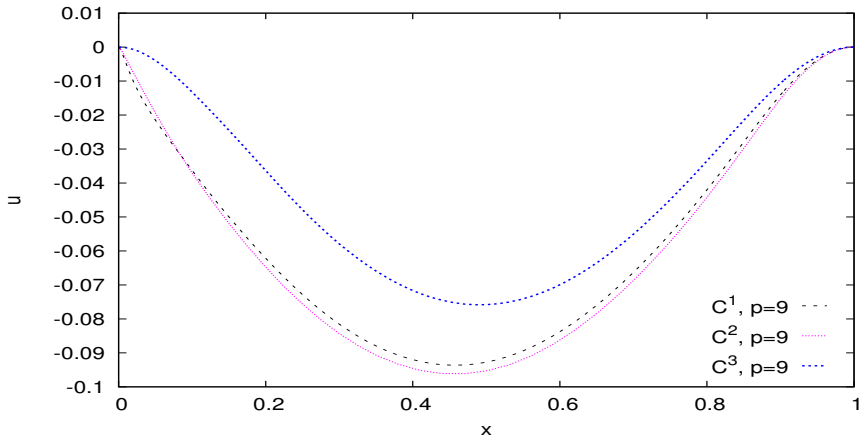

(a) Velocity u versus x at y=0.5

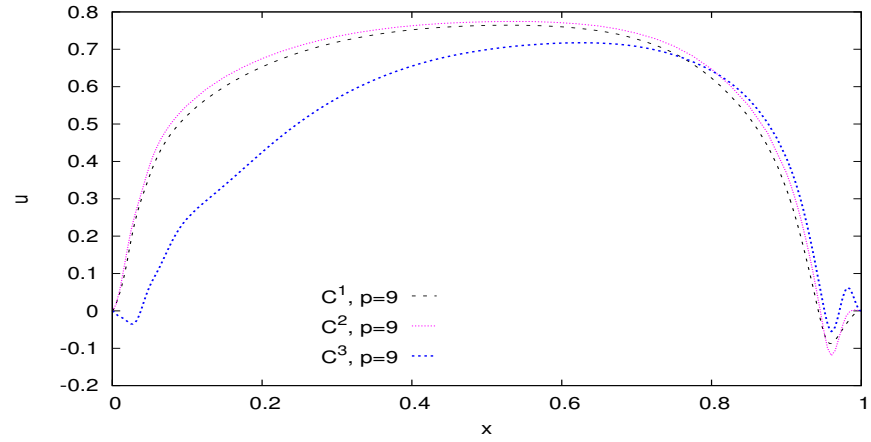

(b) Velocity u versus x at y=0.99

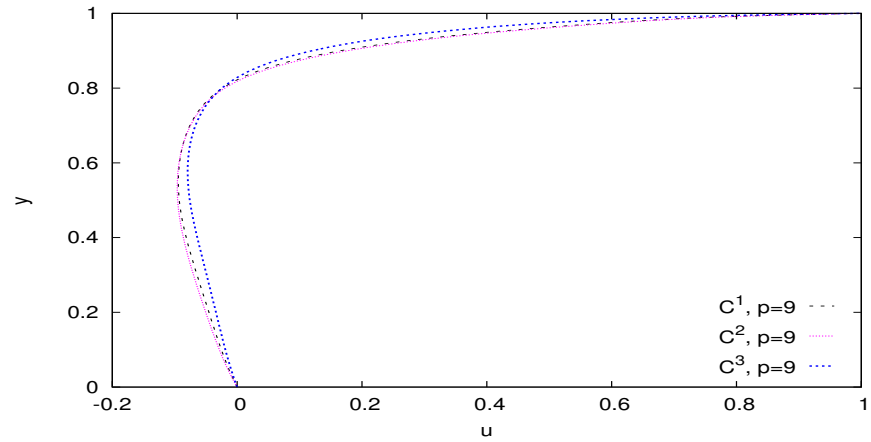

(c) Velocity u versus y at x=0.5

Figure 4.70: Comparison of solutions for mesh M3 (49 elm, h_d = 0.05); $De = 1.2$

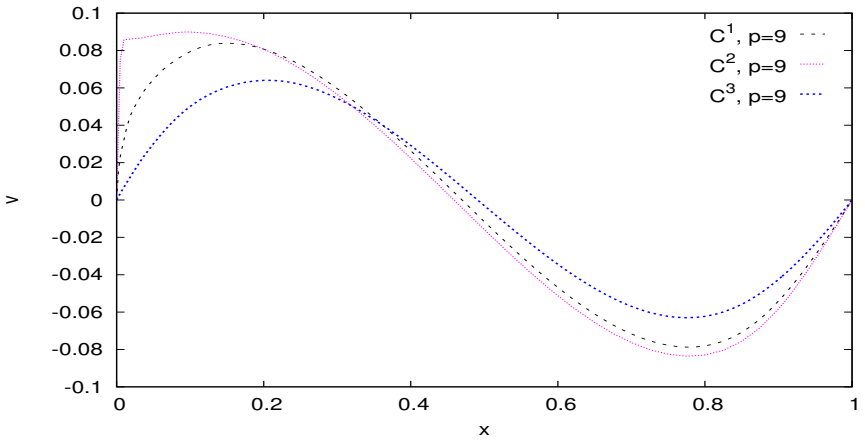

(a) Velocity v versus x at y=0.5

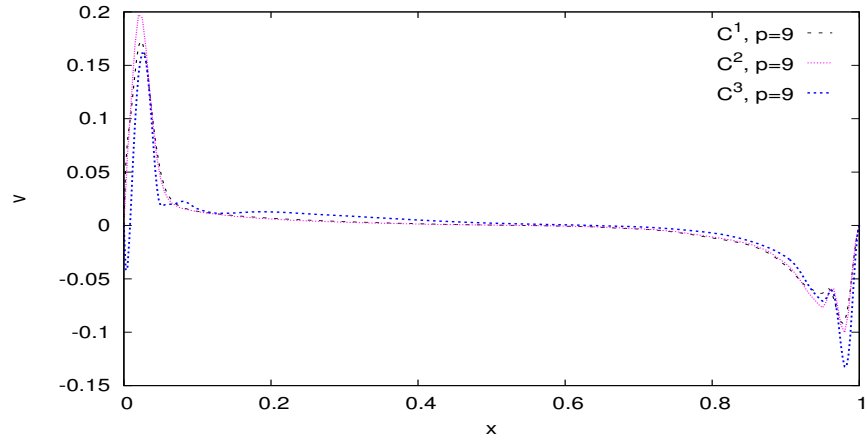

(b) Velocity v versus x at y=0.99

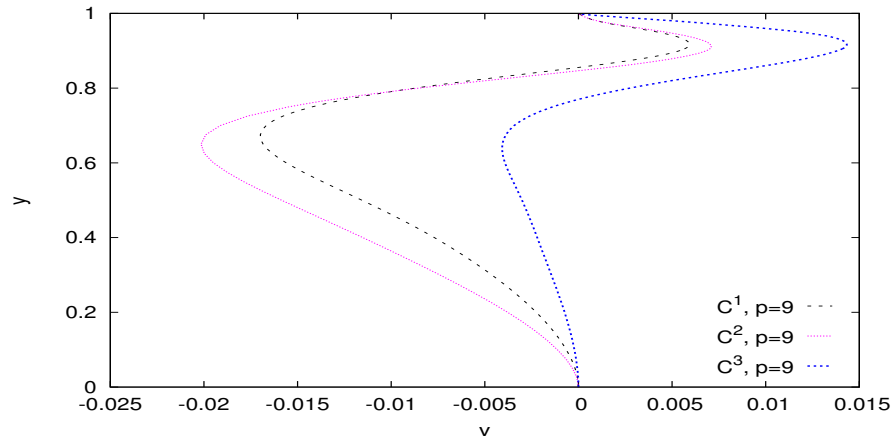

(c) Velocity v versus y at x=0.5

Figure 4.71: Comparison of solutions for mesh M3 (49 elm, h_d = 0.05); $De = 1.2$

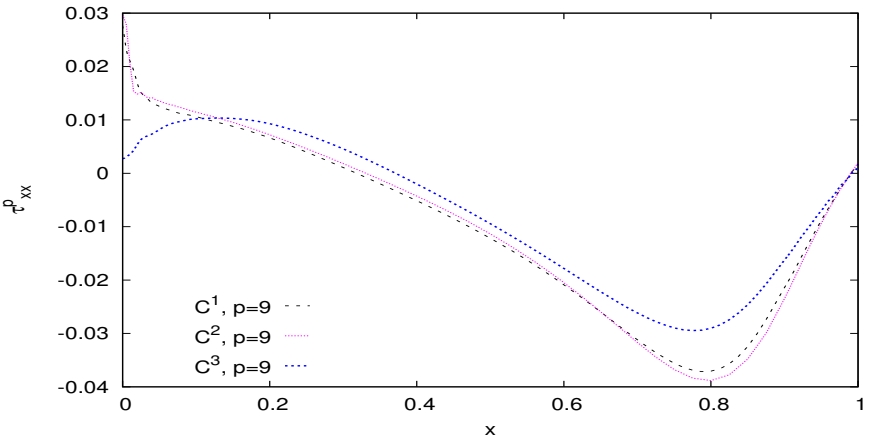

(a) Normal Stress τ^p_{xx} versus x at y=0.5

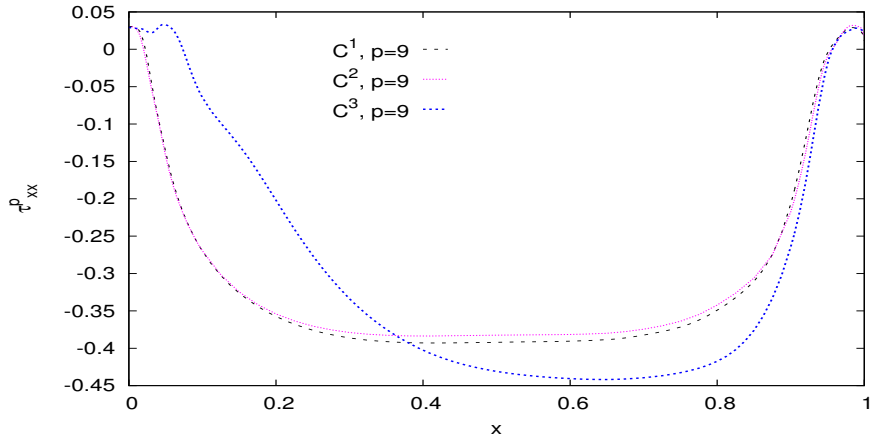

(b) Normal Stress τ^p_{xx} versus x at y=0.99

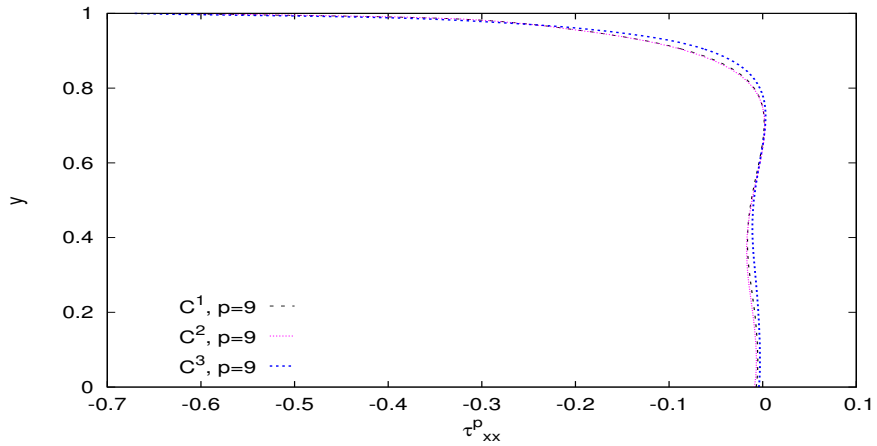

(c) Normal Stress τ^p_{xx} versus y at x=0.5

Figure 4.72: Comparison of solutions for mesh M3 (49 elm, h_d = 0.05); $De = 1.2$

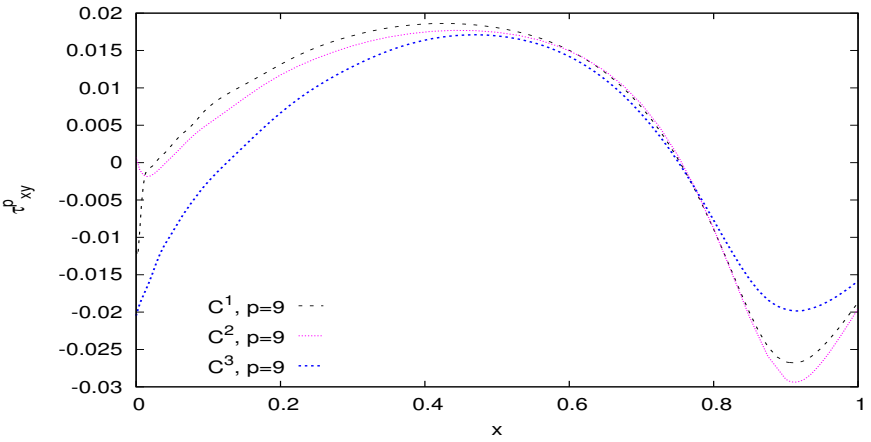

(a) Shear Stress τ^p_{xy} versus x at y=0.5

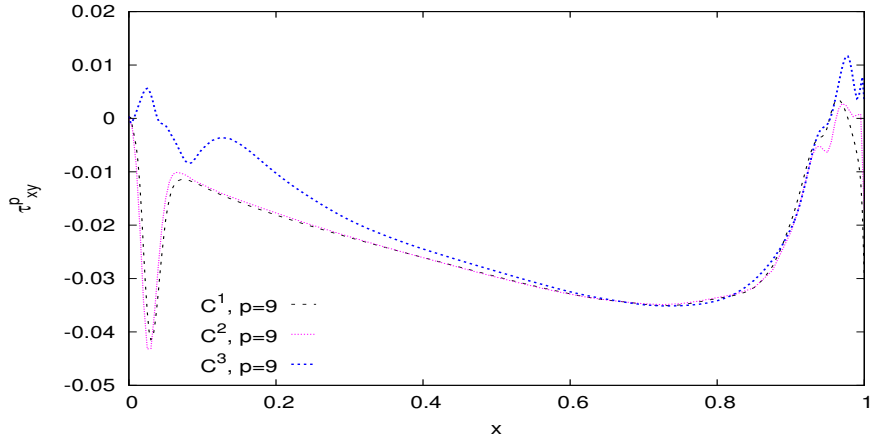

(b) Shear Stress τ^p_{xy} versus x at y=0.99

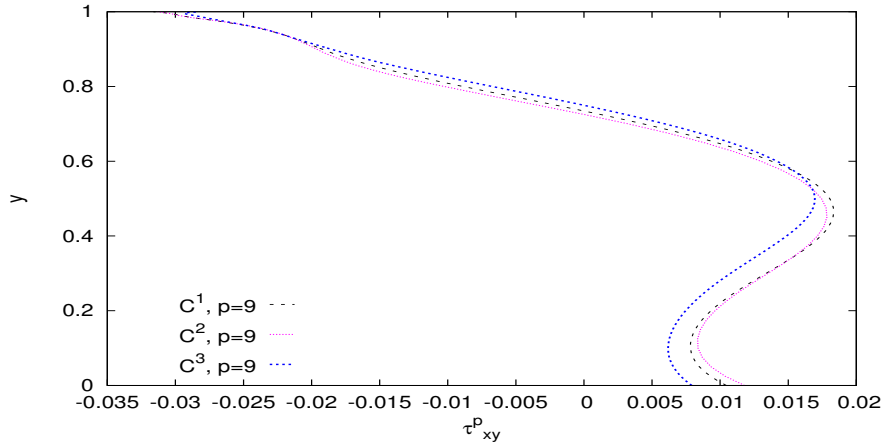

(c) Shear Stress τ^p_{xy} versus y at x=0.5

Figure 4.73: Comparison of solutions for mesh M3 (49 elm, h_d = 0.05); $De = 1.2$

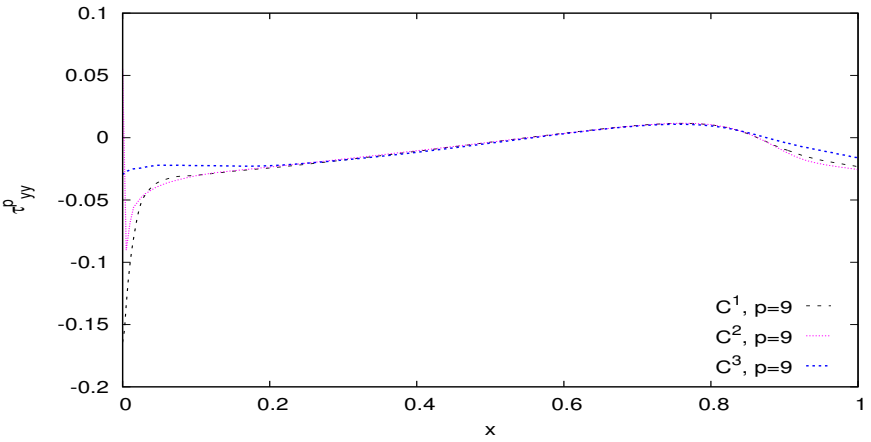

(a) Normal Stress τ^p_{yy} versus x at y=0.5

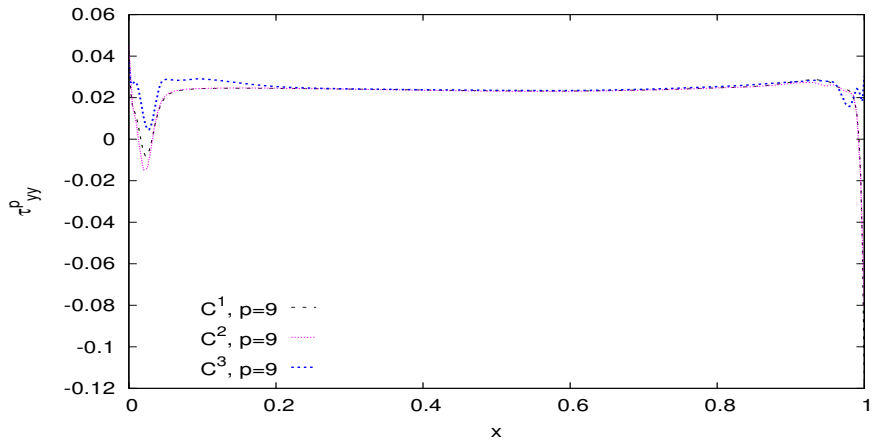

(b) Normal Stress τ^p_{yy} versus x at y=0.99

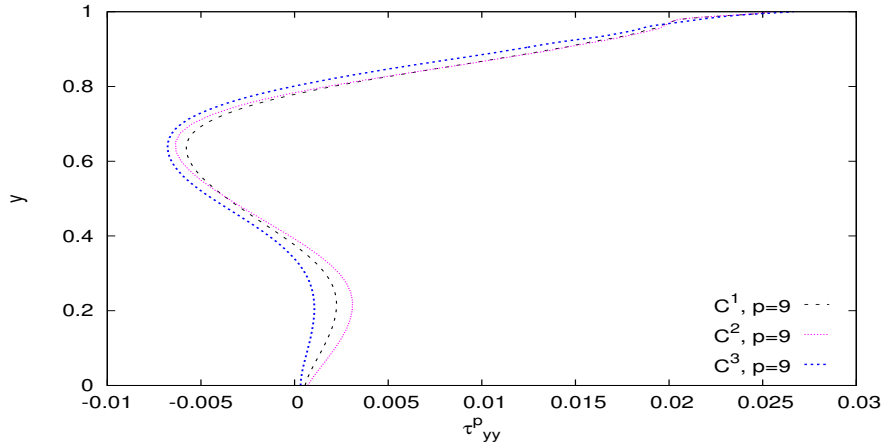

(c) Normal Stress τ^p_{yy} versus y at x=0.5

Figure 4.74: Comparison of solutions for mesh M3 (49 elm, h_d = 0.05); $De = 1.2$

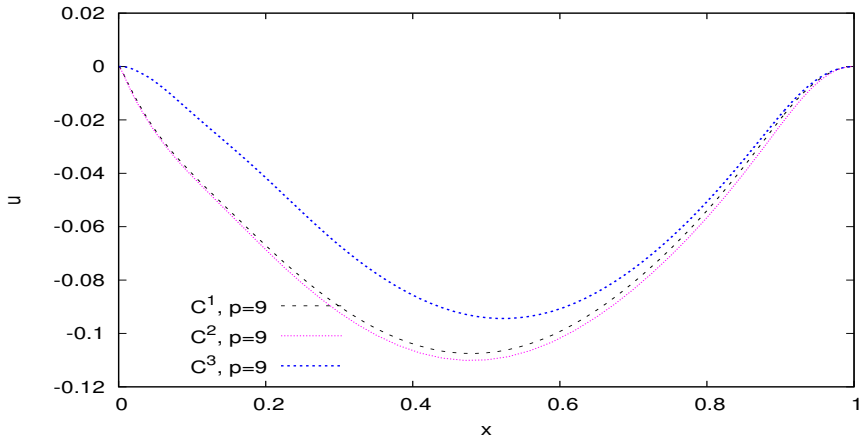

(a) Velocity u versus x at y=0.5

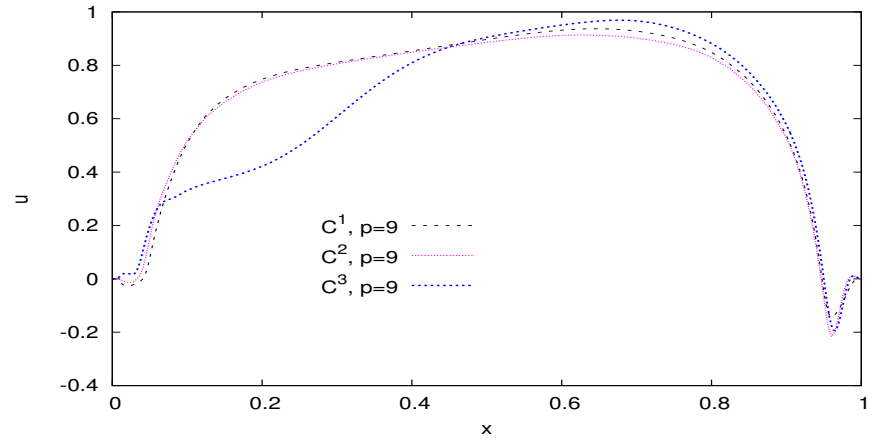

(b) Velocity u versus x at y=0.99

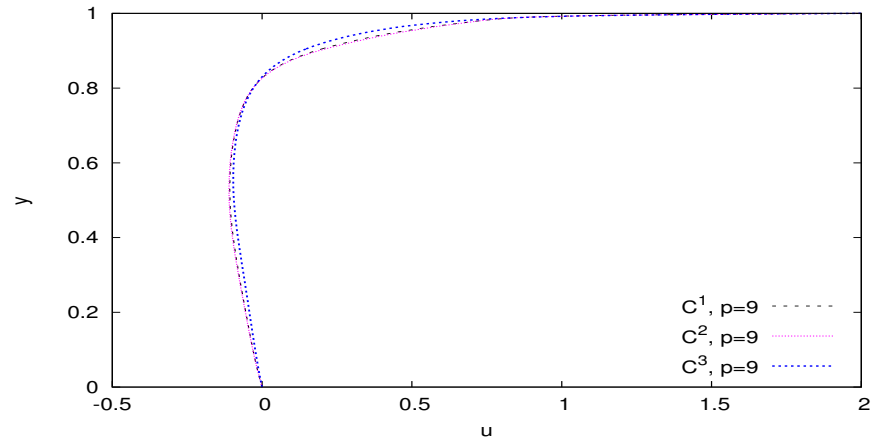

(c) Velocity u versus y at x=0.5

Figure 4.75: Comparison of solutions for mesh M3 (49 elm, h_d = 0.05); $De = 2.4$

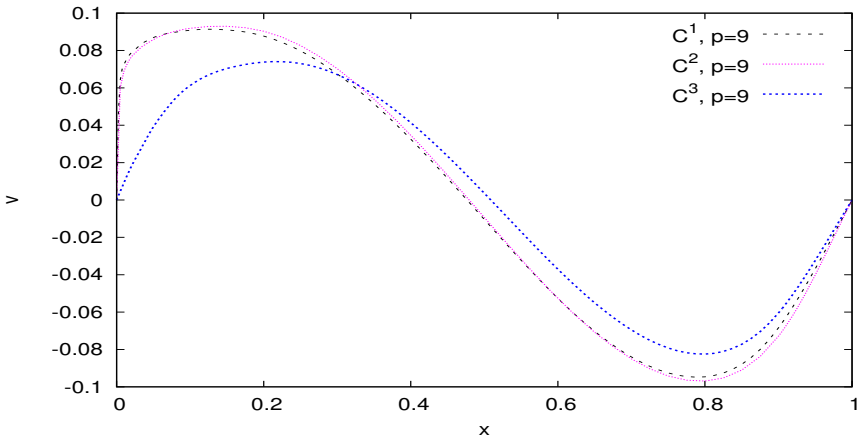

(a) Velocity v versus x at y=0.5

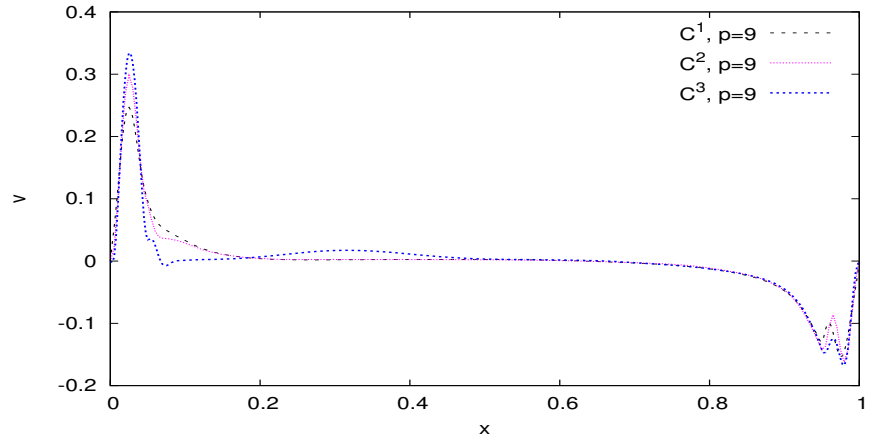

(b) Velocity v versus x at y=0.99

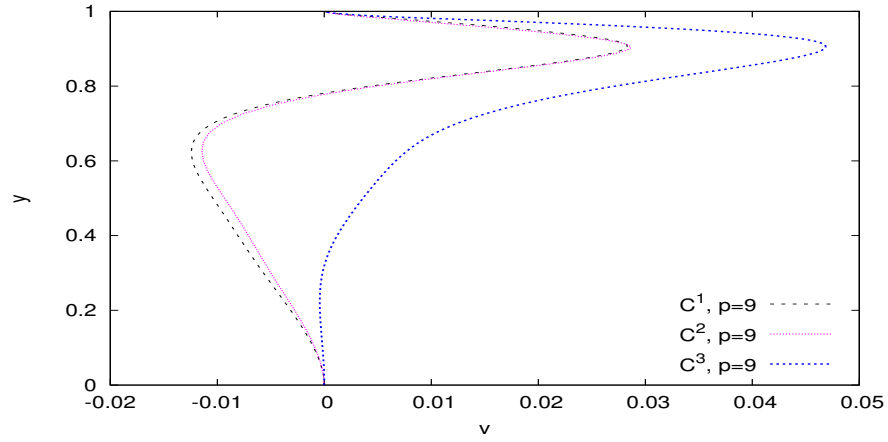

(c) Velocity v versus y at x=0.5

Figure 4.76: Comparison of solutions for mesh M3 (49 elm, h_d = 0.05); $De = 2.4$

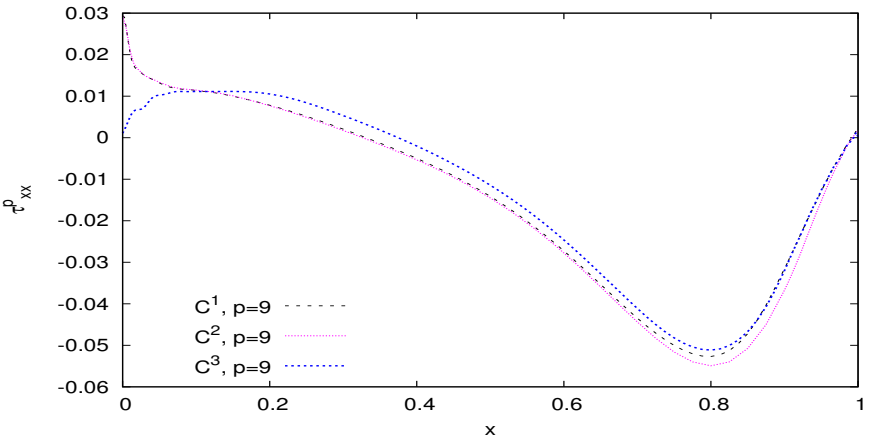

(a) Normal Stress τ^p_{xx} versus x at y=0.5

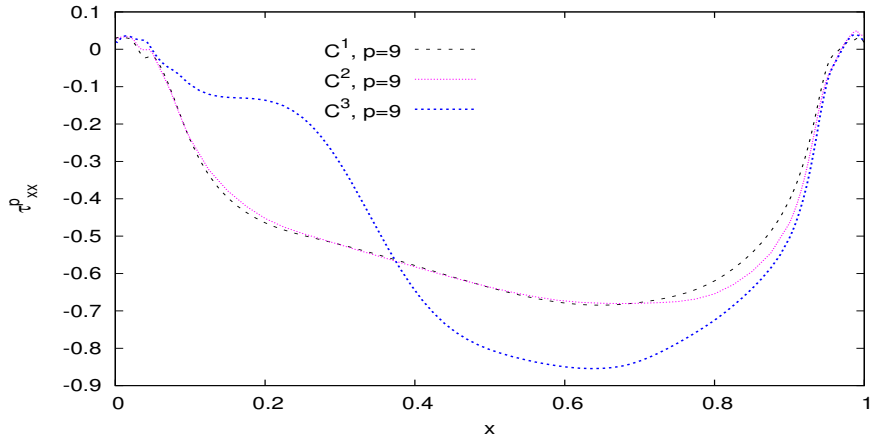

(b) Normal Stress τ^p_{xx} versus x at y=0.99

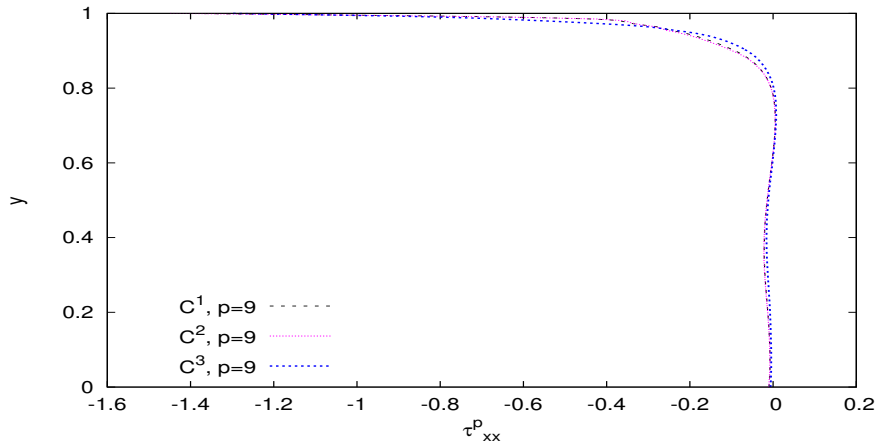

(c) Normal Stress τ^p_{xx} versus y at x=0.5

Figure 4.77: Comparison of solutions for mesh M3 (49 elm, h_d = 0.05); $De = 2.4$

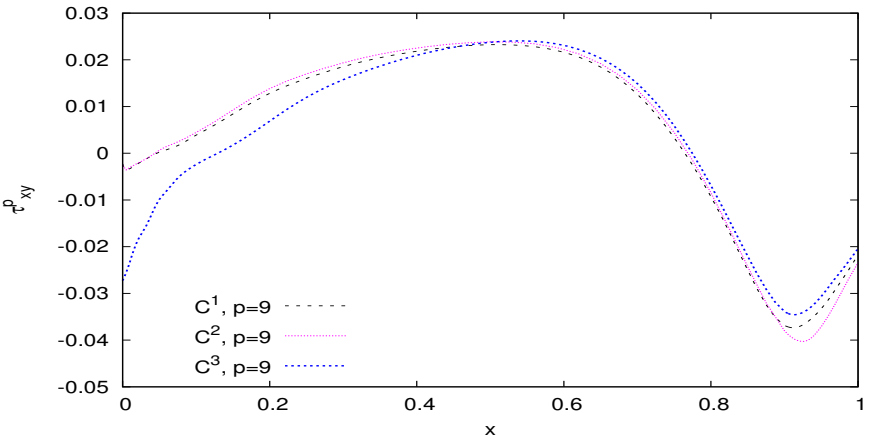

(a) Shear Stress τ^p_{xy} versus x at y=0.5

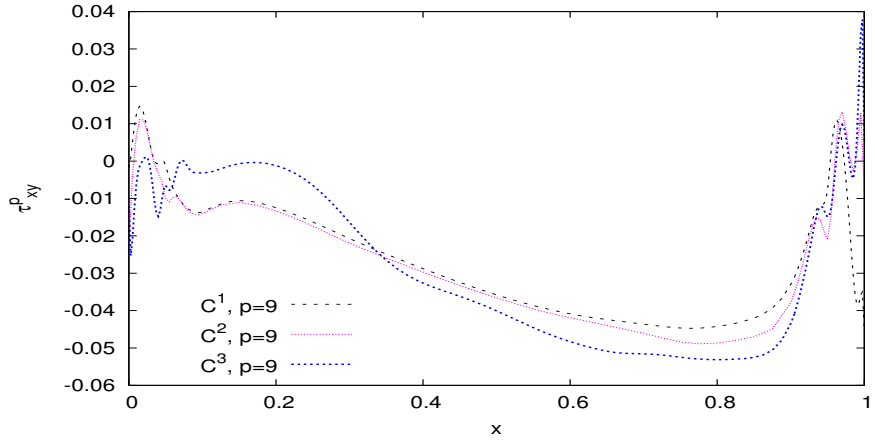

(b) Shear Stress τ^p_{xy} versus x at y=0.99

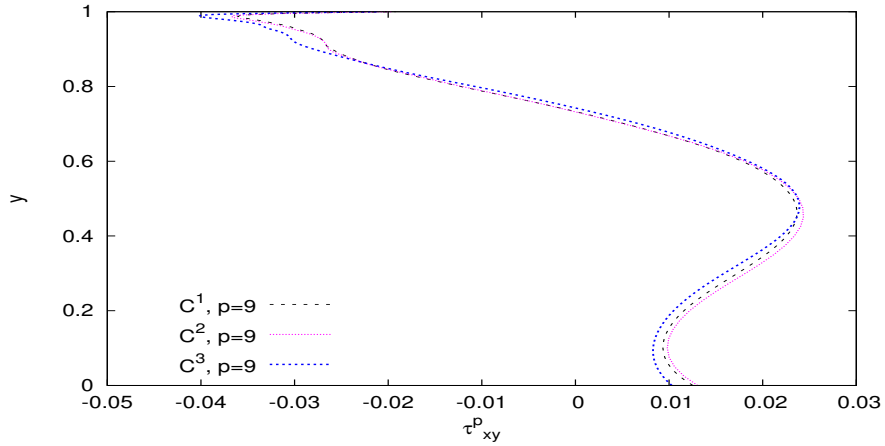

(c) Shear Stress τ^p_{xy} versus y at x=0.5

Figure 4.78: Comparison of solutions for mesh M3 (49 elm, h_d = 0.05); $De = 2.4$

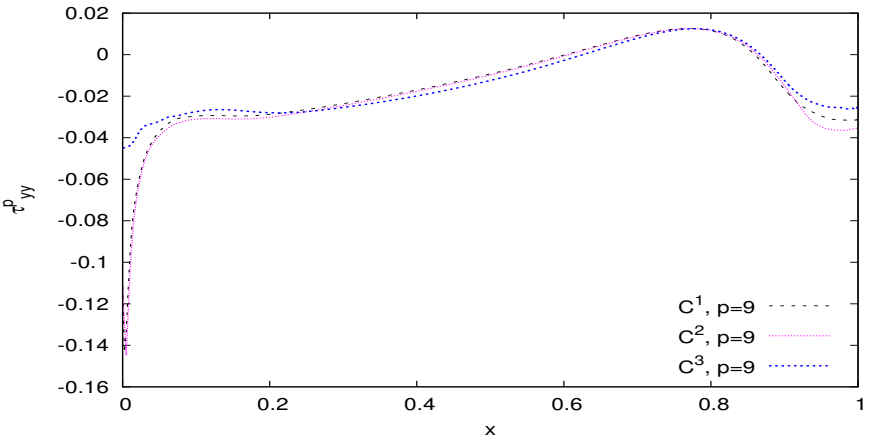

(a) Normal Stress τ^p_{yy} versus x at y=0.5

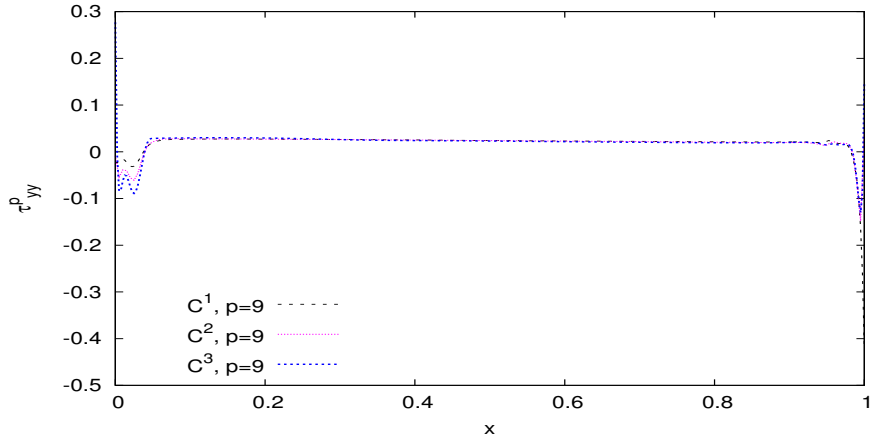

(b) Normal Stress τ^p_{yy} versus x at y=0.99

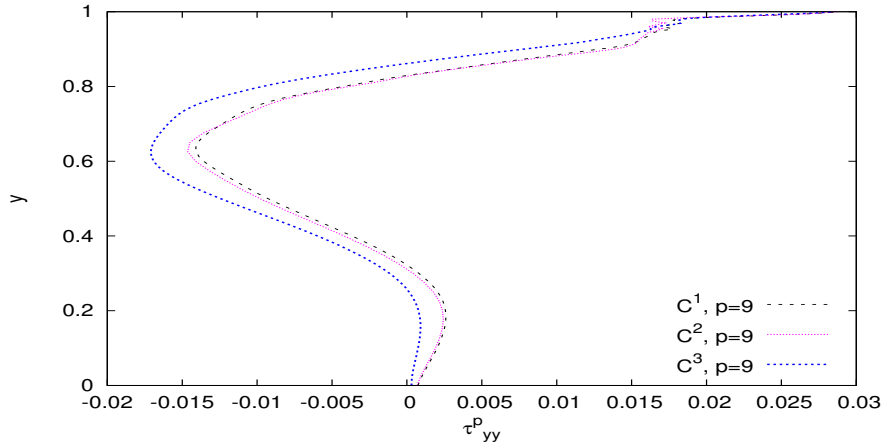

(c) Normal Stress τ^p_{yy} versus y at x=0.5

Figure 4.79: Comparison of solutions for mesh M3 (49 elm, h_d = 0.05); $De = 2.4$

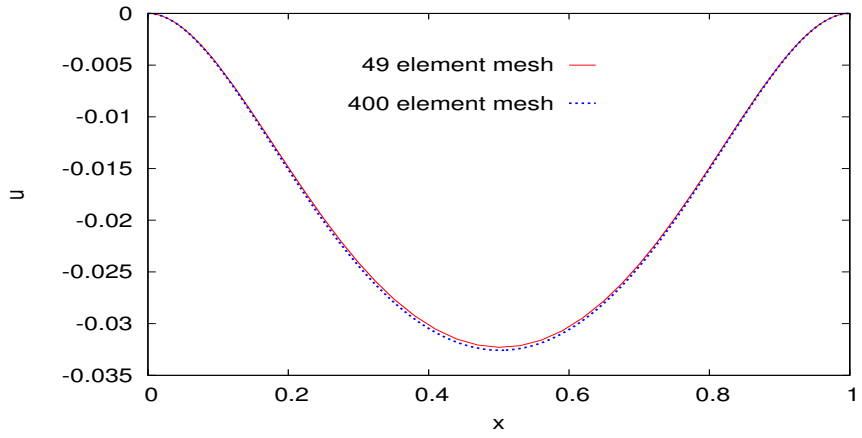

(a) Velocity u versus x at y=0.5

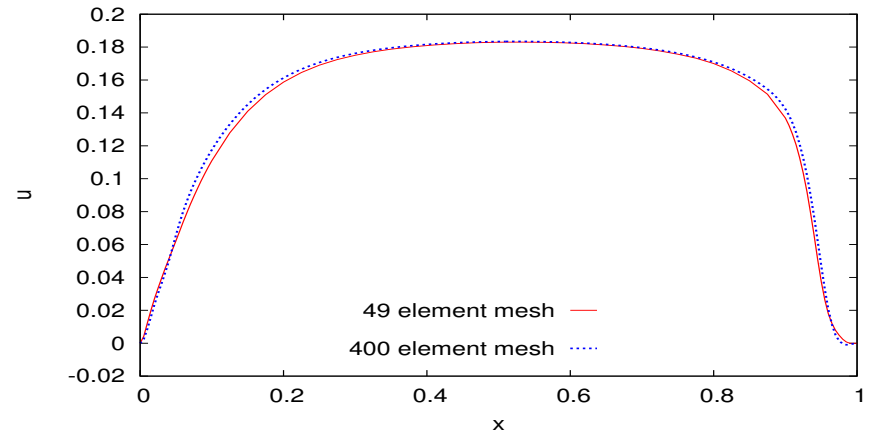

(b) Velocity u versus x at y=0.99

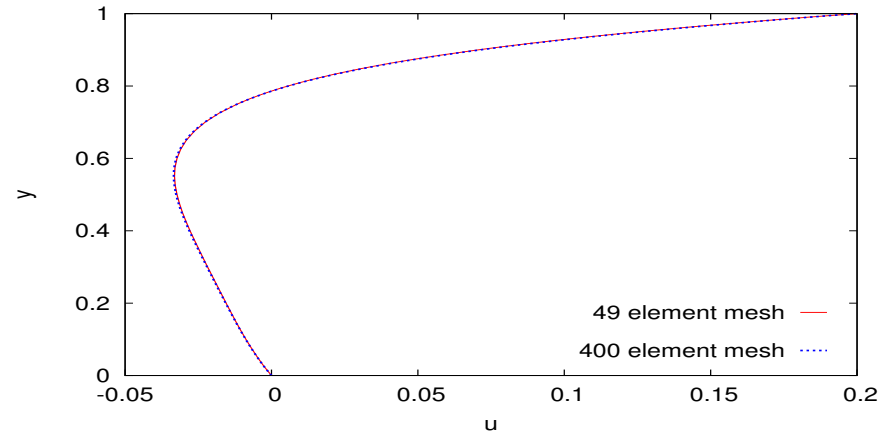

(c) Velocity u versus y at x=0.5

Figure 4.80: Solutions of class C^2 for mesh M3 (h_d = 0.05) ; p=9 and mesh M4 (h_d = 0.05) ; p=7, $De = 0.24$

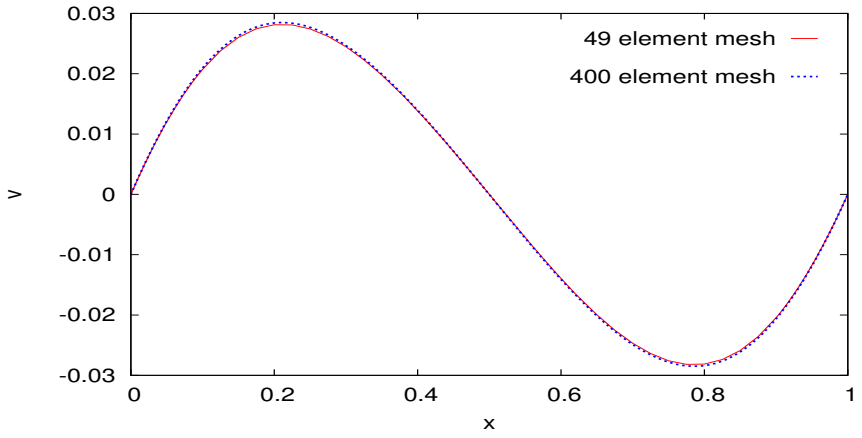

(a) Velocity v versus x at y=0.5

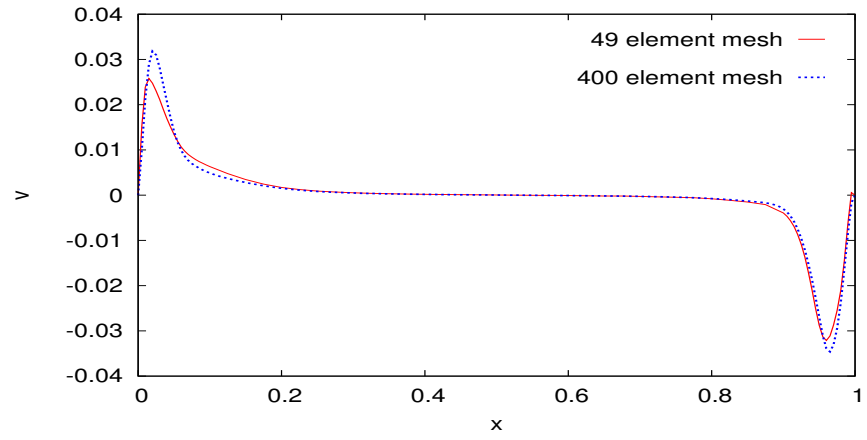

(b) Velocity v versus x at y=0.99

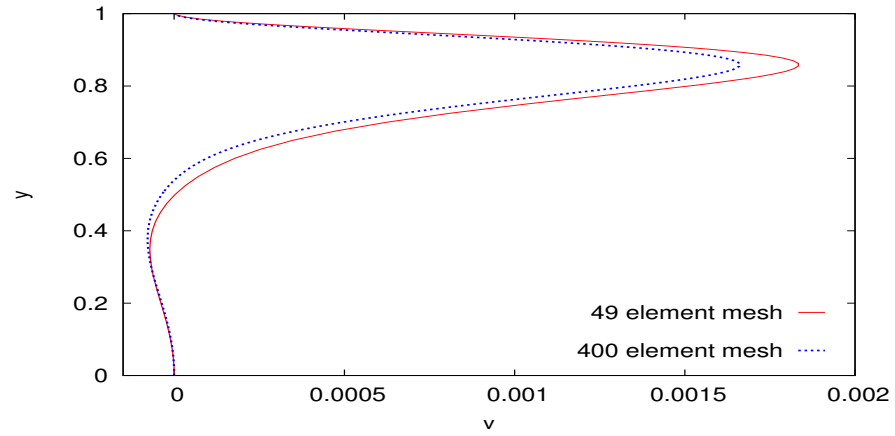

(c) Velocity v versus y at x=0.5

Figure 4.81: Solutions of class C^2 for mesh M3 (h_d = 0.05) ; p=9 and mesh M4 (h_d = 0.05) ; p=7, $De = 0.24$

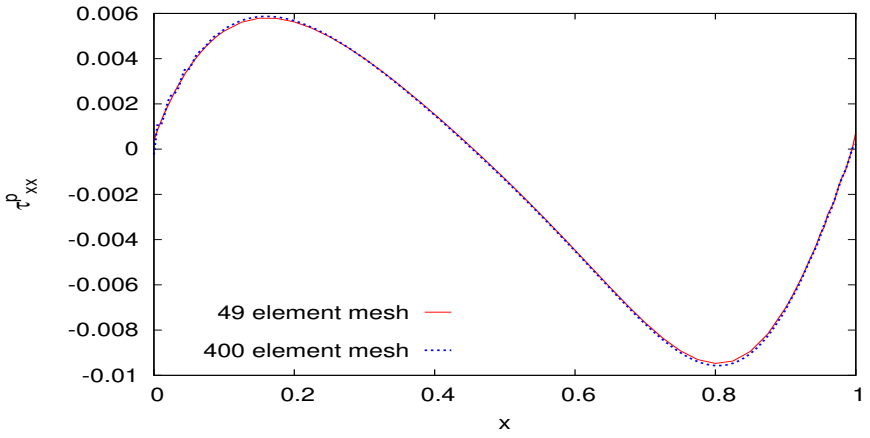

(a) Normal Stress τ^p_{xx} versus x at y=0.5

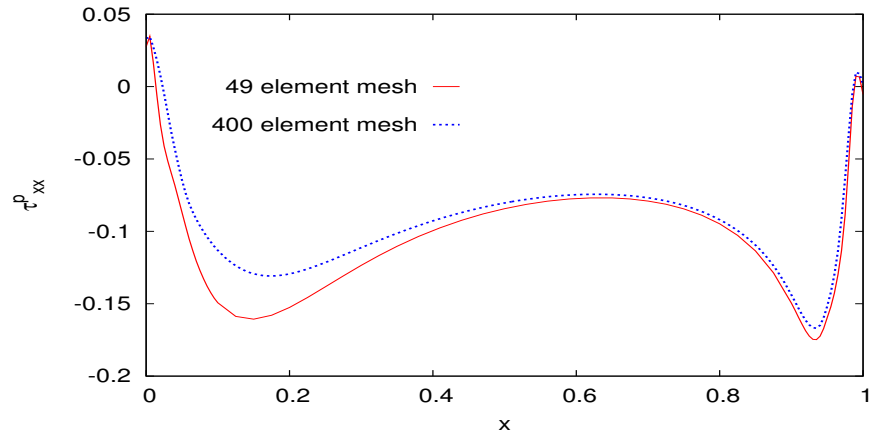

(b) Normal Stress τ^p_{xx} versus x at y=0.99

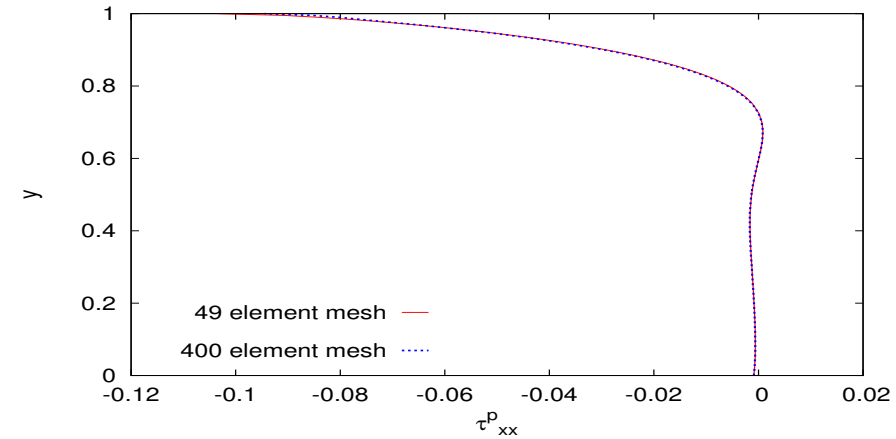

(c) Normal Stress τ^p_{xx} versus y at x=0.5

Figure 4.82: Solutions of class C^2 for mesh M3 (h_d = 0.05) ; p=9 and mesh M4 (h_d = 0.05) ; p=7, $De = 0.24$

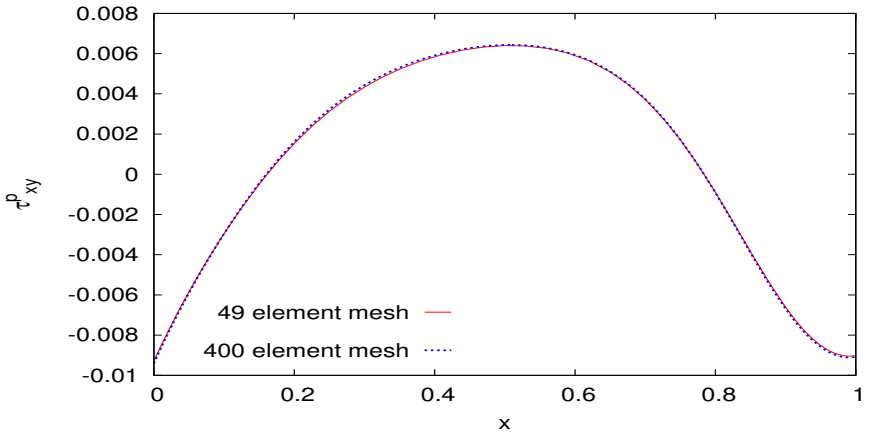

(a) Shear Stress τ^p_{xy} versus x at y=0.5

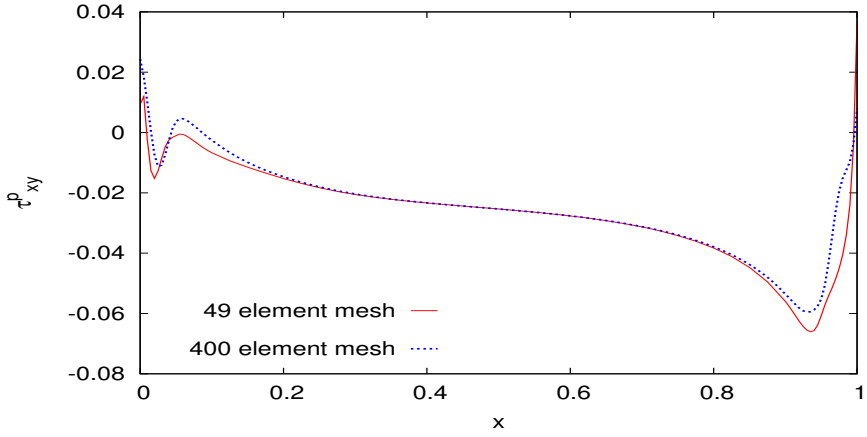

(b) Shear Stress τ^p_{xy} versus x at y=0.99

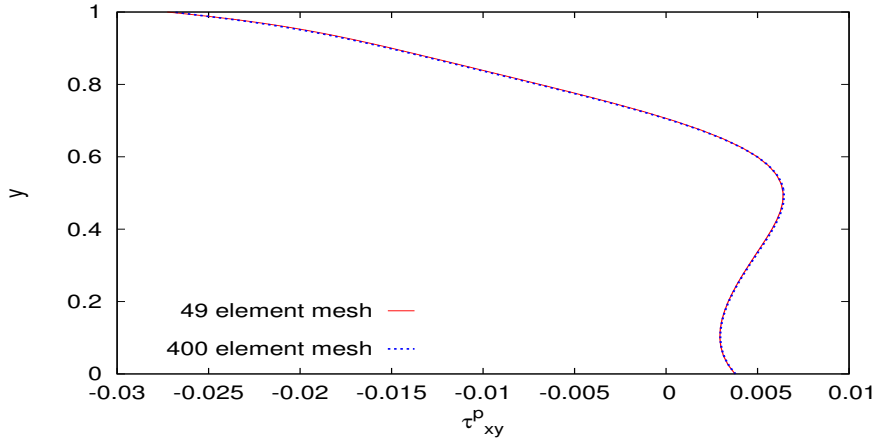

(c) Shear Stress τ^p_{xy} versus y at x=0.5

Figure 4.83: Solutions of class C^2 for mesh M3 (h_d = 0.05) ; p=9 and mesh M4 (h_d = 0.05) ; p=7, $De = 0.24$

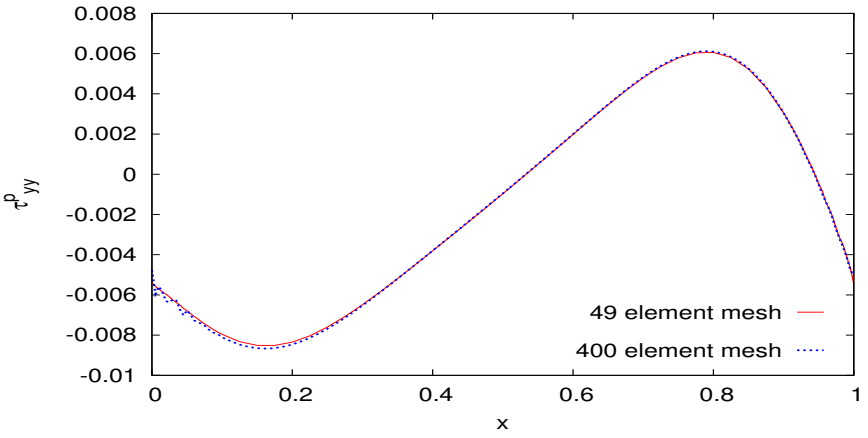

(a) Normal Stress τ^p_{yy} versus x at y=0.5

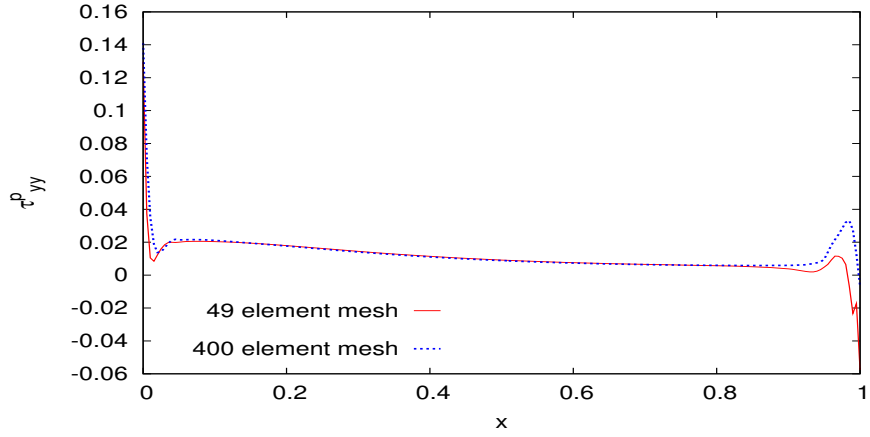

(b) Normal Stress τ^p_{yy} versus x at y=0.99

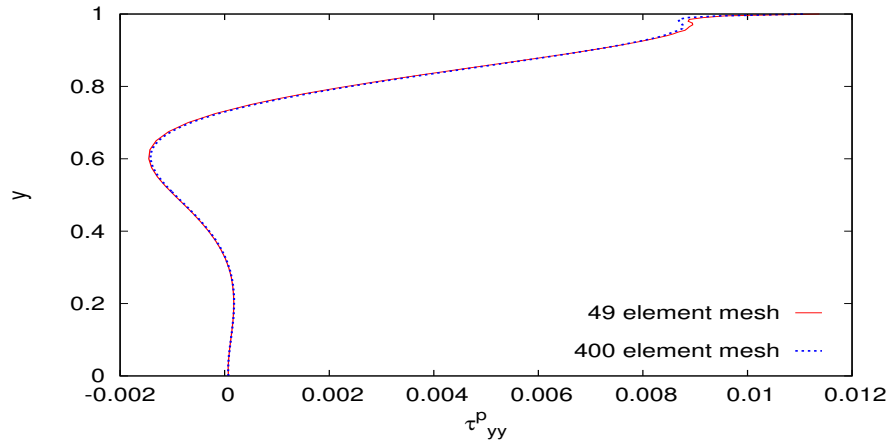

(c) Normal Stress τ^p_{yy} versus y at x=0.5

Figure 4.84: Solutions of class C^2 for mesh M3 (h_d = 0.05) ; p=9 and mesh M4 (h_d = 0.05) ; p=7, $De = 0.24$

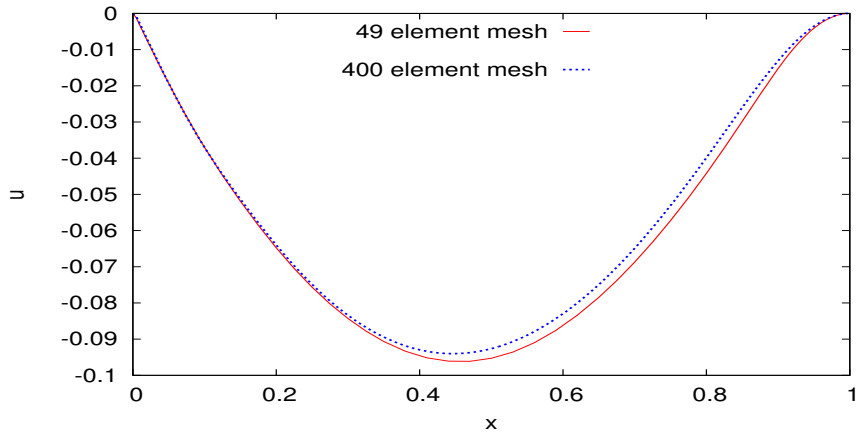

(a) Velocity u versus x at y=0.5

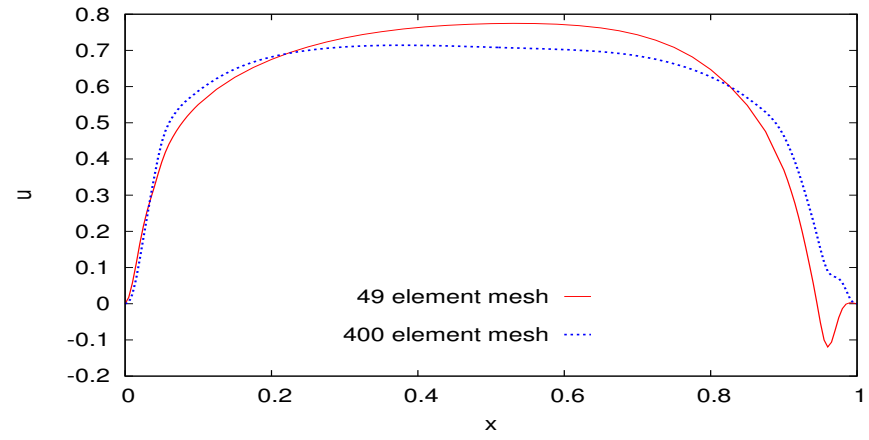

(b) Velocity u versus x at y=0.99

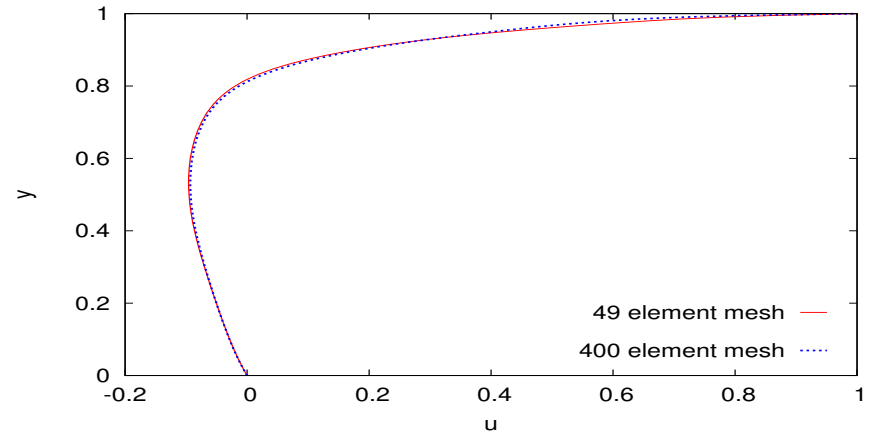

(c) Velocity u versus y at x=0.5

Figure 4.85: Solutions of class C^2 for mesh M3 (h_d = 0.05) ; p=9 and mesh M4 (h_d = 0.05) ; p=7, $De = 1.2$

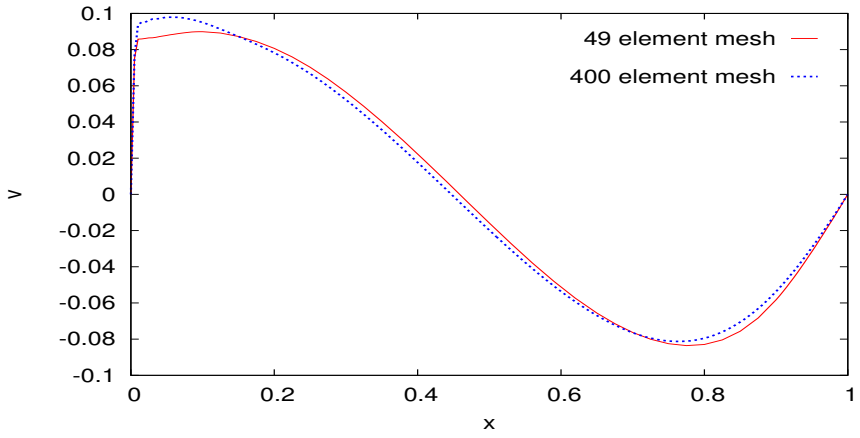

(a) Velocity v versus x at y=0.5

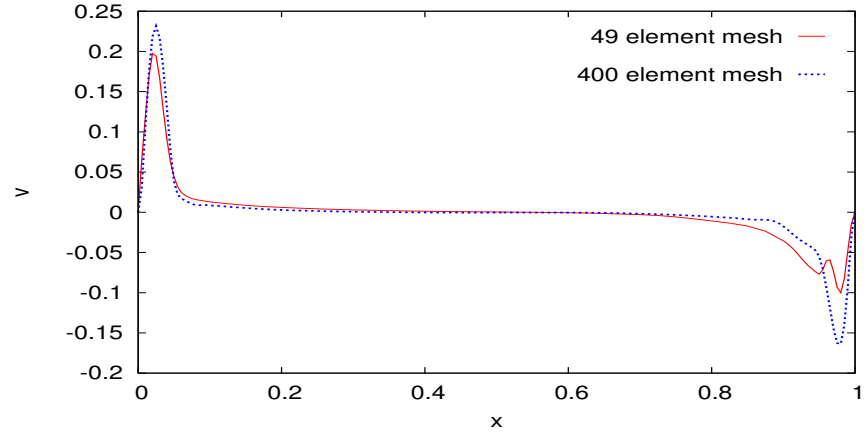

(b) Velocity v versus x at y=0.99

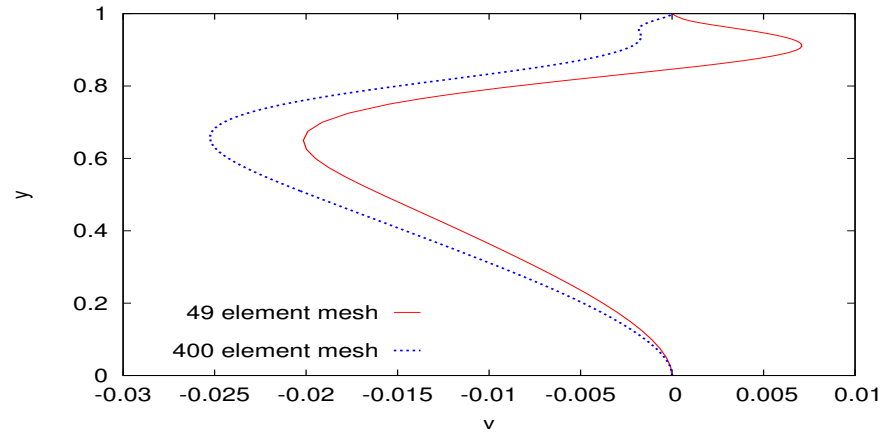

(c) Velocity v versus y at x=0.5

Figure 4.86: Solutions of class C^2 for mesh M3 (h_d = 0.05) ; p=9 and mesh M4 (h_d = 0.05) ; p=7, $De = 1.2$

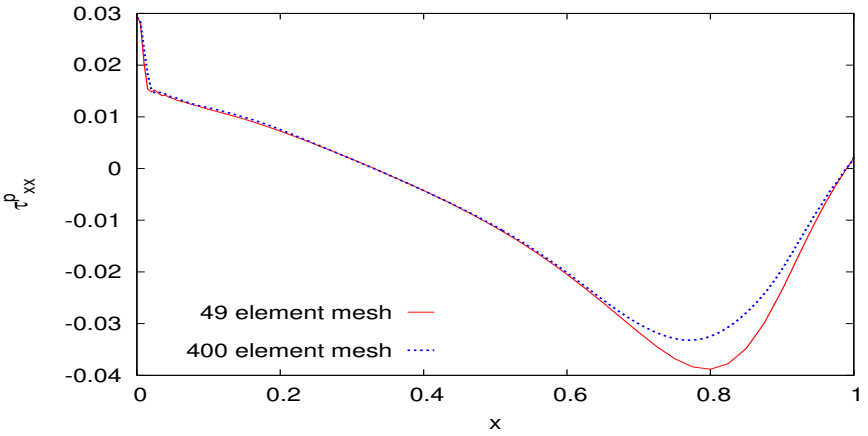

(a) Normal Stress τ^p_{xx} versus x at y=0.5

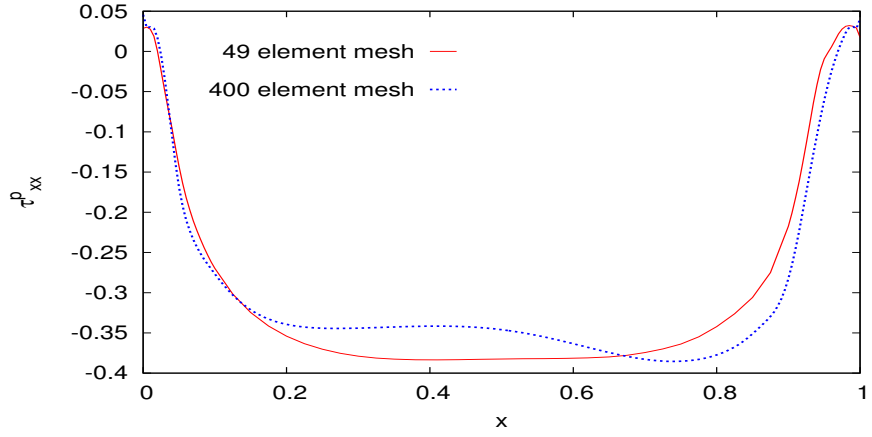

(b) Normal Stress τ^p_{xx} versus x at y=0.99

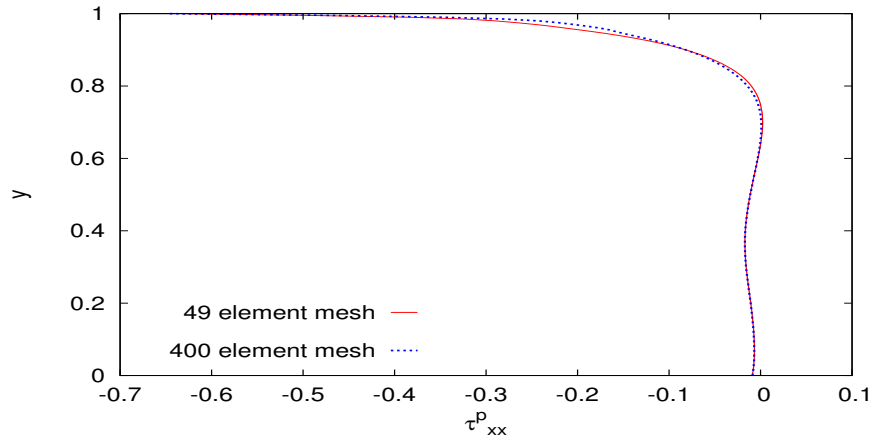

(c) Normal Stress τ^p_{xx} versus y at x=0.5

Figure 4.87: Solutions of class C^2 for mesh M3 (h_d = 0.05) ; p=9 and mesh M4 (h_d = 0.05) ; p=7, $De = 1.2$

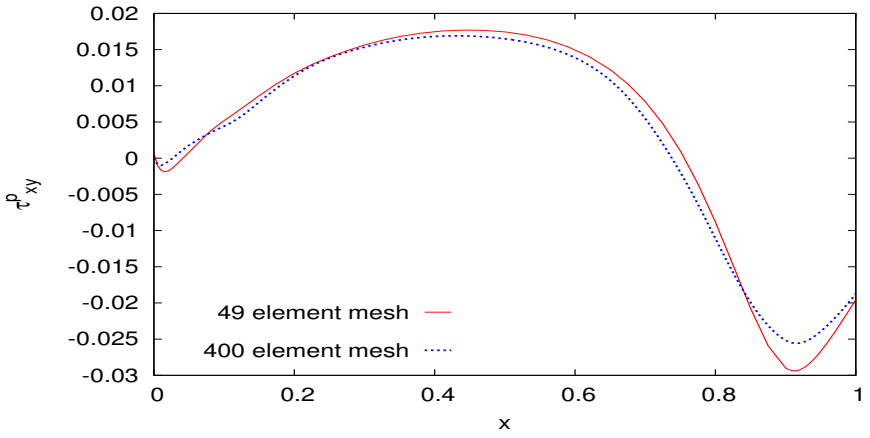

(a) Shear Stress τ^p_{xy} versus x at y=0.5

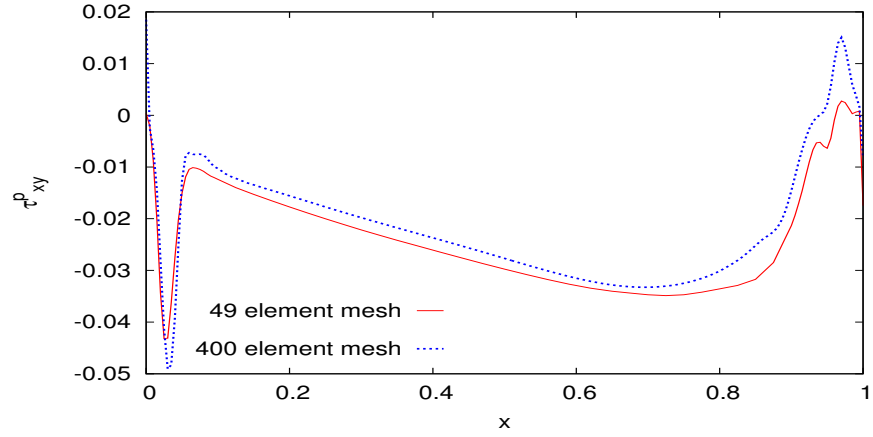

(b) Shear Stress τ^p_{xy} versus x at y=0.99

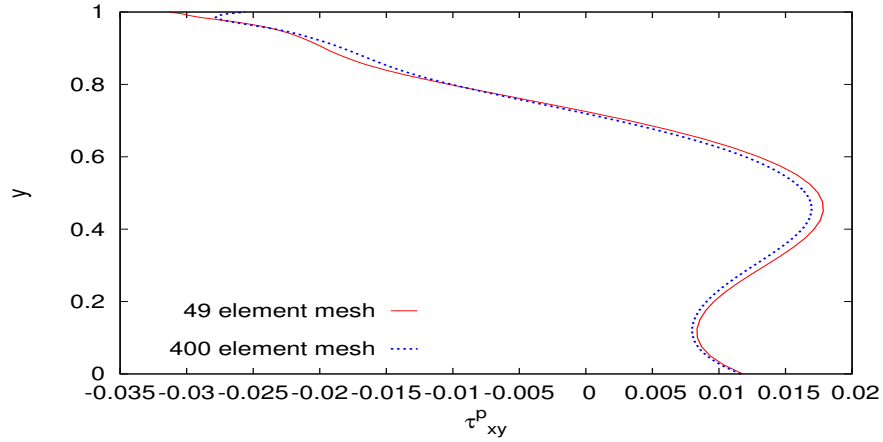

(c) Shear Stress τ^p_{xy} versus y at x=0.5

Figure 4.88: Solutions of class C^2 for mesh M3 (h_d = 0.05) ; p=9 and mesh M4 (h_d = 0.05) ; p=7, $De = 1.2$

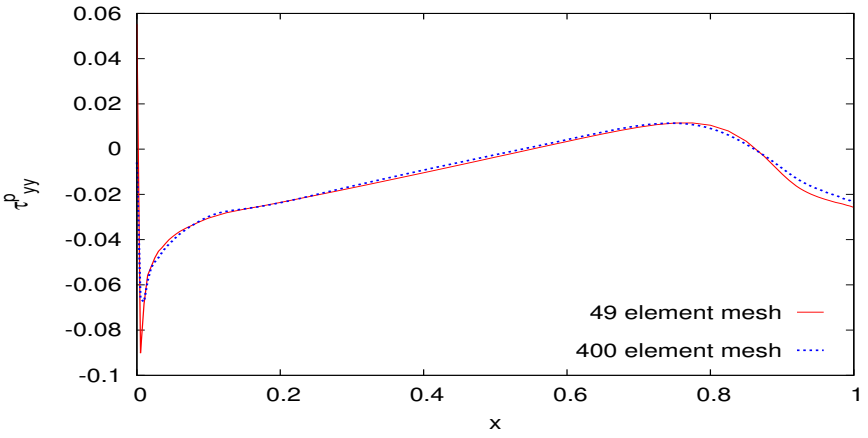

(a) Normal Stress τ^p_{yy} versus x at y=0.5

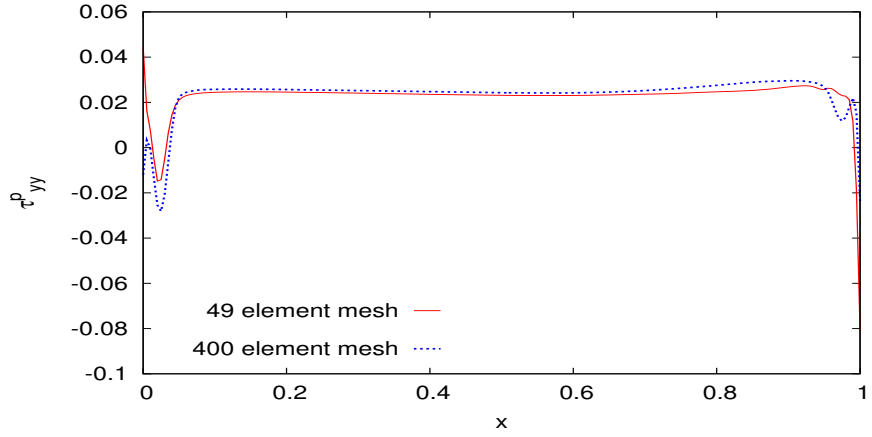

(b) Normal Stress τ^p_{yy} versus x at y=0.99

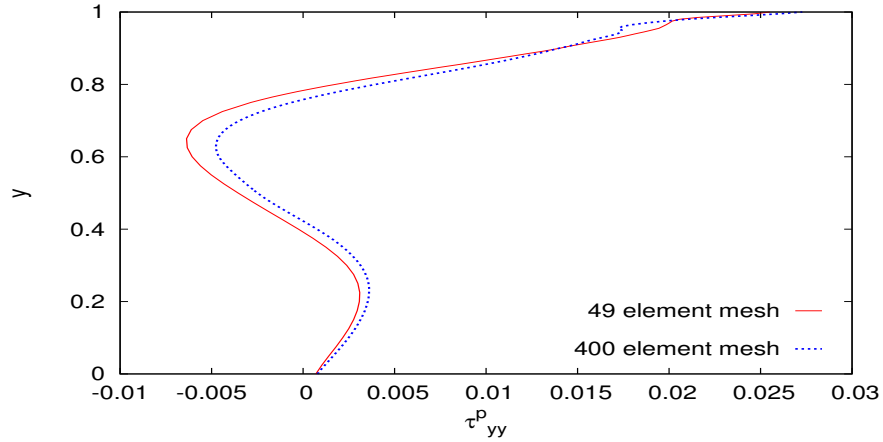

(c) Normal Stress τ^p_{yy} versus y at x=0.5

Figure 4.89: Solutions of class C^2 for mesh M3 (h_d = 0.05) ; p=9 and mesh M4 (h_d = 0.05) ; p=7, $De = 1.2$

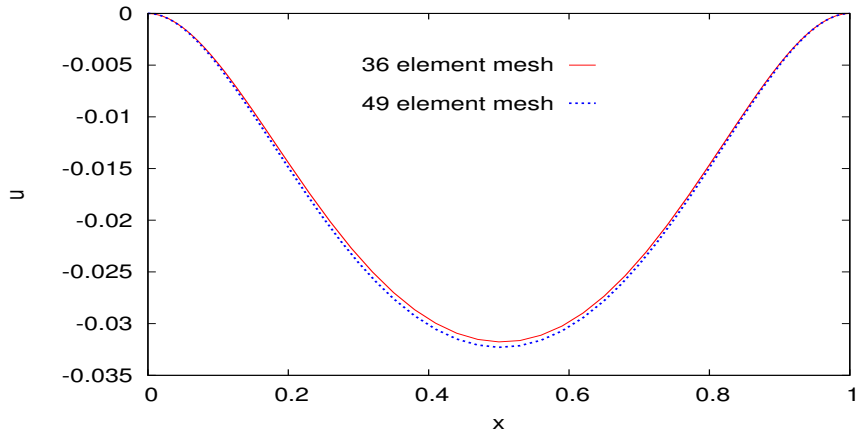

(a) Velocity u versus x at y=0.5

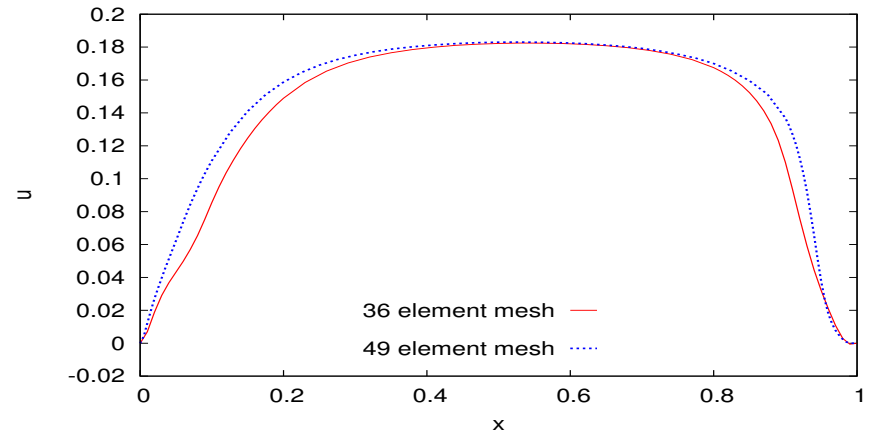

(b) Velocity u versus x at y=0.99

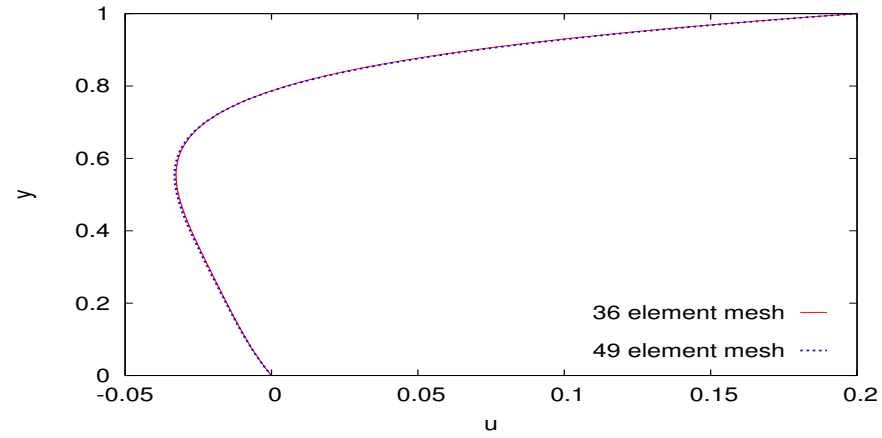

(c) Velocity u versus y at x=0.5

Figure 4.90: Solutions of class C^2 for mesh M1 (h_d = 0.1) ; p=9 and mesh M3 (h_d = 0.05) ; p=9, $De = 0.24$

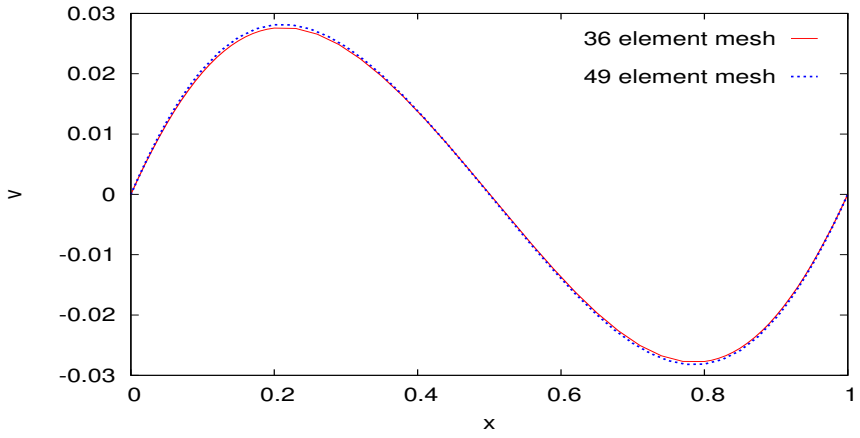

(a) Velocity v versus x at y=0.5

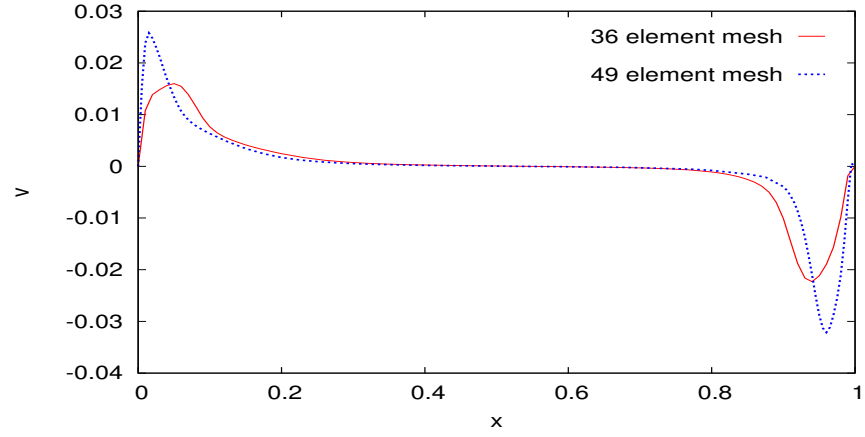

(b) Velocity v versus x at y=0.99

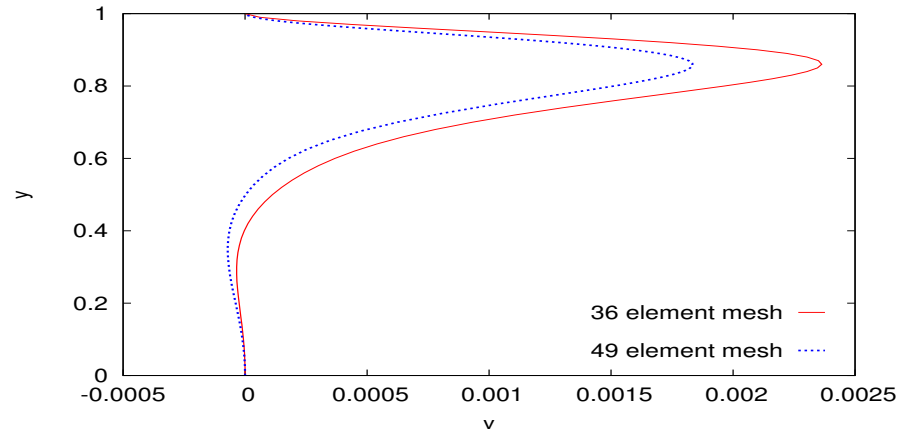

(c) Velocity v versus y at x=0.5

Figure 4.91: Solutions of class C^2 for mesh M1 (h_d = 0.1) ; p=9 and mesh M3 (h_d = 0.05) ; p=9, $De = 0.24$

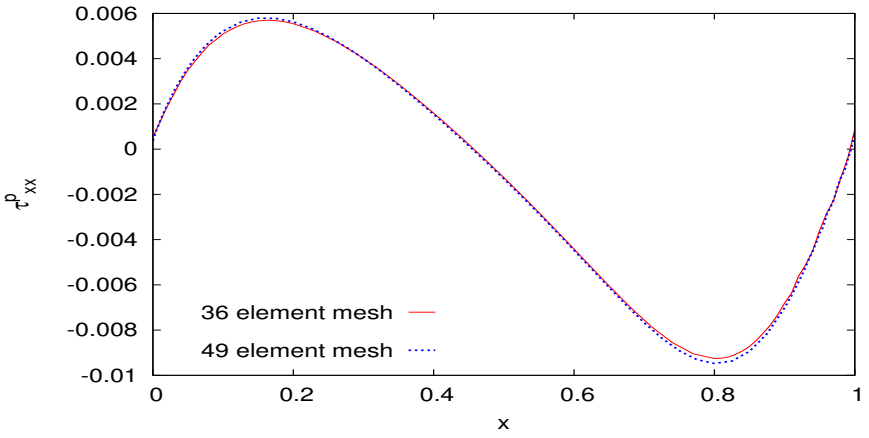

(a) Normal Stress τ^p_{xx} versus x at y=0.5

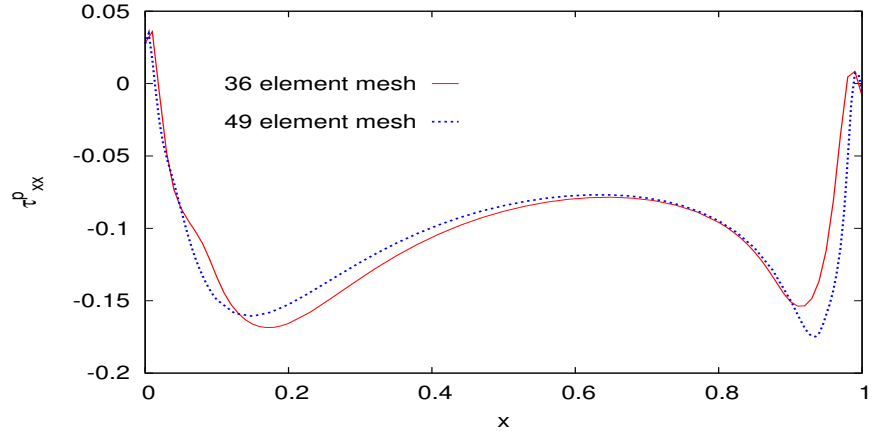

(b) Normal Stress τ^p_{xx} versus x at y=0.99

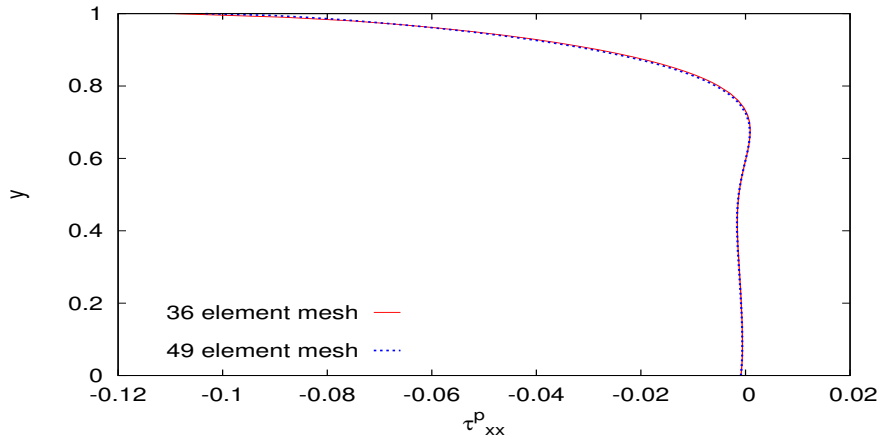

(c) Normal Stress τ^p_{xx} versus y at x=0.5

Figure 4.92: Solutions of class C^2 for mesh M1 (h_d = 0.1) ; p=9 and mesh M3 (h_d = 0.05) ; p=9, $De = 0.24$

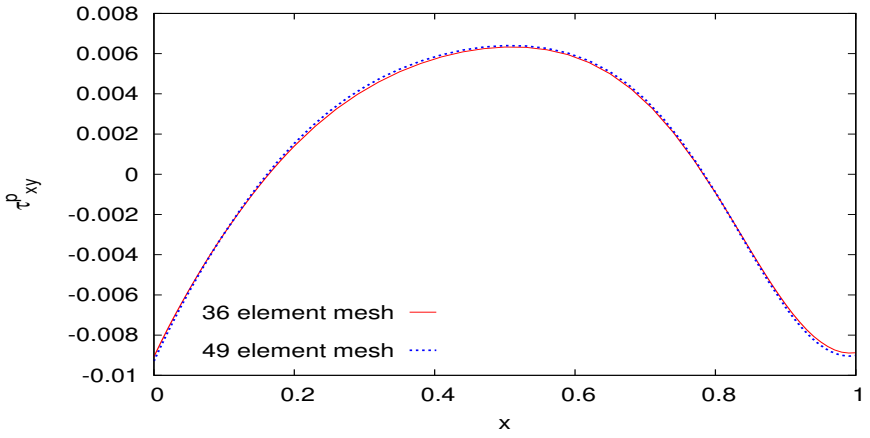

(a) Shear Stress τ^p_{xy} versus x at y=0.5

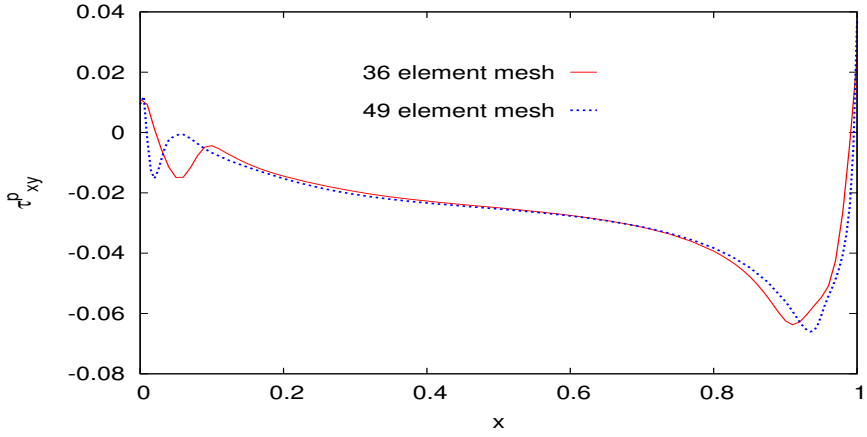

(b) Shear Stress τ^p_{xy} versus x at y=0.99

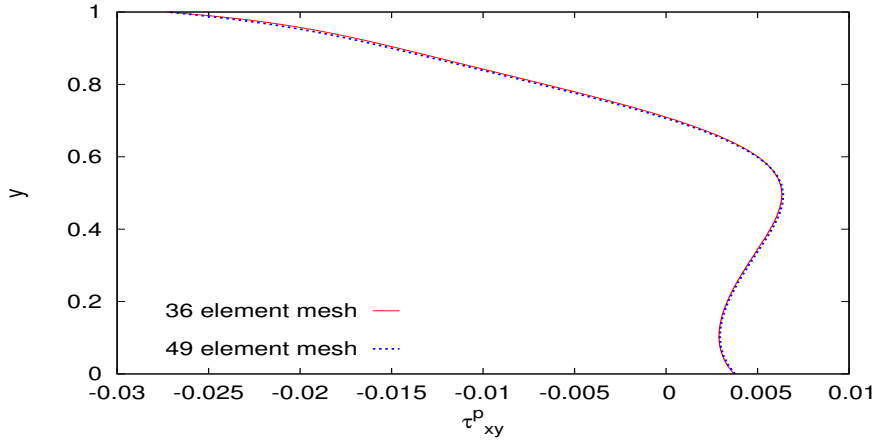

(c) Shear Stress τ^p_{xy} versus y at x=0.5

Figure 4.93: Solutions of class C^2 for mesh M1 (h_d = 0.1) ; p=9 and mesh M3 (h_d = 0.05) ; p=9, $De = 0.24$

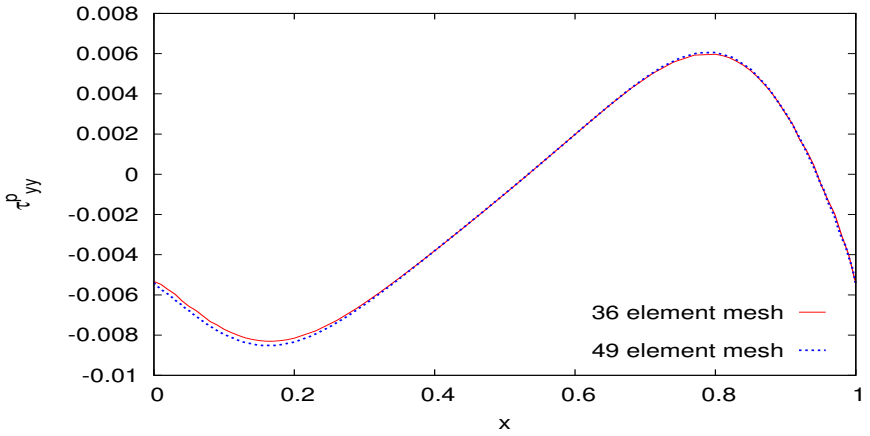

(a) Normal Stress τ^p_{yy} versus x at y=0.5

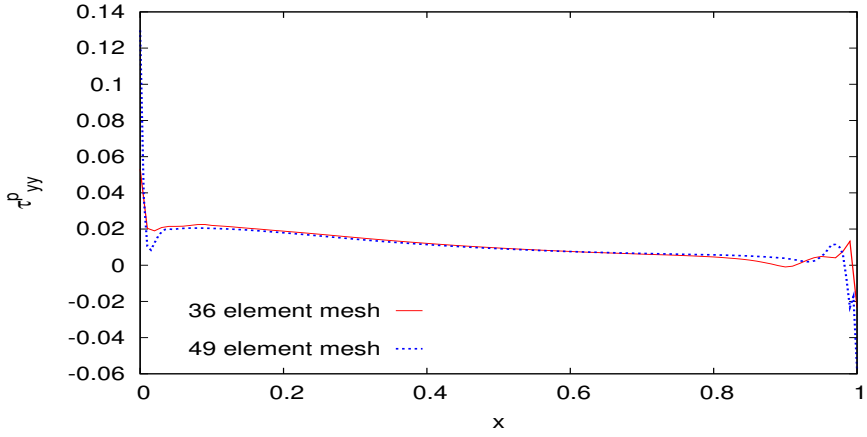

(b) Normal Stress τ^p_{yy} versus x at y=0.99

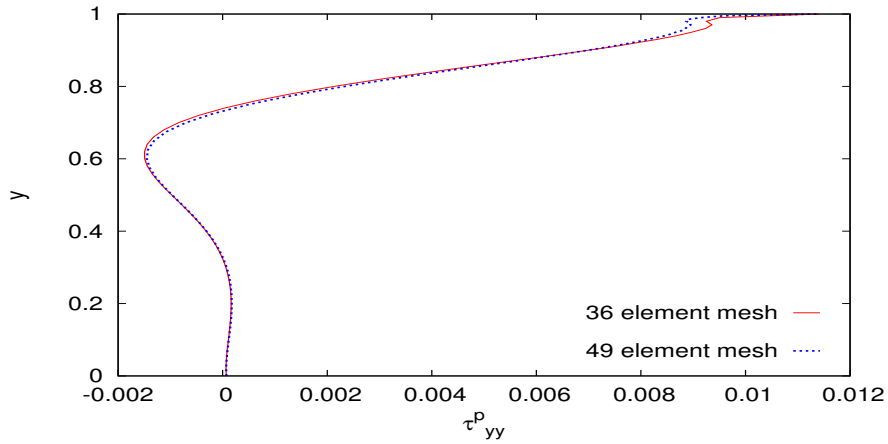

(c) Normal Stress τ^p_{yy} versus y at x=0.5

Figure 4.94: Solutions of class C^2 for mesh M1 (h_d = 0.1) ; p=9 and mesh M3 (h_d = 0.05) ; p=9, $De = 0.24$

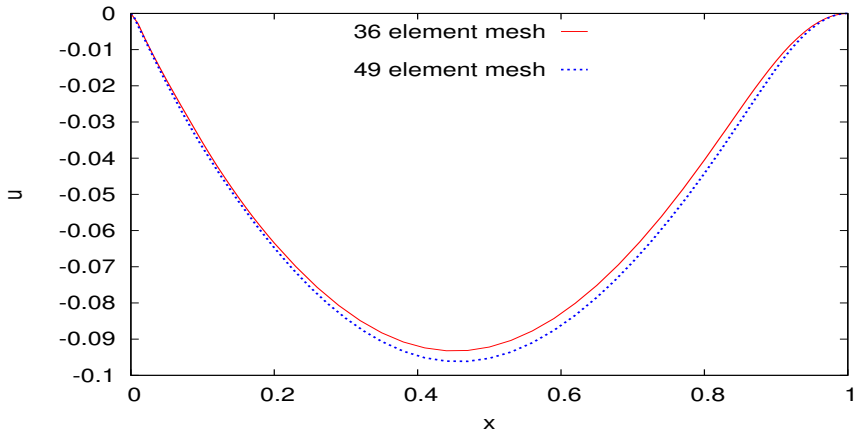

(a) Velocity u versus x at y=0.5

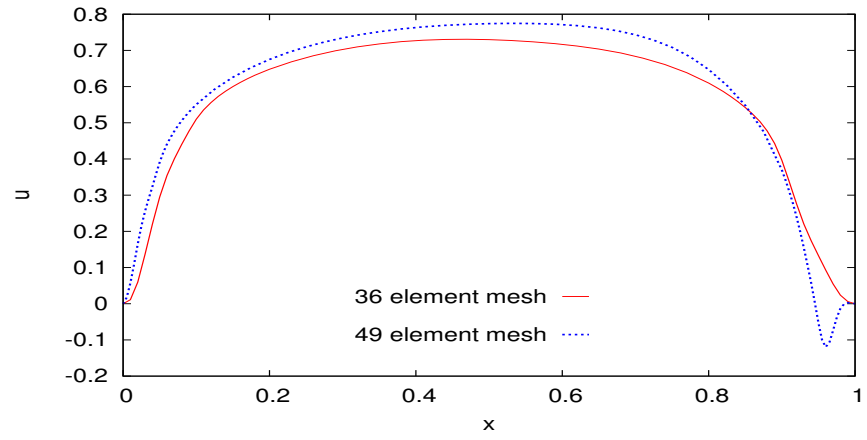

(b) Velocity u versus x at y=0.99

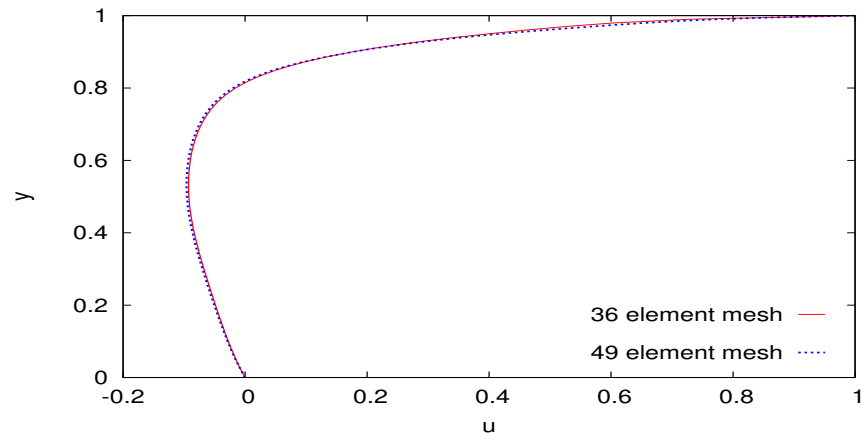

(c) Velocity u versus y at x=0.5

Figure 4.95: Solutions of class C^2 for mesh M1 (h_d = 0.1); p=9 and mesh M3 (h_d = 0.05) ; p=9, $De = 1.2$

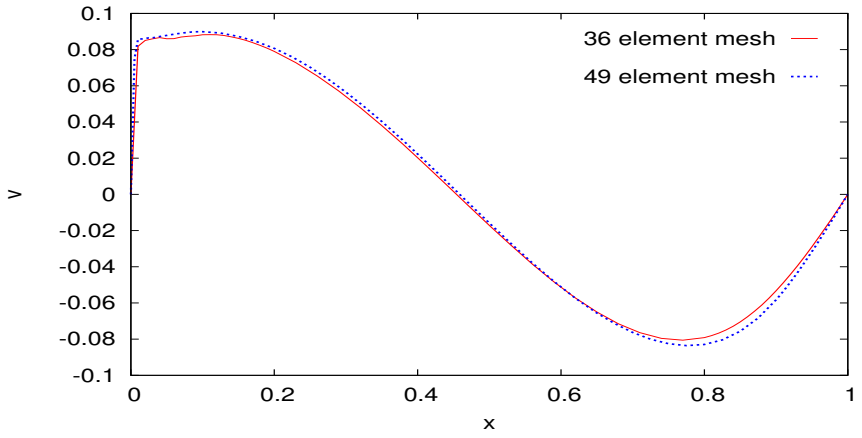

(a) Velocity v versus x at y=0.5

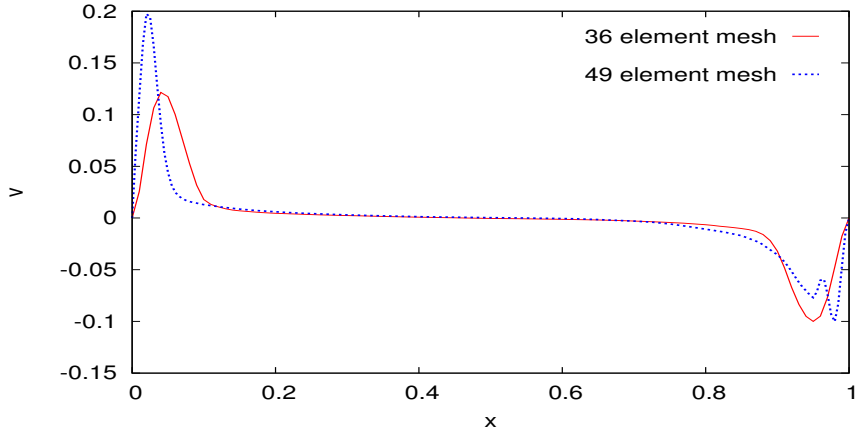

(b) Velocity v versus x at y=0.99

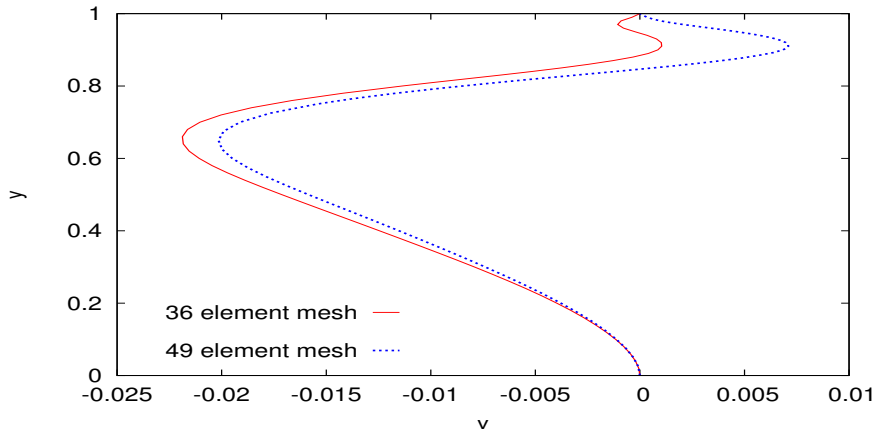

(c) Velocity v versus y at x=0.5

Figure 4.96: Solutions of class C^2 for mesh M1 (h_d = 0.1) ; p=9 and mesh M3 (h_d = 0.05) ; p=9, $De = 1.2$

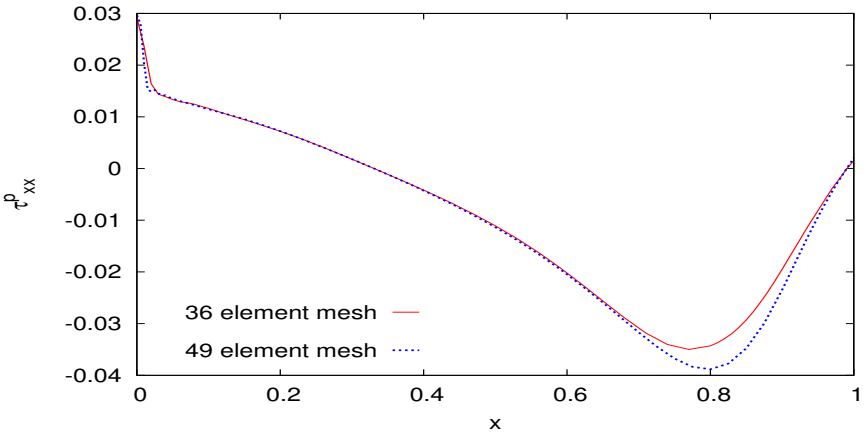

(a) Normal Stress τ^p_{xx} versus x at y=0.5

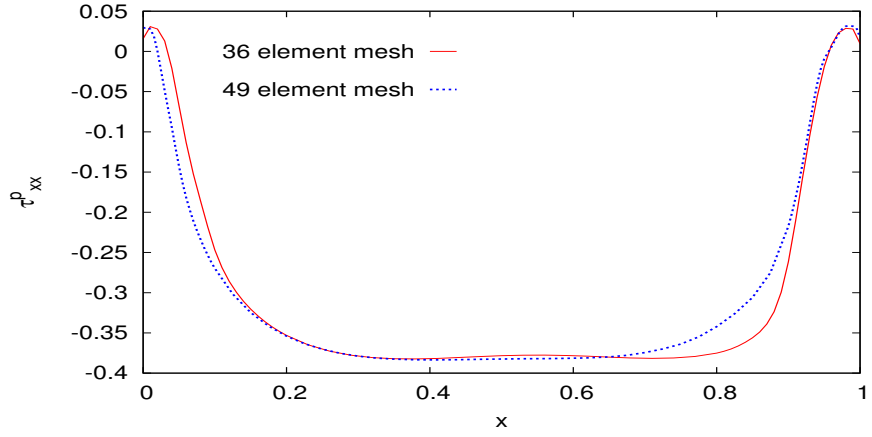

(b) Normal Stress τ^p_{xx} versus x at y=0.99

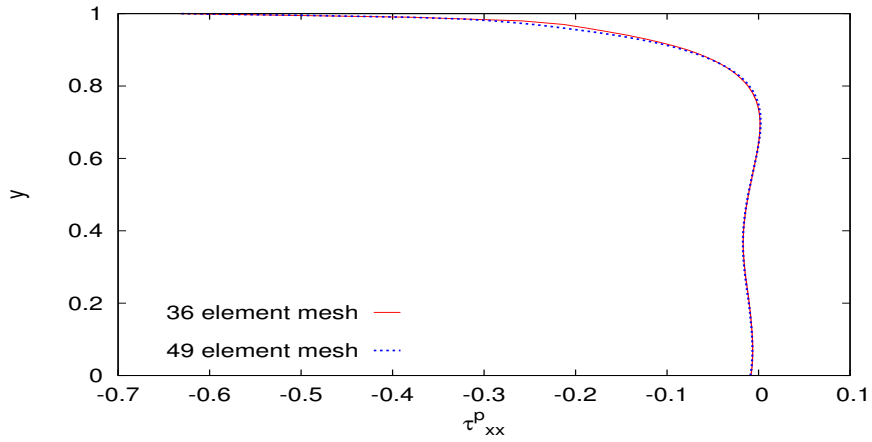

(c) Normal Stress τ^p_{xx} versus y at x=0.5

Figure 4.97: Solutions of class C^2 for mesh M1 (h_d = 0.1) ; p=9 and mesh M3 (h_d = 0.05) ; p=9, $De = 1.2$

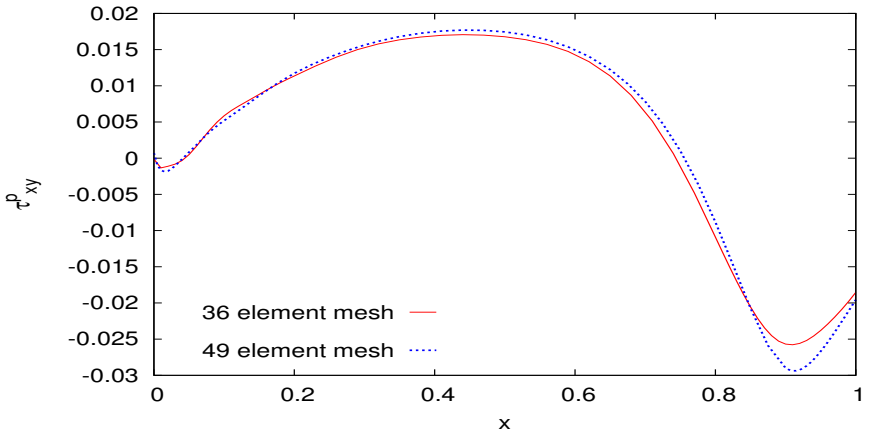

(a) Shear Stress τ^p_{xy} versus x at y=0.5

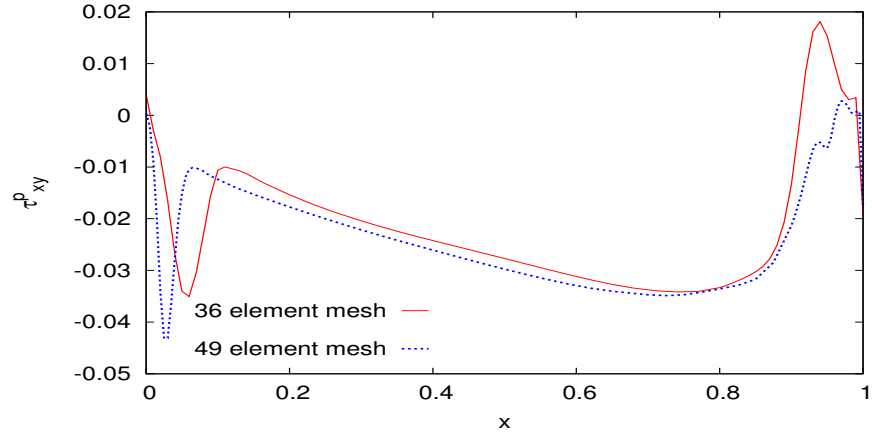

(b) Shear Stress τ^p_{xy} versus x at y=0.99

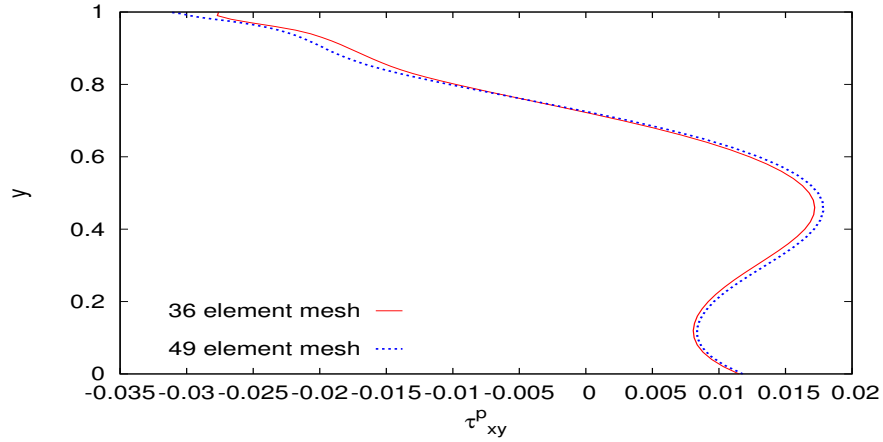

(c) Shear Stress τ^p_{xy} versus y at x=0.5

Figure 4.98: Solutions of class C^2 for mesh M1 (h_d = 0.1) ; p=9 and mesh M3 (h_d = 0.05) ; p=9, $De = 1.2$

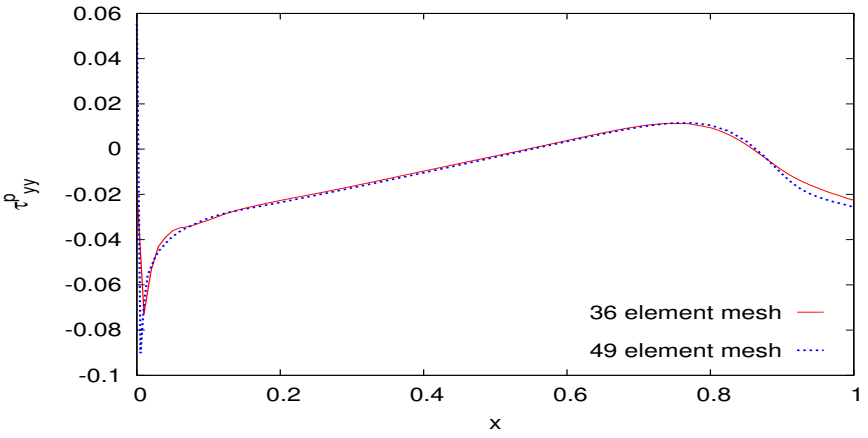

(a) Normal Stress τ^p_{yy} versus x at y=0.5

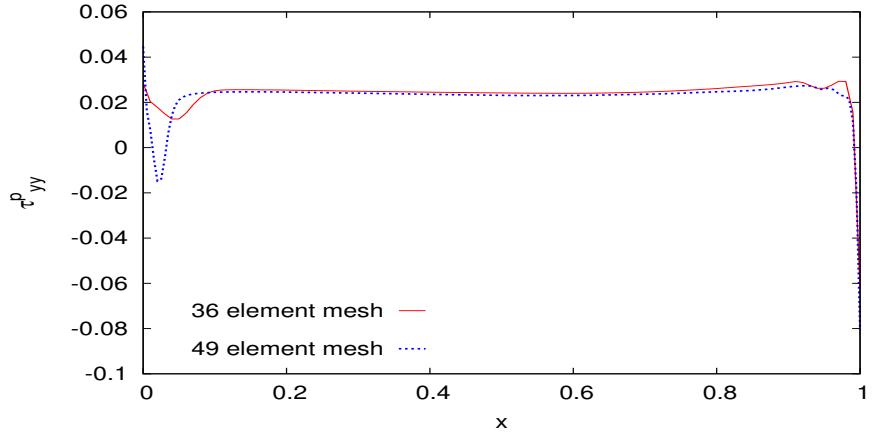

(b) Normal Stress τ^p_{yy} versus x at y=0.99

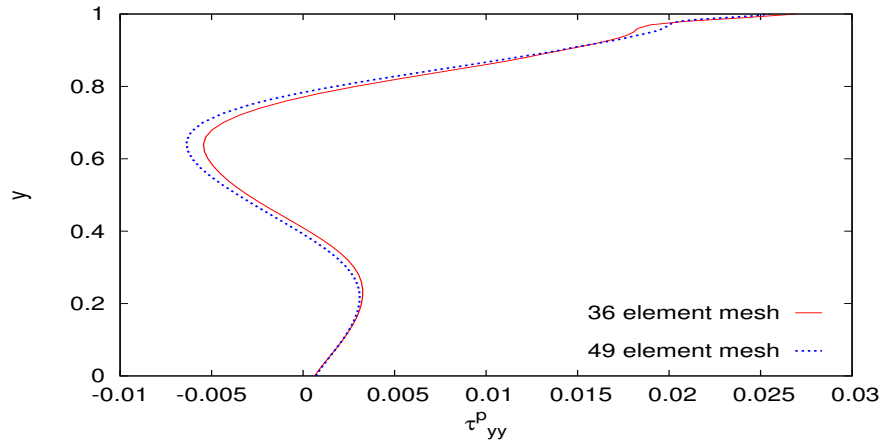

(c) Normal Stress τ^p_{yy} versus y at x=0.5

Figure 4.99: Solutions of class C^2 for mesh M1 (h_d = 0.1) ; p=9 and mesh M3 (h_d = 0.05) ; p=9, $De = 1.2$

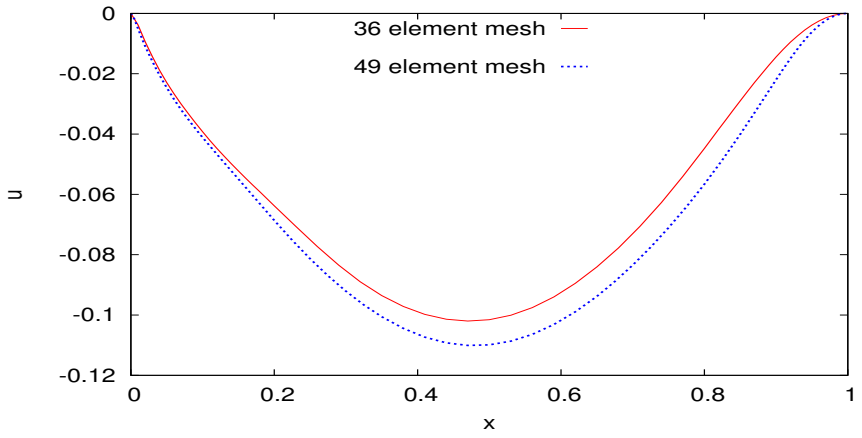

(a) Velocity u versus x at y=0.5

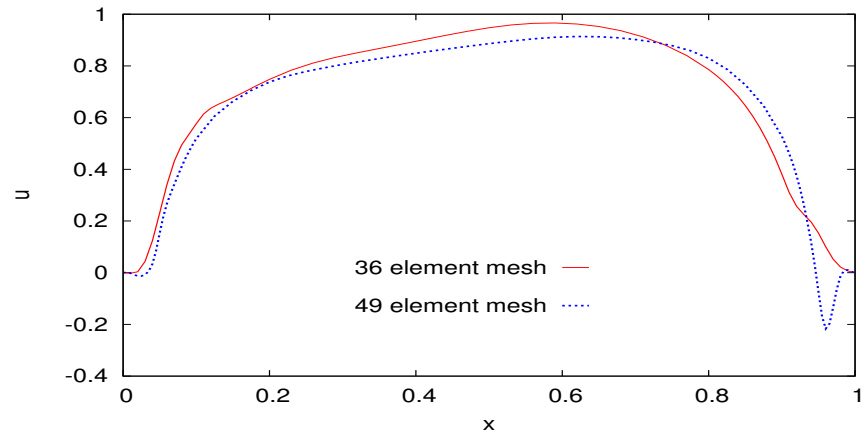

(b) Velocity u versus x at y=0.99

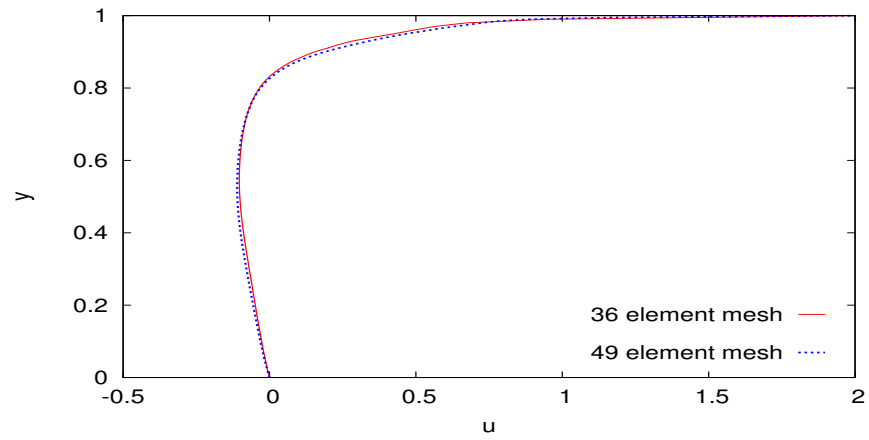

(c) Velocity u versus y at x=0.5

Figure 4.100: Solutions of class C^2 for mesh M1 (h_d = 0.1) ; p=9 and mesh M3 (h_d = 0.05) ; p=9, $De = 2.40$

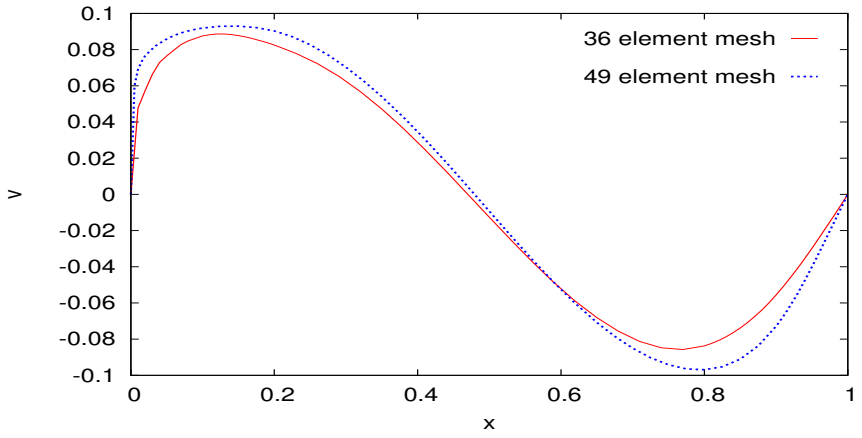

(a) Velocity v versus x at y=0.5

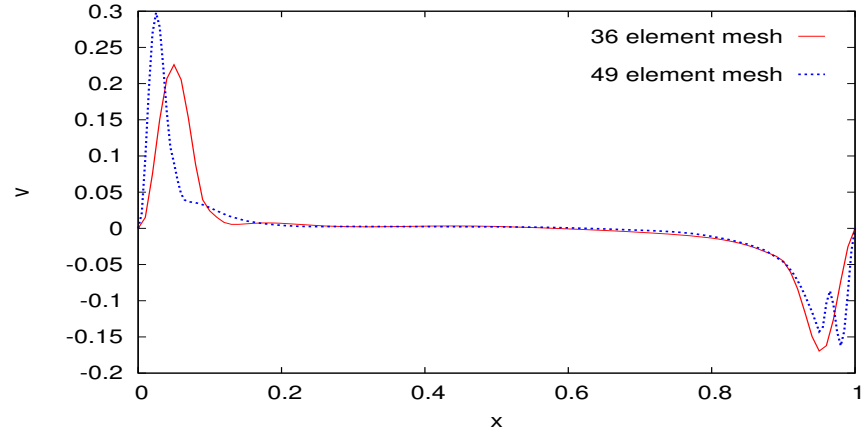

(b) Velocity v versus x at y=0.99

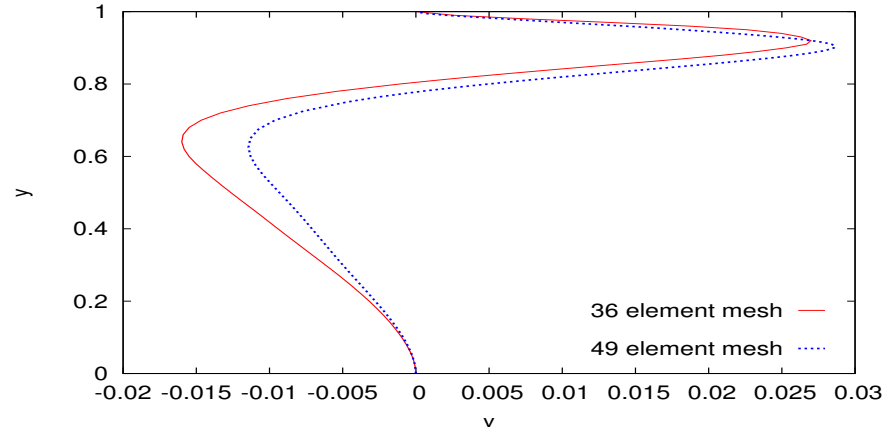

(c) Velocity v versus y at x=0.5

Figure 4.101: Solutions of class C^2 for mesh M1 (h_d = 0.1) ; p=9 and mesh M3 (h_d = 0.05) ; p=9, $De = 2.40$

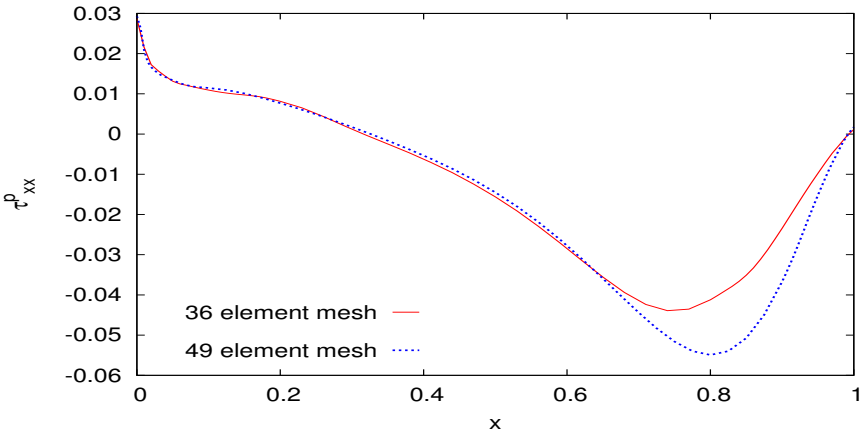

(a) Normal Stress τ^p_{xx} versus x at y=0.5

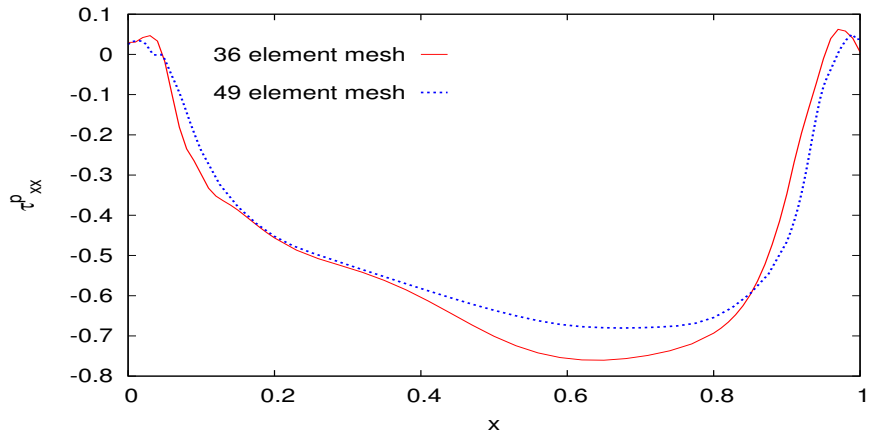

(b) Normal Stress τ^p_{xx} versus x at y=0.99

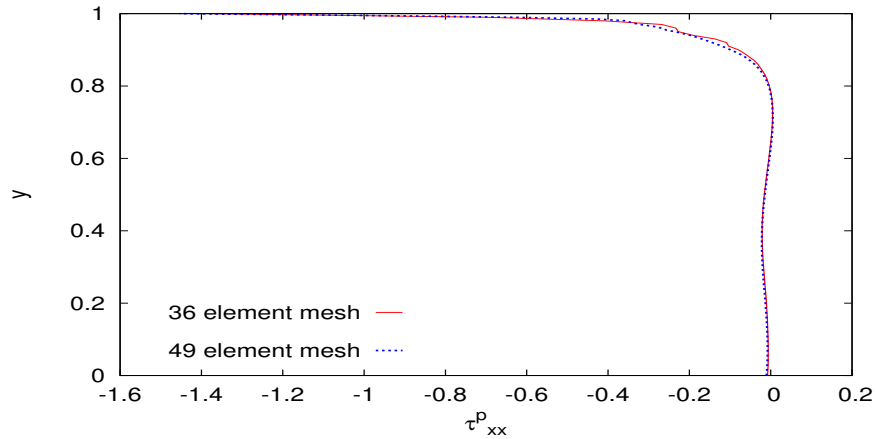

(c) Normal Stress τ^p_{xx} versus y at x=0.5

Figure 4.102: Solutions of class C^2 for mesh M1 (h_d = 0.1) ; p=9 and mesh M3 (h_d = 0.05) ; p=9, $De = 2.40$

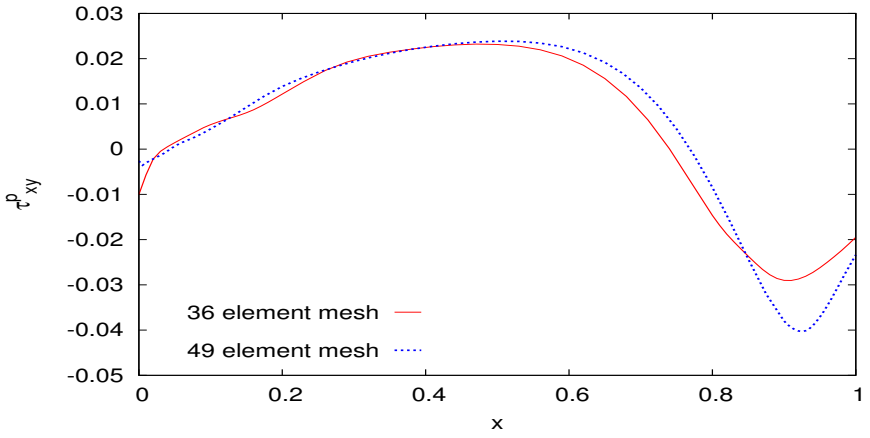

(a) Shear Stress τ^p_{xy} versus x at y=0.5

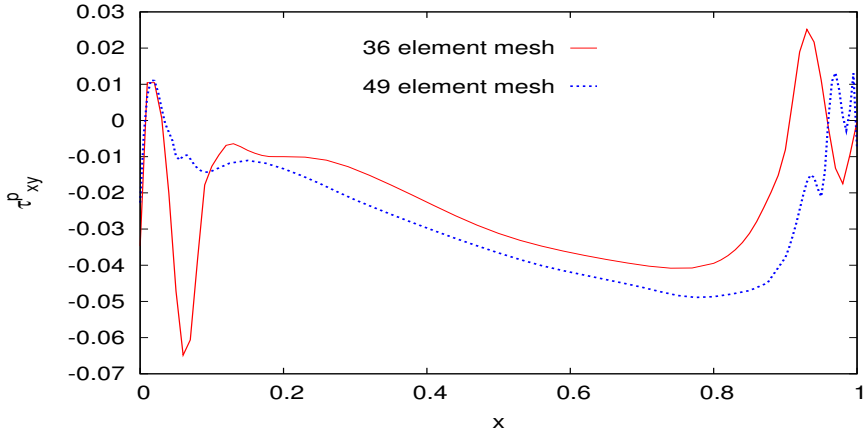

(b) Shear Stress τ^p_{xy} versus x at y=0.99

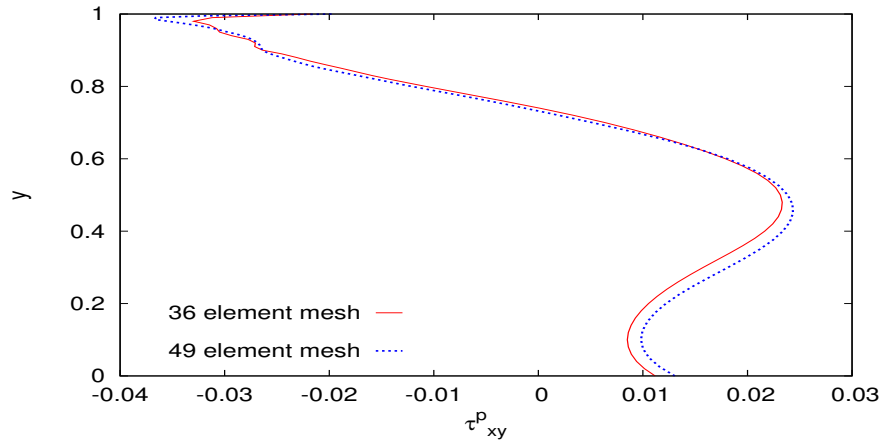

(c) Shear Stress τ^p_{xy} versus y at x=0.5

Figure 4.103: Solutions of class C^2 for mesh M1 (h_d = 0.1) ; p=9 and mesh M3 (h_d = 0.05) ; p=9, $De = 2.40$

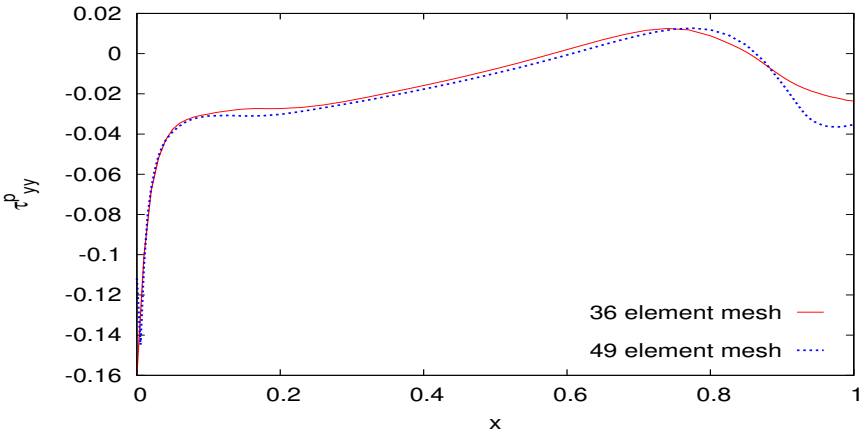

(a) Normal Stress τ^p_{yy} versus x at y=0.5

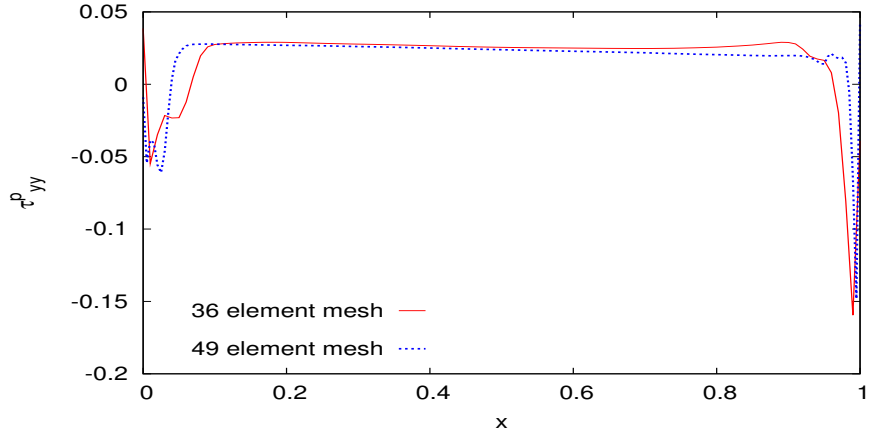

(b) Normal Stress τ^p_{yy} versus x at y=0.99

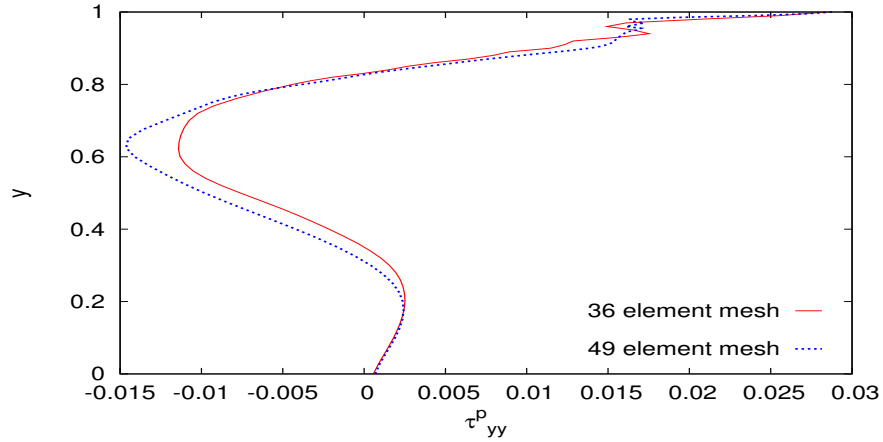

(c) Normal Stress τ^p_{yy} versus y at x=0.5

Figure 4.104: Solutions of class C^2 for mesh M1 (h_d = 0.1) ; p=9 and mesh M3 (h_d = 0.05) ; p=9, $De = 2.40$

4.4 Summary

A variety of numerical studies are presented in this chapter for different model problems. The one dimensional fully developed flow between parallel plates is used as a model problem to investigate the performance of different mathematical models based on different choices of stresses as variables for progressively increasing Deborah numbers. In particular the mathematical models utilizing **U**, p, $\boldsymbol{\tau}^p$; **U**, p, $\boldsymbol{\tau}$ and **U**, p, $\boldsymbol{\tau}^e$ as variables are considered. Numerical studies show that the mathematical models based on **U**, p, $\boldsymbol{\tau}^p$ and **U**, p, $\boldsymbol{\tau}$ as variables show excellent agreement with each other upto Deborah number as high as $De = 6514.52$ and there does not appear to be any limit on Deborah number in the computations. The formulation based on **U**, p, $\boldsymbol{\tau}^e$ as variables performs well upto $De = 21.05$ and the results are in agreement with the other mathematical models. Beyond Deborah number of 21.05 the computations experience difficulty in the Newton's method with line search and eventually result in lack of convergence.

Numerical studies are also presented for developing flow between parallel plates upto Deborah number of 21.13. In all cases sufficient length is used to ensure fully developed flow at the outflow boundary. For all Deborah numbers, the fully developed outflow is in excellent agreement with results obtained using 1-D fully developed flow formulation. In these studies, the flow at the inlet is two dimensional (as opposed to 1-D fully developed flow) with progressively higher gradients for high deborah numbers that eventually becomes fully developed one dimensional flow at the outflow boundary.

Numerical studies for the lid driven cavity are presented using a mathematical idealization of the physics at the corners where the lid meets the stationary walls. A continuous and differentiable distribution of the lid velocity based on interpolants over a small length h_d at the corners make the solution analytic and permits the recovery of the true physics in the limiting process of $h_d \rightarrow 0$ and $k \rightarrow \infty$. Two values of h_d (0.1 and 0.05) are used to present numerical solutions that are independent of h, p and k upto deborah number of 2.4. A comparison of the converged solution for the two values of h_d shows that decreasing h_d only results in solution changes in a very small

neighborhood of the corners which remain localized and hence has virtually no effect on the solution in the rest of the cavity. The numerical studies with uniformly refined discretization and those with graded discretization show that the graded discretization yield almost the same accuracy as those from highly refined uniform discretization but only for small fraction of the degrees of freedom.

Chapter 5

Fiber Spinning in Polymer flows

5.1 Introduction

The time dependent polymer flows has been simulated numerically using finite difference, finite volume, finite element methods using space-time coupled and decoupled approaches. We consider fiber spinning in polymer flows as a model problem. Apart from the industrial applications, fiber spinning technique is dominantly used as an extensional rheometer. The schematic of fiber spinning process is shown in figure 5.1. Polymer melt exits the spinneret and is taken up at position L downstream by take up spool at a speed which is greater than the extrusion velocity, so that the thread is actually stretched. The important parameter in the melt spinning process is the draw ratio which is the ratio of velocity at take up spool to the velocity of polymer melt at the spinneret. The draw ratio can also be defined as the ratio of area of the polymer fiber at spinneret to the area at take up spool. The important parameters for the melt spinning process involves velocity at the inlet, velocity at take up spool, melt spinning length and transport properties of polymers. The literature review presented is an attempt to comprehensively include different mathematical models, effect of various parameters in the mathematical models and various numerical and experimental techniques to study the melt spinning problem in polymers.

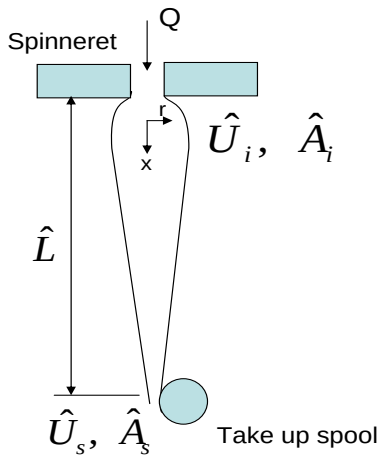

Figure 5.1: Fiber spinning process

5.2 Literature review

The fundamental set of equations describing the physics of the melt spinning process were first introduced by Kase and Matsuo [49] and further discussed by Matovich and Pearson [50] for the incompressible isothermal extensional flow characteristics of a molten threadline. Avenas et al. [51] used slight generalization of the classical Maxwell equation to solve the steady state isothermal spinning of viscoelastic material using Runge-Kutta-Gill method for a maximum draw ratio of 20. In [52, 53], the isothermal melt spinning is studied with a spectrum of relaxation times and it is concluded that relaxation spectrum predicts a more linear velocity and higher elongational stress than the computations with single relaxation time. Dupret et al. [54] explained the importance of evolutionary character of a system and elucidated how the different constitutive models lose evolutionary character. The studies indicate that Maxwell model maintains the evolutionary character under all circumstances while Johnson Segalman and White Metzner models do not. Addition of pure viscous terms to Johnson Segalman and white Metzner models alleviates the problem in certain situations. The effect of process variables on the stability of isothermal melt spinning is studied in [55, 56, 57]

for variety of polymers and the phenomenon of draw resonance is reported in the melt spinning process.The experimental and numerical results for isothermal fiber spinning of molten polyethylenes and Newtonian fluid are studied in [58, 59, 60, 61, 62, 63] using Maxwell model, Bird Carreau model, Bogue-white model and Peterlin model.

Papanastasiou et al. [64] studied the BVPs and IVPs for fiber spinning using a non-linear integral constitutive equation for Newtonian liquid, extension thinning and extension thickening liquids at high draw ratios and high elasticity. The numerical simulations are performed using finite element technique with galerkin method for both steady and transient cases. In [65, 66, 67, 68], the development of molecular orientation within the fiber for polystyrene and glass fibers is studied to determine the effect of molecular parameters on the relaxation spectrum of polymer. Zieminski and Spruiell [69] presented a mathematical model for high speed non-isothermal melt spinning for crystalline polymers (Nylon 66)involving the gravity effect, inertia effect, air friction and the effects of temperature and amorphous molecular orientation on the crystallization kinetics for the melt spinning process. Sampers and leblans [70]studied and compared the behavior of polymer flow for isothermal melt spinning and isothermal creep under a constant force and reported that the flow prehistory plays a dominant role on velocity profiles for higher flow rates. Giesekus [43, 71] presented a constitutive equation which is non-linear in stresses, predicts shear thinning behavior and gives non-vanishing first and second normal stress differences. Yoo and Choi [72] used the single mode Giesekus constitutive equation and obtained analytical solution for plane couette flow and poiseuille flow. The quadratic term in the constitutive equation gives rise to two branched solutions and studies have been presented for different value of mobility parameter (α) and wiessenberg number.

The major instabilities associated with fiber spinning and film casting are draw resonance which is the variation in the cross sectional area and spinnability which is the ability to pull a melt into a long thread. An elaborate review of the process of melt spinning for commercially important polymers and different fiber spinning process such as dry spinning, wet spinning is presented in [73, 74, 75, 76]. Beris et al. [77] presented four first order quasi linear hyperbolic equation representing one dimen-

sional approximation to the transient fiber spinning process. The mathematical analysis concluded the relationship between maximum attainable draw ratio and Deborah number as $Dr <= 1 + 1/De$. Liu and Beris [78] investigated the numerical simulation of the truncated one dimensional fiber spinning equation using finite difference methods, Pseudo spectral methods and finite element method. The central finite difference techniques and galerkin finite element method becomes unstable at a certain point, whereas the upwinding techniques are mostly stable for different deborah numbers and draw ratios.

Papanastasiou et al. [79, 80] proposed a technique which precludes the need to impose unknown boundary condition at the synthetic inlet in various flow situations such as film formation and fiber spinning. The free boundary condition is same as relation between variation of a weighted quantity and its flux through the synthetic boundary which is inherent property of Galerkin method with weak form. Bechtel et al. [81] elucidates the importance of draw ratio for optimization of the fiber spinning process using Den, Petrie and Avenas (DPA) model. Iyengar et al. [82, 83] presented theoretical studies for isothermal steady state film casting process using modified Giesekus constitutive model. Ramanan et al. [84] designed and applied an experimental technique to determine the fiber profile and initial axial force near the spinneret. The initial data obtained was coupled with Giesekus constitutive equation for material characterization of the Boger fluid. Gunter et al. [85] solved the highly convective extensional flow using taylor galerkin method for coupled and decoupled formulations and advocated effective measures to remove the numerical oscillations from the solution. The dynamic evolution of viscoelastic fluid columns during elongation and subsequent stress relaxation is studied by Yao et al. [86]. Comprehensive comparison studies have been reported for single mode and multi mode formulations of the Giesekus model to elucidate the differences in the predicted viscoelastic behavior using relaxation spectrum.

Georgiou et al. [87] studied the transient couette flow problem for Johnson Segalman fluid with added Newtonian viscosity. The studies concluded that transient solutions are always bounded and converge to steady state and there are no regimes of self sustained oscillations. The numerical simulation of two dimensional plane cou-

ette flow and pressure driven flow for UCM and Oldoroyd-B model is examined by sureshkumar et al. [88]. The linear and non linear dynamics of viscoelastic flow is probed using DEVSS-G/SUPG methods. Bernaridin [89] studied three typical transient couette flows of viscoelastic fluids with the inertia of the moving cylinders into consideration. Forest et al. [90, 91] applied 1-D thin filament model for liquid crystalline polymers to simulate isothermal fiber spinning to study the effect of interaction between macroscopic hydrodynamics and internal orientation of fibers. Slattery et al. [92] applied the slattery analysis for commercial high speed non-isothermal fiber spinning. Doufas et al. [93] developed a mathematical model for the simulation of both high and low speed melt spinning which includes the combined effects of flow induced crystallization (FIC), viscoelasticity, air drag, filament cooling, inertia, surface tension and gravity. The formulation explained is a compromise between a molecular and continuum approach making a distinction between the amorphous and semi crystalline phases in the rheological response of the system. The strongly coupled differential equations for the melt spinning are solved as in initial value problem with a variable-step fourth order Runge-Kutta algorithm combined with a shooting method. McKinley et al. [94] underscores the importance of filament stretching devices to generate the experimental data for number of dilute, semi-dilute, entangled polymer solutions, melts and liquid crystalline solution.

Lee et al. [95] investigated the influence of fluid viscoelasticity on the draw resonance dynamics of melt spinning using white Metzner and Phan Thien Tanner fluid models. The increase in viscoelasticity increases tension and decreases tension sensitivity and thus helps in stabilizing the spinning process for extension thickening fluids and vice-versa for extension thinning fluids. Joo et al. [96] performed numerical simulation of two dimensional non-isothermal melt spinning for amorphous polystyrene and fast crystallizing Nylon 66. The set of nonlinear GDES including non-isothermal Giesekus constitutive equation is solved using the DEVSS-G/SUPG finite element method. Gou and Mchugh [97] predicted the dynamics of dry spinning of polymer fibers based on two dimensional model for the temperature using finite difference techniques. The proposed constitutive equation describes viscous and viscoelas-

tic effects and is based on an equivalent parallel combination of non-linear Giesekus model and a simple Newtonian part. The numerical simulation of time dependent viscoelastic flows using finite volume formulation is discussed by Xue et al. [98] with emphasis on numerical accuracy, efficiency and stability of the solution algorithms involved in solving the GDEs. The numerical simulations are performed for the startup and decay of poiseuille flows between parallel plates for Newtonian fluid and viscoelastic fluids with solvent viscosity described by Oldoroyd-B model. The numerical studies corroborate the fact that using stabilizing methods such as both side diffusion (BSD), EVSS, and adaptive viscous split stress (AVSS) causes change in type of equation and leads to diffusion in transient velocity field calculations and hence such forms should be avoided.

5.3 Scope of present study

In the present study we utilize the mathematical framework and associated finite element computational infrastructure presented by Surana et al. [41] to numerically simulate one dimensional unsteady flows of polymeric liquids described by Giesekus constitutive model. In this study the integral forms are space-time integral forms that are variationally consistent and hence the resulting computational processes are unconditionally stable non-degenerate during the entire evolution.

In this study the main focus is on the numerical simulation of time dependent melt spinning process. The numerical studies presented here involves,

(i) Development of the Governing Differential Equations for steady (BVP) and unsteady (IVP) melt spinning process.

(ii) Numerical simulation of BVP and IVP for four different polymeric fluids at very high draw ratios.

(iii) Investigation of the choice of reference quantities and their consequences on the numerical simulation of melt spinning process.

(iv) Various measures are employed to ensure that the partial differential equations

are accurately satisfied by the computed solutions in the pointwise sense in the entire domain and that the converged solutions indeed are in conformity with the physics of the model problem.

(v) Numerical studies presented in this study demonstrates the benefits of proposed Governing Differential Equations, and significance of the variationally consistent and space-time variationally consistent integral forms in hpk framework.

Chapter 6

Development of GDEs and Computational framework for Fiber Spinning

In this chapter, we shall discuss the most widely used Governing Differential Equations (GDEs) for numerical simulation of fiber spinning their shortcomings and present the development of new GDEs that are more in conformity with the physics. The problem of fiber spinning will be considered as two point boundary value problem as well as initial value problem. The GDEs for the fiber spinning process involve constitutive equations which relates the velocity gradients with the stresses. In this work Giesekus constitutive equation is used for computations of both steady and unsteady fiber spinning. The important parameters for the melt spinning process involves velocity at the inlet, velocity at take up spool, melt spinning length and transport properties of polymer.

6.1 GDEs using $U, A, \boldsymbol{\tau}^p, \boldsymbol{\tau}^s$

Consider the flow to be axisymmetric and vertically downward, hence a cylindrical coordinate system is suitable for the development of the mathematical model. The origin of the coordinate system is centered at the location where axial velocity and stresses

are virtually uniform over the cross-section area of the fiber reducing the coordinate system to a radial (r) and axial (x) component. We assume thin filament approximation, thus, the dynamic quantities related to the flow do not vary substantially in the radial direction as compared to the axial direction and hence flow variables can be assumed to be dependent only on the axial (x) direction and time t. The variables for the melt spinning process involves cross sectional area (A), velocity (U), polymer stress $\boldsymbol{\tau}^p$, solvent stress $\boldsymbol{\tau}^s$. The following assumptions are most widely used in the numerical simulation of melt spinning process :

(i) Variables depend only on axial position x and time t.

(ii) Surface tension, circumferential friction, inertia and gravity effects are neglected.

(iii) Origin of the coordinate system is at a point where velocity is constant (After die swell).

The most commonly used GDEs in the literature [73],[95] involves,

1. Continuity Equation

$$\frac{\partial \hat{A}}{\partial \hat{t}} + \frac{\partial(\hat{A}.\hat{U})}{\partial \hat{x}} = 0 \tag{6.1}$$

2. Force Balance Equation

   By conservation of linear momentum the axial force must be constant. Based on assumptions, we get, $\hat{\tau}_{rr} = \hat{p}$ and hence,

$$\frac{\partial \left(\hat{A}.(\hat{\tau}_{xx} - \hat{\tau}_{rr}) \right)}{\partial \hat{x}} = 0 \tag{6.2}$$

3. Constitutive Equation : Giesekus

$$\hat{\boldsymbol{\tau}}^p + \lambda. \left(\frac{\partial \hat{\boldsymbol{\tau}}^p}{\partial \hat{t}} + (\hat{U}.\hat{\nabla})\hat{\boldsymbol{\tau}}^p - (\hat{\nabla}.\hat{U})\hat{\boldsymbol{\tau}}^p - \hat{\boldsymbol{\tau}}^p(\hat{\nabla}.\hat{U})^T \right) + \frac{\alpha.\lambda}{\hat{\eta}_p}(\hat{\boldsymbol{\tau}}^p\hat{\boldsymbol{\tau}}^p) = 2.\hat{\eta}_p.\dot{\boldsymbol{\gamma}} \tag{6.3}$$

$$\hat{\boldsymbol{\tau}}^s = 2.\hat{\eta}_s.\dot{\boldsymbol{\gamma}} \tag{6.4}$$

We make following remarks for the equations (6.1-6.4) :

1. The equations (6.1-6.4) are believed to form an idealized model of fiber spinning process which provides a good qualitative description of the process parameters for fiber spinning.

2. The important aspect to note in the continuity equation is the presence of both Area ($\hat{A}$) and Velocity ($\hat{U}$) as dependent variables. Since $\hat{\rho}$ is constant, $\hat{Q}_i = \hat{Q}_s = \hat{Q}(x,t) = constant$. Hence $\hat{U}$ and $\hat{A}$ both cannot be dependent variables.

3. The momentum equation is obtained without the surface tension, circumferential friction, inertia and gravity, these effects are not substantial for the viscous fluids. The momentum equation mentioned above is widely used in literature and is believed to perform well for industrial melt spinning conditions.

4. The momentum equation does not have a convective term $\hat{A}\hat{U}\frac{\partial \hat{U}}{\partial \hat{x}}$. This term can be significant for the melt spinning process at high draw ratios.

5. The GDEs (6.1) - (6.4) are solved in the literature using finite difference techniques, finite element method and finite volume methods. The computational techniques used in the literature always have stability problems and the problems of computations at high draw ratios. The computational methodology used in this work is based on hpk framework with space-time variationally consistent integral forms and hence is unconditionally stable and non-degenerate.

6. The computations in hpk framework ensure the higher order global differentiability of the solutions in space and time.

6.2 Development of new GDEs for Initial Value Problem

As mentioned in the previous section, the continuity equation cannot have both area and velocity as variables, therefore we have to substitute area in terms of velocity in the GDEs.

1. Continuity Equation:

$$\hat{Q}_i = \hat{Q}_s = \hat{Q}(x,t) = \hat{U}(x).\hat{A}(x) = constant$$

$$\frac{\partial \hat{Q}}{\partial \hat{x}} = 0, \;\; \frac{\partial \hat{Q}}{\partial \hat{t}} = 0$$

$$\hat{A} = \frac{\hat{Q}}{\hat{U}}$$

$$\frac{\partial \hat{A}}{\partial \hat{x}} = \hat{Q}(\frac{-1}{\hat{U}^2})\frac{\partial \hat{U}}{\partial \hat{x}}$$

The above derived expression for $\frac{\partial \hat{A}}{\partial \hat{x}}$ is substituted in the momentum equation.

2. Momentum Equation: Assuming $\hat{p} = \hat{\tau}_{rr}$ and adding the convective term in equation 6.2 we get,

$$\hat{A}.\hat{\rho}\frac{\partial \hat{U}}{\partial \hat{t}} + \hat{A}.\hat{\rho}.\hat{U}\frac{\partial \hat{U}}{\partial \hat{x}} - \frac{\partial \hat{A}.(\hat{\tau}_{xx} - \hat{\tau}_{rr})}{\partial \hat{x}} = 0 \tag{6.5}$$

3. Constitutive Equation:

$$\hat{\boldsymbol{\tau}}^p + \lambda.\left(\frac{\partial \hat{\boldsymbol{\tau}}^p}{\partial \hat{t}} + (\hat{U}.\hat{\nabla})\hat{\boldsymbol{\tau}}^p - (\hat{\nabla}.\hat{U})\hat{\boldsymbol{\tau}}^p - \hat{\boldsymbol{\tau}}^p(\hat{\nabla}.\hat{U})^T\right) + \frac{\alpha.\lambda}{\hat{\eta}_p}(\hat{\boldsymbol{\tau}}^p\hat{\boldsymbol{\tau}}^p) = 2.\hat{\eta}_p.\dot{\boldsymbol{\gamma}} \tag{6.6}$$

$$\hat{\boldsymbol{\tau}}^s = 2.\hat{\eta}_s.\dot{\boldsymbol{\gamma}} \tag{6.7}$$

we use, $\hat{\rho} = \rho_o.\rho,\ \hat{U} = U_o.U,\ \hat{\boldsymbol{\tau}_{ij}} = \boldsymbol{\tau}_o.\boldsymbol{\tau}_{ij},\ \hat{x} = L_o.x\ \hat{\eta}_p = \eta_o.\eta_p,\ \hat{\eta}_s = \eta_o.\eta_s$ to non dimensionalize the GDEs. Substituting $\frac{\partial \hat{A}}{\partial \hat{x}} = \hat{Q}(\frac{-1}{\hat{U}^2})\frac{\partial \hat{U}}{\partial \hat{x}}$ into momentum equation and simplifying we get,

Momentum Equation :

$$U.\left(\frac{\partial U}{\partial t} + U.\frac{\partial U}{\partial x}\right) + f_1\frac{\partial U}{\partial x}(\tau^p_{xx} - \tau^p_{rr}) - f_1.U\left(\frac{\partial \tau^p_{xx}}{\partial x} - \frac{\partial \tau^p_{rr}}{\partial x}\right)$$

$$+3.\eta_s.f_1.\left(\frac{\partial U}{\partial x}\right)^2 - 3.\eta_s.f_1.U.\left(\frac{\partial^2 U}{\partial x^2}\right) = 0 \tag{6.8}$$

Constitutive equations :

$$\tau_{xx}^{p} + De\left(\frac{\partial \tau_{xx}^{p}}{\partial t} + U.\frac{\partial \tau_{xx}^{p}}{\partial x} - 2.\frac{\partial U}{\partial x}\tau_{xx}^{p}\right) + \frac{De.\alpha}{\eta_p}.f_2.(\tau_{xx}^{p}.\tau_{xx}^{p}) - 2.\eta_p.f_2.\frac{\partial U}{\partial x} = 0 \tag{6.9}$$

$$\tau_{rr}^{p} + De\left(\frac{\partial \tau_{rr}^{p}}{\partial t} + U.\frac{\partial \tau_{rr}^{p}}{\partial x} - 2.\frac{\partial U}{\partial x}\tau_{rr}^{p}\right) + \frac{De.\alpha}{\eta_p}.f_2.(\tau_{rr}^{p}.\tau_{rr}^{p}) + \eta_p.f_2.\frac{\partial U}{\partial x} = 0 \tag{6.10}$$

$$where \;\; Re = \frac{\rho_o.L_o.U_o}{\eta_o}$$

$$De = \frac{\lambda.U_o}{L_o}$$

$$where \;\; f_1 = \begin{cases} 1 & if\ \tau_0 = \rho_0 u_0^2 = (\tau_0)_{cke} \\ Re & if\ \tau_0 = \eta_0 u_0 / L_0 = (\tau_0)_{cvs} \end{cases} \tag{6.11}$$

$$f_2 = \begin{cases} 1/Re & if\ \tau_0 = \rho_0 u_0^2 = (\tau_0)_{cke} \\ 1 & if\ \tau_0 = \eta_0 u_0 / L_0 = (\tau_0)_{cvs} \end{cases} \tag{6.12}$$

$Where, (\tau_0)_{cke}$: reference stress based on characteristic kinetic energy.

$(\tau_0)_{cvs}$: reference stress based on characteristic viscous stress.

6.3 GDEs for Boundary Value Problem

The equations (6.8-6.10) represents the GDEs for the time dependent melt spinning process. The corresponding mathematical model for stationary process (BVP) is obtained by setting time dependent terms to zero in (6.8) - (6.10).

Momentum Equation :

$$U.\left(U.\frac{\partial U}{\partial x}\right)+f_1\frac{\partial U}{\partial x}\left(\tau_{xx}^p-\tau_{rr}^p\right)-f_1.U\left(\frac{\partial \tau_{xx}^p}{\partial x}-\frac{\partial \tau_{rr}^p}{\partial x}\right)+3.\eta_s.f_1.\left(\frac{\partial U}{\partial x}\right)^2 -3.\eta_s.f_1.U.\left(\frac{\partial^2 U}{\partial x^2}\right)=0 \tag{6.13}$$

Constitutive equations :

$$\tau_{xx}^p+De\left(U.\frac{\partial \tau_{xx}^p}{\partial x}-2.\frac{\partial U}{\partial x}\tau_{xx}^p\right)+\frac{De.\alpha}{\eta_p}.f_2.(\tau_{xx}^p.\tau_{xx}^p) -2.\eta_p.f_2.\frac{\partial U}{\partial x}=0 \tag{6.14}$$

$$\tau_{rr}^p+De\left(U.\frac{\partial \tau_{rr}^p}{\partial x}-2.\frac{\partial U}{\partial x}\tau_{rr}^p\right)+\frac{De.\alpha}{\eta_p}.f_2.(\tau_{rr}^p.\tau_{rr}^p) +\eta_p.f_2.\frac{\partial U}{\partial x}=0 \tag{6.15}$$

$$where\ \ Re=\frac{\rho_o.L_o.U_o}{\eta_o},\ \ De=\frac{\lambda.U_o}{L_o}$$

$$where\ \ f_1=\begin{cases}1 & if\ \tau_0=\rho_0u_0^2=(\tau_0)_{cke}\\ Re & if\ \tau_0=\eta_0u_0/L_0=(\tau_0)_{cvs}\end{cases} \tag{6.16}$$

$$f_2=\begin{cases}1/Re & if\ \tau_0=\rho_0u_0^2=(\tau_0)_{cke}\\ 1 & if\ \tau_0=\eta_0u_0/L_0=(\tau_0)_{cvs}\end{cases} \tag{6.17}$$

$Where, (\tau_0)_{cke}$: reference stress based on characteristic kinetic energy.

$(\tau_0)_{cvs}$: reference stress based on characteristic viscous stress.

6.4 Computational framework : BVP

The GDEs describing the time dependent and stationary state melt spinning process are non-linear partial differential equations. Surana et al. has shown that when the

differential operators in the BVPs are non-linear only least squares processes in which non-linear algebraic equations are solved using Newton's linear method are variationally consistent with the approximation that the term containing the second variation of residual be neglected in the second variation of the least squares functional. The VC integral forms yield unconditionally stable and non degenerate computational processes, this cannot be ensured for the integral forms that are variationally inconsistent and hence for non-linear GDEs the least squares finite element method is highly meritorious over all others. The details of the Least Squares Finite Element process are same as those described in chapter 3. We note the following,

1. GDEs describing the melt spinning process are non-linear.
2. Galerkin method, Galerkin method with weak form, Petrov Galerkin method are Variationally Inconsistent (VIC) [3] for the non-linear problems.
3. Least Squares Process using Newton's linear method is Variationally Consistent (VC) [3] for the non-linear problems.
4. Numerical simulations for BVP are based on LSP in hpk framework.

6.5 Computational framework : IVP

Based on [41], the space-time Galerkin method and the space-time Galerkin method with weak form are STVIC regardless of the problem, but the space-time coupled least-squares process (STLSP) is always space time variationally consistent (STVC) for non-self-adjoint as well as non-linear space time differential operators. Thus the STLSP is the only viable alternative to have as a computational process that is unconditionally stable and non-degenerate. Also, the STLSP based on the strong form of GDEs is highly meritorious over the STLSP based on the weak form of GDEs [46] and hence used in the present work.

The details of the STLSP process are followed as explained in reference [41] for equations (6.8-6.10). The time evolution of the solution is obtained using space-time strip with time marching. The STLSP is applied to the first space-time strip (from

$t = 0$ to t = Δt) using BCs and ICs and a solution ${}^1\varphi_h$ is computed. Appropriate h, p and k refinement is used so that the solution for the first space time strip is within the specified tolerance limit(i.e. ${}^1I({}^1\varphi_h) \leq \Delta$). This ensures that GDEs for each space-time element of ${}^n\bar{\Omega}^T_{xt}$ are satisfied accurately in the point-wise sense. Now we consider second space-time strip $t = \Delta t$ to $t = 2\Delta t$. The initial conditions at $t = \Delta t$ for this space-time strip are obtained from the ${}^1\varphi_h$ for first space-time strip at $t = \Delta t$. Using these ICs and the BCs, a solution is computed for the second space-time strip. During the computations for the second space-time strip we maintain same p_1^i ,p_2^i, k_1^i and k_2^i as in case of first space-time strip. This process is continued until the desired value of time is reached. We note that in this time marching approach it is essential to obtain a converged solution for the current space-time strip before time marching to the next due to the fact that the solution from the current space-time strip serves as initial conditions for the next space-time strip. In general we make following remarks,

1. The transient melt spinning process is described by non-linear space-time differential operator.

2. STGAL, STGAL/WF, STPGM are all STVIC and hence are not used in this work.

3. STLSP with Newton's first order method is STVC and is used for computations in this work.

4. Numerical Simulation based on STLSP in hpk framework considers:

   Approximations in $H^{k,p}$ $(\bar{\Omega}^e_{xt})$ spaces

   $k = (k_1, k_2)$; where,

   k_1 = Order of approximation space in spatial direction

   k_2 = Order of approximation space in time direction

   $p = (p_1, p_2)$; where,

   p_1 = Degree of approximation in space

   p_2 = Degree of approximation in time

6.6 Summary

In this chapter the most widely used mathematical model for numerical simulation of fiber spinning process is presented and discussed. This mathematical model is derived using U, A, $\boldsymbol{\tau}^p$ and $\boldsymbol{\tau}^s$ as variables. It is shown that this mathematical model is spurious in the sense that it does not recognize that for incompressible polymer flow the flow rate is constant in the fiber spinning process. The development of new mathematical model for time dependent as well as stationary fiber spinning processes is presented using Giesekus constitutive equations based on constant flow rate resulting in axial velocity U and polymer stress $\boldsymbol{\tau}^p$ as dependent variables. The resulting GDEs are in the strong form as opposed to a first order system (weak form). The merits of the strong form of GDEs have already been discussed in chapter 3. Since the mathematical model is a system of nonlinear partial differential equations, LSP and STLSP [3] are utilized to construct the finite element formulations.

Chapter 7

Numerical Studies for Fiber Spinning

In this chapter we present numerical studies for time dependent and stationary fiber spinning processes using the mathematical model and the computational framework described in chapter 6. The numerical studies in this section are designed to demonstrate that : (i) the numerical solution for BVP and IVP are possible for all ranges of draw ratio and (ii) importance of the choice of reference quantities on the performance of computational processes.

7.1 Fiber spinning : BVP

The fiber spinning process is modelled as a two point boundary value problem. Figure 7.1 shows a schematic of the computational domain and a typical three node p-version C^k element. The problem description involves specification of the velocity at inlet (U_i), and at the take up spool (U_s) depending on the desired draw ratio of the fiber spinning process. The computational technique utilized in this work precludes the need of imposition of the unknown value of stresses at the inlet and hence the fiber spinning process can be solved as a two point boundary value problem. We consider four different polymeric fluids that are used in the literature. The properties of the polymeric fluids and the processing parameters of the fiber spinning process are listed

in table 7.1.

Table 7.1: Polymer Properties

Fluid No.	Type	$\hat{L}$	$\hat{\eta}_p$	$\hat{\eta}_s$	λ	(Dr)max
1	Boger[84]	0.08080m	2.936	8.004	0.9148	13
2	Polyisobutylene[20]	0.2m	1.424	0.002	0.06	100
3	Polystyrene[96]	1.72m	413.6859	0.4141	0.05	273
4	Nylon[93]	1.35m	147.4498	15.5502	0.001	2823

Fluid 1 :

We consider 10 and 20 element uniform discretizations in the spatial directions with local approximations of class C^1. For both discretizations at various draw ratios, Newton's method with line search is used to obtain converged solution of the non-linear algebraic equation. When $|\mathrm{g_i}|_{\max} \leq 10^{-6}$, the iterative process for nonlinear algebraic equations is considered converged. The degree of local approximations p, residual function I, $|\mathrm{g_i}|_{\max}$, total degrees of freedom (dofs) and the number of iterations for various studies are presented in table 7.2 for fluid 1. The choice of reference quantities to non dimensionalize the GDEs plays an important role in convergence of the computational process. The different choices of reference quantities results in different deborah number (De) and reynolds number (Re) in the computational domain and is one of the important factor that affects convergence of the computational process. As shown in figure 7.3(a) different combinations of reference velocity (U_o) and reference length (L_o) are possible, certain combinations converged within the tolerance limits and are indicated as okay in the figure 7.2(a). The choice of reference velocity $U_o = \hat{U}_i$ and reference length $L_o = \hat{L}$ are used for computations for fluid 1. The plots of U versus x and dU/dx are shown in figures 7.5(a) and 7.5(b). The graphs of τ^p_{xx} versus x and $d\tau^p_{xx}/dx$ versus x are shown in figures 7.6(a) and 7.6(b). Figures 7.7(a) and 7.7(b) shows plot of τ^p_{rr} versus x and $d\tau^p_{rr}/dx$ versus x. Since the polymeric liquid is in tension, the axial stress τ^p_{xx} has positive values and radial stress τ^p_{rr} has negative values.

Fluid 2 :

The Fluid 2 (Giesekus fluid) is a dense polymeric liquid. The numerical simulations are performed using 20, 40 and 60 element uniform discretizations in the spatial directions for draw ratio of 100. The solutions are computed for class C^1 with $p = 7$. In this case the reference velocity of $U_o = 1$ and reference length ($L_o = \hat{L}$) are utilized for computations, the effect of different choices of reference quantities is shown in figure 7.2(b). The degree of local approximations p, residual function I, $|\mathrm{g_i}|_{\max}$, total degrees of freedom (dofs) and the number of iterations for 20, 40 and 60 element meshes are presented in table 7.3. The plots of U versus x and first derivative of velocity in spatial direction, du/dx versus x are shown in figures 7.8(a) and 7.8(b). The graphs of τ^p_{xx} versus x and $d\tau^p_{xx}/dx$ versus x are shown in figures 7.9(a) and 7.9(b). Figures 7.10(a) and 7.10(b) shows plots of τ^p_{rr} versus x and $d\tau^p_{rr}/dx$ versus x respectively.

Fluid 3 :

The numerical simulation for Fluid 3 (Polystyrene) is performed using 20, 40 and 80 element uniform discretizations in spatial directions for draw ratio of 273. The solutions are computed for class C^1 with $p = 9$. In this case the reference velocity of $U_o = \hat{U}_s$ and reference length ($L_o = 1$) are utilized for computations, the effect of different choices of reference quantities is shown in figure 7.3(a). The degree of local approximations p, residual function I, $|\mathrm{g_i}|_{\max}$, total degrees of freedom (dofs) and the number of iterations for 20, 40 and 80 element meshes are reported in table 7.4. The plots of velocity U versus x and du/dx versus x are shown in figures 7.11(a) and 7.11(b) respectively. The graphs τ^p_{xx} versus x and $d\tau^p_{xx}/dx$ versus x are shown in figures 7.12(a) and 7.12(b) respectively. Figures 7.13(a) and 7.13(b) shows plots of τ^p_{rr} versus x and $d\tau^p_{rr}/dx$ versus x.

Fluid 4 :

The numerical simulation for Fluid 4 (Nylon) is performed using uniform 20, 40 and 80 element discretization in spatial direction for draw ratio of 2823. The solutions are computed for class C^1 with $p = 9$. In this case the reference velocity

of $U_o = \hat{U}_s$ and reference length ($L_o = 1$) are utilized for computations, the effect of different choices of reference quantities is shown in figure 7.3(b). The degree of local approximations p, residual function I, $|\mathrm{g_i}|_{\max}$, total degrees of freedom (dofs) and the number of iterations for 20, 40 and 80 element meshes are reported in table 7.5. The plots of U versus x and du/dx versus x are shown in figures 7.14(a) and 7.14(b). The graphs of τ^p_{xx} versus x and $d\tau^p_{xx}/dx$ versus x are shown in figures 7.15(a) and 7.15(b). Figures 7.16(a) and 7.16(b) shows plots of τ^p_{rr} versus x and $d\tau^p_{rr}/dx$ versus x.

Table 7.2: Fluid 1 : Solutions of class C^1, Draw ratio (Dr) = 13 (BVP)

Fluid No.	No.of elements	p-level	LSF (I)	$\|g_i\|$max	dof	Iterations
1	10	9	0.2084360E-14	0.4459E-08	244	30
1	20	9	0.33873140E-13	0.8301E-06	364	15

Table 7.3: Fluid 2 : Solutions of class C^1, Draw ratio (Dr) = 100 (BVP)

Fluid No.	No.of elements	p-level	LSF (I)	$\|g_i\|$max	dof	Iterations
2	20	7	0.5444874E-12	0.1772E-07	364	7
2	40	7	0.1945729E-15	0.3137E-10	724	8
2	60	7	0.3727629E-13	0.3821E-06	1084	7

Table 7.4: Fluid 3 : Solutions of class C^1, Draw ratio (Dr) = 273 (BVP)

Fluid No.	No.of elements	p-level	LSF (I)	$\|g_i\|$max	dof	Iterations
3	20	9	0.2334941227E-18	0.872596E-09	484	13
3	40	9	0.6906198649E-14	0.368765E-06	964	12
3	80	9	0.2967274093E-14	0.243976E-06	1924	14

Table 7.5: Fluid 4 : Solutions of class C^1, Draw ratio (Dr) = 2823 (BVP)

Fluid No.	No.of elements	p-level	LSF (I)	$\|g_i\|$max	dof	Iterations
4	20	9	0.2115708657E-14	0.848114E-07	484	29
4	40	9	0.4272324848E-15	0.225834E-06	964	29
4	80	9	0.3367408576E-19	0.114178E-07	1924	29

7.2 Fiber Spinning : IVP

Figure 7.4 shows a schematic of the computational domain and a typical space-time strip for an increment of time. The boundary conditions are shown as in figure 7.4(a). At inlet the velocity U_i is kept constant for all the time steps. At the take up spool the velocity changes from U_i to U_s over a single time step Δt and maintains constant value of U_s after that. Initial conditions are applied as shown in figure 7.4(b), the velocity U_i is applied as initial condition along spatial direction at t = 0. Also at time t = 0, the axial stress τ^p_{xx} and radial stress τ^p_{rr} are assumed zero along spatial direction. We consider local approximations of class C^{11}. When $|\mathrm{g_i}|_{\max} \leq 10^{-6}$, the iterative process for nonlinear algebraic equations is considered converged.

Fluid 1 :

The time evolution for the boger fluid (Fluid 1) is computed using 10 element uniform discretization in the spatial direction with $\Delta t = 0.01$. The local approximations of class C^{11} at $p = 9$ are considered for $De = 0.01949$ and $Re = 0.062751$ at draw ratio of 13 and the evolution is continued till the stationary state is reached. The value of the least squares functional (I) when the transient solution reaches the steady state is 0.190068E-07. The time evolution of velocity (u) and first derivative of velocity in spatial direction(du/dx) is shown in figures 7.5(a) and 7.5(b) respectively for $1^{st}, 5^{th}, 15^{th}$ and 50^{th} time steps. The time derivatives are close to zero by the end of 50^{th} time step indicating that the stationary state has been reached. Excellent agreement between the BVP solution and the steady state solution obtained from the time evolution process is shown in figures 7.5(a) and 7.5(b). Similarly the time evolution of axial stress (τ^p_{xx}) and $d\tau^p_{xx}/dx$ is shown in figures 7.6(a) and 7.6(b) respectively. Figures 7.7(a) and 7.7(b) shows time evolution of radial stress (τ^p_{rr}) and $d\tau^p_{rr}/dx$ respectively. The BVP solution for the axial and radial stresses matches well with the steady state solution of the IVP for Fluid 1.

Fluid 2 :

A 40 element mesh with uniform discretization of $\Delta x = 0.025$ in spatial direction and time step of $\Delta t = 0.2$ is used for transient simulation of Fluid 2 (Giesekus fluid). After an initial time step of 0.2, a time step of 0.1 is used for time marching process over the entire length of time domain. The local approximations of class C^{11} at $p = 7$ are considered for $De = 0.3$ and $Re = 112.20$ at draw ratio of 100 and the evolution is continued till the stationary state is reached. The value of the least squares functional (I) when the transient problem reaches the steady state is 0.2181349258E-10. The time evolution of velocity (u) and first derivative of velocity in spatial direction(du/dx) is shown in figures 7.8(a) and 7.8(b) respectively for $1^{st}, 20^{th}, 40^{th}$ and 100^{th} time steps. By the end of 100^{th} time step, the derivatives with respect to time are close to zero and thus the unsteady state problem has reached the steady state. There is an excellent match between the BVP solution and the steady state solution obtained from the time evolution process as indicated in figures 7.8(a) and 7.8(b). Similarly the time evolution of axial stress (τ^p_{xx}) and $d\tau^p_{xx}/dx$ are shown in figures 7.9(a) and 7.9(b) respectively. Figures 7.10(a) and 7.10(b) shows time evolution of radial stress (τ^p_{rr}) and $d\tau^p_{rr}/dx$ respectively.

Fluid 3 :

The transient simulation for the polystyrene (Fluid 3) is performed using 10 element mesh with uniform discretization of $\Delta x = 0.172$ in spatial direction and time step of $\Delta t = 2.0$. After an initial time step of 2.0, a time step of 0.05 is used for time marching process over the entire length of time domain. For Fluid 3, the local approximations of class C^{11} at $p = 9$ are considered for $De = 0.2252$ and $Re = 11.313$ at draw ratio of 273 and the evolution is continued till the steady state is reached. The value of the least squares functional (I) when the transient problem reaches the steady state is 0.1071440665E-14. The time evolution of velocity (u) and first derivative of velocity in spatial direction(du/dx) is shown in figures 7.11(a) and 7.11(b) respectively for $1^{st}, 10^{th}, 20^{th}$ and 60^{th} time steps. The time derivatives are close to zero by the end of 50^{th} time step and thus, the IVP solution has reached the steady state. There is an excellent match between the BVP solution and the steady state solution obtained from the time evolution pro-

cess as indicated in figures 7.11(a) and 7.11(b). Similarly the time evolution of axial stress (τ^p_{xx}) and $d\tau^p_{xx}/dx$ is shown in figures 7.12(a) and 7.12(b) respectively. Figures 7.13(a) and 7.13(b) shows time evolution of radial stress (τ^p_{rr}) and $d\tau^p_{rr}/dx$ respectively. The BVP solution for the axial and radial stresses matches well with the steady state solution of the IVP for Fluid 3.

Fluid 4 :

A 10 element mesh with uniform discretization of $\Delta x = 0.135$ in spatial direction and time step of $\Delta t = 0.25$ is considered for transient simulation of Nylon (Fluid 4). After an initial time step of 0.25, a time step of 0.025 is used for time marching process over the entire length of time domain. The local approximations of class C^{11} at $p = 9$ are considered for $De = 0.091691$ and $Re = 551.27$ at a very high draw ratio of 2823. The value of the least squares functional (I) when the transient problem reaches the steady state is 0.7660470157E-12. The time evolution of velocity (u) and first derivative of velocity in spatial direction(du/dx) is shown in figures 7.14(a) and 7.14(b) respectively for $1^{st}, 20^{th}, 40^{th}$ and 100^{th} time steps. By the end of 100^{th} time step, the derivatives with respect to time are close to zero and thus the unsteady state problem has reached the steady state. There is an excellent match between the BVP solution and the steady state solution obtained from the time evolution process as indicated in figures 7.14(a) and 7.14(b). Similarly the time evolution of axial stress (${\tau^p}_{xx}$) and $d\tau^p_{xx}/dx$ is shown in figures 7.15(a) and 7.15(b) respectively. Figures 7.16(a) and 7.16(b) shows time evolution of radial stress (τ^p_{rr}) and $d\tau^p_{rr}/dx$ respectively.

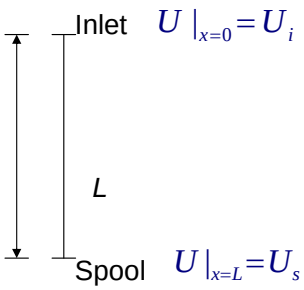

(a) Schematic for BVP

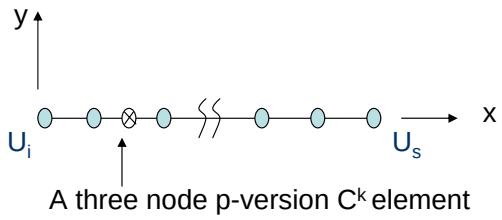

(b) Discretization

Figure 7.1: Schematic and Discretization for BVP : Fiber spinning process

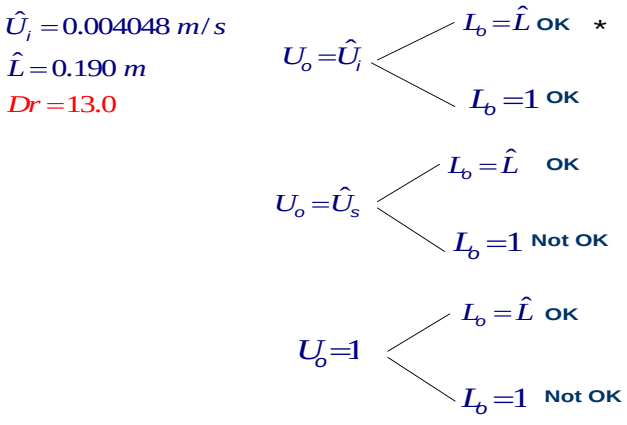

(a) Fluid 1 (Boger Fluid)

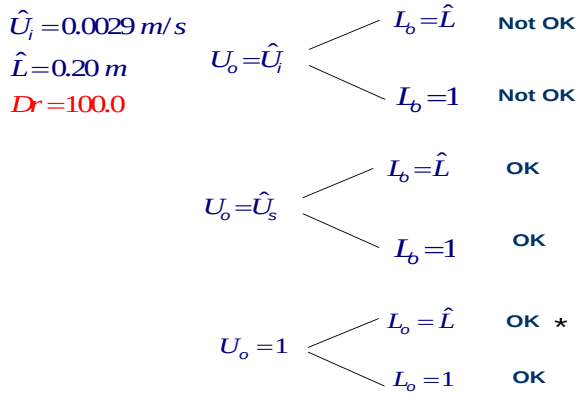

(b) Fluid 2 (Giesekus Fluid)

Figure 7.2: Choice of Reference Quantities; Fluid 1 and Fluid 2

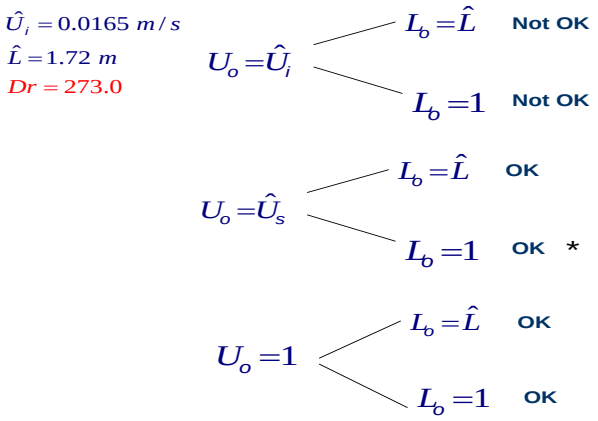

(a) Fluid 3 (Polystyrene)

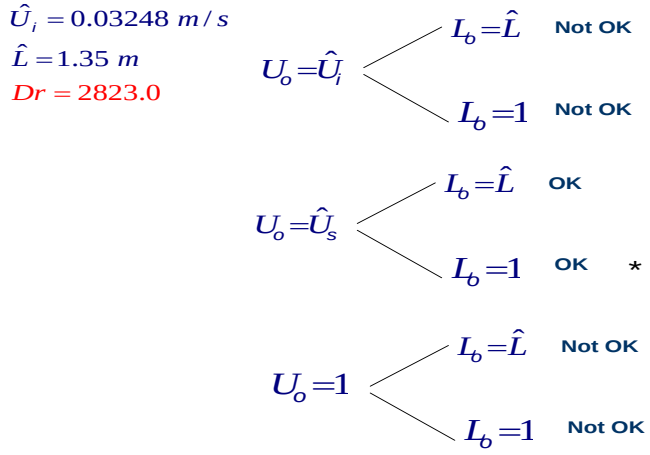

(b) Fluid 4 (Nylon)

Figure 7.3: Choice of Reference Quantities; Fluid 3 and Fluid 4

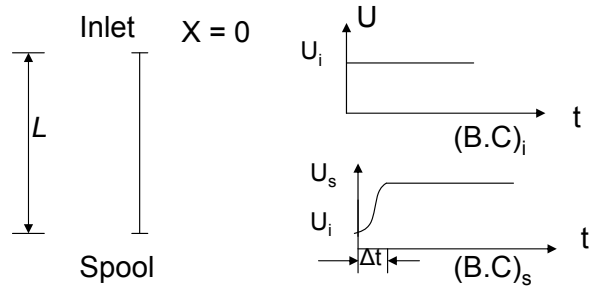

(a) Schematic

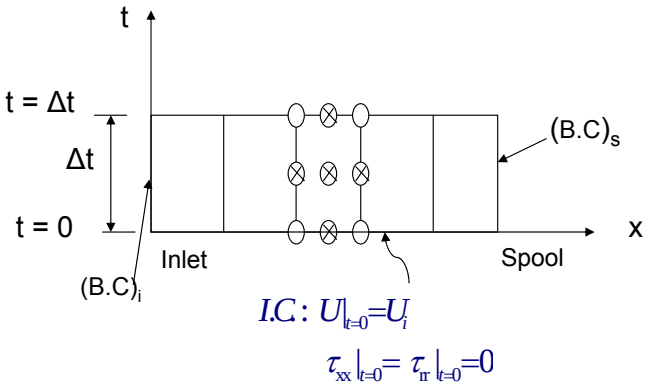

(b) Space time Strip

Figure 7.4: Schematic and Discretization for IVP : Fiber spinning process

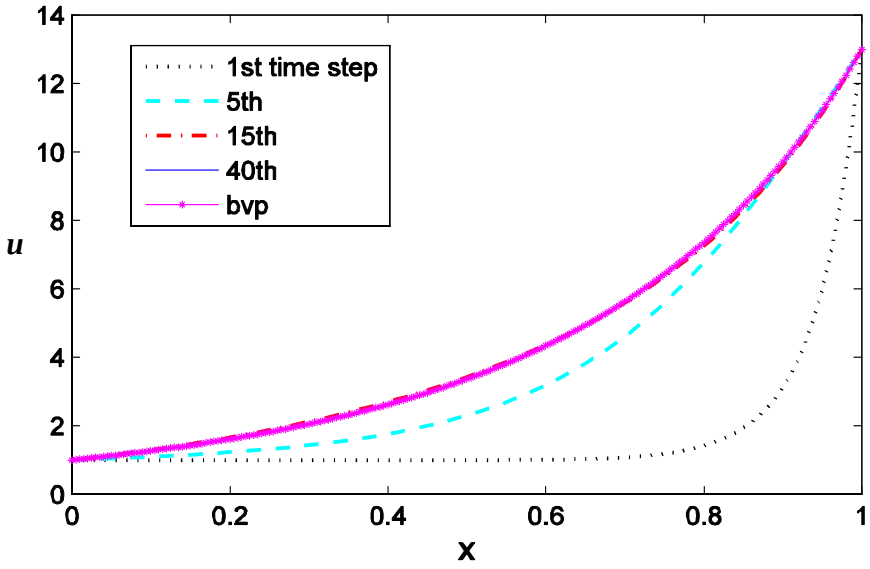

(a) Velocity u versus x

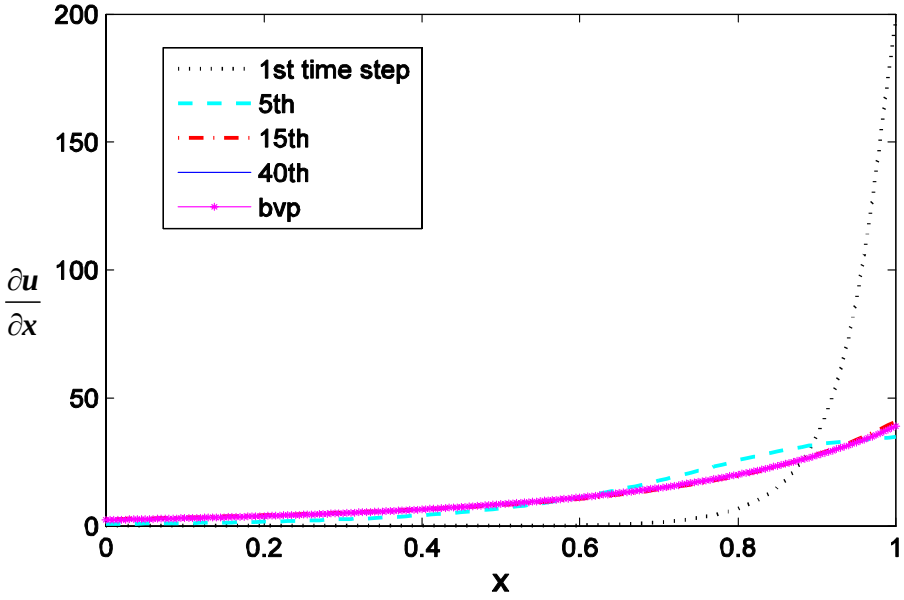

(b) $\frac{\partial u}{\partial x}$ versus x

Figure 7.5: Fluid1, Solutions of class C^1, $p = 9$, Dr = 13, De = 0.01949. BVP solutions for 10 and 20 element mesh, IVP for 10 element mesh

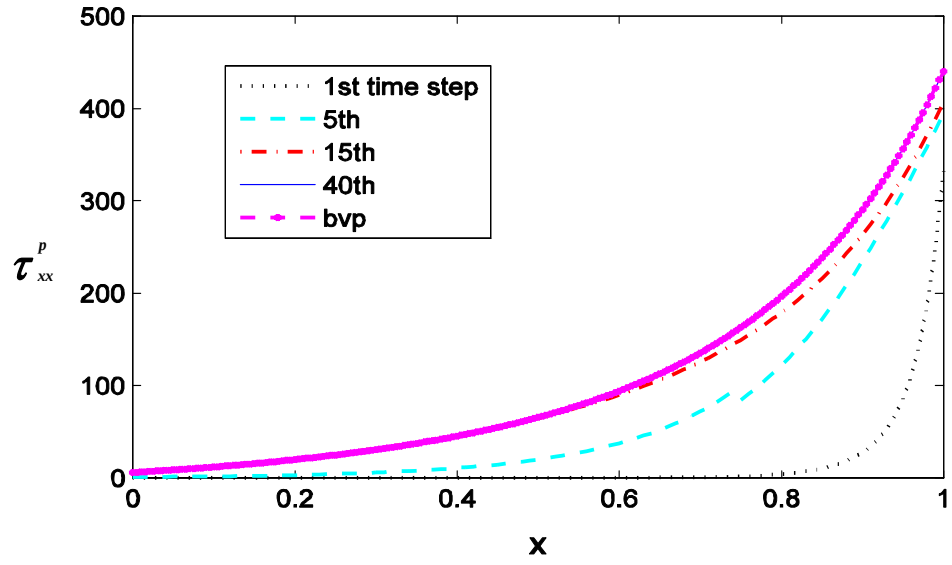

(a) τ_{xx}^{p} versus x

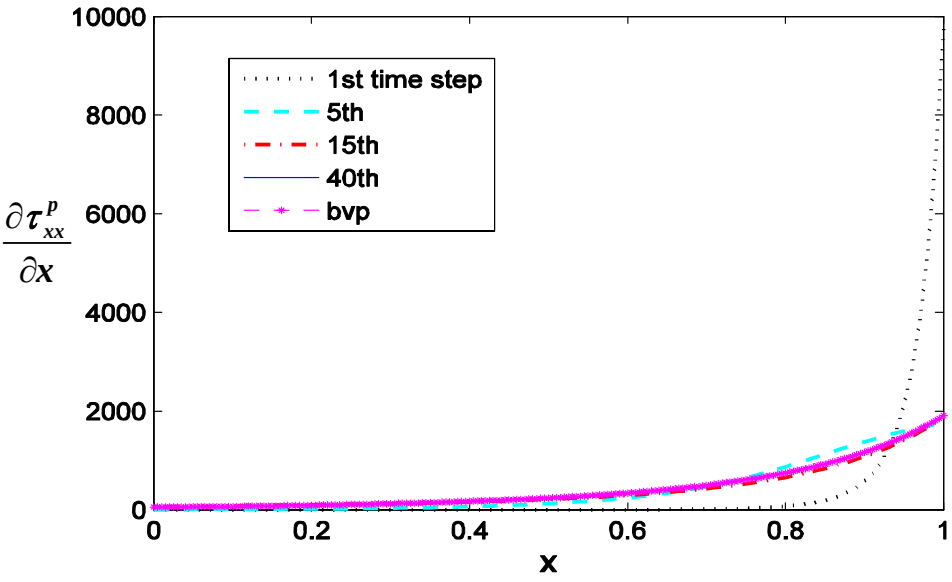

(b) $\frac{\partial \tau_{xx}^{p}}{\partial x}$ versus x

Figure 7.6: Fluid1, Solutions of class C^1, $p = 9$, Dr = 13, De = 0.01949. BVP solutions for 10 and 20 element mesh, IVP for 10 element mesh

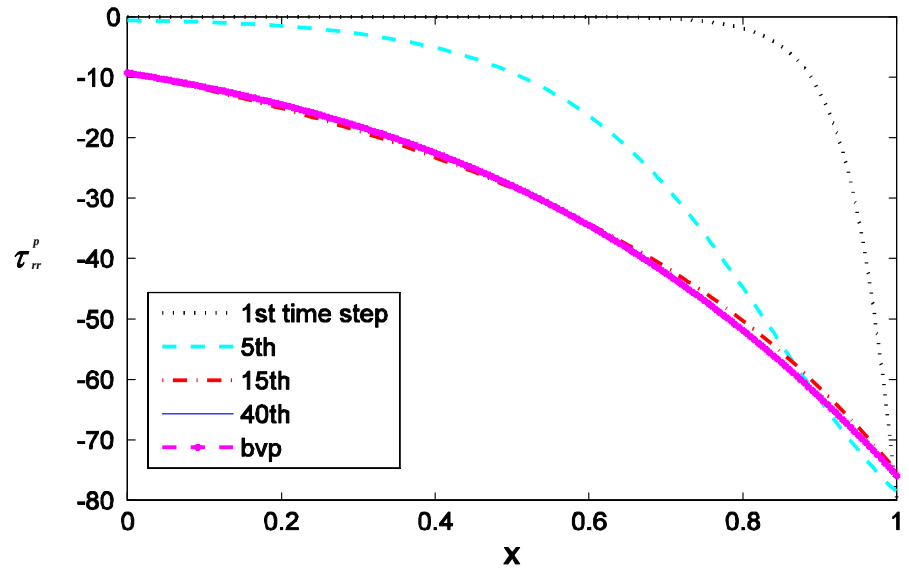

(a) τ_{rr}^{p} versus x

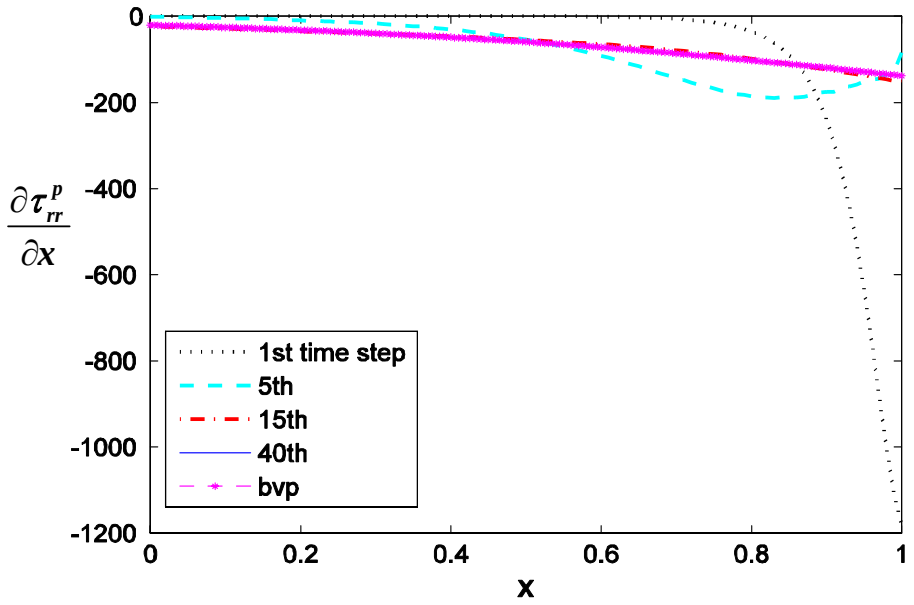

(b) $\frac{\partial \tau_{rr}^{p}}{\partial x}$ versus x

Figure 7.7: Fluid1, Solutions of class C^1, $p = 9$, Dr = 13, De = 0.01949. BVP solutions for 10 and 20 element mesh, IVP for 10 element mesh

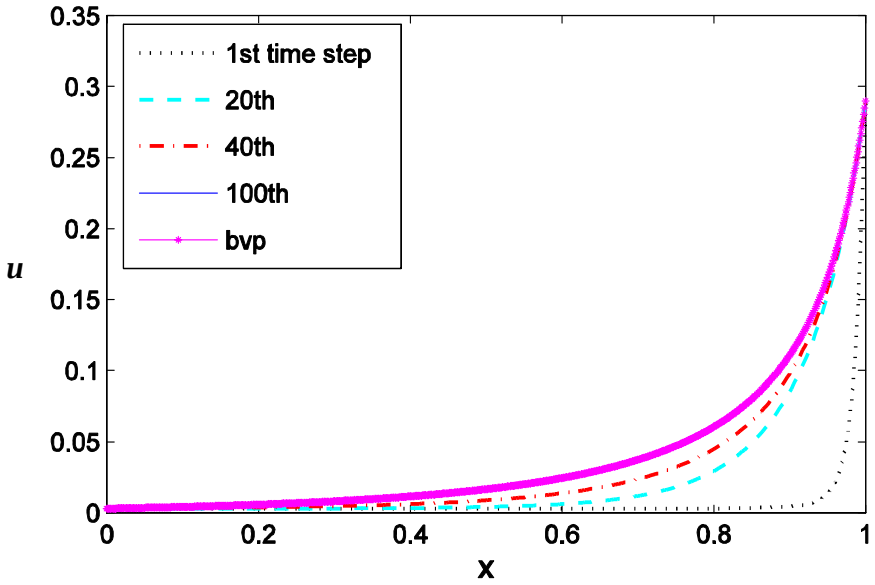

(a) Velocity u versus x

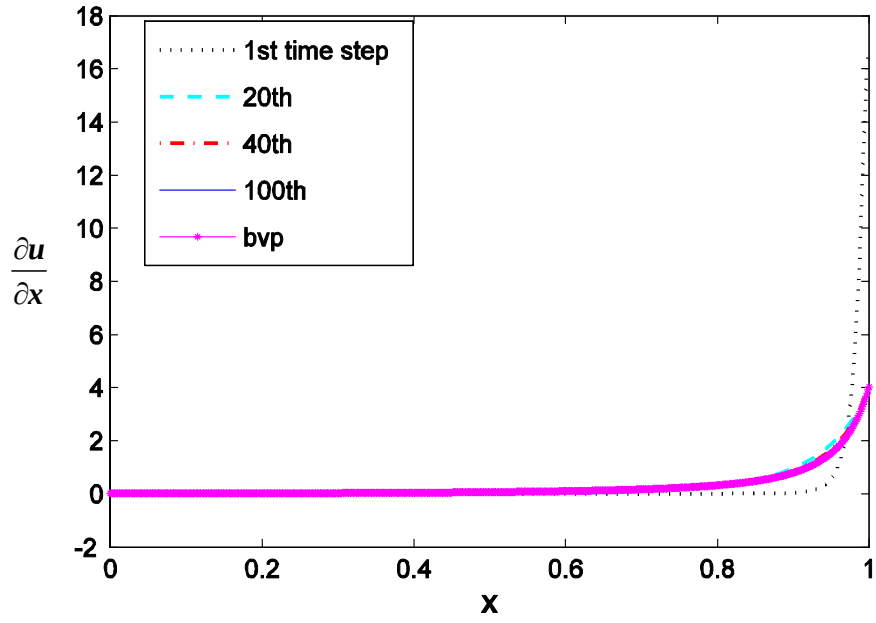

(b) $\frac{\partial u}{\partial x}$ versus x

Figure 7.8: Fluid2, Solutions of class C^1, $p = 7$, Dr = 100,De = 0.3. BVP solutions for 20, 40 and 60 element mesh,IVP for 40 element mesh

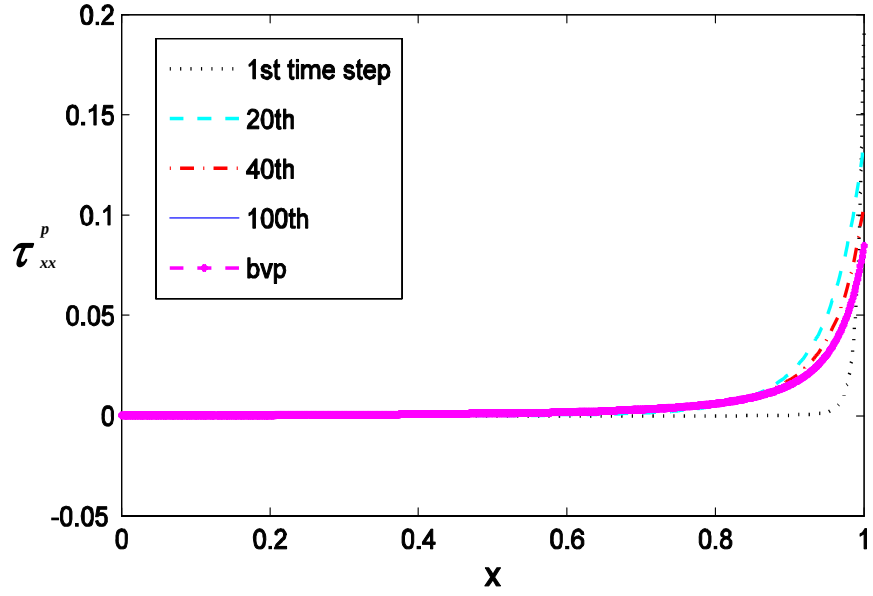

(a) τ_{xx}^{p} versus x

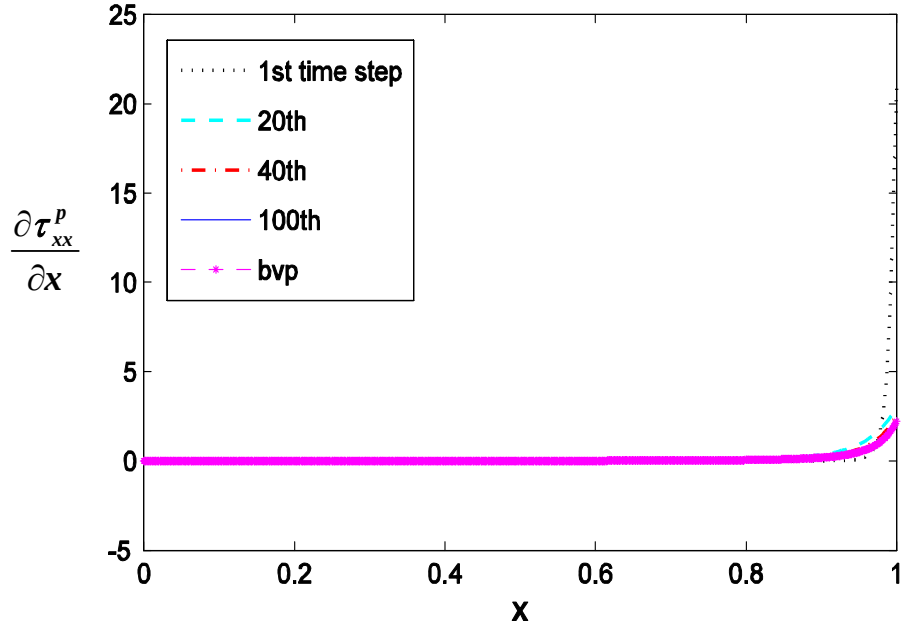

(b) $\frac{\partial \tau_{xx}^{p}}{\partial x}$ versus x

Figure 7.9: Fluid2, Solutions of class C^1, $p = 7$, Dr = 100,De = 0.3. BVP solutions for 20, 40 and 60 element mesh,IVP for 40 element mesh

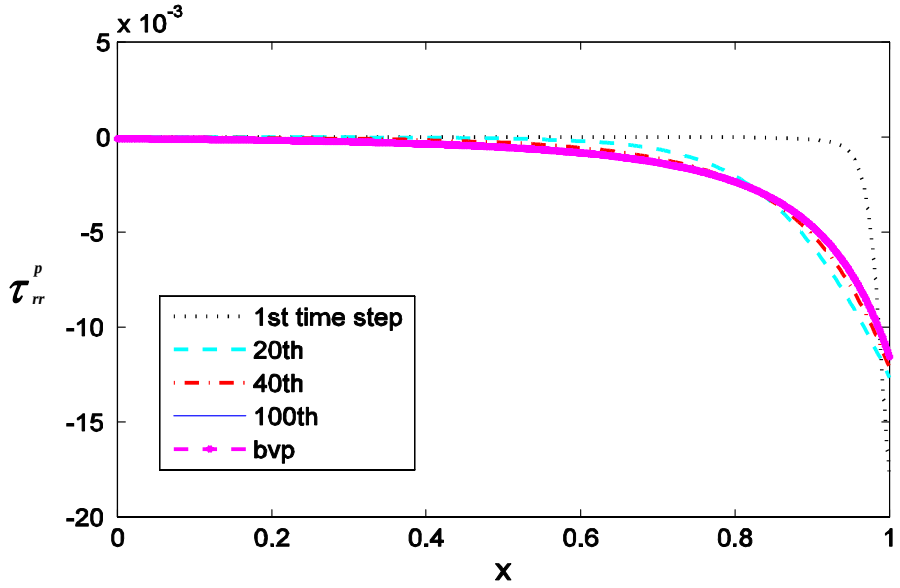

(a) τ_{rr}^{p} versus x

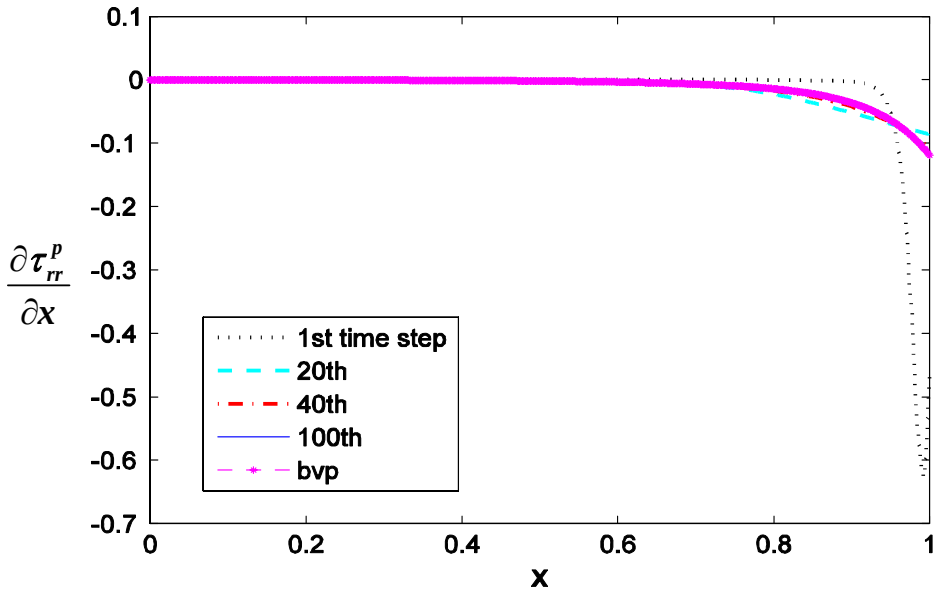

(b) $\frac{\partial \tau_{rr}^{p}}{\partial x}$ versus x

Figure 7.10: Fluid2, Solutions of class C^1, $p = 7$, Dr = 100,De = 0.3. BVP solutions for 20, 40 and 60 element mesh,IVP for 40 element mesh

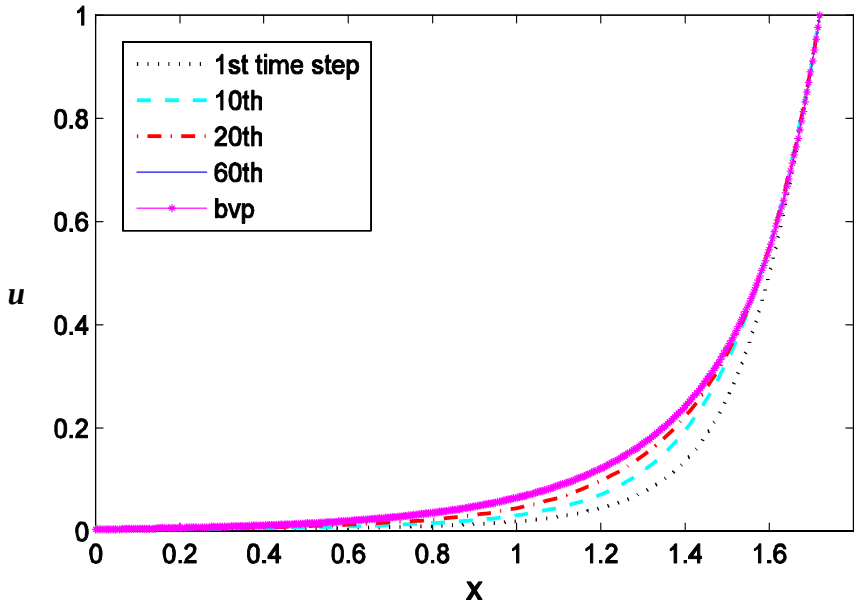

(a) Velocity u versus x

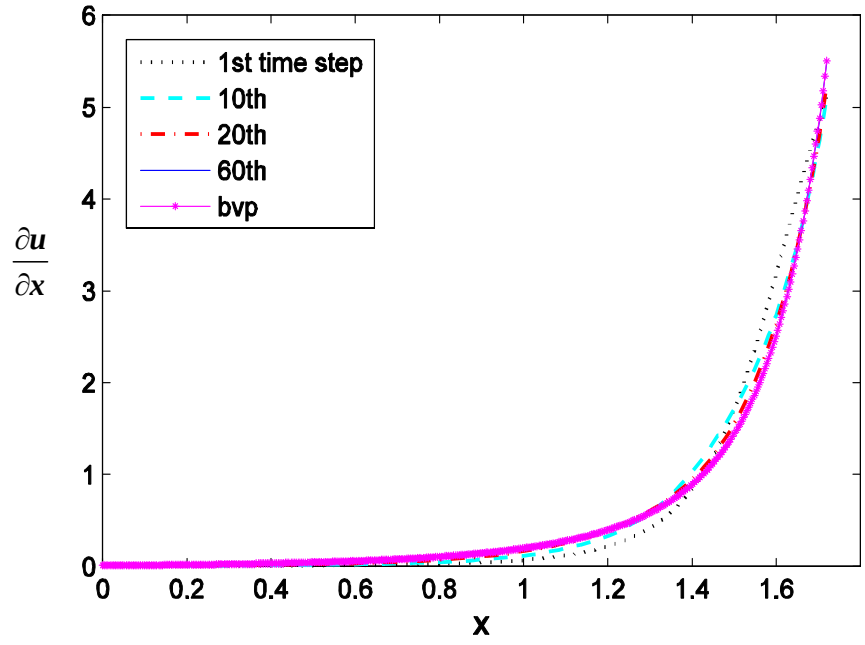

(b) $\frac{\partial u}{\partial x}$ versus x

Figure 7.11: Fluid3, Solutions of class C^1, $p = 9$, Dr = 273, De = 0.2252. BVP solutions for 20, 40 , 80 ele. mesh, IVP for 10 element mesh

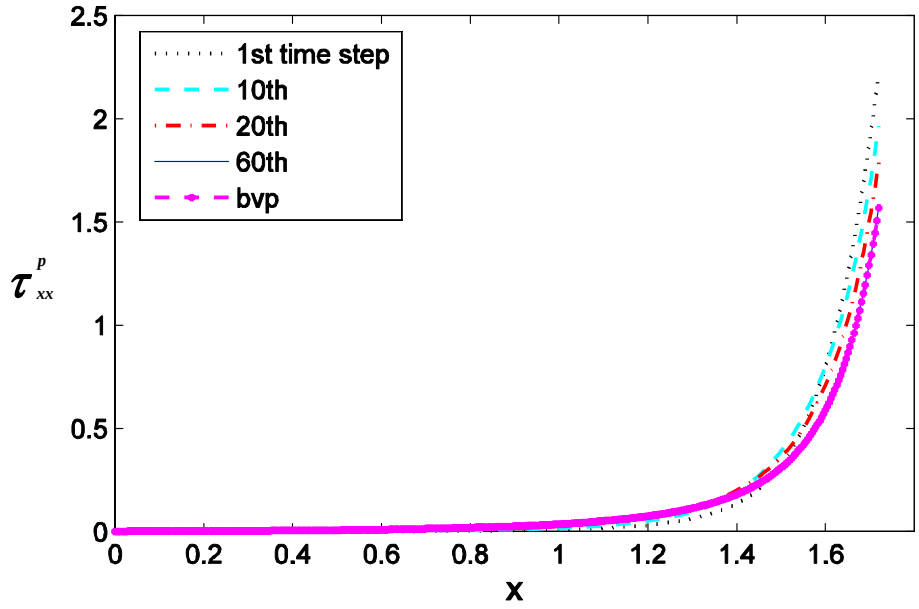

(a) τ^{p}_{xx} versus x

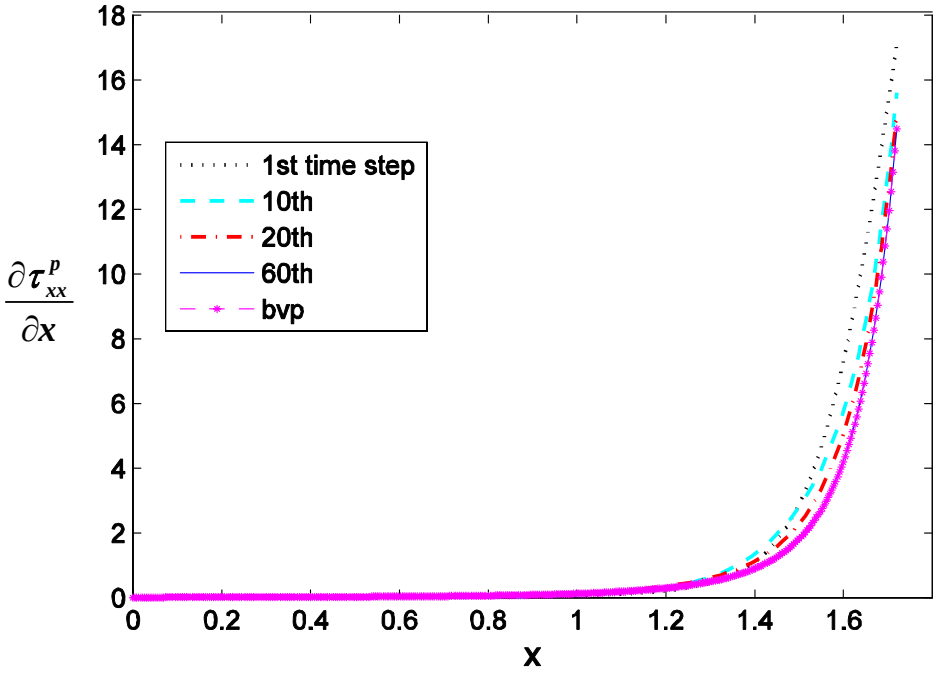

(b) $\frac{\partial \tau^{p}_{xx}}{\partial x}$ versus x

Figure 7.12: Fluid3, Solutions of class C^1, $p = 9$, Dr = 273, De = 0.2252. BVP solutions for 20, 40 , 80 ele. mesh, IVP for 10 element mesh

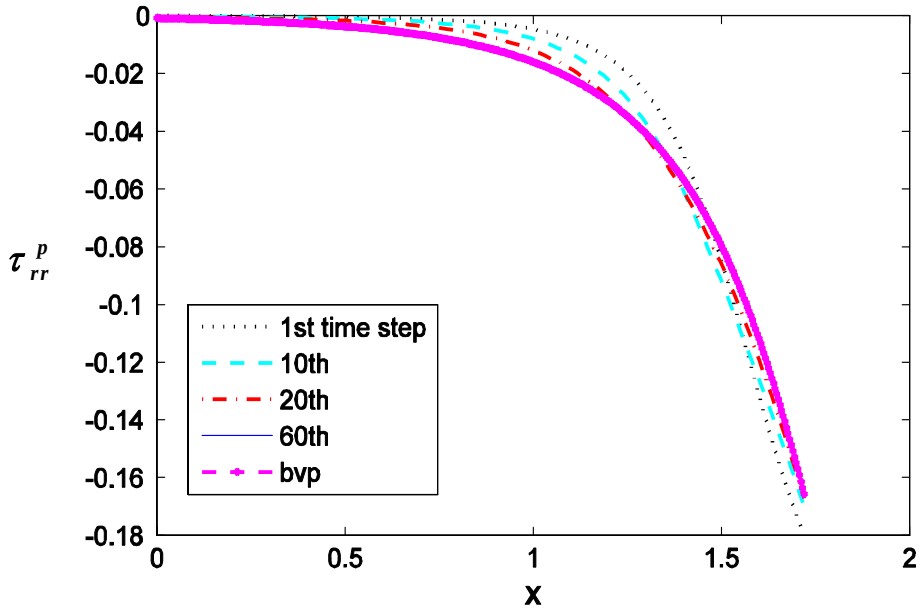

(a) τ_{rr}^{p} versus x

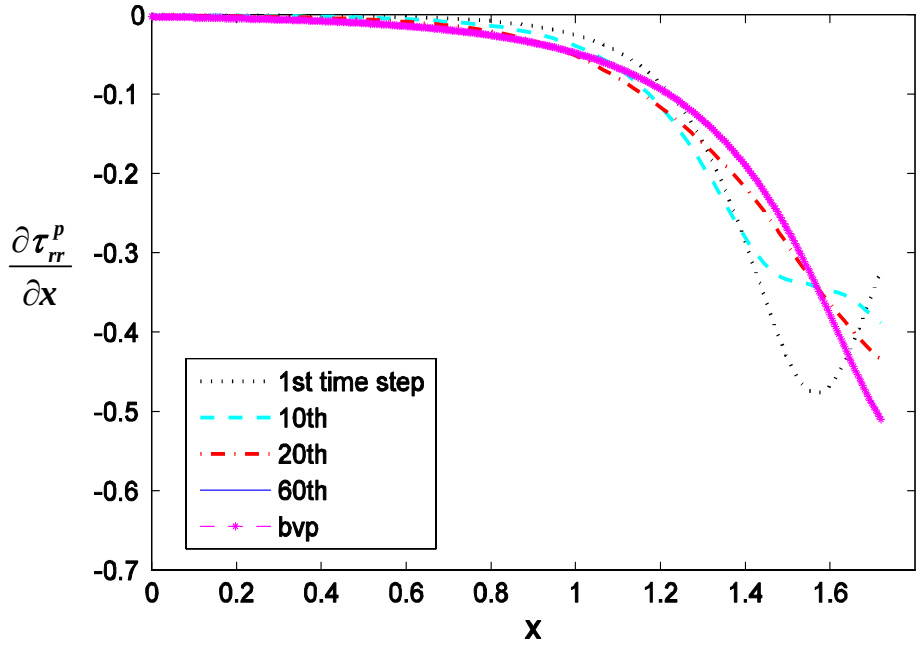

(b) $\frac{\partial \tau_{rr}^{p}}{\partial x}$ versus x

Figure 7.13: Fluid3, Solutions of class C^1, $p = 9$, Dr = 273, De = 0.2252. BVP solutions for 20, 40 , 80 ele. mesh, IVP for 10 element mesh

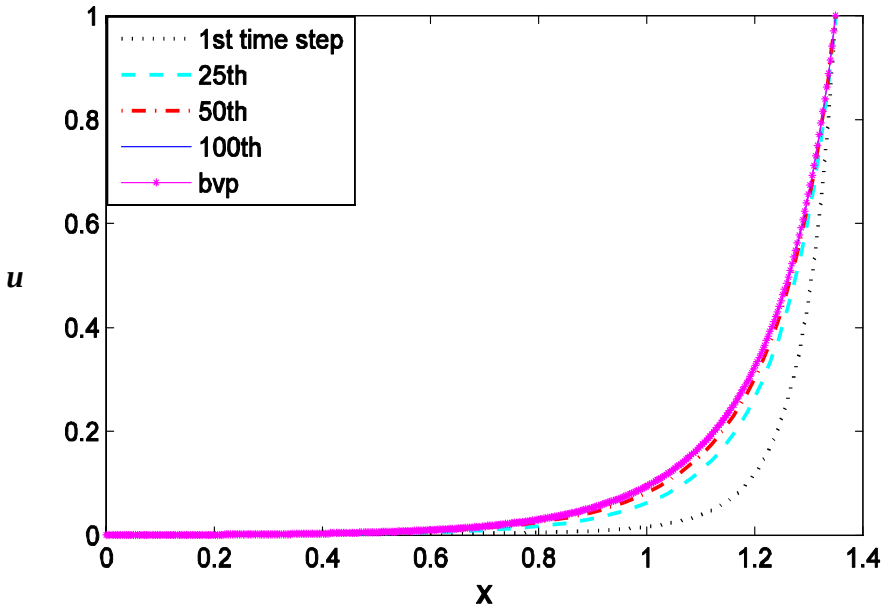

(a) Velocity u versus x

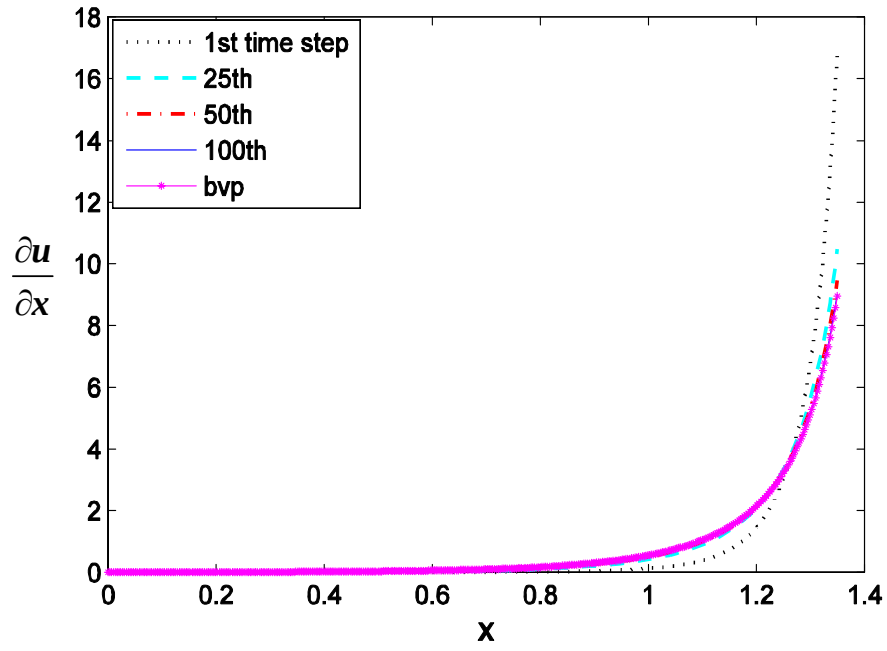

(b) $\frac{\partial u}{\partial x}$ versus x

Figure 7.14: Fluid4: Solutions of class C^1, $p = 9$, Dr=2823,De = 0.0916. BVP solutions for 20,40,80 ele. mesh, IVP for 10 element mesh

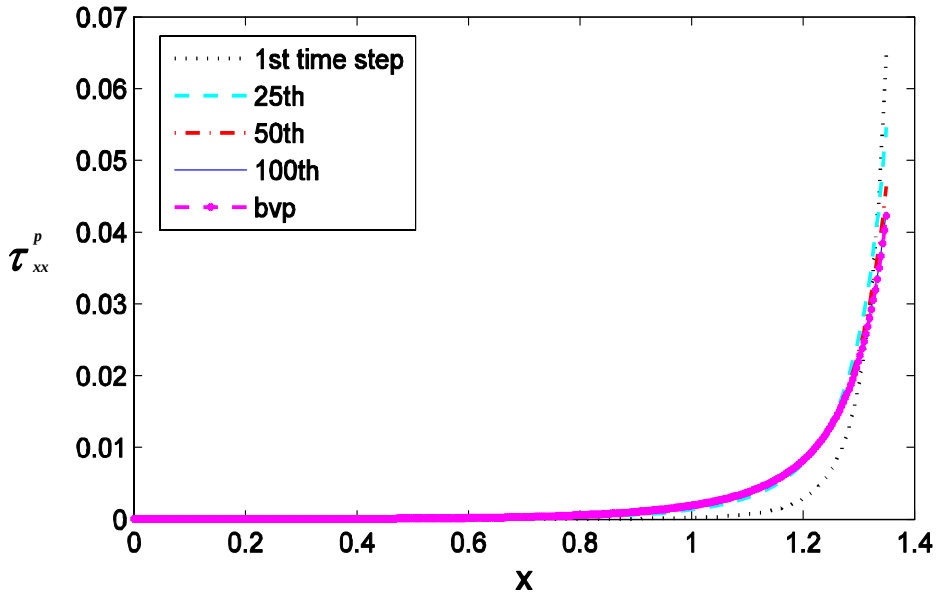

(a) τ_{xx}^{p} versus x

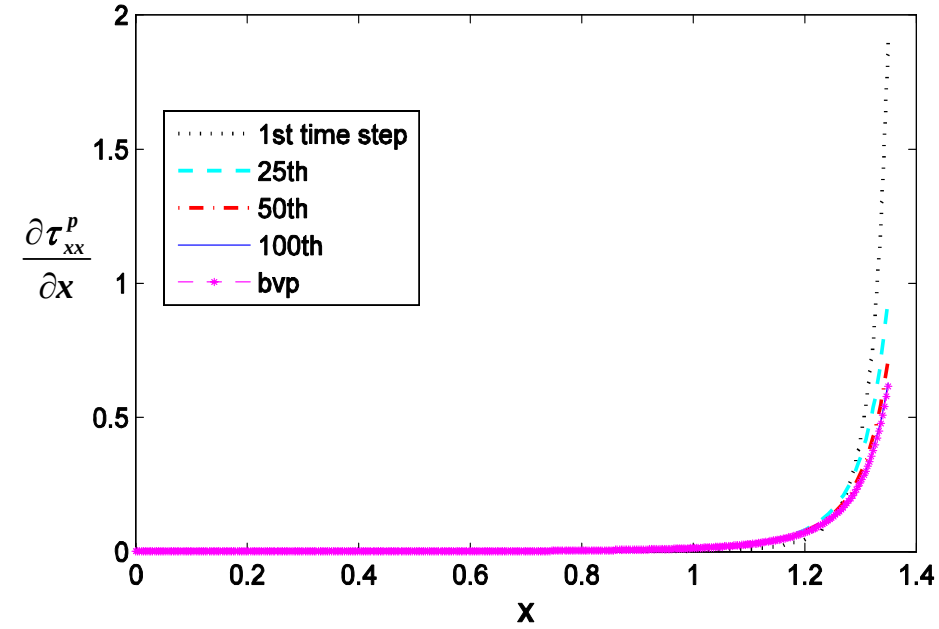

(b) $\frac{\partial \tau_{xx}^{p}}{\partial x}$ versus x

Figure 7.15: Fluid4: Solutions of class C^1, $p = 9$, Dr=2823,De = 0.0916. BVP solutions for 20,40,80 ele. mesh, IVP for 10 element mesh

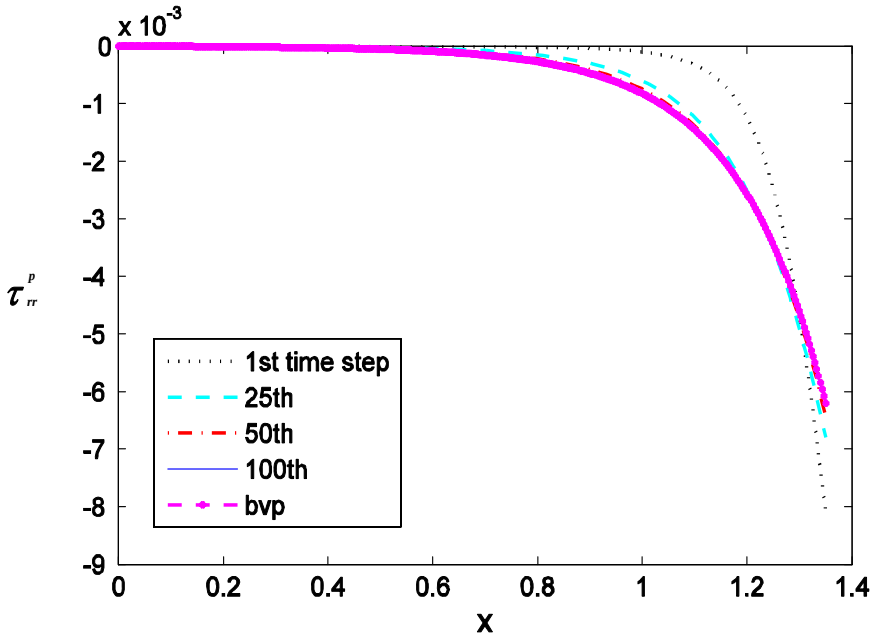

(a) τ_{rr}^{p} versus x

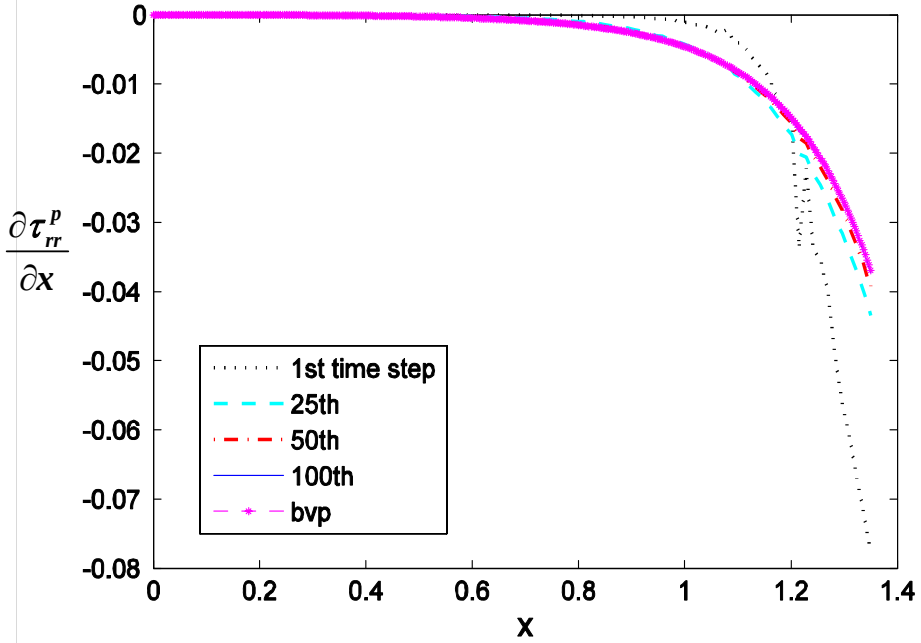

(b) $\frac{\partial \tau_{rr}^{p}}{\partial x}$ versus x

Figure 7.16: Fluid4: Solutions of class C^1, $p = 9$, Dr=2823,De = 0.0916. BVP solutions for 20,40,80 ele. mesh, IVP for 10 element mesh

7.3 Summary

The numerical studies for stationary and time dependent fiber spinning processes are presented using the new mathematical model and the Least Squares and Space Time Least Squares computational framework described in chapter 6. The fiber spinning process is simulated for four different polymeric fluids at high draw ratios based on the reported literature. The solutions of the boundary value problems and stationary state of initial value problems match identically for all fluids and all draw ratios. The numerical studies in this chapter demonstrates that : (i) the solution of BVP and IVP for all ranges of draw ratios are obtainable using variationally consistent least squares processes for BVP problems and variationally consistent space time least squares process for IVP problems without any stability issues and (ii) the choice of reference quantities has a significant effect on the performance of the computational processes. The newly developed GDEs for BVP and IVP in fiber spinning along with space time variationally consistent integral forms in hpk framework provides an excellent simulation methodology that aids in determining important process parameters for fiber spinning process.

Chapter 8

Summary and Conclusions

In this thesis the new mathematical framework [3, 39, 40] based on $h,\ p,\ k$ and variationally consistent integral forms is utilized to develop a finite element computational processes for 1-D and 2-D BVPs and 1-D IVPs in polymer flows utilizing Giesekus constitutive model. In the following, we present a summary of the work and draw some conclusions.

(1) Various choice of dependent variables for the GDEs are discussed. While, there are many alternatives possible, it is shown that the mathematical characteristics of the proposed computational process remain unaffected by these. It is pointed out that a most prudent choice is one that yields most simplified form of the GDEs that are free of redundancies and inconsistencies. Using $\mathbf{U}$, p, $\boldsymbol{\tau}^p$ as dependent variables yields GDEs that are in the strong form and conform to the guidelines presented in this thesis and hence are the GDEs of choice.

(2) The GDEs using $\mathbf{U}$, p, $\boldsymbol{\tau}^e$ breaks down after $De = 21.05$ for one dimensional fully developed flow. Computations are reported for formulations using $\mathbf{U}$, p, $\boldsymbol{\tau}^p$; $\mathbf{U}$, p, $\boldsymbol{\tau}$ upto deborah number of 6514.53 and there does not seem to be any limit on computations with appropriate hpk refinement.

(3) It is shown that local approximations of $\mathbf{U}$, p, $\boldsymbol{\tau}^p$ need to be in $H^{k,p}(\bar{\Omega}^e)$, $k \geq 3$ spaces in which $k = 3$ is the minimally conforming space. If we permit weak convergence of the highest order derivatives (which is acceptable if the theoret-

ical solutions are sufficiently smooth), then k = 2 could be viewed as minimally conforming space. Need for spaces of order higher than 3 is necessitated if one requires convergence of the higher order derivatives of the computed solution to their theoretical values. When the theoretical solutions are not known, one obtains the converged solutions in various order spaces (highest order space determined by the convergence of the highest order derivatives desired) for different discretizations to arrive at a solution that represents the converged solutions in the converging sequence of solutions and hence independent of h, p and k.

(4) Numerical studies have been conducted for (i) One dimensional fully developed flow between parallel plates (ii) developing flow between parallel plates and (iii) lid driven square cavity. Specific findings and conclusions are summarized in the following.

   (a) The one dimensional fully developed flow is used as model problem to investigate the importance of the choice of variables in the GDEs. There does not seem to be any deborah number limit on computations using $\mathbf{U}$, p, $\boldsymbol{\tau}^p$ and $\mathbf{U}$, p, $\boldsymbol{\tau}$ as dependent variables. The formulation using $\mathbf{U}$, p, $\boldsymbol{\tau}^e$ breaks down after $De = 21.05$ and computations get into convergence problems which are not alleviated using 'hpk' refinement.

   (b) For developing flow between parallel plates studies are presented for De upto 20.13. For each De, converged solutions are obtained for solutions of class C^1 and C^2 which show good agreement. Additional studies (not reported here) show that for developing flow between parallel plates solutions of the GDEs are obtainable for any De with proper mesh refinement near the stationary plate (necessary to resolve the boundary layers). The developing flow studies are also used to validate the results of One dimensional fully developed flow. An exact match of the solutions is reported upto $De = 21.13$ for the one dimensional fully developed flow and developing flow between parallel plates.

   (c) For lid driven square cavity; the mathematical idealization of the physics

of the corners A and B where stationary walls meet the lid shown in figure 4.20 (b) is crucial. The higher order global differentiability distribution of velocity u over the length h_d permits us to simulate the true physics in the limiting process in which $h_d \rightarrow 0$ and $k \rightarrow \infty$. For two values of h_d (0.1 and 0.05), solutions independent of computational parameters $h,\ p,\ and\ k$ are presented upto a very high De = 2.4. Comparison of the converged solutions for the two values of h_d show that decreasing h_d only results in the changes in the solutions that remain localized and hence do not influence the far field solution appreciably. Decreasing value of h_d produces higher local solution gradient that become progressively more localized with progressively decreasing h_d. From practical point of view h_d lower than $0(10^{-3})$ only influences the solution in the local region of $0(10^{-3})$ which may be of little consequence as far as the global solution behavior is concerned.

(5) As reported by other researchers [37, 47, 48], with progressively increasing De, the Newton's method with line search requires progressively more iterations for convergence . This problem has been resolved by using the solution of lower deborah number as the initial solution for higher deborah numbers, i.e. continuation in Deborah number.

(6) It is significant to note that, the mathematical framework and Least Squares computational process based on $h,\ p,\ \text{and}\ k$ utilized here is free of inherent and numerical diffusion [99] and that the upwinding techniques such as SUPG, SUPG/DC, SUPG/DC/LS and their many variations are neither needed nor used in the present work. Furthermore, various methods such as Elastic-Viscous decomposition of stress, EEME, EEME/SUPG, EVSS/SUPG etc though may show some benefits in Galerkin methods with weak form, but are of little or no consequence in the present computational framework due to the fact that regardless of the nature of GDEs, Least Squares process are always VC.

(7) The development of new GDEs for Fiber spinning process is presented. These new GDEs are more descriptive of the true physics compared to the GDEs that

are currently used in the literature. Numerical results presented demonstrate the importance of STVC integral forms and also the importance of higher order spaces $H^{k,p}({}^n\bar{\Omega}^e_{xt})$ in space and time. The computational process used in this work is unconditionally stable and non-degenerate.

(8) The use of higher order local approximations in space and time in $H^{k,p}({}^n\bar{\Omega}^e_{xt})$ permits use of strong form of the GDEs instead of weak form and avoids redundancies and inconsistencies associated with weak form of the GDEs. hpk framework permits the desired global differentiability in space and time, which is generally dictated by the physics.

(9) The fiber spinning process is simulated for four different polymeric fluids at high draw ratios based on the reported literature. The solutions of the boundary value problems and stationary state of initial value problems match identically for all fluids and all draw ratios.

(10) Investigation of the choice of reference quantities and their consequences on the numerical simulation of the melt spinning process is presented for the four different polymeric fluids.

(11) The solution of BVP and IVP for all ranges of 'Dr' are obtainable using VC LSP for BVP problems and VC STLSP for IVP problems without any stability issues.

   (a) For a given $\hat{L}$ there is maximum Draw ratio attainable which is possible to be determined by numerical simulations.

(12) The newly developed GDEs for BVP and IVP in fiber spinning along with STVC integral forms in hpk framework provides an excellent simulation methodology that aids in determining important process parameters for fiber spinning process.

Bibliography

[1] D. Rajagopalan, RC. Armstrong, and RA. Brown. Finite element methods for calculation of steady viscoelastic flow using constitutive equations with a Newtonian viscosity. *J. Non-Newtonian Fluid Mech*, 36:159–192, 1990.

[2] D. Rajagopalan, JA. Byars, RC. Armstrong, RA. Brown, JS Lee, and GG Fuller. Comparison of numerical simulations and birefringence measurements in viscoelastic flow between eccentric rotating cylinders. *Journal of Rheology*, 36(7):1349–1375, 1992.

[3] KS Surana, AR Ahmadi, and JN Reddy. k-version of finite element method for non-linear differential operators in BVP. *Internat. J. Comp. Engng. Sci*, 5(1):133–207, 2004.

[4] D. Rajagopalan, RJ. Phillips, R.C. Armstrong, R.A. Brown, and A. Bose. The influence of viscoelasticity on the existence of steady solutions in two-dimensional rimming flow. *Journal of Fluid Mechanics Digital Archive*, 235:611–642, 1992.

[5] D. Rajagopalan, RC Armstrong, and RA Brown. Comparison of computational efficiency of flow simulations multimode constitutive equations: integral and differential models. *Journal of non-newtonian fluid mechanics*, 46(2-3):243–273, 1993.

[6] R. Guenette and M. Fortin. A new mixed finite element method for computing viscoelastic flows. *J. Non-Newtonian Fluid Mech*, 60(1):27–52, 1995.

[7] MT Arigo, D. Rajagopalan, N. Shapley, and GH McKinley. The sedimentation of a sphere through an elastic fluid. Part 1. Steady motion. *Journal of Non-Newtonian Fluid Mechanics*, 60(2):225–257, 1995.

[8] M. Fortin, R. Guenette, and R. Pierre. Numerical analysis of the modified EVSS method. *Computer methods in applied mechanics and engineering*, 143(1-2):79–95, 1997.

[9] A Fortin. On the discrete EVSS method. *Computer Methods in Applied Mechanics and Engineering*, 189(1):121–139, 2000.

[10] H. Matallah, P. Townsend, and MF Webster. Recovery and stress-splitting schemes for viscoelastic flows. *J. Non-Newtonian Fluid Mech*, 75:139–166, 1998.

[11] HS. Dou and N. Phan-Thien. The flow of an Oldroyd-B fluid past a cylinder in a channel: adaptive viscosity vorticity (DAVSS-omega) formulation. *Journal of Non-Newtonian Fluid Mechanics*, 87(1):47–73, 1999.

[12] Y. Fan, RI Tanner, and N. Phan-Thien. Galerkin/least-square finite element methods for steady viscoelastic flows. *J. Non-Newtonian Fluid Mech*, 84:233–256, 1999.

[13] FPT. Baaijens. Mixed finite element methods for viscoelastic flow analysis: A review. *Journal of Non-Newtonian Fluid Mechanics*, 79(2):361–385, 1998.

[14] L. Thais, L. Helin, and G Mompean. Numerical simulation of viscoelastic flows with Oldroyd-B constitutive equations and novel algebraic stress models. *J. Non-Newtonian Fluid Mech*, 140:145–158, 2006.

[15] FJ Lim and WR Schowalter. Pseudo-spectral analysis of the stability of pressure-driven flow of a Giesekus fluid between parallel planes. *Journal of non-newtonian fluid mechanics*, 26(1):135–142, 1987.

[16] F. Brezzi, J. Douglas, R. Duran, and M. Fortin. Mixed finite elements for second order elliptic problems in three variables. *Numer. Math.*, 51:237–250, 1987.

[17] AN Beris, M. Avgousti, and A. Souvaliotis. Spectral calculations of viscoelastic flows: evaluation of the Giesekus constitutive equation in model flow problems. *Journal of non-newtonian fluid mechanics*, 44:197–228, 1992.

[18] S. Xu, AR Davies, and TN Phillips. Pseudospectral method for transient viscoelastic flow in axisymmetric channel. *Numer. Meth. Partial Differential Equations*, 9:691–710, 1993.

[19] T. Kajiwara, S. Ninomiya, Y. Kuwano, and K. Funatsu. Numerical simulation of converging flow of polymer melts through a tapered slit die. *Journal of non-newtonian fluid mechanics*, 48(1-2):111–124, 1993.

[20] LM Quinzani, RC Armstrong, and RA Brown. Use of coupled birefringence and LDV studies of flow through a planar contraction to test constitutive equations for concentrated polymer solutions. *J. Rheol*, 39(6):1201–1227, 1995.

[21] AM. Grillet, ACB. Bogaerds, GWM. Peters, and FPT. Baaijens. Stability analysis of constitutive equations for polymer melts in viscometric flows. *J. Non-Newtonian Fluid Mech*, 103:221–250, 2002.

[22] KK Talwar and B. Khomami. Flow of viscoelastic fluids past periodic square arrays of cylinders: inertial and shear thinning viscosity and elasticity effects. *Journal of Non-Newtonian Fluid Mechanics*, 57(2):177–202, 1995.

[23] KK Talwar and B. Khomami. Higher order finite element techniques for viscoelastic flow problems with change of type and singularities. *Journal of Non-Newtonian Fluid Mechanics*, 59(1):49–72, 1995.

[24] MJ Szady, TR Salamon, AW Liu, DE Bornside, RC Armstrong, and RA Brown. A new mixed finite element method for viscoelastic flows governed by differential constitutive equations. *Journal of Non-Newtonian Fluid Mechanics*, 59(2):215–243, 1995.

[25] Y. Fan. A comparative study of the discontinuous Galerkin and continuous SUPG finite element methods for computation of viscoelastic flows. *Computer Methods in Applied Mechanics and Engineering*, 141(1):47–65, 1997.

[26] P. Wapperom and MF Webster. Second-order hybrid finite-element/volume

method for viscoelastic flows. *Journal of Non-Newtonian Fluid Mechanics*, 79(2):405–431, 1998.

[27] AW Liu, DE Bornside, RC Armstrong, and RA Brown. Viscoelastic flow of polymer solutions around a periodic, linear array of cylinders: comparisons of predictions for microstructure and flow fields. *Journal of Non-Newtonian Fluid Mechanics*, 77(3):153–190, 1998.

[28] AM. Grillet and ESG. Shaqfeh. Observations of viscoelastic instabilities in recirculation flows of Boger fluids. *Journal of Non-Newtonian Fluid Mechanics*, 64(2-3):141–155, 1996.

[29] AM Grillet, B. Yang, B. Khomami, and ESG Shaqfeh. Modeling of viscoelastic lid driven cavity flow using finite element simulations. *Journal of Non-Newtonian Fluid Mechanics*, 88(1):99–131, 1999.

[30] GH McKinley, P. Pakdel, and A. Oztekin. Rheological and geometric scaling of purely elastic flow instabilities. *Journal of Non-Newtonian Fluid Mechanics*, 67(1):19–47, 1996.

[31] P. Pakdel, SH. Spiegelberg, and GH. McKinley. Cavity flows of elastic liquids: Two-dimensional flows. *Physics of Fluids*, 9(11):3123–3140, 2006.

[32] P. Pakdel and GH. McKinley. Cavity flows of elastic liquids: Purely elastic instabilities. *Physics of Fluids*, 10(5):1058, 1998.

[33] PJ. Oliveira. On The Numerical Implementation Of Nonlinear Viscoelastic Models in a Finite-Volume Method. *Numerical Heat Transfer: Part B: Fundamentals*, 40(4):283–301, 2001.

[34] C. Chauviere and RG Owens. A new spectral element method for the reliable computation of viscoelastic flow. *Computer Methods in Applied Mechanics and Engineering*, 190(31):3999–4018, 2001.

[35] J. Bonvin and M. Picasso. A finite element/Monte-Carlo method for polymer dilute solutions. *Computing and Visualization in Science*, 4(2):93–98, 2001.

[36] M. Behr, D. Arora, OM. Coronado, and M. Pasquali. GLS-type finite element methods for viscoelastic fluid flow simulation. *Computational Fluid and Solid Mechanics*, pages 586–589, 2005.

[37] VJ. Ervin and H. Lee. Defect Correction Method for Viscoelastic Fluid Flows at High Weissenberg Number. *Numerical Methods For Partial Differential Equations*, 22(1):145, 2006.

[38] OM. Coronado, D. Arora, M. Behr, and M Pasquali. Four-field Galerkin/least-squares formulation for viscoelastic fluids. *J. Non-Newtonian Fluid Mech*, 140:132–144, 2006.

[39] KS Surana, AR Ahmadi, and JN Reddy. The K-version of finite element method for self-adjoint operators in BVP. *International Journal of Computational Engineering Science(IJCES)*, 3(2):155–218, 2002.

[40] KS Surana, AR Ahmadi, and JN Reddy. The k-Version Of Finite Element Method For Non-Self-Adjoint Operators In BVP. *International Journal of Computational Engineering Sciences*, 4(4):737–812, 2003.

[41] KS. Surana, Allu S., and JN. Reddy. The k-Version of Finite Element Method for Initial Value Problems: Mathematical and Computational Framework. *International Journal for Computational Methods in Engineering Science and Mechanics*, 8(3):123–136, 2007.

[42] R. B. Bird, R. C. Armstrong, and O. Hassager. *Dynamics of Polymeric Liquids*, volume 1. John Wiley and Sons, second edition, 1987.

[43] H. Giesekus. A simple constitutive equation for polymer fluids based on the concept of deformation-dependent tensorial mobility. *J. Non-Newtonian Fluid Mech*, 11(1-2):69–109, 1982.

[44] BC Bell and KS. Surana. S., 1994. p-version least squares finite element formulations for two-dimensional, incompressible, non-Newtonian isothermal and non-isothermal fluid flow. *Int. J. Numer. Methods Fluids*, 18:127–162.

[45] BC Bell and KS Surana. 'p-version space-time coupled least squares finite element formulation for two dimensional unsteady incompressible Newtonian fluid flow,' Presented at 1993 ASME Winter Annual Meeting.

[46] KS. Surana, LR. Anthoni, Allu S., and JN. Reddy. Strong and Weak Form of the Governing Differential Equations in Least Squares Finite Element Processes in h,p,k Framework. *International Journal for Computational Methods in Engineering Science and Mechanics*, 9(1):1–24, 2008.

[47] AN Beris, RC Armstrong, and RA Brown. Finite element calculation of viscoelastic flow in a Journal bearing: I, Small eccentricities. *J. Non-Newtonian Fluid Mech*, 16:141–172, 1984.

[48] MA Hulsen and J. Van Der Zanden. Numerical simulation of contraction flows using a multi-mode Giesekus model. *Journal of non-newtonian fluid mechanics*, 38(2-3):183–221, 1991.

[49] S. Kase and T. Matsuo. Studies on melt spinning. II. Steady-state and transient solutions of fundamental equations compared with experimental results. *Journal of Applied Polymer Science*, 11(2):251–287, 1967.

[50] MA Matovich and JRA Pearson. Spinning a Molten Threadline. Steady-State Isothermal Viscous Flows. *Industrial & Engineering Chemistry Fundamentals*, 8(3):512–520, 1969.

[51] PA Avenas, MM Denn, and CJS Petrie. Mechanics of Steady Spinning of a Viscoelastic Liquid. *AIChE J*, 21:791, 1975.

[52] MM Denn and G. Marrucci. Effect of a relaxation time spectrum on the mechanics of polymer melt spinning. *J. Non-Newtonian Fluid Mech*, 2:159–68, 1977.

[53] JC Chang and MM Denn. An experimental study of isothermal spinning of a Newtonian and a viscoelastic liquid. *J. Non-Newtonian Fluid Mech*, 5:369–385, 1979.

[54] F. Dupret and JM Marchal. Loss of evolution in the flow of viscoelastic fluids. *J. Non-Newtonian Fluid Mech*, 20:143–171, 1986.

[55] JDER. Tsou and DC Bogue. The effect of die flow on the dynamics of isothermal melt spinning. *Journal of non-newtonian fluid mechanics*, 17(3):331–347, 1985.

[56] W. Minoshima and JL White. Instability phenomena in tubular film, and melt spinning of rheologically characterized high density, low density and linear low density polyethylenes. *Journal of non-newtonian fluid mechanics*, 19(3):275–302, 1986.

[57] R. Keunings, MJ. Crochet, and MM. Denn. Profile development in continuous drawing of viscoelastic liquids. *Industrial & Engineering Chemistry Fundamentals*, 22(3):347–355, 1983.

[58] JA Spearot and AB Metzner. Isothermal Spinning of Molten Polyethylenes. *Journal of Rheology*, 16(3):495–518, 1972.

[59] H. Ishihara and S. Kase. Studies on melt spinning. V. Draw resonance as a limit cycle. *Journal of Applied Polymer Science*, 19(2):557–566, 1975.

[60] H. Ishihara and S. Kase. Studies on melt spinning. VI. Simulation of draw resonance using Newtonian and power law viscosities. *Journal of Applied Polymer Science*, 20(1):169–191, 1976.

[61] CB. Weinberger, GF. Cruz-SaenzKase, and GJ. Donnelly. Onset of draw resonance during isothermal melt spinning: A comparison between measurements and Predictions. *AIchE J*, 22(3):441–448, 1976.

[62] RJ. Fisher, MM. Denn, and RI. Tanner. Initial Profile Development in Melt Spinning. *Industrial & Engineering Chemistry Fundamentals*, 19(2):195–197, 1980.

[63] P. Revenu, J. Guillet, and C. Carrot. Elongational flow of polyethylenes in isothermal melt spinning. *Journal of Rheology*, 37(6):1041–1056, 1993.

[64] TC. Papanastasiou, CW. Macosko, LE. Scriven, and Z. Chen. Fiber Spinning of Viscoelastic Liquid. *AIchE J*, 33:834–842, 1987.

[65] WP Bell and DD Edie. Measured orientation and internal stress distributions in melt-spun fibers. *Journal of applied polymer science*, 33(4):1089–1102, 1987.

[66] WP. Bell and DD. Edie. Calculated internal stress distributions in melt-spun fibers. *Journal of Applied Polymer Science*, 33(4):1073–1088, 1987.

[67] R. Fulchiron, V. Verney, A. Michel, and JC Roustant. Correlations between relaxation time spectrum and melt spinning behavior of polypropylene. II: Melt spinning simulation from relaxation time spectrum. *Polymer engineering and science*, 35(6):513–518, 1995.

[68] R. Fulchiron, V. Verney, A. Michel, and JC Roustant. Correlations between relaxation time spectrum and melt spinning behavior of polypropylene. II: Melt spinning simulation from relaxation time spectrum. *Polymer engineering and science*, 35(6):518–527, 1995.

[69] KF. Zieminski and JE. Spruiell. On-line studies and computer simulation of the melt spinning of nylon-66 filaments. *Journal of Applied Polymer Science*, 35(8):2223–2245, 1988.

[70] J. Sampers and PJR Leblans. An Experimental and Theoretical Study of the Effect of the Elongational History on the Dynamics of Isothermal Melt Spinning. *J. Non-Newton. Fluid Mech.*, 30(2):325–342, 1988.

[71] H. Giesekus. A unified approach to a variety of constitutive models for polymer fluids based on the concept of configuration-dependent molecular mobility. *Rheologica Acta*, 21(4):366–375, 1982.

[72] JY Yoo and HC. Choi. On the steady simple shear flows of the one-mode Giesekus fluid. *Rheologica Acta*, 28(1):13–24, 1989.

[73] RJ. Fisher and MM. Denn. Mechanics of nonisothermal polymer melt spinning. *AIchE J*, 23:23–28, 1977.

[74] CJS. Petrie and MM. Denn. Instabilities in polymer processing. *AIChE Journal*, 22(2):209–236, 1976.

[75] MM. Denn. Continuous Drawing of Liquids to Form Fibers. *Annual Review of Fluid Mechanics*, 12(1):365–387, 1980.

[76] RG Larson. Instabilities in viscoelastic flows. *Rheologica Acta*, 31(3):213–263, 1992.

[77] AN. Beris and B. Liu. Time-dependent fiber spinning equations. I. Analysis of the mathematical behavior. II. Analysis of the stability of numerical approximations. *J. Non-Newtonian Fluid Mech.*, 26:341–394, 1988.

[78] B. Liu and AN Beris. Time-dependent fiber spinning equations. 2. Analysis of the stability of numerical approximations. *J. Non-Newtonian Fluid Mech*, 26:363, 1988.

[79] TC Papanastosiou, N. Malamataris, and K. Ellwood. A new outflow boundary condition. *International journal for numerical methods in fluids*, 14(5):587–608, 1992.

[80] TC. Papanastasiou, VD Dimitriadis, LE Scriven, CW Macosko, and RL Sani. On the inlet stress condition and admissibility of solution of fiber spinning. *Advances in Polymer Technology*, 15(3,237-244), 1996.

[81] SE Bechtel, JZ Cao, and MG Forest. Illustration of an optimization procedure for fiber-spinning operating conditions: Maximum draw ratio under a Maxwell thin-filament model. *Journal of Rheology*, 37(2):237–287, 1993.

[82] VR Iyengar and A. Co. Film casting of a modified Giesekus fluid: a steady-state analysis. *Journal of non-newtonian fluid mechanics*, 48(1-2), 1993.

[83] VR. Iyengar and A. Co. Film casting of a modified Giesekus fluid: stability analysis. *Chem. Eng. Sci*, 51:1417, 1996.

[84] VV Ramanan, SE Bechtel, V. Gauri, KW Koelling, and MG Forest. Exploiting accurate spinline measurements for elongational material characterization. *Journal of Rheology*, 41(2):283–306, 1997.

[85] S. Gunter, P. Townsend, and MF Webster. THE SIMULATION OF SOME MODEL VISCOELASTIC EXTENSIONAL FLOWS. *International Journal for Numerical Methods in Fluids*, 23(7):691–710, 1996.

[86] M. Yao, GH. McKinley, and B. Debbaut. Extensional deformation, stress relaxation and necking failure of viscoelastic filaments. *J NON NEWTONIAN FLUID MECH*, 79(2):469–501, 1998.

[87] GC. Georgiou and D. Vlassopoulos. On the stability of the simple shear flow of a Johnson-Segalman fluid. *J. Non-Newtonian Fluid Mech*, 75:77–97, 1998.

[88] R. Sureshkumar, MD Smith, RC Armstrong, and RA Brown. Linear stability and dynamics of viscoelastic flows using time-dependent numerical simulations. *J. Non-Newtonian Fluid Mech*, 82(57):104, 1999.

[89] D. Bernardin. Theoretical study of some transient Couette flows of viscoelastic fluids in inertial devices. *Journal of Non-Newtonian Fluid Mechanics*, 88(1):1–30, 1999.

[90] MG. Forest, Q. Wang, and SE. Bechtel. 1-D isothermal spinning models for liquid crystalline polymer fibers. *J. Rheology*, 41:821–850, 1997.

[91] MG. Forest, H. Zhou, and QI Wang. Model study of the spinning thermoplastic liquid crystalline polymers: Fiber performance predictions and bounds on throughput. *J. Non-Newtonian Fluid Mech*, 82(57):104, 1999.

[92] JC Slattery and S. Lee. Analysis of melt spinning. *Journal of Non-Newtonian Fluid Mechanics*, 89(3):273–286, 2000.

[93] AK. Doufas, AJ. McHugh, and C. Miller. Simulation of melt spinning including flow-induced crystallization. Part I. Model development and predictions. *J. Non-Newtonian Fluid Mech*, 92(1), 2000.

[94] GH. McKinley, O. Brauner, and M. Yao. Filament Stretching Rheometry AND THE Extensional Viscosity OF Dilute AND Concentrated Polymer Solutions. *1st International Symposium on Applied Rheology*, pages 65–71.

[95] JS. Lee, HW. Jung, SH. Kim, and JC. Hyun. Effect of fluid viscoelasticity on the draw resonance dynamics of melt spinning. *Journal of Non-Newtonian Fluid Mechanics*, 99(2):159–166, 2001.

[96] YL Joo, J. Sun, MD Smith, RC Armstrong, RA Brown, and RA Ross. Two-dimensional numerical analysis of non-isothermal melt spinning with and without phase transition. *Journal of Non-Newtonian Fluid Mechanics*, 102(1):37–70, 2002.

[97] Z Gou and AJ Mchugh. Two-dimensional modeling of dry spinning of polymer fibers. *Journal of Non-Newtonian Fluid Mechanics*, 118(1):121–136, 2004.

[98] SC. Xue, RI. Tanner, and N. Phan-Thien. Numerical modelling of transient viscoelastic flows. *Journal of Non-Newtonian Fluid Mechanics*, 118(1):121–136, 2004.

[99] KS Surana and JS Sandhu. Investigation of diffusion in p-version LSFEand STLS-FEformulations. *Computational Mechanics*, 16(3):151–169, 1995.